

Design and Optimization of a Formula SAE Vehicle

A Major Qualifying Project Submitted to the Faculty of

Worcester Polytechnic Institute

In partial fulfilment of the requirements for the
Bachelor of Science Degree in Mechanical Engineering by:

Andrew Casella

Alex Deneault

Patrick Donaghey

Mark Lightbody

Jeffrey Robinson

Cote Taylor

April 23, 2018

Project Advisors:

Professor David Planchard

Professor John Hall

Abstract

The purpose of this MQP was to design and build a vehicle for use in the 2018 Formula SAE Michigan competition based on a frame built by the 2017 MQP team. The 2016 WPI car served as a benchmark for the 2018 MQP team's work, with the main goals being weight reduction, improved robustness, and improved competition performance. The suspension and drivetrain subsystems were deemed to have the most room for improvement and were given the most focus during the design process. The steering and braking subsystems also required significant modification to fit in the new frame, which is smaller than the 2016 frame. The 2018 MQP team was able to reduce vehicle weight by 100 pounds versus the 2016 car, while improving driving performance. The report details the design process and recommends refinements to be pursued by future WPI Formula SAE teams.

Executive Summary

The major goal for this team's MQP is to design and build a Formula style race car that will compete in the 2018 Formula SAE Competition in Michigan. The 2018 WPI Team is looking to finish the competition in a better place than the 2016 WPI Team did. The 2018 team used the methods, analysis, and takeaways from the 2016 team in order to make the best car possible. The 2016 car performed very well in the 2016 competition and thus served as a model for many of this team's designs.

The car was broken into seven main subsystems by the team in order to further progress the car and divide work. The team started this project with a frame made from last year's MQP team and designed these seven subsystems around its parameters. The team designed concepts using SolidWorks, performed FEA analysis using SolidWorks simulations and ANSYS, prototyped using 3D printers, and manufactured parts with machine mills and lathes. The final product of these methods resulted in an assembled car that will be competing in the 2018 competition.

The Drivetrain was the first major subsystem that was examined. The main component in this system is the differential. The differential in a car is designed to neutralize the distance the inner and outer part of a wheel travel when turning. Differentials are hard and time consuming to make, and therefore, the team decided not to design one in house. Additionally, there are many different types of differentials for cars, so research was done to determine the best option available. After careful consideration, the team decided to purchase a limited slip differential from Drexler Automotive.

The Engine subsystem was the next subsystem that was considered. The major component of this subsystem is the intake system. Extensive research and redesign was put into this system. The intake on the 2016 car performed well, but this year's team wanted a full redesign. FEA analysis and flow simulations were performed to determine the optimal volume of the intake. After the redesign, the team prototyped the intake system and will be testing it with a manufactured metal intake. The other component in the Engine subsystem that was mainly focused on was the fuel tank and fuel system. This was also fully redesigned as a new fuel tank shape is needed due to the new frame.

The Suspension subsystem required considerable attention immediately in the design process. The suspension was also a full redesign in this year's car. The 2016 car and earlier cars were helpful for learning experiences, but the 2018 car contained a new suspension. The a-arms, shocks, and geometry were studied and designed thoroughly.

The Steering subsystem of the car was based off of the system used in the 2016 car. The steering box was redesigned but still uses the miter gears that were used before. The mounting method was also changed to a tab based design that is more compact. The Kaz Technologies steering rack that the 2016 team had originally wanted to use was selected for this car as it is now available for purchase. The tie rods and lower steering shafts were redesigned as well. The upper steering shaft was kept the same to simplify the system.

The Brake subsystem was partially based off the 2016 car and partially redesigned. For the 2018 car, the brake calipers, master cylinders, and rotors came to be the same as the 2016 car. However, the brake pedal needed a full redesign due to a smaller frame forcing the template named Percy not to fit. A new brake pedal was designed and machined, as well as the assembly for mounting it to the frame. The floorplate was also designed and manufactured as well.

The Ergonomic subsystem was not the main focus during A and B term. The firewall and headrest were both fully redesigned. All of the ergonomic components will have to be fully redesigned due to the new frame. In C term, the seat and body panels were manufactured as well as the impact attenuator.

The last subsystem was shifting. This system involved multiple designs and analyses. In order for this system to be accomplished the Mechanical Engineering team and the Electrical Engineering team had to coordinate. The end result was a 6 bar design, which was validated through FEA analysis.

In C and D term the MQP team validated designs through testing. The team completed all technical documentations and prepared the vehicle for competition. Finally, the team offered recommendations for the continuation of this car for next year's MQP team.

Table of Contents

Abstract	ii
Executive Summary	iii
Table of Contents	v
Table of Figures	viii
Table of Tables	xii
Units (SI and US)	xiii
Competition Overview	1
Introduction	2
Drivetrain I – Power Transmission	3
Differential Selection	3
Differential Mounts	4
Mount Concepts	5
Final Drive Ratio Selection	5
Differential Positioning and Tab Design.....	8
Design Refinement and Completion	9
Sprocket Carrier	13
Axles	15
Engine Mounts	15
Finite Element Analysis	18
Shifting	20
Initial Mechanism Designs	22
6 Bar Linkage	24
Kinematic Analysis	25
Static and Stress Analysis	28
Load Determination and Stress Calculations: Shifter Link	28
Load Determination and Stress Calculations: Limiting Link	30
Engine Mount Modification	31
Hand Clutch.....	32
Testing Results and Modifications	34
Drivetrain II – Engine Performance	42
Engine Modification	43
Air Intake	45

Background Research	45
Restricted Air Intake Theory of Operation	45
Subdivision of Design and Concept Refinement	48
Forced Air Induction	52
Design Software	56
Intake Simulation Model	56
Getting Started with SolidWorks Flow Simulation	56
Pressure Wave Simulation Spreadsheet.....	59
Model Calibration	61
Prototype Intake Design	64
Prototype Manufacturing	66
Physical Testing and Refinements	69
Intake Mounting	72
Future Recommendations	74
Exhaust Tuning.....	76
Header Pipe Modifications.....	76
Fuel system	78
Cooling System.....	80
Testing.....	81
Simulation Method.....	83
Comparison Method	84
Radiator Selection	85
Radiator Mounting	87
Fan Research and Selection	89
Future Recommendations	91
Suspension.....	92
Overview.....	92
Design Formulation	92
How to Choose Suspension Geometry.....	93
Design Process.....	95
Suspension geometry.....	95
A-Arm Design	101
Rocker Design	105
Spring and Damper Selection.....	108
Steering.....	109
Implementation of Ackermann Geometry.....	117
Redesign and Implementation.....	119

Brakes	120
Brake Components	120
Pedal Assembly	124
Background Information	124
Design Process	125
Finite Element Analysis	130
Assumption and Modifications to the Assembly	130
Fixtures and Loads.....	131
Connectors and Contact Sets	131
Mesh	133
Results	134
Post-Manufacturing Design Modifications	136
Optimization Recommendations.....	138
Throttle Pedal Mounting and Placement.....	138
Ergonomics	141
Firewall and headrest	141
Electronics	142
Seat	143
Scheduling Overview	145
Bibliography	146
Appendix A. WR450F Clutch Retrofit Forum Posts	149
Appendix B. Brake Force Calculations	150
Appendix C. Simulation Study for Differential Mount FEA	153
Appendix D. Simulation Study for Sprocket Carrier FEA	165
Appendix E. Simulation Method for Air Intake	172
Appendix F. FEA Analysis of Suspension Components	180
Appendix G. Engine Mount FEA Simulation Report	245
Appendix H. Pedal Assembly FEA Simulation Report	259

Table of Figures

Figure 1. Formula SAE Michigan Event Point Values	1
Figure 2. Render of Complete 2018 WPI Formula SAE CAD Model	2
Figure 3. Chart of Road Speed vs. RPM for 36:13 Final Drive with WR450F	7
Figure 4. Differential Starting Location and Half Shaft Angles, Top and Rear Views.....	8
Figure 5. Pivoting Differential Mount Model in Frame.....	9
Figure 6. Eccentric Bearing Cup Model	10
Figure 7. Sandwich Assembly of final Differential Mounts	11
Figure 8. Differential Mount Assembly for FEA.....	12
Figure 9. Factor of Safety Plot of Differential Mounts.....	13
Figure 10. Completed Differential Mounts in Frame.....	13
Figure 11. Sprocket Carrier FEA Configuration and Results.....	14
Figure 12. Engine Mount Relative Locations	16
Figure 13. 3D Engine Scan.....	17
Figure 14. Engine Mount 2D Profile	18
Figure 15. Engine Mount FEA Assembly.....	19
Figure 16. FOS Fringe Plot	19
Figure 17. Transmission Lever.....	20
Figure 18. Key Hub	22
Figure 19. Interlocking Forks.....	22
Figure 20. Key Hub Concept 2.....	23
Figure 21. Key Hub 6 Bar.....	24
Figure 22. Ball Joint Rod Ends and Turnbuckle	25
Figure 23. Planar Mechanism Positions.....	25
Figure 24. Planar Mechanism.....	26
Figure 25. Graph of Position of Joints 1 and 2.....	27
Figure 26. Graph of Angular Displacement	27
Figure 27. Angle of Shift Linkage.....	28
Figure 28. Key Hub Free Body Diagram 1	29
Figure 29. Key Hub Free Body Diagram 2.....	30
Figure 30. Motor Mounts FEA Setup.....	31
Figure 31. Motor Mounts FEA FOS	32
Figure 32. Hand Clutch Assembly.....	33
Figure 33. Updated Linkage Position.....	34
Figure 34. Shifting Mechanism return Springs	35
Figure 35. Workings of an Assist and Slip Clutch	36
Figure 36. YFZ 450R clutch assembly.....	38
Figure 37. YFZ Clutch installed in WR engine case.....	40
Figure 38. Pingel Electric Speed Shifter Mounted to Car.....	41
Figure 39. Hot Cams Intake and Exhaust Camshafts for 2012-2015 WR450F	43
Figure 40. High Compression Ratio Piston for WR450F.....	44
Figure 41. Intake Restrictor Location	45
Figure 42. Subsections of Air Intake.....	49
Figure 43. Airflow Entering Plain Pipe and Elliptical Bellmouth.....	49
Figure 44. Pressure in 16°/4° “De Laval” Restrictor	50

Figure 45. Required placement for intake components for Turbocharged Formula SAE Cars	53
Figure 46. Compressor graph of Garrett GT1241 turbocharger.....	54
Figure 47. Compressor Graph of Honeywell MGT12 turbocharger.....	55
Figure 48. WR450F Integral Intake Runner Extension and Intake Valve Stems.....	57
Figure 49. Interior of Model of Integral Runner Extension.....	58
Figure 50. 2016 Intake Model with Integral Runner and SWFS Boundary Conditions Set	58
Figure 51. Excerpt of Pressure Output Data from Pressure Wave Spreadsheet	60
Figure 52. Goal Plot Result for a 6000 RPM Calibration Run.....	62
Figure 53. Plenum Prototype Design Cross Sections, 5x Engine Displacement Volume	65
Figure 54. Plenum Design Simulation Assembly, Including Free Air Bubble.....	66
Figure 55. Cross Section of Prototype Intake Design with 1x Volume Plenum.....	68
Figure 56. Intake Prototype Mounted in Car.....	69
Figure 57. Screen Capture of Flow Simulation of Final Intake Design.....	70
Figure 58. Cross Section of Final Intake Design.....	71
Figure 59. 3D Printed Components of Final Intake.....	72
Figure 60. Top View of Upper Air Intake Mount to Frame	73
Figure 61. Side View of Upper Air Intake Mount to Frame	73
Figure 62. Metal Lower Runner Section.....	74
Figure 63. Header Pipe Modification.....	77
Figure 64. Exhaust Slip Fit	77
Figure 65. Fuel Tank Isometric.....	78
Figure 66. Fuel Tank Side View.....	79
Figure 67. Test Bench Radiator and Fan.....	81
Figure 68. Section View of Radiator Segment Simulation Setup.....	83
Figure 69. Kawasaki KFX450R Radiator	86
Figure 70. Two Proposed Radiator Positions.....	88
Figure 71. Radiator Mounted to Jack Point on Car	89
Figure 72. Fan Considered.....	90
Figure 73. Radiator Fan Used	90
Figure 74. WPI Frame, competitor frame.....	93
Figure 75. Wireframe model of suspension geometry.....	93
Figure 76. Suspension mounting bars with tab locations	95
Figure 77. Wireframe sketch of suspension mount point on frame.....	95
Figure 78. Front suspension wire frame.....	96
Figure 79. Wheel offset.....	97
Figure 80. Modified Hub Dimension	98
Figure 81. Caster angle and mechanical trail, Kingpin inclination and scrub radius.....	99
Figure 82. Dynamic Steering and Suspension Sketches	100
Figure 83. Suspension assembly with “suspension mockup” and “wheel” parts.....	100
Figure 84. A-arm tube profiles in “suspension mockup” part.....	101
Figure 85. 2015 Front Suspension.....	102
Figure 86. Pullrod Tab and Crossbar	102
Figure 87. A-Arm part.....	103
Figure 88. Spherical A-Arm fixtures	104
Figure 89. Slider A-Arm Fixture	104
Figure 90. Forces applied to A-Arm	104
Figure 91. Mesh Parameters for Rear A-Arm.....	105
Figure 92. 2016 Front suspension	106

Figure 93. First Iteration of Rocker Design.....	106
Figure 94. Final Rocker Design	107
Figure 95. Simplified steering system diagram.....	109
Figure 96. Steering shaft from the steering wheel to the steering box.....	110
Figure 97. Old Steering Box Design	111
Figure 98. Spiral Cut Miter gears	111
Figure 99. Tapered Roller Bearings.....	112
Figure 100. The new side panel design.....	112
Figure 101. SolidWorks model of the new steering box design.....	113
Figure 102. Old bearing mount.....	114
Figure 103. Kaz Technologies steering rack	115
Figure 104. Optimized driver line through minimum radius corner.....	116
Figure 105. Example of perfect Ackermann steering geometry	117
Figure 106. Sketch used to determine steering geometry	118
Figure 107. Redesigned front upright next to old upright.....	118
Figure 108. Wilwood Billet Dynalite Single, on the right, and Wilwood PS-1, on the left.....	123
Figure 109. 95th Percentile Male Template Dimensions	124
Figure 110. Sketch of 95th Percentile Male Template place in 2017-2018 Frame.....	124
Figure 111. Wilwood Brake Pedal Assembly used in Previous Years.....	125
Figure 112. First Pedal Box Iteration.....	126
Figure 113. Wilwood Hanging Pedal Assembly	126
Figure 114. Placement of Master Cylinder Mounting Brackets in Frame	127
Figure 115. Sketch of Final Pedal Profile.....	129
Figure 116. Final Pedal Assembly.....	130
Figure 117. Pedal Assembly Brackets	131
Figure 118. Pedal Assembly Brackets FEA.....	131
Figure 119. Pedal Assembly Brackets FEA Setup.....	132
Figure 120. Pedal Assembly Brackets FEA Preload.....	132
Figure 121. Pedal Assembly Brackets FEA Contact Sets	133
Figure 122. Pedal Assembly Brackets FEA Mesh.....	133
Figure 123. Pedal Assembly Brackets FEA Results 1.....	134
Figure 124. Pedal Assembly Brackets FEA Results 2.....	135
Figure 125. Pedal Assembly Brackets FEA Factor of Safety	135
Figure 126. Pedal FEA Setup.....	136
Figure 127. Pedal FEA Results	137
Figure 128. Pedal Bracket.....	138
Figure 129. BMW Throtte Pedal	139
Figure 130. Throttle Pedal Assembly Bracket	139
Figure 131. Top View of Mounted Throttle Pedal	140
Figure 132. Bottom View of Mounted Throttle Pedal.....	140
Figure 133. Firewall Sheet Metal.....	141
Figure 134. Headrest Sheet Metal.....	142
Figure 135. Component mount locations on Firewall.....	143
Figure 136. Leather Seat.....	144
Figure 137. Beginning of Year Gantt Chart.....	145
Figure 138. Brake System Design for Original Values.	151
Figure 139. Brake System Design with Final Values.	152
Figure 140. Fixtures and Loads for Differential Mount FEA.....	161

Figure 141. Mesh for Differential Mount FEA.....	162
Figure 142. Von Mises Stress Plot of Differential Mounts, Including Frame Tube Substitutes	163
Figure 143. Factor of Safety Plot of Differential Mounts, Including Frame Tube Substitutes.....	164
Figure 144. Factor of Safety Plot of Differential Mounts, Only Including Mounts and Tabs.....	164
Figure 145. Fixtures and Loads for Sprocket Carrier FEA	168
Figure 146. Mesh for Sprocket Carrier FEA	169
Figure 147. Von Mises Stress Plot of Sprocket Carrier.....	170
Figure 148. Factor of Safety Plot of Sprocket Carrier.....	171
Figure 149. Air Intake Flow Simulation Boundary Conditions	174
Figure 150. Excerpt of Excel Spreadsheet Used for Intake Valve Boundary Condition.....	175
Figure 151. Numerical Integration Formula for Flow Simulation Result Data.....	177
Figure 152. Volume Flow Rate Result Graph for Flow Simulation.....	178
Figure 153. Volumetric Efficiency Calculation from Numerically Integrated Results	178

Table of Tables

Table 1. Weighted design matrix for differential selection	4
Table 2. McMaster Hardware.....	25
Table 3. Data for Joints 1 and 2.....	26
Table 4. 2014 YFZ450R Clutch Components Ordered.....	38
Table 5. Design Matrix for Forced Induction	52
Table 6. Cooling System Test Results	82
Table 7. Cooling System Heat Dissipation Calculations	82
Table 8. Radiator Option Comparison	86
Table 9. Steering rack specifications	115
Table 10. Steering rack decision matrix	115
Table 11. Overall Settings for Differential Mount FEA	153
Table 12. Mesh Settings and Output for Differential Mount FEA.....	162
Table 13. Overall Settings for Sprocket Carrier FEA.....	165
Table 14. Mesh Settings and Output for Sprocket Carrier FEA	169

Units (SI and US)

Quantity	Name	Symbol(s)
length	meter	m
	inch	in
	foot	ft
mass	kilogram	kg
	pound-mass	lb, lbm
time	second	s
	minute	min
	hour	hr
temperature	kelvin	K
	celsius	C
	fahrenheit	F
angle	degree	deg, °
angular velocity	rotations per minute	RPM
speed, velocity	miles per hour	mph
acceleration relative to gravity	g-force	G
area	square inch	in ²
	square meter	m ²
volume	cubic centimeter	cc
	liter	L
	cubic meter	m ³
	cubic inch	in ³
density	kilogram per cubic meter	kg/m ³
energy	joule	J
power	watt	W, J/s, kg·m ² /s ³
volumetric flow rate	cubic meter per second	m ³ /s
mass flow rate	kilogram per second	kg/s
pressure, stress	pounds per square inch	psi, lb/in ²
	pascal	Pa, N/m ²
torque	inch-pound	in-lb
	foot-pound	ft-lb
force, weight	newton	N
	pound-force	lb, lbf

Competition Overview

The Formula SAE competition series is an engineering competition managed by SAE International, in which student teams at various universities around the world act as fictional manufacturing companies to compete to develop and market small race cars for weekend autocross driving. The competition has an extensive rule book that all vehicles must adhere to, which includes an outline of all events. The point values for these events are shown in Figure 1.

FORMULA SAE MICHIGAN	
Static Events	
Presentation	75
Engineering Design	150
Cost Analysis	100
Dynamic Events	
Acceleration	100
Skid-Pad	75
Autocross	125
Efficiency	100
Endurance	275
Total Points	1000

Figure 1. Formula SAE Michigan Event Point Values

Each Formula SAE competition is comprised of both static and dynamic events to gather a complete understanding of the vehicle designs and business strategies produced by each team. The dynamic events judge the performance and capability of the vehicle, while the static events assess the design process and knowledge of the team. All events are judged by experts in the automotive industry, and the pressure of justifying poorly made design decisions can weigh heavily on the team during competition. The disparate judgment criteria used for the different events mean that during the design process, every choice must be evaluated in relation to the car as a whole, balancing optimized performance with cost and reliability in order to produce well-founded design decisions that stand up to the scrutiny of expert review. An overall emphasis on solid, defensible design is thus key to success in Formula SAE competition.

Introduction

Previous WPI Formula SAE teams have followed somewhat irregular development cycles, with the 2015 vehicle taking several years to complete, the 2016 vehicle developed within one year, and the 2018 vehicle completed after a two-year development cycle. Due to the challenges of completing a car within a single year, as was done in 2015-16, the 2017 MQP team decided to focus exclusively on the frame for the 2018 competition car, with the intent of completing the remainder of the car during the 2017-18 academic year. This extended development cycle has provided a more appropriate time span to thoroughly validate all design decisions, but has also taught the team some valuable lessons about the issues inherent with staggering frame and subsystem development. The 2018 WPI Formula SAE car is shown in Figure 2 as a render of the finished SolidWorks assembly.

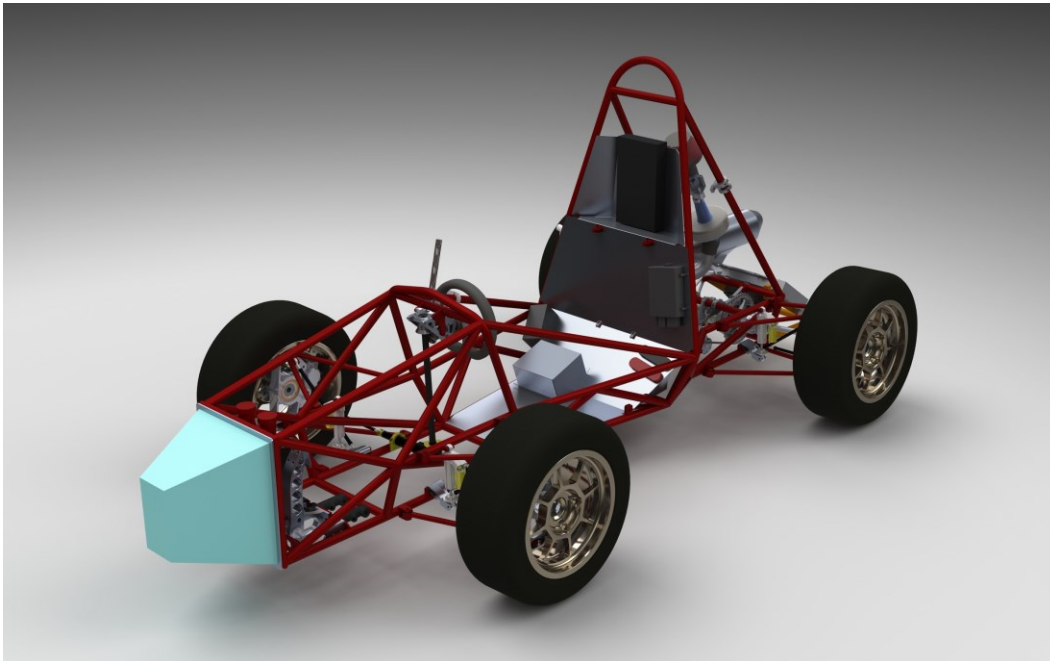


Figure 2. Render of Complete 2018 WPI Formula SAE CAD Model

The organization of this report will reflect the subsystem breakdown used by the 2018 team to organize the development process. This subsystem breakdown includes, in order: drivetrain, suspension, steering, brakes, and ergonomics. Each section of this report details the design processes, validating data, and manufacturing methods that defined each component of the car, along with recommendations for future teams based on the lessons learned during this development cycle. The 2018 MQP team hopes that the information included in this report will not only serve to inform those curious about the development process for the 2018 car, but will also provide a solid reference for future WPI Formula SAE teams to make informed decisions about individual components, as well as the development process as a whole. It is the recommendation of the 2018 WPI Formula SAE team that future teams not modify any part of the current design without a full understanding of the design process used for the 2018 car and thorough validation of improvement.

Drivetrain I – Power Transmission

Differential Selection

The engine selected for this year was a 2015 Yamaha WR450F engine due to its similarity to the YFZ450R that was used in 2016, and that was used for the frame design in 2017. Once this engine was selected, the next step was to decide how best to transfer the power to the ground. The engine is equipped with a five-speed internal gearbox and a sprocket intended for a chain drive to the rear wheel, as implemented in the OEM dirt bike. It was decided that a similar setup will be used, except that a limited slip differential would be used to transfer power to the car's rear wheels. The addition of a differential is the most effective way to transfer power from the engine to both rear wheels and make the best use of both rear tires. A limited slip differential limits the difference of applied torque between the two output shafts, which helps with applying torque to the outside wheel during cornering, which has considerably more traction than the inside wheel. This is needed because during high lateral acceleration during cornering, the inside wheel may not have the frictional force needed to transfer all the torque to the ground and accelerate the vehicle. Because of this, the use of a traditional open differential may cause the wheel to lose traction and spin, which would slow lap times considerably.

The selection of a limited slip differential was not taken lightly, as an incorrect selection could have a large impact on performance. Three differentials were initially considered, the first being an ATV differential made by Can-AM and used in many of their newer vehicles. This was most like the differential used in the 2016 formula car, so the team was already familiar with its benefits and shortcomings. The most appealing characteristic of this option was its price and availability. It is a widely used part, and there is a lot of documentation online about them. However, because this product is a shaft driven final drive, a custom case would have to be machined, which is no small task. If this option were chosen, the axle would also have to be cut and welded to the needed length. The next option was a Torsen type LSD made by Taylor Race Engineering specifically for use in a Formula SAE vehicle. This option was considerably more expensive but offered more benefits. This differential is slightly adjustable by changing out internal components which allows for torque distribution adjustment between wheels. Another benefit to this differential is the availability of drive shaft components. Taylor Race sells everything for the drive shafts individually, allowing the team to pick and choose as they want. Also, judging from positive feedback online, both customer service and the lead time on the product are excellent. The last differential that was looked into was made by Drexler Automotive, a German engineering company that has a great reputation in the racing world. This differential is a clutch pack LSD, that offers adjustable lockup with the turn of a bolt and is by far the lightest option. Drexler also offers custom length drive shafts and will ship everything ready to be dropped into the car. The down side to this option was cost and lead time. It costs around \$5,700 and has a lead time of 12 weeks. This differential is completely rebuildable and could be used in many cars to come.

Table 1. Weighted design matrix for differential selection

		ATV front Differential		Taylor Formula SAE Differential		Drexler Differential	
Criterion	Weight	Score	Total	Score	Total	Score	Total
Cost	5	9	45	4	20	2	10
Adjustability	8	2	16	5	40	10	80
Weight	7	4	28	8	56	8	56
Simplicity	8	1	8	5	40	8	64
Lead time	3	8	24	6	18	8	24
Total			121		172		234

The final decision on a differential was made using a weighted matrix, see Table 1. Five key characteristics were used in order to make the decision, with the first being cost. Cost was weighed in the middle because the team’s defined budget would allow for the purchase of any of the options, with minor reallocation of resources. A higher cost may limit freedom with other parts of the car but would not impede the team from finishing the vehicle. The next was adjustability, which was weighted highly due to a lack of knowledge of suspension and tire performance. The ability to tune the lockup easily could greatly increase the drivability of the car. The next factor was weight, which was also weighted somewhat high due the importance of weight reduction. Another key factor was ease of implementation, as the team had limited man power and time. Spending less time on implementation would allow for more time to tune the car and focus on other areas that were lacking on the 2016 car. The last parameter was lead time. This was given a fairly low weight because the team was being proactive and thinking about this decision early in the build. Even with a long lead time the team was well prepared. As the weighted matrix clearly shows, the Drexler LSD was the best option and was purchased for implementation in the car.

Differential Mounts

Along with the differential itself, the differential mounts are a crucial part of the drivetrain. In addition to holding the differential in place, they also define the chain line of the drivetrain and the angle of the half shafts. They thus not only need to be strong enough, but also must ensure the differential is properly located in all three dimensions. For this year, the team has also added the complicating factor of integrating the chain tensioner into the differential mounts in an effort to improve on the mounts designed for the 2016 WPI vehicle and ultimately reduce weight.

Mount Concepts

In 2016, the differential mounts attached the differential rigidly to the frame with bulky, 1/2-inch plate aluminum brackets and custom shaft collars. This design used a separate chain tensioner located near the rear engine mount, which used a torsional spring, tensioning bolt, and idler pulley. Due to the intersection of the chain line and a frame cross member supporting the rear of the engine, a Delrin chain guide was made to redirect the chain around this member. Although this mount and chain guide system functioned properly for the majority of the time, the chain guide failed on at least one occasion due to an engine lock-up during dyno testing, causing the tensioning bolt to snap.

The main goal of the new differential mount design was to incorporate chain tensioning functionality into the mounts in order to reduce the complexity and weight of the system. This tensioning system would need to provide at least half of one chain link worth of linear adjustment in the tensioning system. Any less would risk being unable to properly tension the chain. The team also decided that the differential mounts would attach to the frame with welded tabs and shoulder bolts instead of shaft collars. This would ideally reduce weight and complexity while increasing strength. The team came up with three main concepts to accomplish these goals:

- Linear tensioning with bolts in slots - mounts held in place by bolt torque
- Rotational tensioner – pivot mount around top or bottom frame tabs, adjust with turnbuckle
- Eccentric bearing cups – pivot diff within fixed mount, hold in place with pinch bolts

After discussing the goals for the system, and the potential advantages and disadvantages of each, designs for the latter two were created, as they were more viable options. The first idea was discarded early due to the likelihood of higher system weight and the difficulty of securely fixing the mounts in place under the projected loads. However, no extensive calculation or design work was done to fully invalidate this option. Once the prospective designs had been identified, the final drive ratio needed to be determined to begin work on the mounts in earnest, since the size of the driven sprocket will have a large influence on the available range of chain tensioning adjustment.

Final Drive Ratio Selection

In determining the final drive ratio, that being the ratio between the engine output sprocket and the driven sprocket at the differential, several concerns needed to be addressed, including packaging due to sprocket size, and performance due to the influence gearing would have on driver experience. The first step taken by the team was to review previous methodologies used for final drive determination.

According to documentation left by the 2016 WPI Formula SAE team, the final drive ratio for their car was decided by tabulating road speed values according to engine RPM and gear selection. Seeking to maximize use of the full gearing range available on their closely geared YFZ450R, the team tried to adjust their final drive ratio to make the car reach its maximum desired road speed at redline in fifth gear. This resulted in a final drive ratio of 38:14, or 2.714:1, with the car reaching about 65 mph at 6000 rpm in fifth gear. Due to issues with engine performance, the redline of the

2016 car was considered to be 6000 rpm, as performance steeply declined at higher speeds. According to accounts from some current team members who drove the 2016 car, forcing all five gears into a 65 mph limit resulted in near constant shifting when driven on the track, causing annoyance and slowing the car due to time wasted shifting. A review of the gear ratio analysis tables generated by the 2016 team showed that most gears would only keep the engine in its power band for less than 10 mph hence the rapid pace of shifting required to drive the car.

For the Cal Poly team, their gear ratios were narrowed down through calculations of “tractive effort,” top speed, and time to speed. By completing physical testing with previously designed Formula SAE cars, the Cal Poly engine team was also able to observe the effects of certain final drive ratios and gear selections on acceleration. Instead of comparing the total road speed spread offered by each final drive choice, the Cal Poly team narrowed their comparisons to the specific gears each final drive ratio would use. For example, when comparing the relatively high drive ratio of 33:14 to the relatively low ratio of 48:14, they compare the two from first to third gear, and second to fourth gear, respectively. By specifying the gears they intended to use, rather than assuming all would be used, the Cal Poly team allowed themselves to more finely tune the behavior of their drivetrain to match driver preference and engine tuning. While they did not specify exactly which gear ratio they intended to use in their report, their approach to final drive selection seemed remarkably thorough.

The 2018 WPI team intended to strike a balance between these two approaches to final drive selection, since certain attributes of each method would be useful for the design of the new car. Due to a lack of information about torque and power figures for the WR450F, even at the level of conjecture, calculations of tractive effort and acceleration time would be essentially pointless, so the total speed range of each gearing option became the primary design metric. The first step of the design process was thus a determination of the limits of possible final drive choice, to narrow the field of options. After browsing through online aftermarket parts stores, front (engine) sprocket selection was limited to a range of 12-15 teeth, all using standard 520 motorcycle chain since only sprockets using this specification would fit the splined output shaft of the WR450F engine. With this information in mind, the frame was then examined to determine the maximum rear sprocket size that would feasibly fit. Using a guide found online, an adaptable model of a 520 sprocket was made, and its size was adjusted from 36 teeth upward to find the limit. In checking the fit of each sprocket size, the outer edge of the sprocket was kept at minimum 1/2 inch from any frame members, and less than 1/2 inch below the bottom of the frame, also keeping in mind a desired one-half link of chain length adjustment. From this exercise, the largest rear sprocket that was observed to comfortably fit into the frame was 38 teeth, since a 39 tooth sprocket did not leave enough room for the required adjustment range.

With this information in mind, a spreadsheet of road speed values per gear was created, in the same vein as the approach taken by the 2016 WPI team. Taking into account 20-inch diameter tires, the 2.652:1 primary drive ratio of the WR450F engine, and its five gear ratios, a table of road speeds was laid out from 500 RPM to the 11500 RPM stock redline of the WR450F, with specific fields for front and rear sprocket tooth counts. Figure 3 below is a chart of these road speeds for one of the

gear ratios considered. After playing with different gear ratios, the ratios 38:12 and 36:13 began to look most appealing.

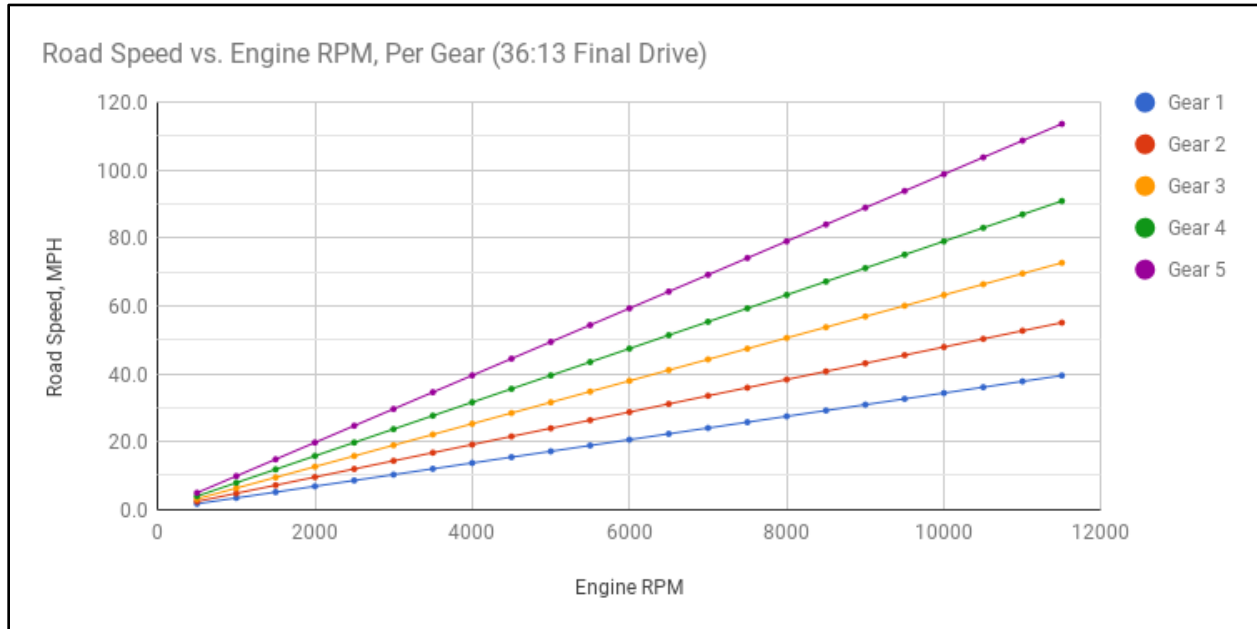


Figure 3. Chart of Road Speed vs. RPM for 36:13 Final Drive with WR450F

In addition to being the lowest gear ratio possible for the car, 38:12 would allow for full usage of all five gears, and assuming a power band of 6000-8000 RPM, would place the top speed of the vehicle at just under 70 MPH. Considering that the engine already has a 13 tooth drive sprocket attached from the factory, and the wider speed spread possible with a higher gear ratio, 36:13 is an appealing option. This higher ratio would allow for full usage of gears one through four, and would place the top speed of the car at just under 80 MPH.

Due to the concurrent work being done to improve intake plenum performance, and thereby increase the effective “redline” of the engine, 8000 rpm was assumed to be a reasonable redline for the 2018 car, with any improvement beyond this limit allowing for further spacing between shifts. If engine redline could be pushed up to 10000 rpm later in development, the 36:13 gearing would allow the car to achieve the maximum speed expected during competition, 65 mph, in third rather than fourth gear, further spreading required shifts. If engine redline were limited to 6000 rpm, as it had been in previous years, the car would still be able to reach 60 mph at the top of fifth gear with a 36:13 final drive.

The 36:13 gear ratio was selected for its versatility with different engine behaviors, as well as the smaller size of the 36 tooth driven sprocket. However, since gearings using a 38 tooth driven sprocket were also found to be viable, this slightly larger sprocket size was used for the design of the differential mounts.

Differential Positioning and Tab Design

With a rear sprocket size now selected, the basic layout of the differential mounts was arranged, starting with the location of the differential, this being the point in the adjustment range of the mounts where the rear sprocket would be closest to the frame. Since the centers of the rear wheels are positioned nearly in plane with the rear of the car, setting the differential as far rearward as possible would produce the minimum possible half shaft deflection. This location was set with the differential 125 mm on center from each of the rearmost frame cross members, placing a 38 tooth 520 sprocket just under 1/2 inch away from each frame member for the smallest comfortable clearance. This location was chosen while checking the fit of different sprocket sizes and is shown in Figure 4 below. Also note the differential and half-shaft models, which were given to the team by Drexler immediately following the confirmation of the differential order. These assemblies were imported from another CAD software before they were sent to us and required much work to arrange into an assembly usable for packaging.

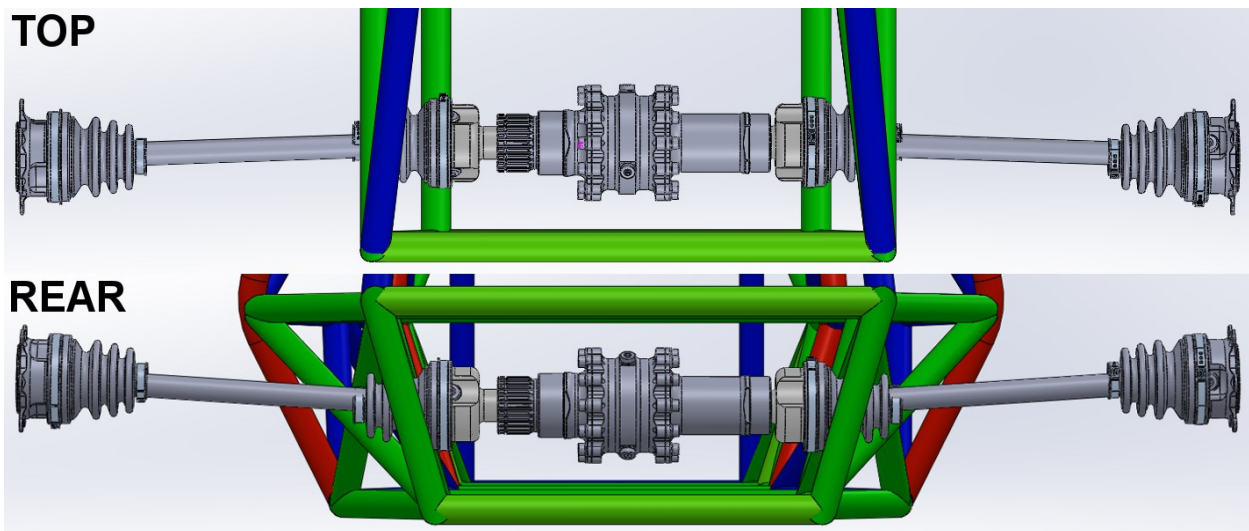


Figure 4. Differential Starting Location and Half Shaft Angles, Top and Rear Views

With the position of the differential chosen, the mounting tabs that would be welded to the frame to support the mounts were then designed. Before creating any concrete designs, a static analysis was run by hand to approximate the loading the mounts would need to withstand. For determining the maximum load, the assumed worst-case scenario involved an engine lock-up as seen during dyno testing in 2016, where the force of the chain tension on the mounts far outweighed the mass of the differential. For this case, the tires were assumed to break traction at 1.5 G of deceleration, with a total vehicle weight of 750 pounds including the driver. With 50/50 weight distribution, as would roughly be the case on a dynamometer, this placed 562.5 pounds-force tangentially on the rear wheels. For a tire diameter of 20 inches, assuming no compression, and a sprocket diameter of roughly 4 inches as found from the earlier model, the approximate tension force applied to the chain would be 1406 pounds, as expected making the mass of the differential negligible in comparison. With this force applied at the drive side of the differential, and properly functioning mount bearings, the vast majority of the force would be transmitted to the mounts as a

linear forward pull on the drive side mount. For a differential mount attached to the frame at both top and bottom, this 1406-pound force would split into two 703 pound forces at the mount tabs. If perfect shear is assumed, this force then splits into two 301.5 pound forces at each tab.

Since previous WPI vehicles had experienced some issues with tab failure, the differential mount tabs were significantly overbuilt to ensure that they would be the least likely component to break in the event of any accident, since the mounts would be far easier to repair than the tabs. To do so, 0.16-inch-thick steel was chosen for the tabs, along with 3/8-inch shoulder bolts as the mounting hardware. Early in designing the first differential concept, the length of the tabs was set at one inch from the center of the frame tubes to the center of the mount bolts, leaving a small amount of free space for different mount designs later on, if required.

In hindsight, these choices produced significantly stronger tabs than required, even for an “overbuilt” configuration according to the assumed worst-case scenario, with a minimum FOS of 12 due to bearing stress in the tabs. In retrospect, the team does not think that this degree of excess is advisable for other components of the car, or for future iterations of this design.

Design Refinement and Completion

The design of the pivoting mount concept involved attaching the differential mount to the mounting tabs on the lower of the two rear frame cross members, using separate mounts for the drive side and non-drive side of the differential. With the lower end of the mount riding on shoulder bolts, the mount would be allowed to pivot around this lower bolt to tension the chain. This pivoting would be controlled by a small turnbuckle attached between the top of the mount and the upper frame tabs. Figure 5 below shows the layout of this first completed mount assembly.

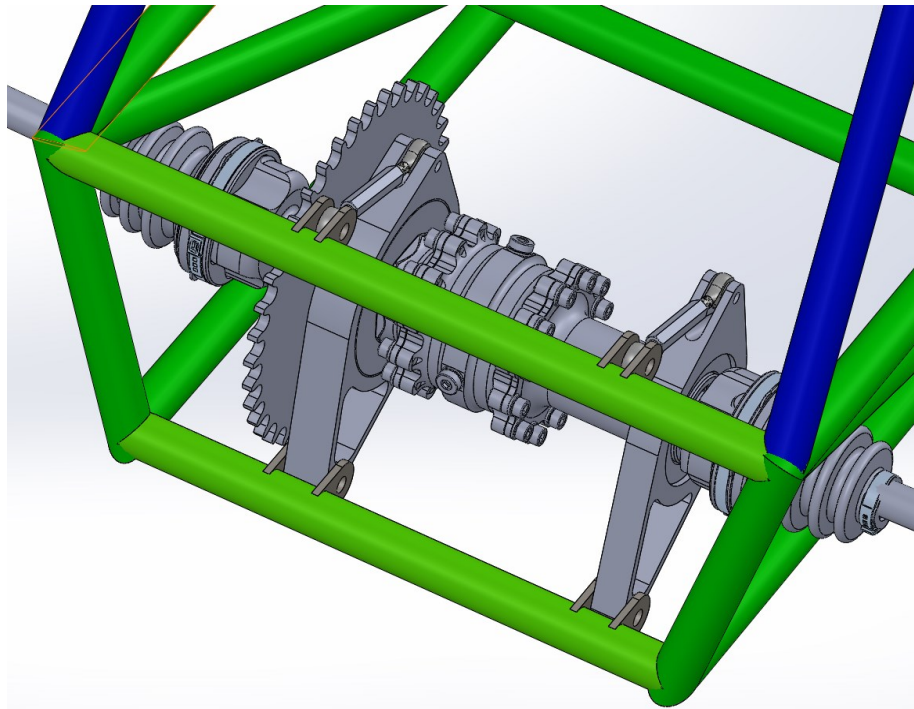


Figure 5. Pivoting Differential Mount Model in Frame

When this design was modeled in SolidWorks, a number of potential complications were noticed with this theoretically simple design, primarily regarding the miniature size of the turnbuckles. Due to the small size of the mounts relative to most turnbuckles, those used on the differential mounts would be among the smallest commercially available, likely requiring overall lengths of less than four inches. While these turnbuckles were stated on the manufacturer website to be capable of withstanding the worst case 700-pound axial load predicted, the mounts themselves would be somewhat more complex than was preferable, in order to provide a clevis joint for the turnbuckles to attach to. Due to a general wariness about using turnbuckles as a structural component of the differential mount, as well as concerns about the manufacturing complexity of the mounts, the team decided to scrap this concept as well, and focus on the third of the original ideas.

The eccentric cup mount was thus the one that was carried through to completion and was chosen over the other two competing concepts primarily for its simplicity. This mount concept works by pressing each differential bearing into a cup with an outer diameter off-center from the bearing seat. The distance between the center of the bearing seat and the center of the outer diameter of the cup thus becomes the radius around which the differential is able to rotate. The benefit of this design is that the differential is allowed to pivot about an axis within its physical envelope, meaning that the diameter of this rotation can be finely tuned to offer the required linear displacement while requiring only a small amount of extra material over a fully rigid mount.

To suit the pitch of the 520 chain that would be used on the car, the offset of the eccentric cups was set at 7 mm, to provide a total linear adjustment range of 14 mm, and thus a total chain length adjustment range of 28 mm, or just under 1 full chain link at 32 mm. Adjustment was limited due to the fact that a full link of adjustment would simply be cause for shortening the chain, and the additional offset would make the sprocket protrude farther below the frame than any other components. Additionally, increasing the offset further would risk interference between the rubber half-shaft boots and the nearby suspension rocker/shock absorber assembly when the eccentric cups were in the fully forward position. From here, the bearing sizes required to fit the Drexler differential were determined, those being 6211 and 6010, and work began on modeling the two potential designs for the mounts. Figure 6 shows one of the eccentric cups, which has holes in its side to aid rotation of the cup in its mount and to reduce weight.

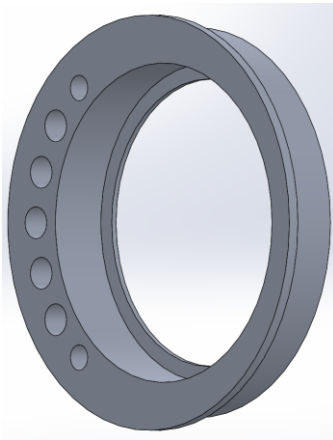


Figure 6. Eccentric Bearing Cup Model

Since the differential mount would see a large amount of vibration, and continuous loading, it was important to consider the stability of the differential as a package. To prevent horizontal slippage, the differential included inboard flanges to locate the bearings horizontally on their seats, and the eccentric cups were designed to include matching flanges on the outboard side to lock the bearing in place between the two horizontally. This was also done for the cups themselves, with a flange on the inboard face of each cup to prevent it from sliding outward horizontally in the mount bracket. The combined effect of these flanges, when assembled, is to prevent the assembly from coming apart without removing the whole assembly from the frame tabs, thus making any additional axial positive locking for the bearings and cups redundant. This is illustrated by Figure 7.

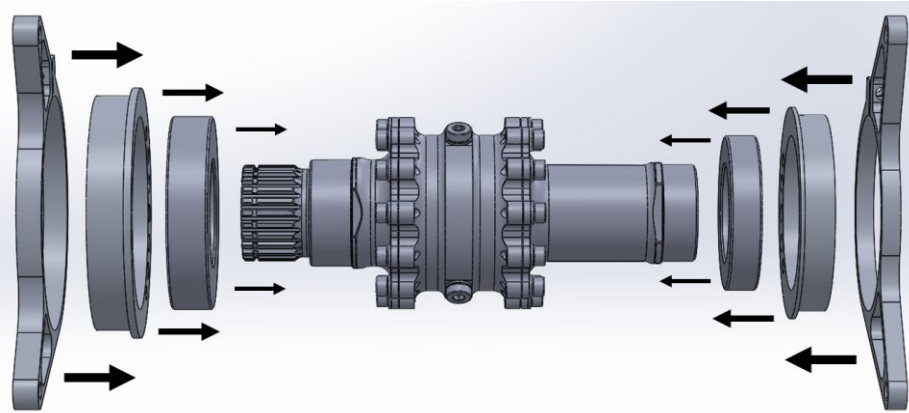


Figure 7. Sandwich Assembly of final Differential Mounts

For the drive side mount, 1/2-inch AL6061 plate is used, and 3/8-inch plate is used for the non-drive side mount since any force on the chain will present far more significantly in the nearer drive-side mount. Since the mounting tabs had already been welded to the frame by the time this design was completed, with equal 1/2 inch spacing on both mounts, the non-drive side mount used a 1/8-inch spacer to offset it horizontally in the 1/2-inch spacing between each pair of tabs. While the eccentric cups are thicker than the mounts to accommodate the bearings, this has been deemed acceptable to properly house the bearings and has no effect on the functionality of the mounts. The mounts are also almost entirely flat, with the only machining process necessary after cutting the horizontal profiles being the drilling of the pinch bolt holes. This has allowed for the usage of waterjet cutting to make the differential mounts instead of the extensive milling procedures that would be required to cut thicker plate, or the previous pivoting design.

After completing the design, FEA was run using the same 1406-pound force calculated as the worst-case scenario earlier. Figure 8 below shows the full arrangement of the FEA assembly. For this analysis, the frame tabs were attached to modeled tubes of equivalent length to the real frame members they would be welded to, and blanks of all fasteners were made to simulate the behavior of the mounts as they would be assembled in practice. A simplified model of the differential assembly was also made, with cylindrical segments substituting for the bearings and the sprocket. In the static simulation environment, the mount tabs were attached to the frame tubes with “Bonded” contact constraints, and all contacts between the mount components and differential blank were accounted for with “No Penetration” constraints. All fastener representations and the differential blank were

set to behave as rigid components, to simplify their behavior. The remaining components were assigned the materials they would be made of in reality, those being AL6061 for the mount brackets and cups, and 4130 chromoly steel for the tabs and frame tubes. Appendix C provides a more thorough explanation of the setup used for this FEA simulation.

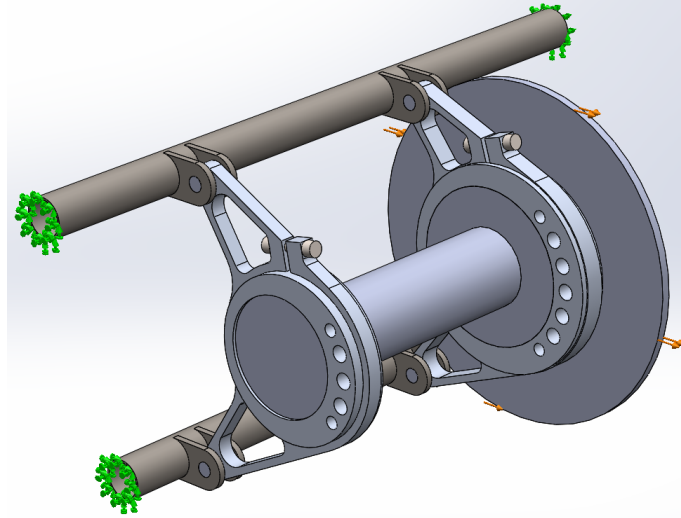


Figure 8. Differential Mount Assembly for FEA

When tested with this FEA procedure, the FOS of the mounts is about 2, which is a safe value also considering the extreme loading used for the worst-case scenario. Figure 9 below shows a plot of the FOS of the mount design, and Figure 10 shows the assembled mounts in the frame. This completed mount design was manufactured and fitted to the car in B Term. One recommendation for future WPI teams if this same mount design is used is to design some form of wrench or locating system to verify that both bearing cups are properly aligned, as this is somewhat difficult to do with the current design and can take time to correct after installing the chain.

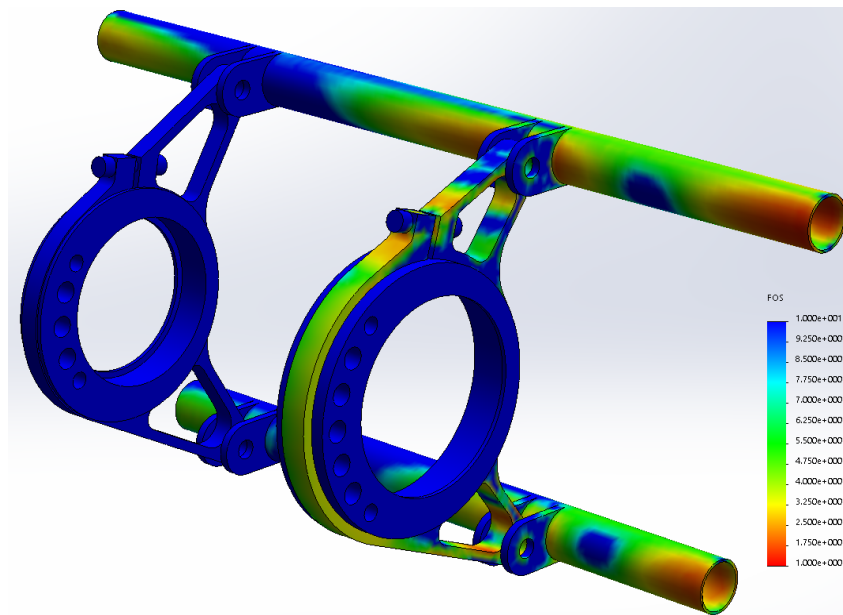


Figure 9. Factor of Safety Plot of Differential Mounts (fastener and differential substitutes hidden for clarity)



Figure 10. Completed Differential Mounts in Frame

Sprocket Carrier

Also shown in Figure 10 above is the Sprocket Carrier, the component which connects the sprocket to the splines on the Drexler differential. This component is highly important to the vehicle design for two main reasons: its purpose in transmitting power to the rear wheels, and the high stakes of its manufacturing. The meaning of the former is obvious, but the latter is due to its splined interface with the differential. When selling a differential and axles, Drexler includes an approximately 8-inch diameter by 2-inch thick cylindrical aluminum blank which has a splined hole matching the differential machined into its center. This blank is intended to be machined into an adapter for whatever final drive system the purchasing team intends to use to transmit power to the differential, since the exact dimensions of the splined interface are evidently considered proprietary and are not available to teams to manufacture their own differential adapters. Due to the several-month lead time involved with shipments of parts from Drexler, the team only had one try to machine this blank to the required dimensions.

To design the sprocket carrier, the dimensions of the sprocket were first determined to find the required bolt pattern dimensions, and to determine the ‘keep-out’ zone that would prevent the chain from interfering with the sprocket carrier. The 36 tooth sprocket chosen for the car uses the bolt pattern from a Yamaha YFZ450R, which was chosen arbitrarily since the team had a YFZ450R engine in a previous car, and no bolt pattern specifications could be determined prior to purchase. The bolt pattern was determined to be a 144.5 mm diameter circle with four equally spaced 10 mm bolts, and the keep-out diameter was set at roughly 3.25 inches based on the standard side plate width of 520 motorcycle chain.

The exact design of the sprocket carrier was mainly arbitrary, but an “I-Beam” profile was used for the arms to ideally minimize weight. The thickness of the adapter along the axis of the

splined bore was set to just over one inch, that being the distance between the shoulder of the splined area of the differential and a shallow notch in the splines used to hold a spiral retention ring. A spiral retention ring with an inner diameter of 2 inches was used in this notch to retain the sprocket adapter on the differential, since Drexler did not include any other way to retain the adapter in the design of the differential, and little side load was expected. The design also took into account the necessity of simple manufacturing processes to reduce the likelihood of failure, and ultimately required only one lathe operation and one mill operation to complete. Since the exact dimensions of the spline interface are not known, their location was simply modeled as a cylindrical hole with an outer diameter equal to the outer diameter of the splined interface, i.e. leaving the smallest amount of material in the sprocket adapter.

Once the design was completed, a FEA scenario was arranged to ensure its strength. The assembly created for this FEA included the sprocket carrier, a model of the sprocket, and four rough models of the shoulder bolts that would be used to join the two. To simplify the calculations and focus the stress on the sprocket carrier exclusively, the four bolts and sprocket were set to behave as rigid bodies in the assembly, with their geometry only used to place the loads appropriately. Figure 11 below shows a screenshot of the FEA results, including the locations of the applied forces and fixtures. Appendix D provides a more thorough description of the steps taken to arrange this FEA simulation.

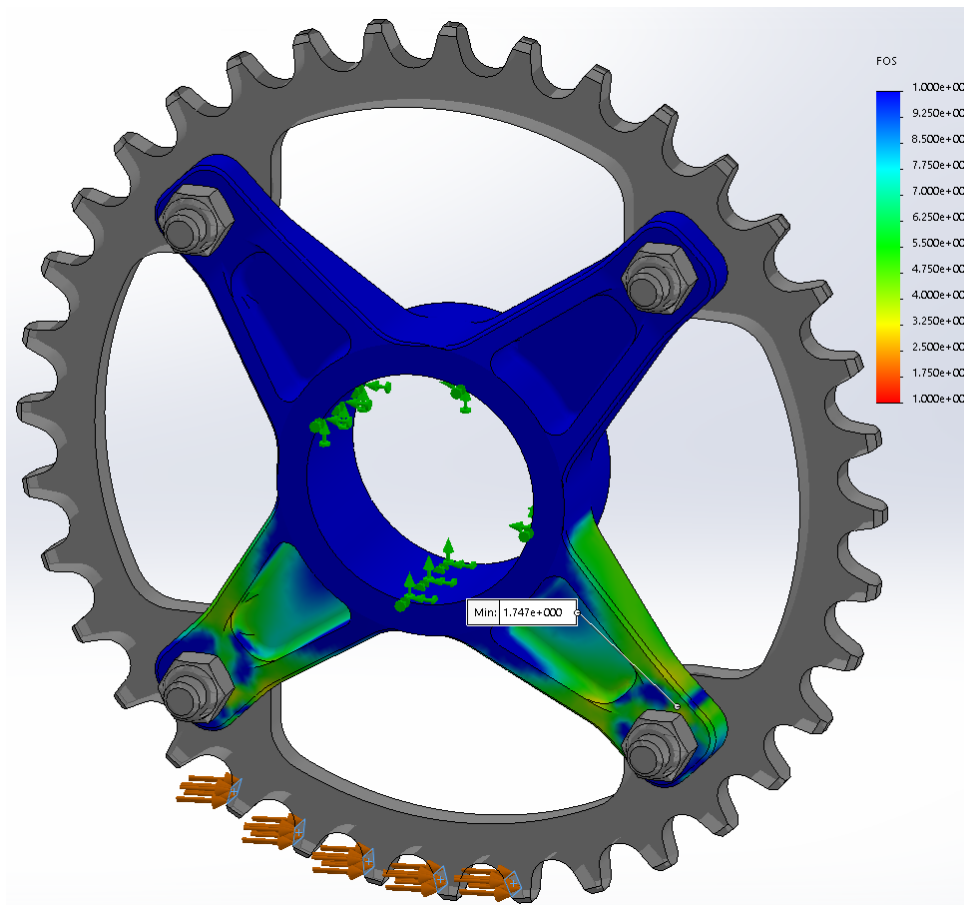


Figure 11. Sprocket Carrier FEA Configuration and Results

This cylindrical face was used as the fixture for the analysis. Two loads were applied to the assembly in alternating tests, one being a linear, nearly tangential force simulating the tensile force of the chain on the sprocket in the worst-case engine lockup scenario discussed earlier. The other was a torque applied to the faces of the sprocket with a total value of 4218 in-lb, a translation of the 1406 pound tension in the chain into a torque about the sprocket carrier when applied about the approximately 3.6-inch pitch radius of the 36 tooth sprocket. Of the two forces, the linear tension force produced a more conservative factor of safety estimate due to the distribution of the force primarily between only two of the four arms of the sprocket carrier. This factor of safety, as shown in Figure 11 above, is about 1.75, though this is likely an anomaly due to the way SolidWorks handles the bearing stress of bolts and pins, as the highest factor of safety observed elsewhere on the sprocket carrier was around 3. Regardless, these results confirmed that the sprocket adapter was sufficiently strong to withstand the worst-case scenario established for power transmission components of the drivetrain, and with a high enough factor of safety that it would be unlikely to be the weakest link in the system in the event of a failure.

Axles

Along with the Drexler differential came custom length axles, however because of the lead-time, all measurements were taken from a rough CAD model of the car near the beginning of the design process. As the model was updated, these measurements changed slightly. The end result was a smaller gap between the wheel bearings and the end of the axle cv joint than originally thought, because of this the original design for a connection between the cv end would not work. This piece would have been a simple design the bolted up to the cv joint and splined into the hub clamping on the bearing. The whole system would have comprised of three components, the cv joint end, the backer plate, and the hub. The solution for the space issue was to make the cv joint end and the backer plate one piece. This would eliminate the need for bolts and let us condense these components. This part was machined from 4340 chromoly steel. The design for the cv joint end was copied from the existing components and the spline was made to match the spine in the hub. Doing it this way tuned out to be lighter and far less complicated than the original design but was far more difficult to machine.

Engine Mounts

As mentioned in a previous section of this report, the frame and drivetrain were not designed in parallel, in an ideal world, the frame would have been designed with integral engine mounts, but since the frame began its design cycle with a separate team of students, one year before the drivetrain and the rest of the car, this was not possible.

Despite the rear section of the frame remaining the same as the 2015-2016 vehicle, the slight differences between the YFZ450R of the previous year and the current WR450F, along with the allocation of a brand new differential and axles, warranted the design of a new set of engine mounts. When designing the mounts a few things must be taken into consideration, the engine needs to be as low in the frame as possible, without leaving the envelope of the primary structure. As the engine is one of the single heaviest components, the lower it can be mounted, the lower the vehicle's center

of gravity is, which will only aid performance. The mounts must also place the engine far enough towards the rear of the vehicle to allow for clearance between the J-pipe and the firewall, but not too far rearwards, as the differential, differential mounts, chain, chain tensioner, chain guard and shifting components all must be packaged in the frame, behind the engine.

In previous years, time has been devoted to trying to procure 3D models of the engines for mounting and packaging purposes. Last years MQP team made an attempt to get a model of the WR450F from Yamaha but was not able to succeed. Instead wasting more time on a venture that was not guaranteed to be successful, mount locations were initially measured manually, using a tape measure and threaded rod, while the engine was mounted on a stand. These measurements were used to triangulate the mounting points relative to one another

Calipers were used to measure mount hole diameters and widths, it was assumed that all mounting points were horizontally symmetrical. A tape measure was also used to approximate the location of the sprocket centerline with respect to the rear engine mounts, this will be important for finding the chain line to the differential and for creation of SolidWorks model, to be used for mount design, that will incorporate all of the measurements taken by hand.

With all of the measurements taken, some rough front engine mounts were drawn up and laser cut using spare 1/8" balsa wood that was hanging around the shop. The shape of the mount was solely based on looking at the engine and did not fit very well, however, using threaded rod extending out from the mounting points on the engine, the placement of the connections points on the mounts were verified. This allowed for the creation of a simplistic 3D model that had all the critical mounting dimensions of the engine, shown in Figure 12.

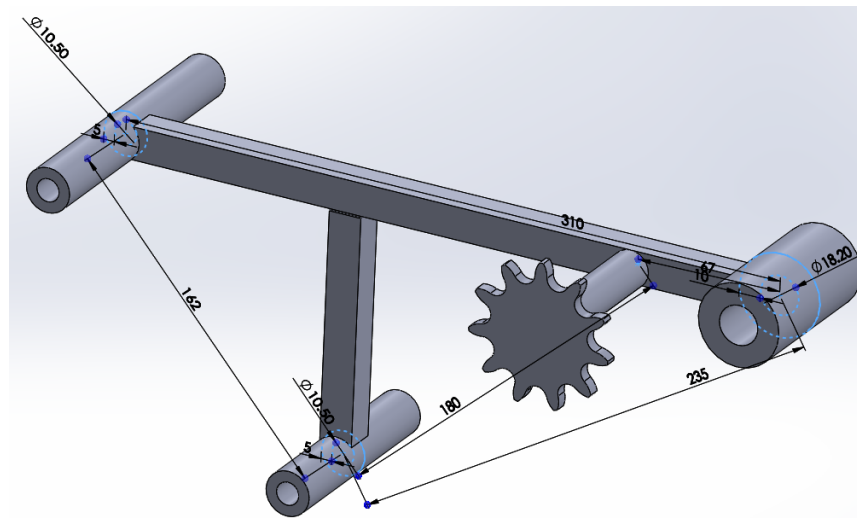


Figure 12. Engine Mount Relative Locations

As evidenced by the prototyped front engine mounts, interference with the engine would be an issue when designing the final shape of the mounts, so in order to design the mounts properly it is necessary to model the overall space that the engine will take up. In the past, MQP teams have used the Autodesk's "123d Catch" app to scan the engine and import the 3D surface into SolidWorks to use for packaging, this app was discontinued in January 2017, but got the team

thinking about options for 3D scanning. Through advisor Professor David Planchard, the team learned that WPI's Dr. Erica Stults had access to a mobile 3D scanner that should have been able to produce a scan that would be good enough for the purpose at hand. The scanner itself was mounted to an Ipad, and produced a very low quality scan, shown in Figure 13, but it did a fine job defining the space that the engine occupies. Using datum planes and axes, the engine scan was mounted onto model of hand measured mounts from before, this created a full engine model of the correct size and with workable mounting geometry.

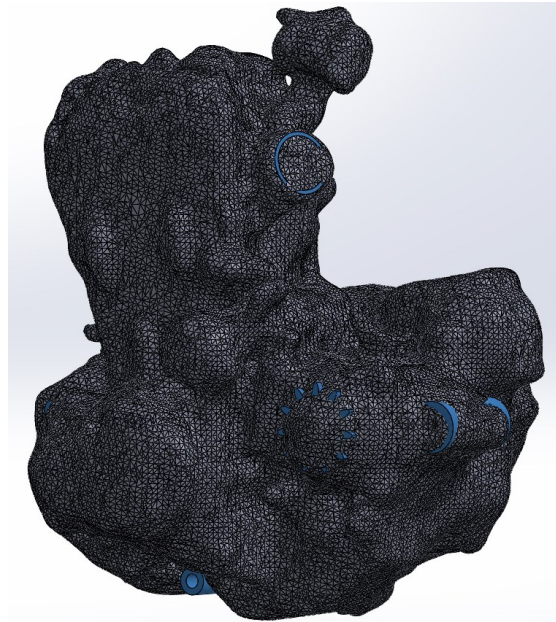


Figure 13. 3D Engine Scan

This assembly was placed in a SolidWorks model of the frame, to align the engine model laterally in the frame, the driver side face of the engine sprocket was mated coincident to the driver side face off the differential sprocket, as the differential assembly was already in the top level assembly of the entire vehicle. A datum plane was created in the engine model and was matted to the top plane of the frame to control engine height and pitch, the engine was constrained such that its lowest point was coincident with the plane created by the bottom surface of the lowest frame members. A model J-pipe was created and mated to the engine model, this was used to verify that there was space between the firewall and the exhaust to allow for heat dispersion. All other degrees of freedom were eliminated using distance mates between the engine mount centerlines and frame tube centerlines. With the engine fully constrained, engine mounts were sketched originating at the mounting points on the engine and terminating at the nearest frame rail(s). The shape was fine-tuned to fit around the shape of the engine with rather large tolerance, in an effort to avoid unforeseen interferences come final assembly. Once the final shape was determined, holes were made to reduce the overall weight of the mounts. If issues arose during simulation, these holes and the material thickness would be the first things to be modified.

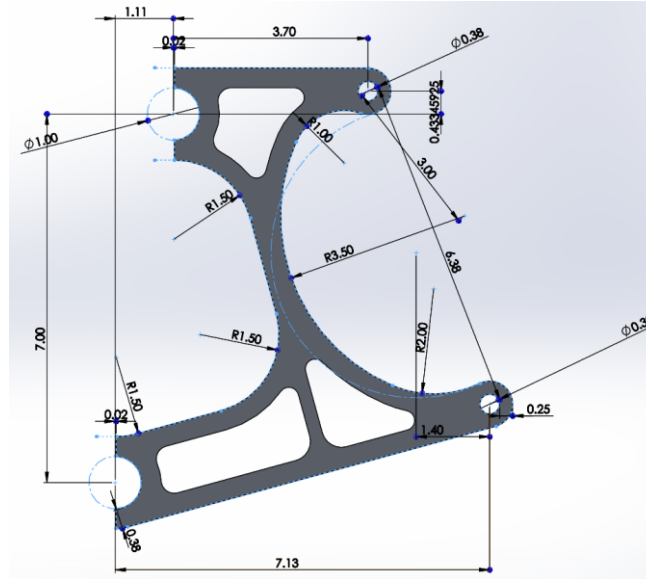


Figure 14. Engine Mount 2D Profile

In order to simplify manufacturing, the engine mounts are limited to a 2D profile with a .375” thickness, as this facilitates laser cutting or water jetting, which can be done by one of the team sponsors, Howe and Howe Technologies. Figure 14 shows this 2D profile for the forward mounts. The Mounts were also designed to mount to the frame with off-the-shelf 1/2” shaft collars in an effort to reduce manufacturing time. The selected hardware would be 1/4-20 bolts, standard for the selected shaft collars. Due to the design, the hardware must be threaded into the edge of the .375” aluminum plate, as there is a very minor concern that thread tear out will be a failure point for the mounts, the team looked into having a spare mount pull-tested on an Instron Machine in order to determine the failure load and lay rest to any concern, but this was never done.

Finite Element Analysis

To validate the design of the engine mounts, a static simulation was conducted in SolidWorks in order to obtain a factor of safety for all four mounts. Before the simulation could be set up, the applied loads needed to be determined. At this stage of the design process, the engine had not been tested, thus the torque output was unknown. Similar to load determination used for the differential mounts, engine lockup was assumed, which results in a 1400 in-lbf torque at the engine sprocket. The engine weight was also unknown, as the scale the team has easy access to tops out at 30kg (~66lbs), a conservative value of 90 lbs was assumed. Based on the target deceleration, a 1.5G engine forward force was assumed and a 1400 lbf chain tension force was used, as with the differential mounts. To contain the engine model, three tubes mimicking the tubes used for the frame construction were put into an assembly that preserved the orientation of the frame members that the engine mounts bolt to. The ends of these tubes were assigned fixed geometry.

Six models of the a 1/2” shaft collar were inserted into the assembly and mated to the frame tubes using a fixed-hinge boundary condition to permit rotation around the tube, but not translation. The motor mounts are attached to the shaft collars using a simulated 1/4” bolted connector torqued

to 100 lbf-in. The final component in the simulation is the engine model, without the engine scan, which is mated to the engine mounts, the front mounts and the engine model fully define the position of the rear mounts and shaft collars. Figure 15 shows the FEA assembly, with constraints and loads highlighted.

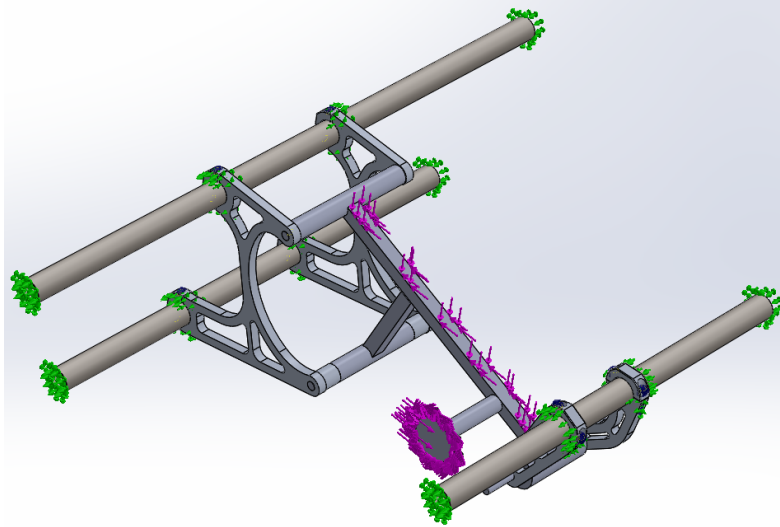


Figure 15. Engine Mount FEA Assembly

In addition to the constraints mentioned above, no penetration contact sets were used at surface contact locations, and all components except the engine mounts themselves were made rigid, serving as a path for load to travel to the mounts. The selected material was 6061-T6 aluminum due to its relatively low cost, low weight, and availability. As mentioned above, the thickness of the mounts was $\frac{3}{8}$ " and with the above loading, the mounts passed the simulation with factor of safety around 1.5, shown in Figure 16, so no further modifications were made.

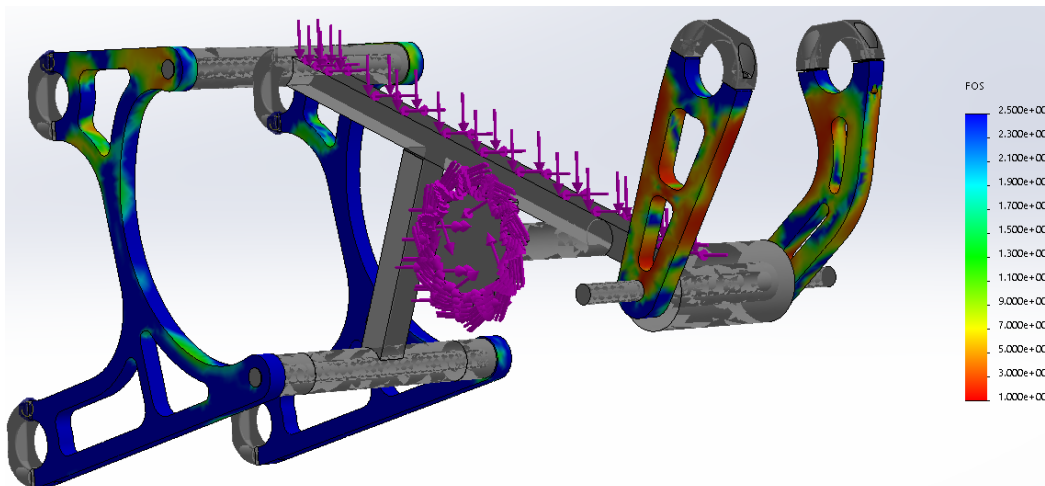


Figure 16. FOS Fringe Plot

Another simulation was done with assuming 1G side load due to cornering, and the mounts passed with a factor of safety of 3.

Shifting

In previous years, the WPI Formula SAE vehicle has utilized a variety of engine/transmission combinations for competition. In 2015, an odd fire two-cylinder engine from a Yamaha snowmobile was mated to a continuously variable transmission, which required no outside input from the driver to work. In 2016, a 450cc single cylinder engine sourced from a Yamaha YFZ450R ATV was used, which had a sequential 1-down-4-up 5 speed manual transmission with a wet clutch integrated into the engine casing. The manual transmission required input from the driver, so a driver controlled pneumatic shifting system was designed to actuate the shifting. It used three pneumatic actuators, one for upshifts, one for downshifts, and one for clutch disengagement when shifting between gears. The pneumatic cylinders were all fed from a single supply tank kept pressurized by a small onboard compressor. The whole system was controlled separate from the engine control unit, using a custom-built PCB and a series of microcontrollers. The shifts were initiated by the driver using two momentary buttons mounted on the steering wheel. This system was heavy and took up a lot of space behind the firewall and in the engine bay. The goal for this year's vehicle is to drastically reduce the weight of the whole system, as well as the amount of space the subsystem occupies. As stated previously, the competition engine will be a four stroke, 449cc single cylinder sourced from a 2015 Yamaha WR450F dirt bike. Like the YFZ450R of the previous years, this engine has an integral 5 speed sequential gearbox that also utilizes a wet clutch.

A significant portion of new teams, or teams with short build cycles often settle for fully mechanical shift actuation, as it puts all the control in the hands of the driver, and although significantly slower than a pneumatic or electro-mechanical system, has very few failure points. Although there was one advocate for this option, the team opted for the design of a new electro-mechanical system, knowing that the pneumatic system could be retrofit from the 2016 vehicle in the event of a complete design failure. Shifting will still be initiated by the driver via paddles on a steering wheel, however, instead of controlling a pneumatic system, the paddles will activate an electric motor that will initiate upshifts and downshifts. The most critical component of this system is the electric motor, as it must produce enough torque to initiate a shift, and it ideally should have controllable position due to the way the gearbox is shifted.

A 1-down-4-up transmission in a dirt bike application is shifted via the riders left foot, using a lever attached to a splined input shaft on the transmission, circled below in Figure 17.

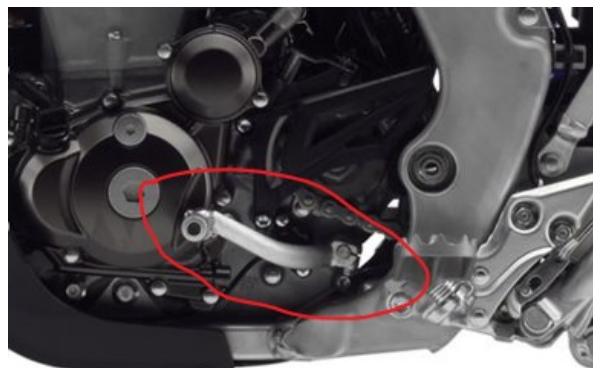


Figure 17. Transmission Lever

The lever position does not correspond to the gear that the transmission is in, instead the shifter has a “home” location that it returns to every time a gear is selected. When the transmission starts in neutral, the lever is depressed downward to engage first gear, when the force no longer being applied to the lever, it springs back up into its “home” position. To engage second gear, the lever is pulled upward, and when the force is removed, it springs back down to the same home position. All subsequent upshifts work the same as the 1-2 shift, with neutral being a half shift between 1 and 2. The angular displacement of the splined input on the transmission is a finite value between each full gear shift, hence the importance of positional control of the electric motor. From experimentation with the engine on the engine stand, it was determined that the required angular displacement of the splined input for either an upshift or downshift was ~ 17 degrees and the torque required to initiate a shift without the engine running was ~ 8 lb-ft.

The desire for positional control led to the search for a servo motor, as their angular position can be controlled rather precisely, and a large angular displacement is not required for this application. The search for the motor was headed by a member of the ECE side of the MQP, as they had considerably more experience working with electric motors. Ultimately, a servo could not be found at a reasonable price with the required torque output, however, he was able to source a regular 12VDC motor and gearbox combination that produces double the required torque (16.6 lb-ft) at a free speed of 75 rpm, weighed only 2 lbs, and came with a hall effect encoder for position control. The motor was sourced from AndyMark.com, a popular supplier for FRC and FTC teams, and is sold as the PG71 Gearmotor, 10mm round output with a 775 Motor (part number: am-2971). The hall effect encoder outputs seven pulses for every revolution of the motor shaft (497 pulses per revolution of the output shaft). This pulse resolution seemed suitable for positional control of the shifting mechanism, but it was decided that as a failsafe, a mechanical stop would be implemented to prevent the motor from holding a torque on the splined input, which if done continually, will damage the shift forks in the transmission. Because the design timeline was rather compressed, and the team wanted to test the system by the end of C-term, this motor was purchased in addition to a 10mm key hub (am-095a) and machine key (am-1249) for attaching components to the motor. The CAD files and technical drawings for all three components were available for download directly from the website, which expedited the next step of the process.

The question then became, mount the motor first and design a shifting mechanism around the placement of the motor, or design a mechanism and hope that the motor could be mounted in such a way to maintain the functionality of the mechanism? The first option seemed like the wisest given the timeframe. Although the rear engine mounts had already been designed, they had not yet been manufactured, so instead of making a separate mount for the electric motor, both mounts were incorporated in a single two-dimensional piece. It would have been possible to tuck the electric motor up under the engine, but this would drastically limit the space to package a shifting mechanism, as well as there was a concern that the electric motor would become heat-soaked, affecting its operability. The radius between the centerline of the motor output and the centerline of the splined input on the transmission was chosen to be 4.5”, as this placed the motor away from engine, with enough space to design either a linkage or an interlocking fork for torque transfer.



Figure 18. Key Hub (bottom center of image)

Figure 18 above shows the electric motor and key hub mounted in their final positions, the mounts were simply sketched on the previously design engine mounts, extruded, and the two bodies merged. The driver side mount contains a 4-bolt pattern to fasten the motor with M3 screws, the passenger side mount incorporates a cradle to minimize vibration of the motor when the engine is running.

Initial Mechanism Designs

The first mechanism that was designed to transfer motion from the electric motor to the transmission input was a pair of interlocking forks, the basic concept is shown below in Figure 19, with the left fork attached to the transmission input and the right fork attached to the electric motor.

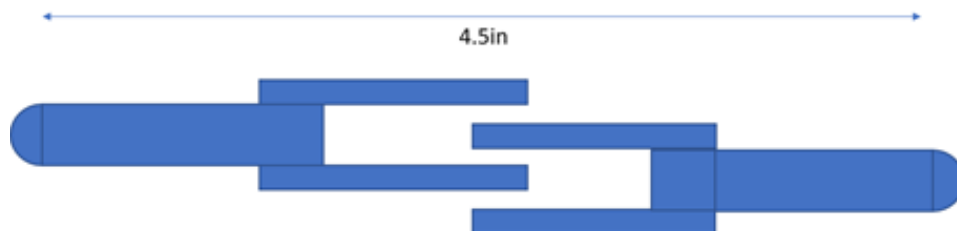


Figure 19. Interlocking Forks

Essentially, as the electric motor rotates, either clockwise or counterclockwise, the right fork will contact the left fork, causing it to rotate in the opposite direction, initiating a shift. This

mechanism is very rudimentary, imprecise and would cause a momentary delay before a shift, as the forks are not always in contact. This idea was quickly scrapped in favor of something more refined.



Figure 20. Key Hub Concept 2

Figure 20 above shows the next iteration of the design, the concept is the same as the interlocking forks, however, the fork on the electric motor side is replaced with an actuating arm that would be bolted to the key hub and the fork in the transmission side is designed so the actuating arm is always in contact with the internal profile of the fork, like a cam and follower, which would eliminate any delay between electric motor movement and shift initiation. As stated above, the motor selected was a regular 12VDC unit, so some kind of mechanical stop was required. This is accomplished in this design concept by the contact between a flat face in the internal profile of the fork and a flat face on the actuating arm, the stopped position is shown above.

This design was also scrapped relatively quickly, before any analysis was done, due to the lack of adjustability. As the mechanism is pictured above, it is designed for 17 degrees of angular displacement, clockwise or counterclockwise, at the transmission input. If for some reason this parameter needed to change, all new parts would have to be designed, manufactured and installed, putting a stop to all dynamic testing of the vehicle and rendering it undriveable.

6 Bar Linkage

At the start of the design phase for the shifting subsystem, the plan was to use a 4-bar linkage in conjunction with a servo motor, after deciding on the use of a regular 12VDC motor and exploring other methods of motion transfer, the final design ends up being a 6 bar linkage, shown below in Figure 21.

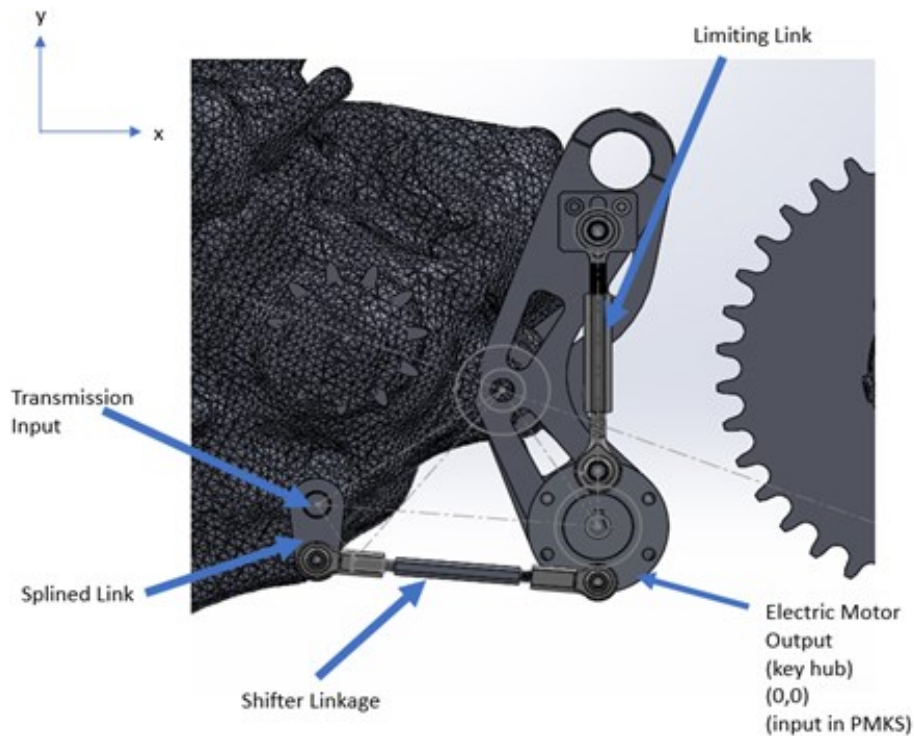


Figure 21. Key Hub 6 Bar

A simple 4-bar linkage consists of an input link, a coupler, a follower, and the ground link. Depending on the task at hand, either the coupler or the follower can be the output link. In the mechanism depicted above, the key hub, driven by the electric motor is the input, the shifting link is the coupler and the splined link on the transmission input shaft is the follower as well as the output link. As there is no control over the exact position of the motor, another link, the limiting link needed to be added to the mechanism, this link rides in a slotted boss attached to the motor mount and is mounted opposite the shifter linkage on the key hub. When the shifter is in its “home” position as described in the previous section, this limiting link is vertical. As the key hub rotates, either clockwise or counterclockwise, the link travels downward in the slot, and once it bottoms out, planar motion stops and a shift is completed. Ideally, as soon as the limiting link bottoms out, power to the motor is cut and the splined input shaft on the transmission will back-drive the linkage to its home position in time for the next shift.

Both the shifter link and the limiting link are constructed from rod ends and turnbuckle style connects sourced from McMaster-Carr, the parts are listed below in Table 2, and pictured in Figure 22. The shifter link and the limiting link use $\frac{1}{4}$ -28 hardware, as this was the only size available for the required turnbuckle length

Table 2. McMaster Hardware

Item	Part number (Mcmaster-Carr)
(4) Lightweight Corrosion-Resistant Ball Joint Rod End (LH) (1/4-28)	60685k722
(4) Lightweight Corrosion-Resistant Ball Joint Rod End (RH) (1/4-28)	60685k721
(2) Turnbuckle Style Connecting Rod (1/4-28)	8419k11



Figure 22. Ball Joint Rod Ends and Turnbuckle

The turnbuckle connecting rods will allow the length of each link to be adjusted, which is especially important for the limiting link, as adjusting the length of this link will set the mechanical stopping point of the mechanism.

Kinematic Analysis

As the electric motor chosen produces double the required torque to initiate a shift, no mechanical advantage is required of the linkage; because no mechanical advantage is required, the input link and follower link are designed to have the same length between their joints, which is the radius of the bolt circle on the key hub, .9375". In theory, because these two links have the same length, that angular displacement of the input should correspond directly to the angular displacement of the follower, to verify this, a kinematic analysis was done using PMKS (planar kinematic mechanism simulator).

PMKS: Planar Mechanism Kinematic Simulator introduction + instructions									
Open File		Save Configuration		Export Kinematic Data		Get as URL		Edit Commands ^	
Target Shape = Enter Target Shape Stream Here.									
Input	Links	Type of Joint	X Pos.	Y Pos.	Angle	P	V	A	
<input checked="" type="radio"/>	ground,input	R	0.000	0.000	0.000				
<input type="radio"/>	input,coupler	R	0.000	-0.938	0.000	<input checked="" type="checkbox"/>	<input type="checkbox"/>	<input type="checkbox"/>	
<input type="radio"/>	coupler,follower	R	-4.480	-0.568	0.000	<input checked="" type="checkbox"/>	<input type="checkbox"/>	<input type="checkbox"/>	
<input type="radio"/>	follower,ground	R	-4.480	0.370	0.000				
<input type="radio"/>	input,slider	R	0.000	0.938	0.000	<input checked="" type="checkbox"/>	<input type="checkbox"/>	<input type="checkbox"/>	
<input type="radio"/>	slider,stop	R	0.000	4.000	0.000	<input checked="" type="checkbox"/>	<input type="checkbox"/>	<input type="checkbox"/>	
<input type="radio"/>	stop,ground	P	1.000	4.000	90.000				
Remove Row		Clear All Rows		DOF = 1					

Figure 23. Planar Mechanism Positions

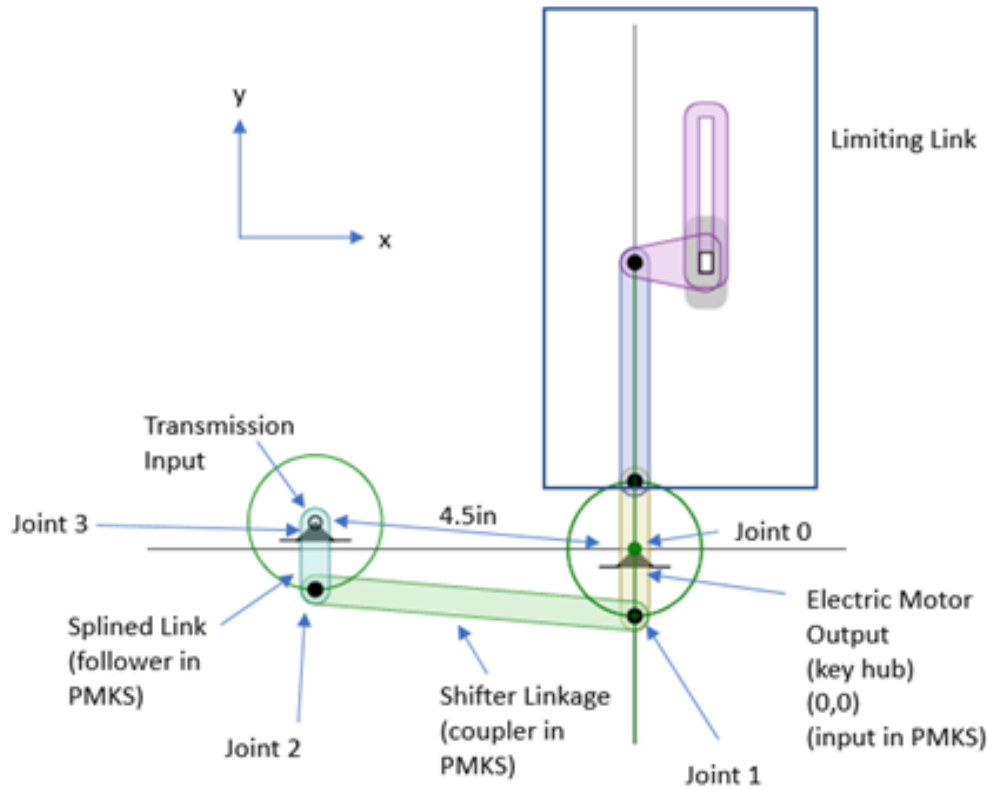


Figure 24. Planar Mechanism

Shown above in Figure 24 and Figure 23 are the planar mechanism model and starting coordinates respectively, which were taken directly from measurements in the SolidWorks model. When using this simulator, the following assumptions are made; all revolute and prismatic joints are frictionless and the links are weightless, thus gravity has no effect on the linkage.

For the simulation, the input rpm was set to 75, which is the unloaded speed of the chosen motor. Ideally, the slider length would have been limited to represent the motion the actual linkage will be restricted to, however this is not available in PMKS, thus the whole system can rotate 360 degrees. However, since the linkage in the vehicle will be limited to a 34-degree total swing, only data from time steps $-.0444s$ to $.0444s$ were analyzed, as these time steps correspond to a 20-degree swing in either direction from the initial position. A sample of the data collected for joints 0 and 1 is shown below in Table 3.

Table 3. Data for Joints 1 and 2

TimeSteps	x_0	y_0	Vx_0	Vy_0	Ax_0	Ay_0	x_1	y_1	Vx_1	Vy_1	Ax_1	Ay_1
-0.044444444	0	0	0	0	0	0	-0.32081	-0.88143	6.922748	-2.51967	19.78948	54.37114
-0.033333333	0	0	0	0	0	0	-0.24277	-0.90604	7.116009	-1.90673	14.97541	55.88901
-0.022222222	0	0	0	0	0	0	-0.16288	-0.92375	7.255113	-1.27927	10.04738	56.98152
-0.011111111	0	0	0	0	0	0	-0.08175	-0.93443	7.339001	-0.64208	5.04288	57.64038
0	0	0	0	0	0	0	0	-0.938	7.367035	0	1.03E-07	57.86056
0.011111111	0	0	0	0	0	0	0.081752	-0.93443	7.339001	0.642079	-5.04288	57.64038
0.022222222	0	0	0	0	0	0	0.162882	-0.92375	7.255113	1.279272	-10.0474	56.98152
0.033333333	0	0	0	0	0	0	0.242772	-0.90604	7.116009	1.906729	-14.9754	55.88901
0.044444444	0	0	0	0	0	0	0.320815	-0.88143	6.922748	2.519674	-19.7895	54.37114

The position data for joints one and two were graphed on a single scatter plot and are shown below in Figure 25. This plot shows the path that both joints travel during -.0444s to .0444s and is a visual verification that the linkage is functioning as expected.

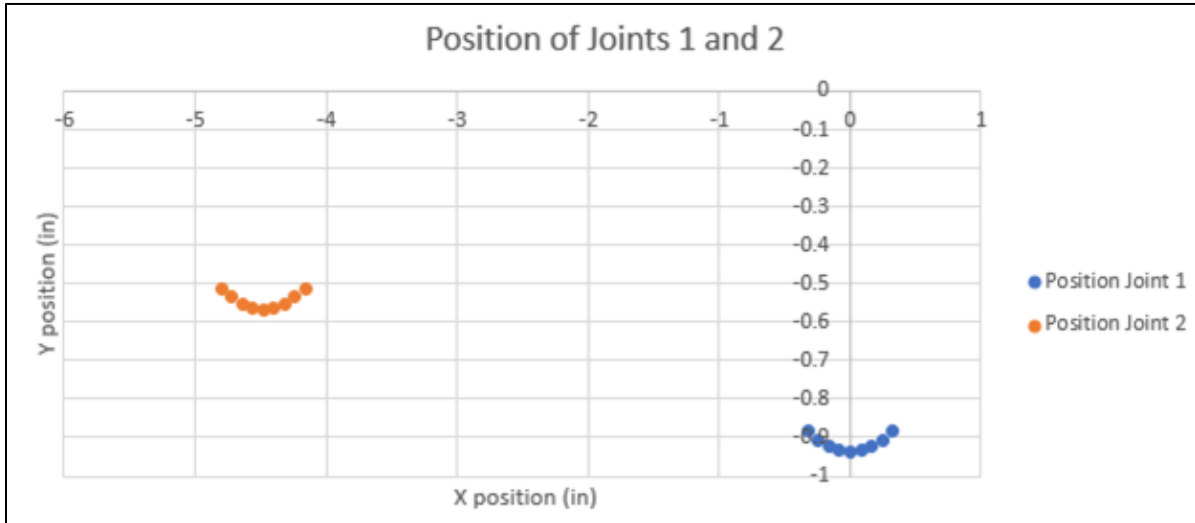


Figure 25. Graph of Position of Joints 1 and 2

Figure 26 below shows the plot of angular displacement vs. time steps for both the input link and the follower link with respect to the origin of the mechanism. The trend lines for each data set show that the rate of change of angular displacement for both the input and follower is the same, meaning that a 17 degree angular displacement at the motor should correspond to a 17 degree angular displacement at the transmission input.

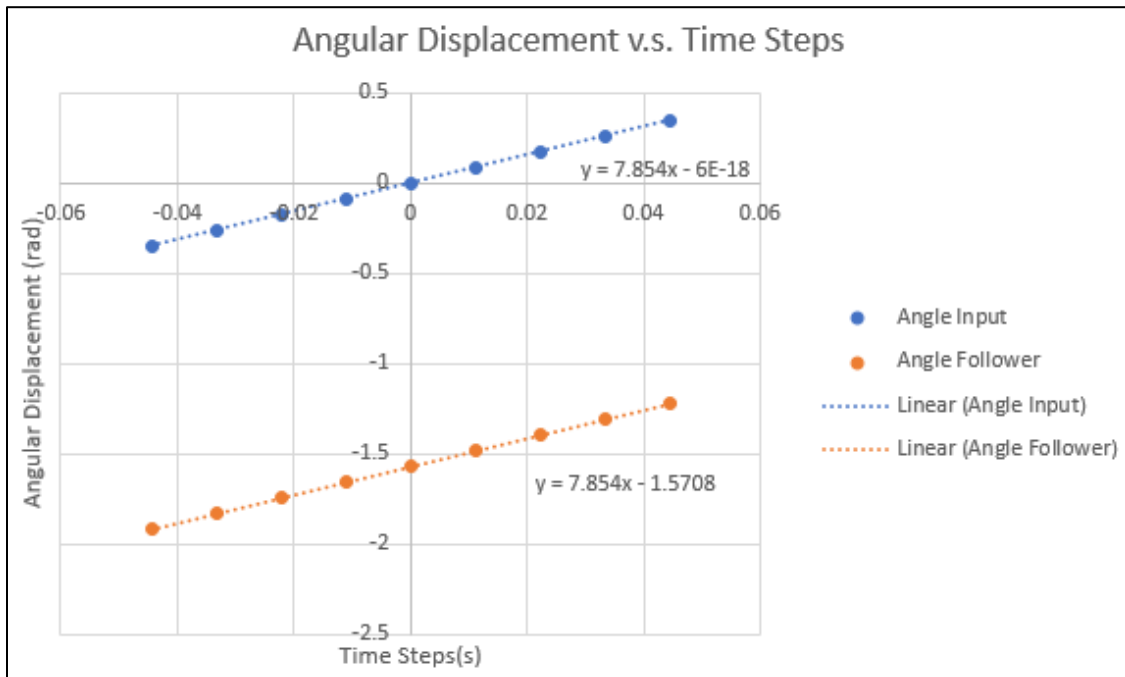


Figure 26. Graph of Angular Displacement

Static and Stress Analysis

Although 16.6 lb-ft does not seem like a considerable amount of torque, the tangential force at the bolt circle of the key hub is about 212.5 lbs, as shown below.

$$F = \frac{16.6 \text{ lb} \cdot \text{ft}}{\left(\frac{.9375 \text{ in}}{12}\right)} = 212.48 \text{ lbs}$$

According to product specifications available on McMaster-Carr's website, the selected rod ends have a maximum radial load of no less than 1,350 lbs, while these components are nowhere near their failure load, there is not strength data available regarding the turnbuckle style connecting rods, which are manufactured from 6061 aluminum. To verify that they would not be a cause of mechanism failure, the axial stress in each turnbuckle needed to be determined and compared to the yield strength to determine a safety factor.

Load Determination and Stress Calculations: Shifter Link

The axial load in each link will be determined at the point where the key hub is at full lock in the counterclockwise direction, as this puts each link in tension. The load in each link will be determined independently, assuming that each link will solely counteract the torque produced by the electric motor. Although this will not actually be the case as both links will share the load, this represents a worst-case scenario should one link fail.

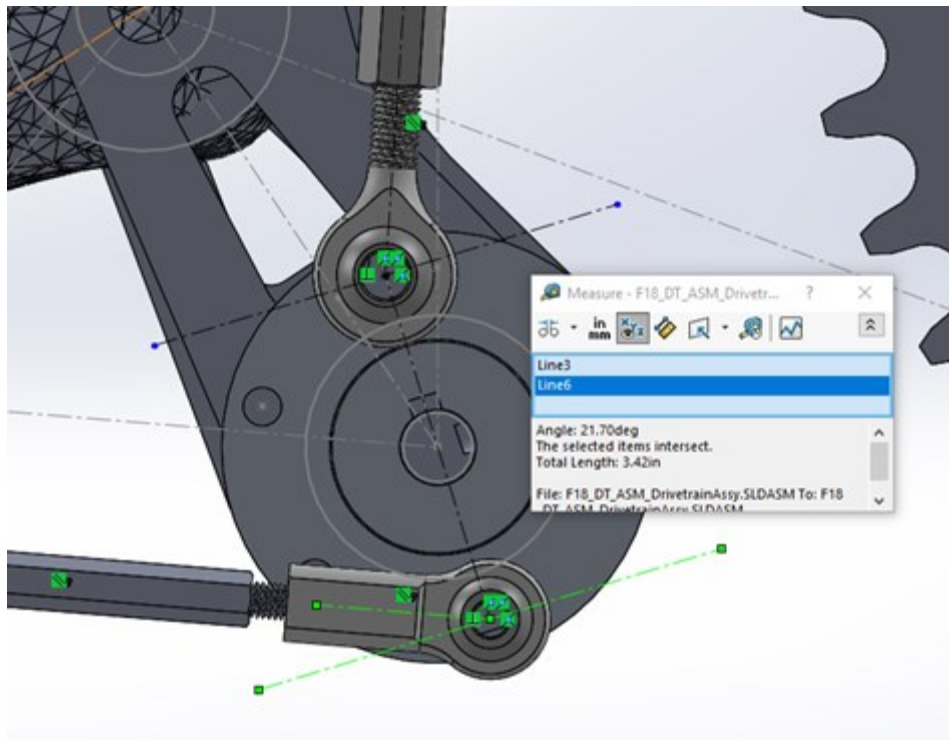


Figure 27. Angle of Shift Linkage

Figure 27 above shows the measured angle between the shift linkage and the tangent line on the bolt circle to be 21.7 degrees. This angle was used in the free body diagram shown below in Figure 28 to determine the axial force in the link. As the link is a two-force member, there is only an axial load, no bending load.

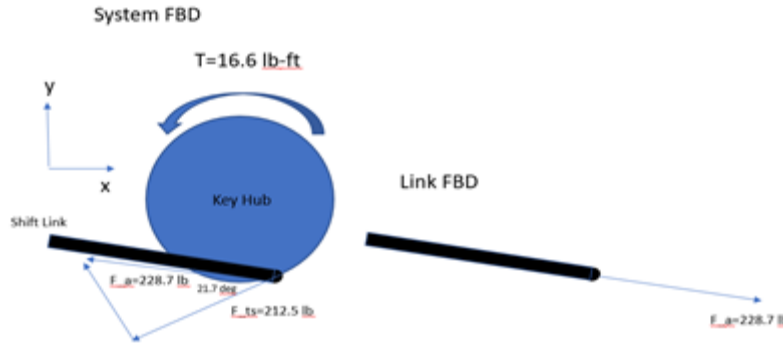


Figure 28. Key Hub Free Body Diagram 1

The axial force in the link, F_a is dependent on the tangential reaction force at the joint, which creates a reaction moment to counteract the torque produced by the motor.

$$F_a = \frac{212.48lb}{\cos(21.7)} = 228.7 lbs$$

This turnbuckle is internally threaded with 1/4-20 left hand and right hand threads and, assuming it will not fail due to thread pullout, it can also be modeled as a hollow rod, with an OD of .376 in and an ID of .25in.

$$\sigma_{nom} = \frac{228.7 lbs}{\pi * (.188in^2 - .125in^2)} = 3692 psi$$

As this turnbuckle is being modeled as a simple rod, there are no geometric features to create stress concentrations, thus sigma nominal is equal to the von Mises effective stress and the factor of safety can be determined using the ultimate yield strength of aluminum, which is typically around 39000 psi

$$N = \frac{39000 psi}{3692 psi} = 10.56$$

Load Determination and Stress Calculations: Limiting Link

A process like that shown above was also used to determine the axial load present in the limiting link. The angle between the link itself and the tangent line on the bolt circle was measured to be 69.17 degrees, using this value and the free body diagrams shown below in Figure 29, the tensile load in the link was found to be 597.6 lbs.

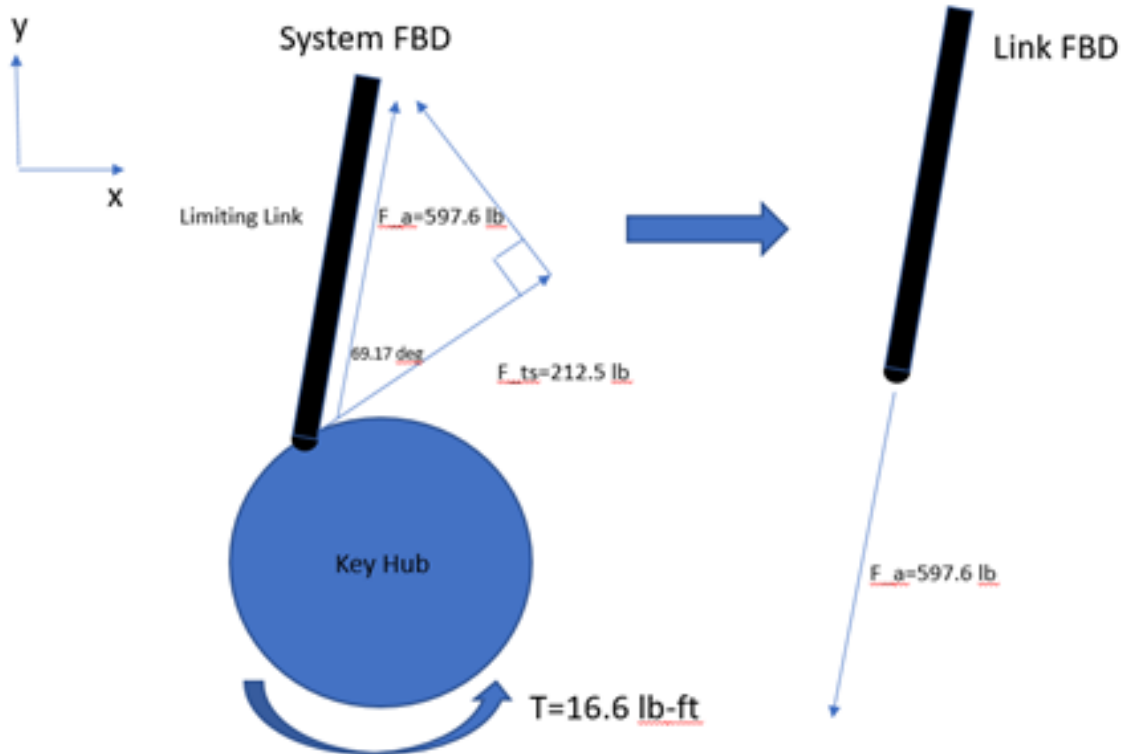


Figure 29. Key Hub Free Body Diagram 2

This turnbuckle is internally threaded and again, assuming it will not fail due to thread pullout, it can also be modeled as a hollow rod, with an OD of .376 in and an ID of .25in.

$$\sigma_{nom} = \frac{597.6 \text{ lbs}}{\pi * (.188in^2 - .125in^2)} = 9647psi$$

The factor of safety is then determined, once again, using the ultimate tensile strength of aluminum.

$$N = \frac{39000psi}{9647psi} = 4$$

Engine Mount Modification

The final step in validating this subsystem was to re-run the FEA previously done on the engine mounts to verify that the added loads on the rear mounts due to shifting will not cause failure of either mount. The loads from the shifting motor were not expected to have any effect on the factor of safety, however it was necessary to validate this assumption.

The entire simulation had already been set up, and is explained in a previous section of this report, the only modifications were; the replacement of the rear engine mounts with the newly designed ones that had the provisions for the shifting motor mount, the addition of a 16.6 lb-ft load on the driver side rear engine mount, and a vertical load of 2lbs, representing the weight of the electric motor, also applied to the driver side rear motor mount. To get the simulation to run properly, new contact sets needed to be built for the newly added rear engine mounts. The assembly with all applied loads, prior to simulation, is shown below in Figure 30.

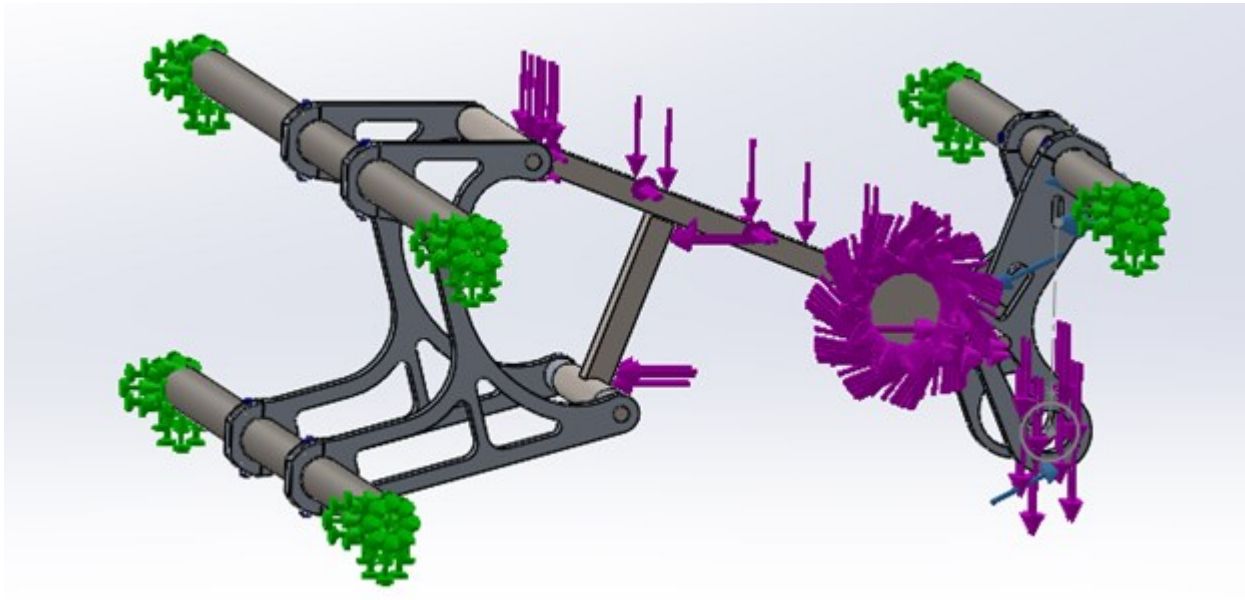


Figure 30. Motor Mounts FEA Setup

As expected, the loads due to the electric motor were so small in comparison to loads produced by the engine/drivetrain that they had little to no effect on the overall FOS for the system. This is proven in Figure 31 below, which shows the FOS fringe plot after the simulation was run. Up where the engine mounts meet the frame, the FOS is between 3 and 4, which was expected based on previous simulations, meanwhile, the factor of safety down by the shifting motor is at or above 200.

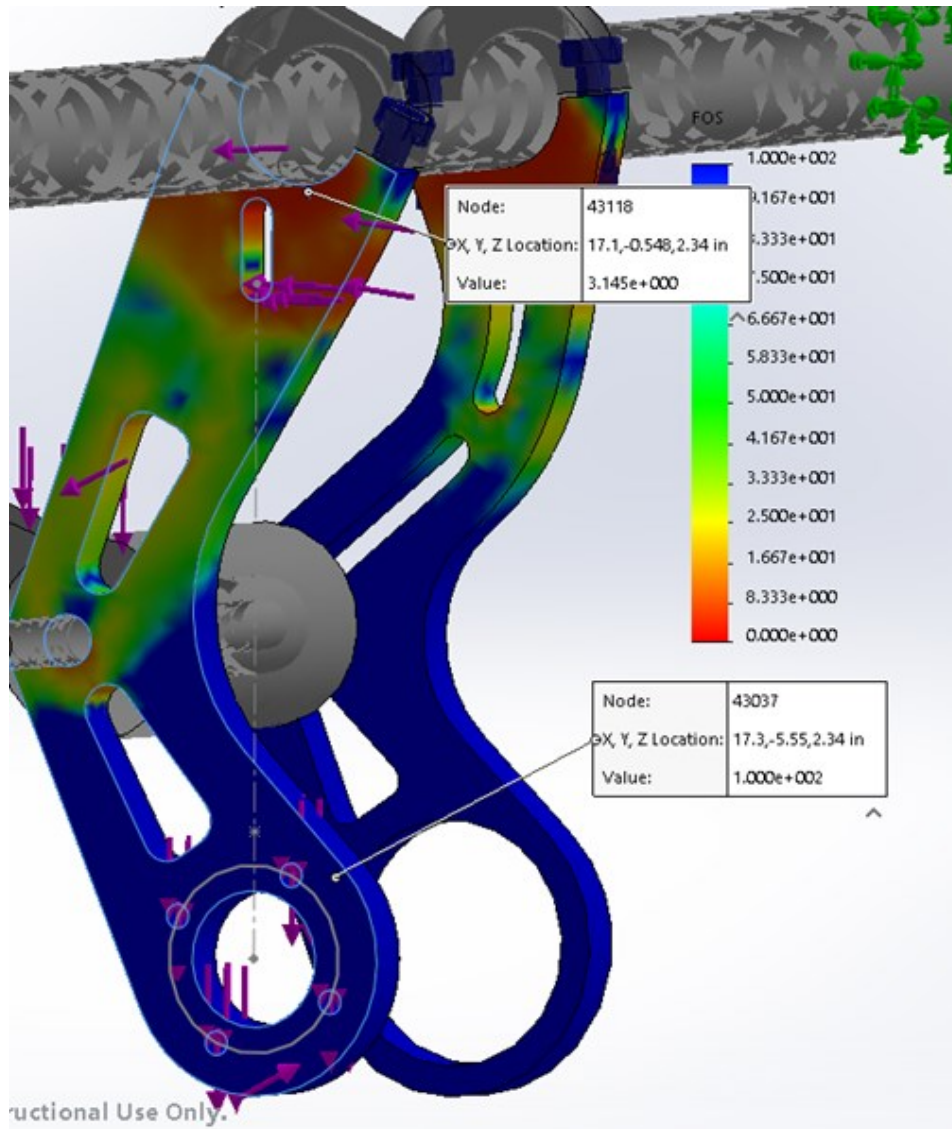


Figure 31. Motor Mounts FEA FOS

The simulation report available in Appendix G shows a minimum factor of safety of .75, near where the passenger side rear motor mount contacts the frame. Based on inspection of nearby areas, it is believed this is a singularity due to the stress concentration at the sharp corner there the radius for the frame tube is cut. Plot inspection and cross sectional views show that the factor of safety in close proximity is not less than 1.5. Throughout the rest of the assembly, the factor of safety ranges from 3 to 20+, the team is confident that the motor mounts will perform adequately in all driving situations.

Hand Clutch

In 2016, WPI's Formula SAE vehicle had a hand operated clutch, specifically for starting, stopping, and launching. The previous design was well liked and easy to use, so the team opted use a similar mechanism for clutch operation this year. Using the previous design as a starting point, the

mechanical advantage of the lever was calculated at 5.4:1, this ratio provided a firm feel to the lever, while still being easy to pull for all of the drivers. The grab location was located 6.75in from the lever pivot, and the clutch cable mounting point was located 1.25in from the pivot point. These dimensions resulted in the 5.4:1 mechanical advantage and a lever that was not obtrusive in the cockpit but was still large enough for the driver to quickly reach in a panicked stopping situation. For the new design, there were no compelling reasons to change these dimensions, but the overall layout of the mechanism was changed. The previous design had upwards of ten components (not including hardware) and three shaft collar attachment points to the frame. Sticking with the goal of reducing weight for this year's vehicle, the system was redesigned, shown below in Figure 32 using two attachment points and six total components.



Figure 32. Hand Clutch Assembly

The assembly mounts to the frame using two shaft collars. The forward shaft collar has a steel $\frac{1}{4}$ -20 stud for mounting the lever itself, which rides on and oil embedded journal bearing. The rear shaft collar has mounting provisions for the clutch cable and the adjustable stop that sets preload on the lever and prevents it from over rotating when released. The clutch cable used is the OEM Wr450f clutch cable, thus no modifications were needed to mate it to engine. On the hand clutch lever side, there is a hole and counterbore on the rear most shaft collar to capture the other end of

the clutch cable housing. The cable itself mount inside a small channel on the hand lever, via a slotted pin with cross drilled holes on either end for a cotter pin or safety wire. The threaded ends of the shaft collars are generic McMaster-Carr parts (pn# 6436K73). The other halves were machined with the .5 radius and mounting geometry for additional parts. Locknuts were used in all possible locations to reduce the possibility of anything vibrating loose during operation. Overall, when fully assembled, the mechanism works very well and packages nicely.

Testing Results and Modifications

Initial assembly went as planned, all parts fit exactly as expected and the entire system was relatively easy to assemble. Once the chain was installed however, it became apparent that there might be a clearance issue between the chain and the hardware for the ball joint rod ends. There was technically clearance when the chain was at rest, but during a hard braking or accelerating situation the chain deflects, possibly causing contact. To eliminate this problem, the solution was to move the rods ends to the other side of the hub on the motor, in the configuration shown below in Figure 33, which eliminated the need for a spacer between the top most rod end and the motor mount.

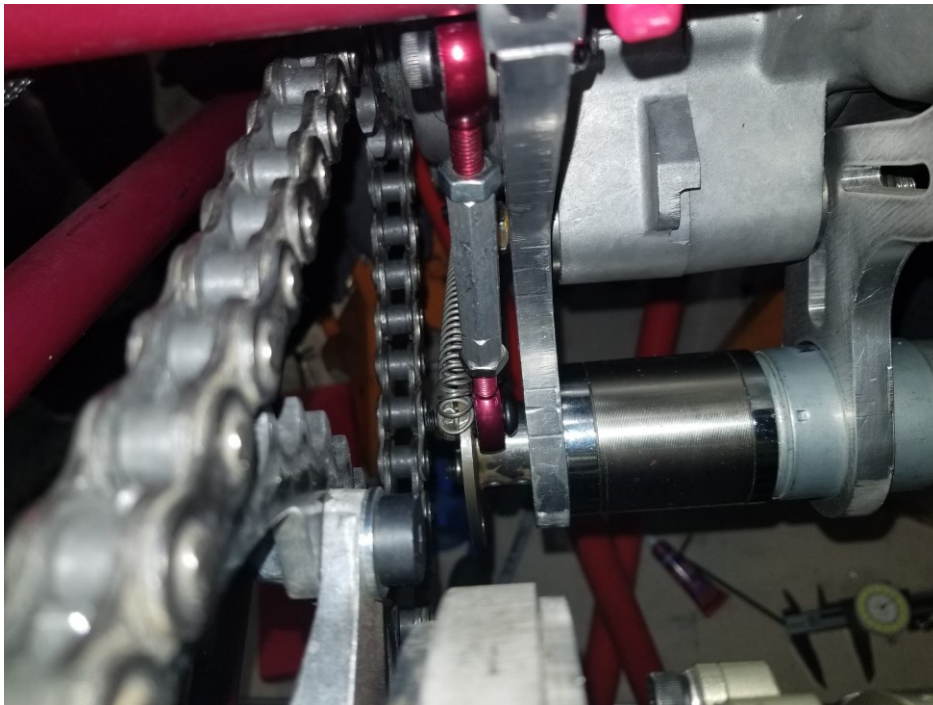


Figure 33. Updated Linkage Position

Minor modifications also needed to be made to the hub itself, the supplied key stock did form a tight fit between the motor shaft and the hub, so instead of a key, two set screw were tapped into the hub. The set screws register in the four millimeter keyway on the motor shaft, to prevent threads from galling the keyway, m6 set screws were used, with the ends turned down to 4mm, removing the threads. Based on the results of all the test driving done so far, it seems as through the two set screws are adequately transmitting torque and do not seem to be galling the keyway.

During the initial test of the shifting mechanism, with the engine not running, the electric motor seemed to produce enough torque to shift gears in all instances, however, an issue arose with the mechanism returning to center for the next shift. The motor was initially directly controlled by the paddle shifters via a dual relay circuit for switching directions. This setup was the simplest option and puts a lot of control in the hands of the driver, but offers no positional control of the motor and no powered return to center. In an effort to quicken the process of returning to center, two return springs were added between the motor hub and the engine case, in the configuration shown below in Figure 34.

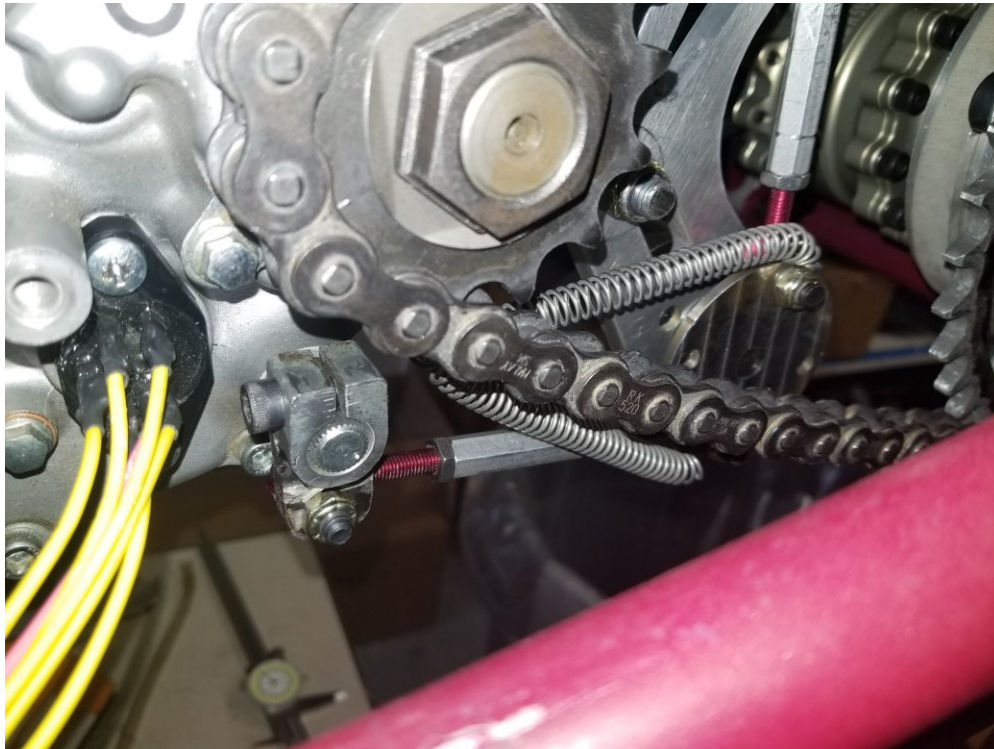


Figure 34. Shifting Mechanism return Springs

Due to space constraints, the spring with the highest spring rate that could be attained through McMaster-Carr was from a 302 stainless steel extension spring, at 4.85 lb/in (pn# 94135K18). Although the springs do help with the return to center, the process is still slower than ideal, at about one second. While this is fine for upshifts, as they are usually spaced apart, it is not ideal for downshifts, which are sometimes done consecutively before entering into a corner. It was at this point where the team decided to move forward and try to utilize the encoder on the back of the motor to implement a powered return to center for the linkage for shortened time between shifts. The brain of the system is a Raspberry Pi 3, which takes input from the paddle shifter and controls the motor through an H bridge circuit instead of the relay circuit. Simultaneously, the Raspberry Pi counts encoder ticks until the transmission has successfully made it into the next gear. The gear information is known via a custom gear indicator sensor, shown above in Figure 34. Six wires, one for each gear and neutral, pass through a delrin plug into the transmission case. On the other side of the plug is a steel drum with a protruding ball, when the ball is in contact with one of the wires,

which are all individually run back to the Raspberry Pi as inputs, continuity is formed and the computer knows what gear it is in. Based on a command, upshift or downshift, via the paddles, the computer knows which direction to turn the motor and to count encoder ticks until the next gear is reached, once the next gear is achieved, the motor reverse for the same amount of encoder ticks, centering for the next shift. More detail regarding the specific coding and wiring procedures can be found in [ECE MQP TITLE/REFERENCE INFO].

The most recent issues that came up was rear wheel lockup when shifting from 2nd gear to 1st gear before entering a corner in an autocross situation. Rear wheel lockup is caused by a difference between engine speed and wheel speed once first gear is engaged. If the wheels are spinning much faster than the engine, then either wheels must decelerate quickly or engine accelerate quickly. Given that the throttle blade is closed and the engine is pulling full vacuum, the wheels tend to decelerate before engine speed increase, resulting in the wheel briefly locking before equilibrium between engine speed and wheel speed is reached. Under normal conditions, this is usually mitigated by slowly letting out the clutch after a shift into lower gear, to slowly equalize engine speed and wheel speed, but because the team opted to do clutchless shifts, this was not an option. As there was still a hand clutch for launching, it would be possible to use that when downshifting, however, it requires the driver to remove their right hand from the wheel during driving, which would not be ideal. The team did not believe there was time to design an automatic clutching mechanism for downshifts, however, an SAE club member recommended the use of a “slipper clutch”, popular in super moto and street bikes, this type of clutch allows for some slip when the wheel(s) are driving the engine (under engine braking). This slip helps reduce the possibility of rear wheel lock up by allowing engine speed and wheel speed to equalize over a longer period of time. As a result of the slip, engine braking is, in some cases, drastically reduced, which is another added benefit, putting more braking control in the hands (feet) of the driver. Figure 35 below shows a schematic of the mechanism for a slipper clutch.

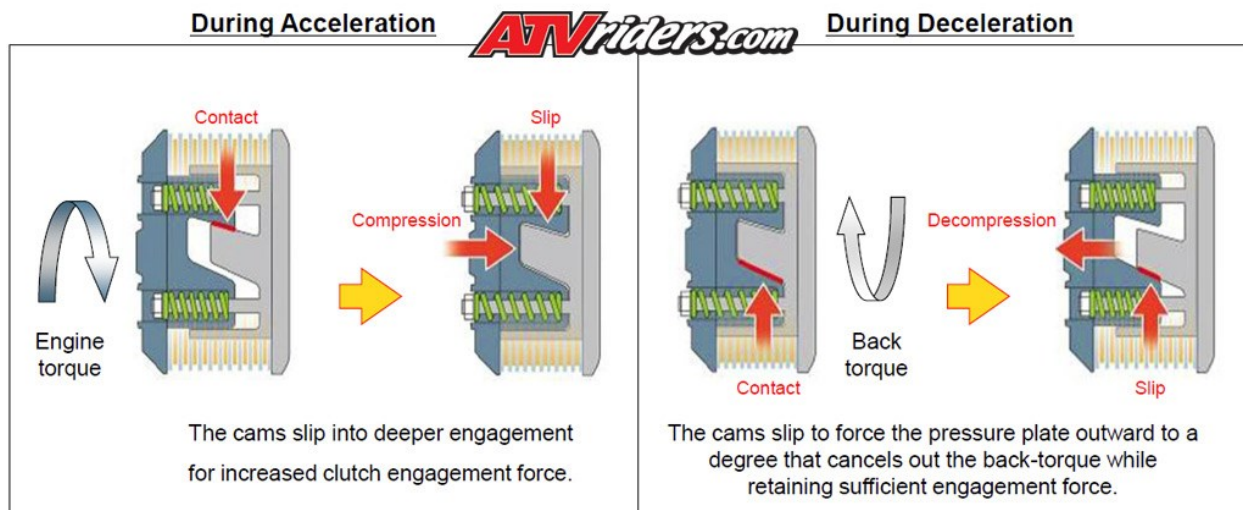


Figure 35. Workings of an Assist and Slip Clutch (atvriders.com)

At first, it seemed like there was only one option for a slipper clutch of the WR450f engine, it was available through Hinson Racing and would cost upwards of \$1200. But after some more research, it was discovered that the 2014 Yamaha YFZ 450R atv cam from the factory with a slipper clutch, dubbed “assist and slip” by Yamaha (atvriders.com). As mentioned previously, the previous WPI Formula SAE vehicle that went to competition utilized this engine, and after talking to two of its drivers who commented on the significantly reduced engine braking and easier down shifting of the previous car, the information was confirmed. Based on two motorcycle forum posts linked in the appendix, it was determined that due to engine and transmission case similarities, the clutch hub and pressure plate and clutch disks from the YFZ, which incorporate the slipping mechanism, can be installed inside the WR clutch basket while still using the WR clutch pushrod and pushrod actuator. The possibility of taking the clutch out of the old car was briefly discussed, but for peace of mind, all new oem Yamaha parts were ordered through Motorsports International in Auburn, Massachusetts.

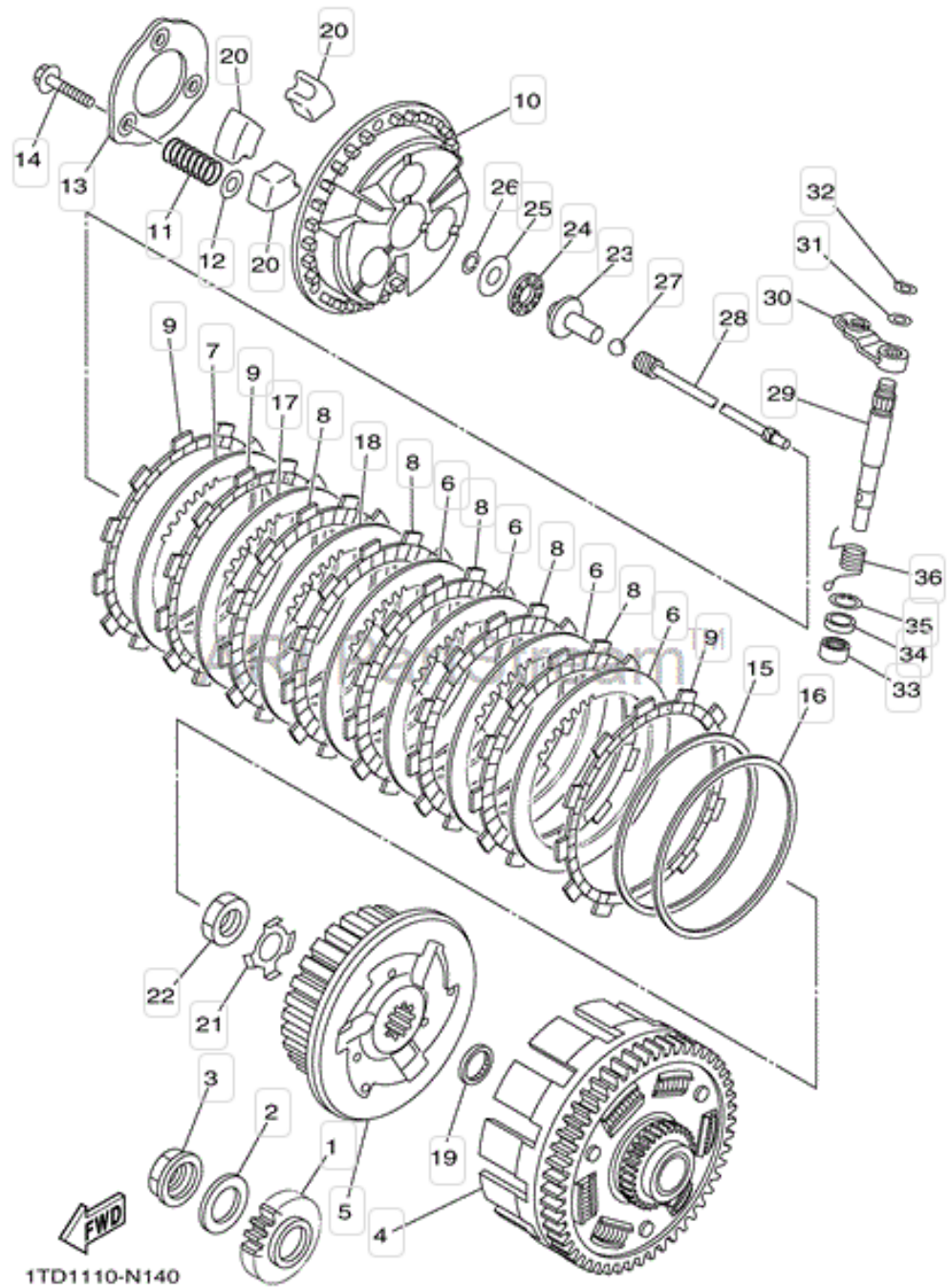


Figure 36. YFZ 450R clutch assembly

Table 4. 2014 YFZ450R Clutch Components Ordered

2014 yfz450 Clutch components.

Diagram #	Part #	Quantity
5	1td-16371-00-00	1
6	4X7-16325-00-00	4
7	1td-16324-00-00	1
8	5VY-16321-00-00	5
9	1td-16331-00-00	3
10	1td-16351-00-00	1
11	1td-16333-00-00	3
12	1td-16774-00-00	3
13	1td-16352-00-00	1
14	1td-16337-00-00	3
15	1TD-16383-00-00	1
16	1TD-16384-00-00	1
17	5JG-16325-00-00	1
18	5JG-16325-00-00	1
20	1td-16178-00-00	3
21	90215-20005-00	1
22	90170-20327-00	1

Figure 35 above shows the parts breakdown of the 2015 YFZ 450R clutch and Table 4 shows all of the parts that were ordered. Technically, the parts highlighted in red are optional, but they were ordered anyway just in case they were needed. All the parts were assembled according to the diagram and inserted in the clutch basket of the WR 450f. Instead of using all of the new friction disk, part number 8 in the diagram, the disks from the WR450f were reused as they were identical and already broken in. Figure 37 below, shows the installed clutch assembly in the WR engine case.

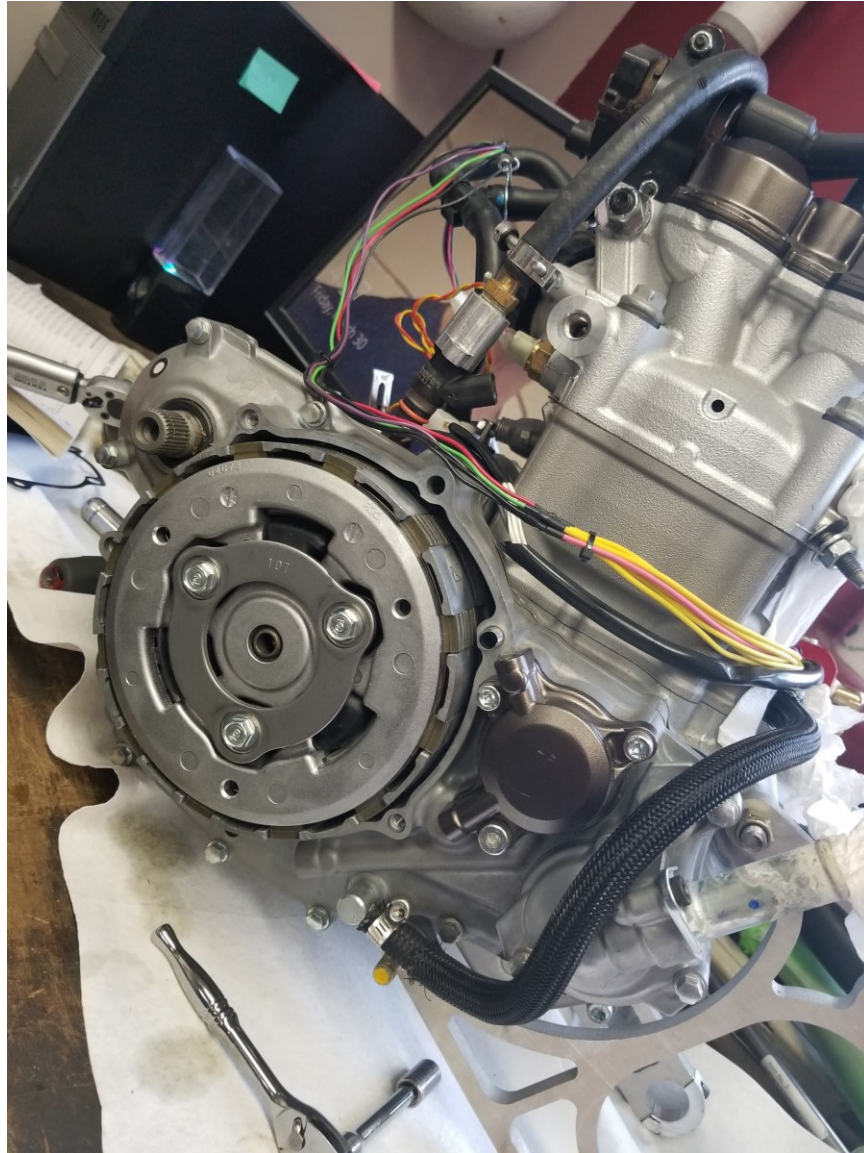


Figure 37. YFZ Clutch installed in WR engine case

As of April 19th, 2018 the electronic shifting via the Raspberry Pi was working and seemed relatively reliable with the car on jackstands and the engine not running. When the car was taken to the dyno, the car began shifting erratically during cranking and would shift while the engine was running. It was at this point the team decided to move away from this style of shifting and install a simpler more reliable system. After much discussion, the team decided to purchase a Pingel Electric Speed Shifter, which is a electronic linear actuator designed to shift sequential transmissions in motorcycles. Manual shifting was also considered as an option, but the actuator was purchased knowing that it would be simple to install and had the ability to produce quick and precise shifts. The actuator itself utilizes the stock foot lever for shifting and is controlled by three wires, one sees constant power and switching ground between the other two change the direction of actuation, when neither wire is grounded, the actuator floats freely, allowing the internal return spring in the transmission to return the actuator to center for the next shift. A simple mount was designed that

locates the actuator between the engine mounts on the back side of the engine, where it extends down to meet the shift lever, the configuration is shown below in Figure 38.



Figure 38. Pingel Electric Speed Shifter Mounted to Car

The electric speed shifter shows excellent potential. The car currently shifts much more reliably and much faster than the original design. However, there is still some more tuning to do with the vertical placement of the actuator and adjusting the rod and lever lengths. After more driving test days, the system will be dialed in and working properly.

Drivetrain II – Engine Performance

For the 2018 competition year, one major area of interest for the team has been lack of engine performance. Little concrete data on the subject is available from the 2015 or 2016 development cycles, but anecdotal evidence suggests that these vehicles were severely limited in maximum power output, maximum achievable RPM, and the consistency of the engine's power curve. Due to the lack of data from previous competition years, it is difficult to determine which components of the engine system, if any in particular, were the main cause of the power problem. This also made it impossible to set specific design goals for the powertrain of the 2018 vehicle, so efforts made this year should be considered as a baseline for later work.

In lieu of attempting to fully characterize the performance of existing hardware from previous years, the 2018 team has decided to direct its efforts toward observing and addressing possible avenues for optimization, purely with regard to the current powertrain. Due to the relatively short time available to develop a powertrain from engine up, and the limited manpower the six-person team could devote to the task, the 2018 team relied heavily on conclusions drawn from scholarly research, other Formula SAE teams, and industry design trends. Although rationale was provided for all design decisions through calculation or simulation, many early design decisions were made on the basis of such generalizations with the intent to narrow the scope of work to a degree manageable within the given schedule limitations.

This report section describes the design trends and possible strategies considered for the design and optimization of the powertrain. Due to an aforementioned reliance on high-level approximations, this section also includes information about some conceptual design choices. The main areas of interest identified for engine optimization were identified as: engine modification, exhaust resonance tuning, forced-air induction, and air intake design. Of these topics, air intake design received by far the greatest degree of effort and attention at the design stage, for reasons which will be addressed later.

Before discussing these areas of interest independently, it is important to note the importance of one key information source to all engine optimization efforts pursued by the 2018 WPI team. This source is a report by the Formula SAE team at California Polytechnic State University specifically regarding the optimization of their engine system for their 2010 vehicle (Ales, Mendoza, Thomas, & Vinokurov; 2010). The work discussed in this report concerns the same engine used in the 2018 WPI vehicle, albeit an earlier version, and their report thus provided much valuable information, particularly about the effects of certain modifications to this engine that would have otherwise been a complete mystery.

Engine Modification

The engine used for the 2018 WPI Formula SAE vehicle is a single-cylinder, 449cc displacement, four-stroke model from a 2015 Yamaha WR450F. Full specifications for this engine and its integral transmission are listed starting on page 53 (2-2) of the 2015 Yamaha WR450F Owner's Manual, which is available for free on the Yamaha website. This engine was chosen by the 2017 team largely due to its similarity to the Yamaha YFZ450R, which was used by the 2015 and 2016 WPI teams, as well as its low cost and high performance potential. Both engines were chosen due to their high power to weight ratio, despite having less power than other engines commonly used in competition. The reasoning for this was primarily that higher powered cars could only rarely be used to their full potential in most Formula SAE competition events, and regardless of other performance benefits, the greater weight implicit in a more powerful engine would hinder the handling of the car.

When initially discussing the powertrain, a popular potential topic of optimization was the subject of engine modification. Within the general category of modification, the team was specifically interested in the possibility of installing an aftermarket piston and camshafts into the engine. Although modifying the engine was a somewhat risky strategy due to the possibility of critically damaging the engine, the idea of simply installing components for performance improvements was highly appealing. If it were possible to simply purchase improvements to the performance of the WR450F, even prior to discussing the design of the intake or exhaust, the time saved and performance gained would be well worth the extra expense. Brief research yielded information about the exact modifications intended to be installed, with additional information on the projected effects available from the Cal Poly report.



Figure 39. Hot Cams Intake (L) and Exhaust (R) Camshafts for 2012-2015 WR450F (Hot Cams, Inc.)

The first method of modification discussed was the installation of Hot Cams, Inc. aftermarket intake and-or exhaust camshafts, shown in Figure 39 above. According to the Cal Poly engine report and the Hot Cams website, the aftermarket camshafts would increase the duration for which the valves are open during both intake and exhaust events by 19 and 15 degrees at the crankshaft, respectively, with corresponding increases in total valve lift of 0.09" and 0.08". Hot Cams claims

only vaguely that these cams will improve mid- and top-end performance, and the Cal Poly report does not make many claims about the effect these cams had on their engine. As camshaft lift, profiles, and timing are possibly the most direct way to alter the performance of an engine, it was disappointing to find such a lack of information about a potentially crucial modification. Similarly, when the team looked into increasing the compression ratio of the WR450F with an aftermarket piston, or boring the cylinder for a larger piston, a lack of information on the expected results dampened interest.



Figure 40. High Compression Ratio Piston for WR450F (Vertex Pistons, Inc.)

According to research into high compression pistons, the most common ratios after the stock 12.3:1 seemed to be 12.8:1 and 13.5:1. Figure 40 above shows one such aftermarket piston, produced by Vertex Pistons. The Cal Poly report includes useful information about the aftermarket piston used in their engine, which provided a 13.5:1 compression ratio, including engine test data from before and after modifying their engine. When the Cal Poly team installed the aftermarket cams and piston along with their custom intake and exhaust designs, a significant performance increase was observed over baseline results. Their engine saw increases from four to six horsepower, from 6500 to 9000 RPM, and torque by 1 to 2 foot pounds over the same range. However, their test data also showed that this improvement was almost entirely produced by their custom designed intake and exhaust, with negligible gains of less than 1 percent after the aftermarket engine modifications were installed. Whether this was due to destructive interference between the effects of the aftermarket piston and camshafts, or simply the magnitude of power gains to be expected from these parts is unclear.

With each camshaft costing \$200, and the piston another \$200, the total cost of modifying the engine would be well over \$600 when accounting for shipping costs and other relevant purchases. This is a steep price for modifications when also considering the time and effort inherent in installing the parts. When the potential risks of modifying the engine are also taken into account the situation becomes even worse. The aftermarket piston and crankshafts greatly increase the probability of valve “crashes,” auto ignition (“knocking”), heat damage, and other miscellaneous problems made possible by interfering with the internals of the engine. Considering on top of these detriments the small percent improvements observed by the Cal Poly team for these modifications, it became clear that modifying the WR450F would not be a worthwhile use of already limited time. The team concluded that Yamaha had done a good enough job optimizing the WR450F engine for maximum performance, and that time should be spent instead on intake and exhaust tuning.

Air Intake

The engine air intake is generally considered to be a highly important component of any engine system when investigating potential avenues for performance improvement. In aftermarket car modification and powertrain development the intake is a frequent focus of optimization efforts as a cost effective alternative to engine internal modifications. The air intake was selected as the primary subject of engine optimization efforts for two main reasons: the Formula SAE mandatory air restrictor, and the greater feasible degree of control over its design relative to the exhaust or engine.

Background Research

In order to determine the best methodology and design concepts for the intake, a significant amount of time was dedicated to researching the fundamental concepts that define the performance of certain components, and to see if optimization could be easily defined by formulas, ratios, or specific values.

Restricted Air Intake Theory of Operation

According to the 2017-18 Formula SAE rules section IC1.6, all gasoline-powered vehicles must restrict airflow to the engine to a 20 mm diameter orifice at some point between the throttle body and cylinder, as shown in Figure 41 below (SAE International, 2017). The restrictor is a key component of the intake system, and as its name suggests, it has the potential to heavily influence the performance and behavior of the engine.

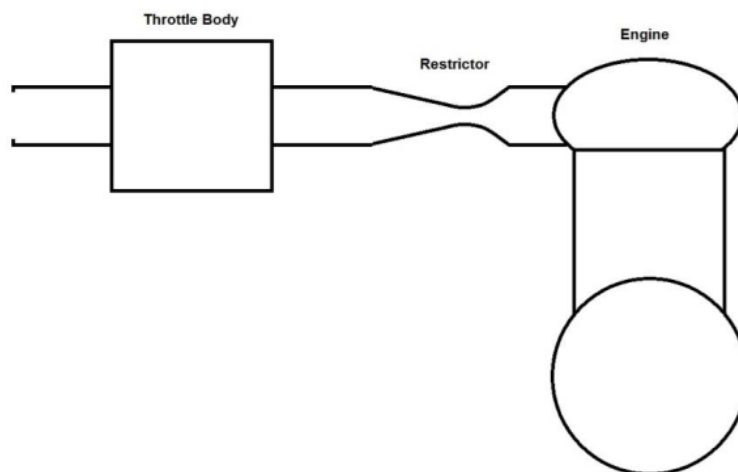


Figure 41. Intake Restrictor Location (SAE International, 2017)

The Formula SAE rules state that this restriction is specifically intended to limit the maximum power output of engines in Formula SAE vehicles. Therefore, this is one aspect of the vehicle that demands priority over other components surrounding the engine during the design process. This is especially important as, unlike the four-cylinder engines many other Formula SAE competition vehicles use, single cylinder engines like the WR450F are particularly vulnerable to the handicapping

effects of the restrictor. To explain why, a description of some fundamental concepts governing the function of a restricted air intake follow.

Due to the cyclical nature of the internal combustion engine, the airflow through the intake of an engine will never be entirely constant, but will pulse whenever the engine is in an “intake stroke” and its intake valves are opened. In a four-stroke engine, the intake valves of each cylinder will open for roughly half of one crank rotation, every other crank rotation, during the intake stroke of the piston. For a single-cylinder engine, this means that in a single combustion cycle of two full crank rotations, the intake valves will only be open for roughly one quarter of the cycle. In a four-cylinder engine, in which the firing of each cylinder is staggered, at least one cylinder will thus always be in its intake stroke at any given point in the combustion cycle. This means that, for single- and four-cylinder engines of the same displacement, the flow of air through the intake is drastically different. While the single-cylinder engine must ingest its full displacement of air within only one quarter of its combustion cycle, the four-cylinder engine distributes its air ingestion relatively evenly, resulting in reduced intensity of intake pulses. The implications of this airflow distribution are significant, as the single cylinder engine is more sensitive to momentary intake airflow disturbances due to its brief intake stroke, and yet simultaneously produces more intense airflow pulses that place greater efficiency demands on the intake manifold. The intensity of airflow pulses during intake is an issue primarily due to the behavior of air itself and derives from the functionality of the restrictor.

While the air restrictor is frequently discussed at an abstract level, the reason for its restriction is seldom described fully, and requires a brief overview of the concept of choked flow for an ideal gas. In ducted airflow, as in an intake restrictor, choked flow occurs where the cross-sectional area of the duct is at a minimum, and the velocity of air in the duct reaches the speed of sound at the “choke point,” or “throat” – the sonic condition. In addition to the occurrence of the sonic condition at the duct throat, choked flow also implies, by its very name, that the mass flow rate of air through the choke point is at a maximum, i.e. that the maximum possible airflow through the duct occurs under choked flow conditions. The choked condition is initiated primarily by a pressure difference between the upstream and downstream areas of the duct around the throat, where a ratio of 0.528 is the highest at which the flow will be choked, and a ratio of 1 translates to a flow velocity of zero. One key purpose of restrictor optimization is thus to minimize pressure drop across the choke point.

The speed of sound in a gas is variable according to temperature and is specified by the formula $a = \sqrt{k \cdot R \cdot T}$, where k is the specific heat ratio, R is the specific gas constant, and T is the temperature of the gas (Sutton & Biblarz, 2017). For air these values are typically $k=1.4$, $R=286$ J/kg-K, and $T=298$ K at room temperature. The mass flow rate of an ideal gas through a frictionless nozzle at the choked condition is governed by the formula:

$$\dot{m} = \frac{APk}{\sqrt{kRT}} \sqrt{\left(\frac{2}{k+1}\right)^{\frac{k+1}{k-1}}}$$

where A is the cross-sectional area of the choke point, P is the pressure of the gas at ambient conditions upstream of the choke point, and the other variables are the same as applied above. If

standard conditions are assumed, such as a sea-level atmospheric pressure of $P=101325$ Pa, $k=1.4$, and $R=286$ J/kg-K, this formula can be simplified for application to the restrictor:

$$\dot{m} = 3222.135 * \frac{D^2}{\sqrt{T}}$$

where D is the diameter of the restrictor in meters, and T is the ambient air temperature in Kelvin. For a restrictor of 20 mm diameter, 0.02 m, as specified in the Formula SAE rules, and room-temperature air, the ideal maximum mass flow rate of air through the restrictor is approximately 0.075 kg/s. Taking into account that this is an optimistic estimate, a comparison with the airflow rate the restrictor will be required to deliver is now in order.

For a single-cylinder engine, the flow rate of air demanded can be assumed to be equivalent to the displacement of the cylinder, 449 cc or 0.000449 m³, at a rate of RPM/120 cycles per second when the four-stroke cycle is taken into account. With a standard air density of $\rho=P/RT=1.19$ kg/m³, this works out to an average of approximately 0.051 kg/s at the 11,500 RPM redline of the WR450F. Since this average mass flow rate is only 68 percent of the choked mass flow rate for the mandatory 20 mm restrictor diameter, choked flow should not occur, and the engine should behave exactly the same with the restrictor as it had without. In fact, according to this idealized formula, a 20 mm restrictor should be sufficient to support even a 750 cc engine operating at 12000 RPM, or a 1.5 L engine at 6000 RPM. However, this simplified model ignores all non-idealities of friction, turbulence, and variable flow rate in the restrictor, which combine to limit performance in practice. The latter is of particular concern here, and the pulsating flow produced by a single-cylinder engine is the primary cause for much of the difficulty of designing single-cylinder restricted air intakes.

If the airflow demanded by the engine is recalculated, taking into account the intake valve open duration, the difficulty of designing an intake for the engine becomes clear. Assuming that the intake valve is open for exactly one quarter of each four-stroke cycle, the duration of the intake stroke is $30/\text{RPM}$ seconds. If an air volume equivalent to the entire engine displacement is transferred into the cylinder within this time, for a volumetric efficiency of 100 percent, the average mass flow rate at redline now becomes approximately 0.205 kg/s while the intake valve is open, or 273 percent of the maximum possible mass flow rate through the restrictor. While neither the average flow scenario above, nor this worst-case scenario would be observed in practice, their contrast clarifies the rationale behind some higher-level aspects of intake design and drivetrain choice.

Returning to the earlier discussion of cylinder count, it is clear now why the four-cylinder engine has an inherent, although slightly counterintuitive advantage over the single-cylinder engine in restricted applications. An intake supplying a four-cylinder engine will experience a flow pattern similar to the averaged flow scenario, in which flow through the restrictor is induced at lower intensity and higher frequency, in turn allowing for larger engine displacements without running into the physical limitations of the restrictor. Along with the performance advantages of four-cylinder engines over single-cylinder, even at sub-one-liter displacements, this is likely a contributing factor in why some highly successful Formula SAE teams have been observed to use engines such as the

four-cylinder Honda CBR600. In the specific context of simplifying intake design, the team recommends that future WPI Formula SAE teams consider the possibility of using an engine with multiple cylinders to simplify intake design. Additionally, this issue of flow rate distribution provides the rationale for a characteristic component of most single-cylinder air intakes – the plenum.

The plenum is a component common to all vehicle air intake systems and is key to reducing the effect of any intake restrictions on engine performance. The purpose of the plenum in ordinary cars is largely to allow for even distribution of intake air between all cylinders, and to reduce effects of turbulence and restriction caused by intake filters and tubing runs (Hamilton & Cowart, 2010). As applied to a single-cylinder engine with a restrictor, the plenum instead functions mainly as an “air capacitor,” a reservoir of unrestricted air for the engine to draw from during its intake stroke. During intake events the plenum provides a cushioning effect to flow at the engine and restrictor, simultaneously allowing for increased volumetric efficiency over a direct restrictor-engine system and allowing for more evenly distributed flow through the restrictor. This is due to the intermittent nature of the intake events for the single-cylinder engine, as each intake event drains the air from the plenum, and during the three-quarters of the combustion cycle during which the intake valves are closed, the plenum can refill through the restrictor. Considering its theory of operation, the ideal plenum volume is infinite, to infinitely smooth the flow through the restrictor, but in practice this is unfeasible both due to size constraints and the delayed throttle response produced by a vastly oversized plenum. The focus of intake design effort by the 2018 team was thus set on the optimization of the shape and volume of the plenum to best reduce the detrimental effects of the restrictor while balancing the similarly important concerns of packaging and throttle response.

Subdivision of Design and Concept Refinement

The design of the intake was started from scratch due to the lack of information from the WPI 2016 Formula SAE team. Discussion with team members involved with the intake for the 2016 vehicle revealed that there was indeed little validation done for the intake design. Due to a lack of publicly available information on intake manifold optimization for single cylinder engines with restrictors, previous applications had been designed partially according to vague and often conflicting rules of thumb. Although research articles and publicly available Formula SAE reports regarding intake design as a whole revealed some relevant papers, none addressed the specific situation aside from the Cal Poly Formula SAE report mentioned earlier (Ales, Mendoza, Thomas, & Vinokurov, 2010). Most of these articles concerned four-cylinder engines, specific experimental design concepts, or efficiency rather than performance, with no discernable agreement as to the ideal end-to-end configuration of a single-cylinder restricted intake. Given the simultaneous abundance of forum posts by Formula SAE teams from other universities regarding intake design, initial concerns that the intake would be a complicated ordeal were confirmed. To make the design process more manageable, and to determine if scholarly research agreed on optimizations for individual components, the team broke the intake system into subsections, including the bellmouth, the restrictor, the plenum, and the runner. The bellmouth, sometimes referred to as a “velocity stack,” is the first component of the intake system to interact with the air stream and is intended to direct the airflow to the throttle as smoothly as possible. After the throttle, the restrictor is the next component of the intake system, followed by the plenum. The runner is the last component of the

intake before the cylinder head and includes the fuel injector port. Figure 42 below clarifies the positions and appearances of these components on the current 2018 intake prototype. The 2016 WPI team gave information on the restrictor and bellmouth, which served as a model for this year's design. The subsections are as follows: A is the Bellmouth, B is the Throttle Body, C is the Restrictor, D is the Plenum, E is the Runner, F is the Fuel Injector Mount, and G is the Engine Integral Runner Extension.

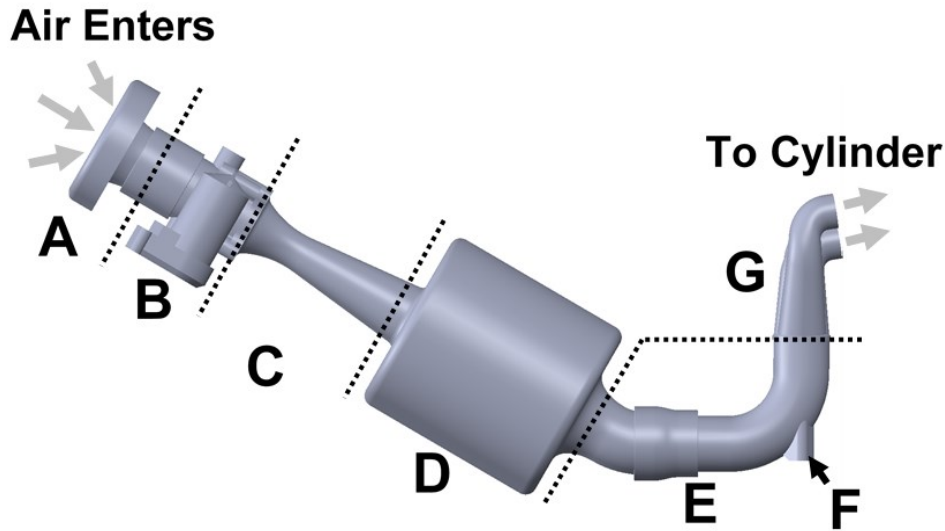


Figure 42. Subsections of Air Intake

A 2006 article by G. P. Blair and W. M. Cahoon in Race Engine Technology Magazine describes the benefits of the bellmouth profile over a plain tube end, and the advantages of specific profiles over a simple radius. This article states that the primary benefit of a bellmouth is the elimination of turbulence and contraction caused by a sharp pipe end, a concept illustrated by Figure 43. The ideal design was specified as a series of dimensions relative to the diameter of the inlet to which the bellmouth is fitted, with an entrance area 2.13 times the inlet diameter, an axial length equal to the diameter of the inlet, a radius of 0.08 times the inlet diameter outside the entrance area, and an elliptical profile connecting the two.

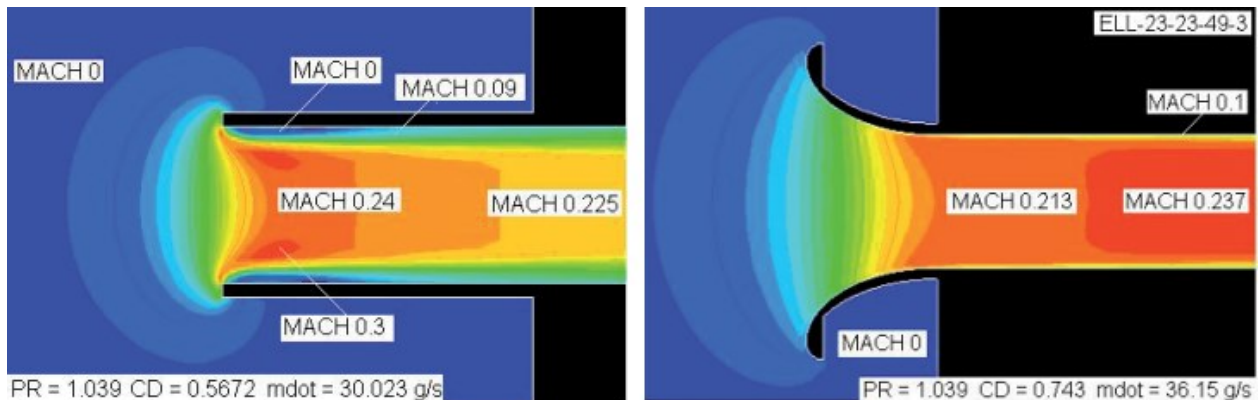


Figure 43. Airflow Entering Plain Pipe and Elliptical Bellmouth (Blair & Cahoon, 2006)

Although the article also stated that this optimized profile only has a small advantage over a simple radius in terms of discharge coefficient, the team chose to adhere to the optimal profile as one of the only optimizations that could be made with relative certainty.

For the restrictor, the article consulted compared several combinations of converging and diverging angles for some common restrictor profiles, providing pressure drop measurements between entrance and exit for each (Deshpande & Narappanawar, 2015). As discussed in the theory section of this report, the pressure drop across the restrictor is possibly its most important characteristic. The promotion of minimal pressure drop delays the initiation of choked flow, and therefore the choking of the engine's air supply. According to the simulation-based study described in the report, the ideal combination of was a "De Laval" nozzle profile, an entrance angle of 16 degrees, and an exit angle of 4 degrees. The De Laval nozzle profile, when viewed as a cross section, involves a convex entrance ramp of constant radius ending tangent to a straight exit ramp, as shown in Figure 44 below.

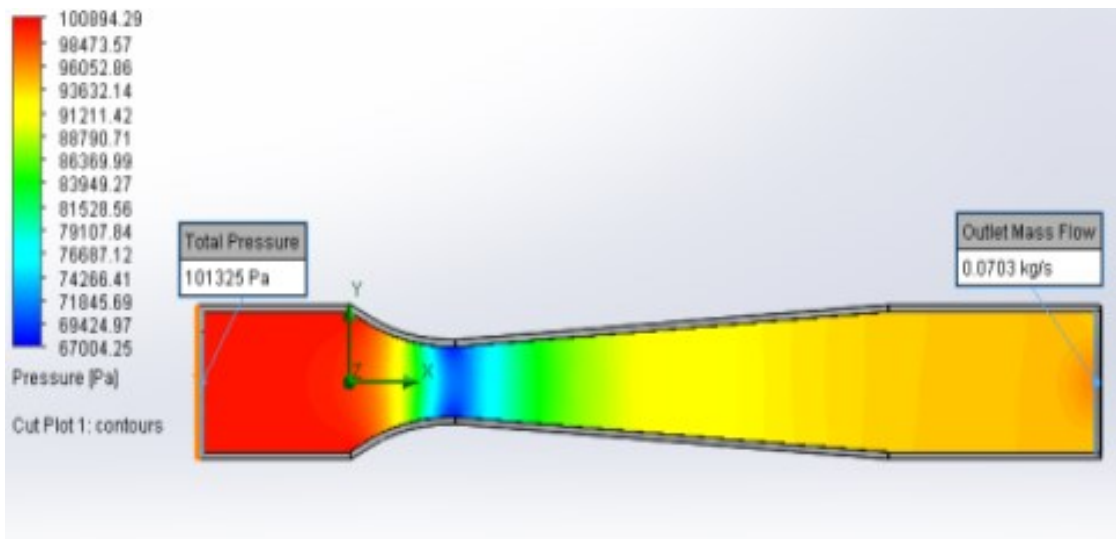


Figure 44. Pressure in 16°/4° "De Laval" Restrictor (Deshpande & Narappanawar, 2015)

The angles specified for the entrance and exit are specified with respect to the axis of the nozzle, representing the 'half-angle' of the converging and diverging sections of the nozzle rather than the included angle. Using SolidWorks Flow Simulation and the test conditions detailed in the report, the restrictor profile was proved optimal within a reasonable degree of certainty.

In researching the runner as well, a study characterizing the effects of runner design features on intake performance in addition to the Cal Poly report referenced earlier, assisted the design decisions made. In a report by researchers at The Ohio State University (OSU) sponsored by Ford, various runner lengths and diameters, in combination with tapered and bellmouth runner entrance profiles, were compared through simulation and physical testing with a single cylinder and a similar 500 cc engine (Mariucci, Selamet, & Miazgowicz, 2007). This report provides a thorough overview of ideal runner design strategies, presenting specific results and conclusions about the advantages runner resonance tuning can provide, as well as the strategies required to reap these benefits.

Some important conclusions of this OSU report can be summarized by observing the magnitude and nature of power improvements produced by a selection of the designs tested. The highest efficiency runner tested in this study was made with a tapered inlet (Mariucci et al., 2007). The test engine gained 5.95 percent in peak power at an offset of -250 RPM from the baseline peak, with a peak volumetric efficiency increase of 3.59 percent at an offset of 625 RPM over baseline, or -125 RPM from the new peak power. These results may seem impressive at first glance, and in terms of peak power and efficiency figures they are. However, when the result data in the report is reviewed with consistency and a smoothed torque curve in mind, even the “best” runner in terms of peak figures has little to claim.

Despite the slight increases in peak power many produced, none of the runners tested by the OSU report had significant positive effects on the volumetric efficiency or power curves of the engine overall (Mariucci et al., 2007). It mainly redistributed local peaks and dips while maintaining overall trends, or in some cases worsened local dips. Although this seems to be a negative result, it did give some relief. Out of runner lengths varying from 6 cm to nearly 30 cm, none had a drastic effect on the performance of the test engine overall. While some designs caused restrictions to flow due to small entry radii or unfortunate resonances, these results were similarly small in scale to the increases reported for the “best” runners. These results showed overall that runner design is a non-critical aspect of intake design, and given an unrestricted flow path between the plenum and engine, the runner has little effect on performance. Similar results were recorded by the Cal Poly engine team in their report, although their data is more irregular and less detailed.

In addition to the relatively small increases in power provided by properly tuned runners, the complexity of ensuring proper resonance makes the intake runner a frustrating component of the intake system to optimize. The intake runner would also have packaging concerns such as avoiding conflicts with the frame members, rule-mandated exclusion zones, and the nearby exhaust. When considering all of this, the small and debatably relevant benefits of a properly designed intake runner become minimal. While it would be ideal to optimize the runner, the optimization can be ignored in order to direct focus more productively to other components of the intake.

When researching the plenum, the conclusions made by research reports aligned with the theory on the point that increasing plenum volume resulted in increased performance. In a report specifically studying plenum volume by professors at the US Naval Academy, eight plenum volumes from two to ten times the displacement of the engine were tested with a four-cylinder, 600 cc engine using a 20mm diameter intake restrictor. This study concluded that plenum volume positively correlated with power and torque, with power increasing by 17 percent from the smallest to largest plenum tested, and torque increasing by 31 percent. This report also concluded that plenum volume had only negligible effects on throttle response time up to a volume of 10 times engine displacement. This alleviated concerns from the team about this aspect of plenum design. Again, the Cal Poly report provided a similar result with lower fidelity, showing that the larger of two plenum volumes they tested produced greater power and torque throughout the speed range tested. As no ideal plenum volume was identified in either case, this research into plenum design did little to advance the design process, but did illustrate the influence intake design can have on performance.

Forced Air Induction

In addition to the previously mentioned options, the possibility of including a turbocharger in the intake system to circumvent some of the challenges posed by a restricted intake was also considered. In 2015, the MQP tasked with creating the initial design of the 2016 Formula SAE car proposed the integration of a Honeywell MGT12 turbocharger system into the final design of the car (Moser, 2015). However, due to time constraints during the car's assembly, the system design was never completed or implemented.

In addition to the previously proposed turbocharger concept, supercharging or running ethanol fuel were also considered. In order to compare these three methods, design requirements were weighted with multiplication values between 1 and 10 by their level of importance, with 10 being the most important. Reliability and availability of parts were rated highest, as a large amount of points can be lost during any Formula SAE competition if a system breaks regularly or parts to repair the system are difficult to obtain. Power increase was weighed next, as the implemented system must produce nearly double the power of the current setup in order to be at a similar power level of other Formula SAE cars. This was followed by cost and complexity, as a large amount of points can be lost during competition due to high car production costs, and because a complex system would be less likely to be implemented due to time constraints when building the car. Efficiency and use of off the shelf parts were rated last, as the 2016 car is currently already highly efficient, and because WPI's Formula SAE Team has the skills and resources to manufacture any custom parts that would be needed. In order for the different designs to be directly compared a design matrix was created to weigh different methods (see Table 5). Each part was given a score from 1 to 10 for each design criteria, and this was multiplied with the weight of each design requirement. From this, it was determined that a turbocharger system aligned best with the design criteria due to its low cost from sponsorships, availability of parts, and ability to increase power.

Table 5. Design Matrix for Forced Induction

Design Criteria	Weight	Turbocharger	Supercharger	E85
Cost	7	7	3	8
Power Increase	8	8	6	4
Complexity	7	5	6	9
Reliability	9	7	7	9
Use of off the shelf parts	5	7	7	9
Efficiency	6	7	5	8
Availability	9	8	4	3
Total		360	275	352

Due to the WR450F's high compression ratio, the engine would most likely not be able to handle more than 10 psi of boost without a high risk of engine failure or pre-detonation. In addition, it was identified that if the boost pressure remained under 7psi, the implementation of an intercooler was not needed (Miller, 2008). As per Formula SAE rules, any intercooler must be placed between the throttle and the engine (see Figure 45), increasing throttle delay (Formula SAE Rules, 2017).

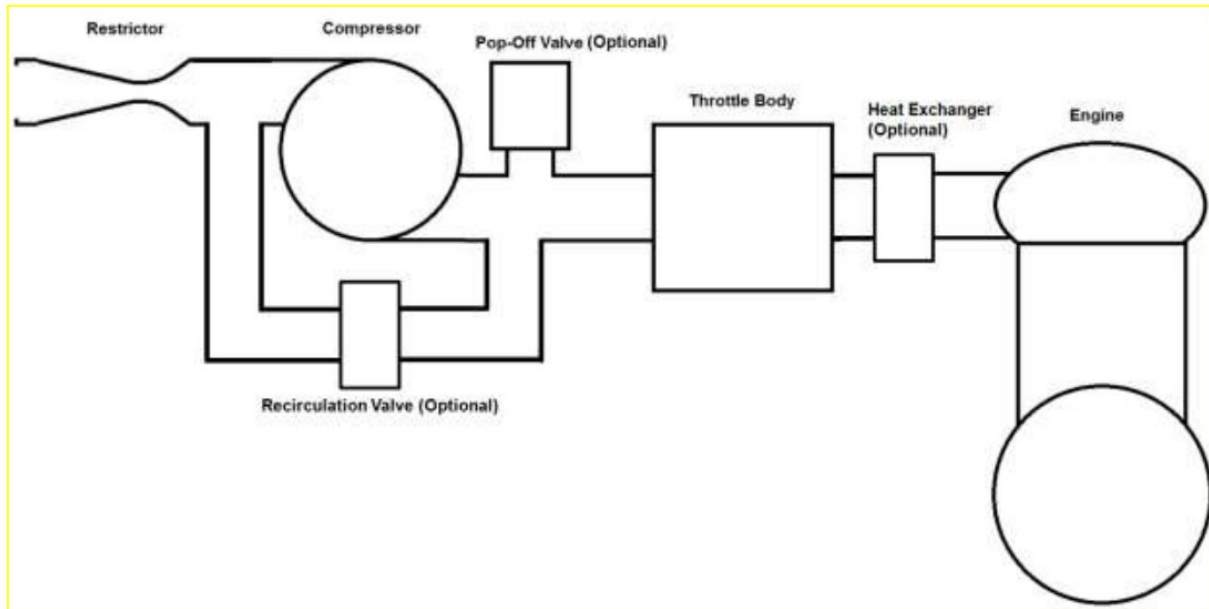


Figure 45. Required placement for intake components for Turbocharged Formula SAE Cars

After weighing all factors it was decided that if a turbocharger system was implemented, it should be designed around running 7 psi of boost without the use of an intercooler. In addition, an engine RPM of 8000 was chosen for optimization calculations as this was the mean RPM value of the desired powerband. For this part of the project, the volumetric efficiency of the engine was estimated to be around 90%, a reasonably conservative number for most engines. Once these values were determined, the airflow and pressure ratio were found using EQ1 and EQ2, shown below. These values were then used to compare the compressor graphs of different turbochargers to determine which ones would be best matched to the engine. The proposed MGT12 turbocharger was compared with a Garrett GT1241 turbocharger; both compressor graphs can be seen in Figure 46 and Figure 47. Comparing these compressor graphs helped to determine if the MGT12 turbocharger recommended by the 2015 MQP was an ideal size for this application. It was found that the MGT12 turbocharger was slightly too large for this application, and that the GT1241, as well as other turbochargers, were slightly better suited. However, it was ultimately decided that for an initial design, the MGT12 turbocharger should be used as the team has two currently available.

$$\text{EQ 1) Airflow} = \text{Displacement} * \text{Target RPM} * \text{VE} * 2.199 * 10^{-6}$$

$$\text{EQ 2) Pressure Ratio} = (\text{Boost Pressure}) / (\text{Atmospheric pressure})$$

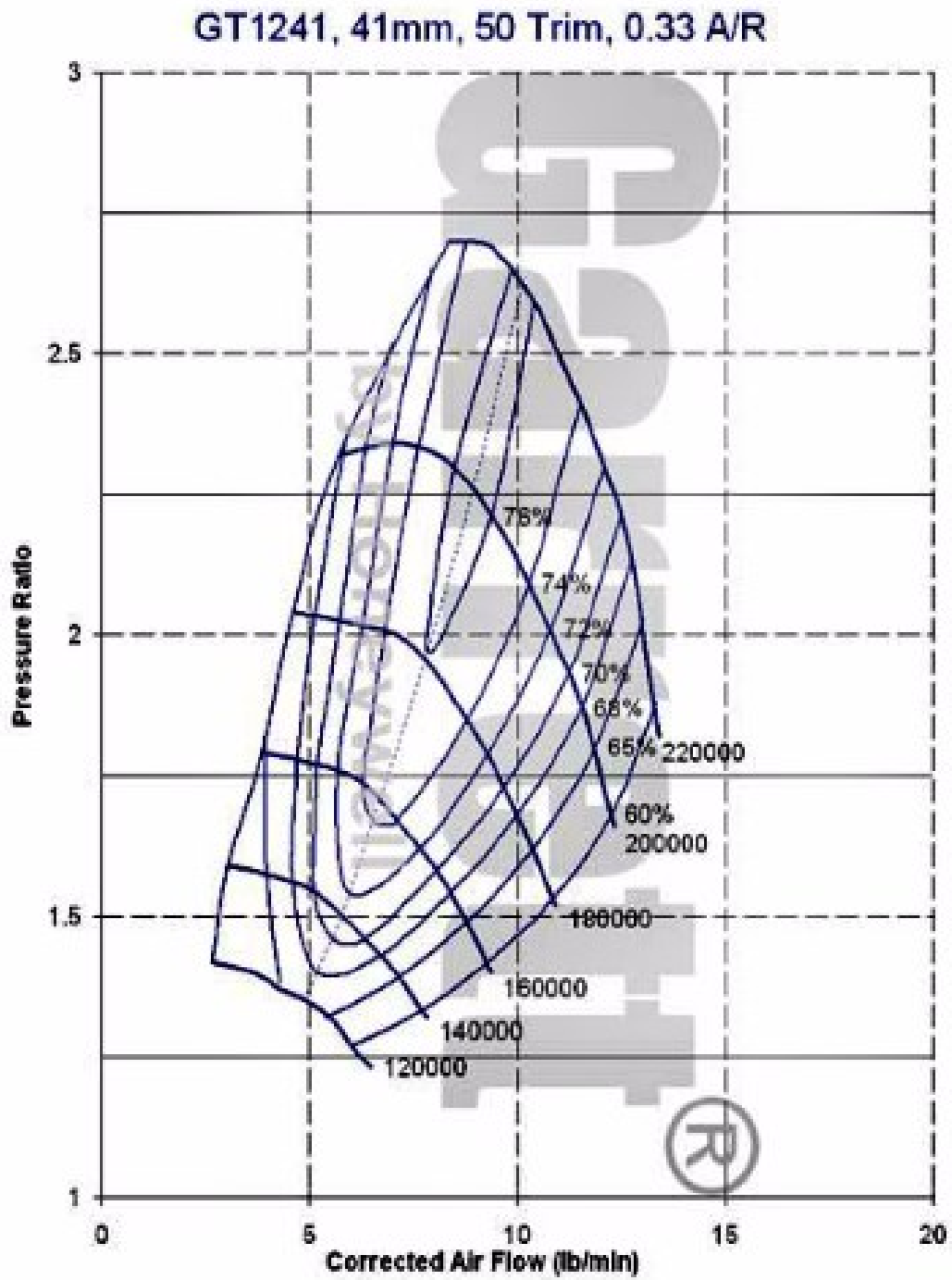


Figure 46. Compressor graph of Garrett GT1241 turbocharger

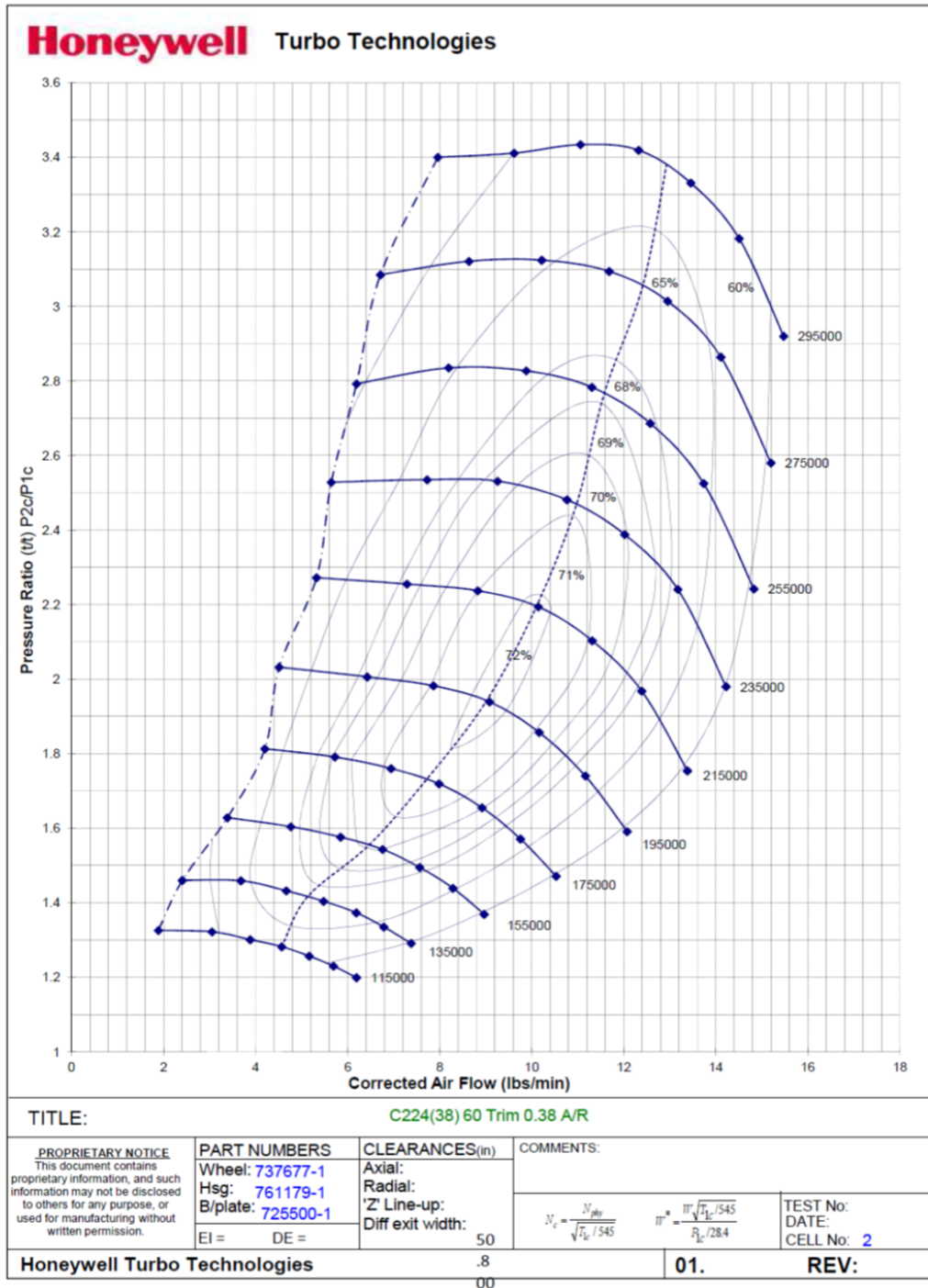


Figure 47. Compressor Graph of Honeywell MGT12 turbocharger

While this report covers some of the basic justifications and calculations for implementation of a turbocharger system, more detailed designs, including suggested turbo placement can be found in a past ISP report (on the SAE Google drive in folder titled: “SAE ISP 4430 (Turbocharger system design)”).

Design Software

During research on intake design, the team found engine simulation software products, most prominently the Ricardo family of software, which promise to simplify and demystify intake and exhaust tuning, as well as engine tuning itself. These software packages were mentioned throughout the Cal Poly design report and in several others as a reliable source of information and validation for often complex designs. The reason the 2018 team did not attempt to gain sponsorship from Ricardo, ANSYS, or others for CFD tools or engine-specific software is primarily due to the complexity of these software products and a lack of time. Due to the compressed timeline imposed by the scheduling of the Formula SAE MQP, the team did not have the man-hours to spend on learning an entire new software suite. Ricardo offers Formula SAE team sponsorships, including free software licenses, and the 2018 team insists that future WPI teams attempt to gain sponsorship or software licenses to hopefully streamline, or at least better inform design decisions.

Intake Simulation Model

Consisting of several subsections, each with their own purpose, flow characteristics, and variety of controlling parameters, the intake was complex and challenging to design. Since there are no simple answers for any part of the intake, iteration has been a key component of its design process, and that process has required the development of unique methodologies to match. For the 2018 vehicle, this involved the development of a time-dependent simulation model using Microsoft Excel and SolidWorks Flow Simulation (SWFS) to approximate the behavior of airflow inside of the intake plenum. This model was developed both to circumvent the lengthy and costly process of acquiring a license for engine-specific CFD software by allowing for precise control of the boundary conditions used in SolidWorks Flow Simulation.

In previous years, SWFS was used to validate intake performance prior to physical manufacturing, but only at a rudimentary level using static analysis. While this was easy to set up in the program, and was “better than nothing,” the static simulation method was essentially useless for determining any numerical descriptions of intake performance, and mainly served to provide pretty pictures of static flow patterns. When the 2018 team began researching intake design and decided to develop a more concrete methodology, there was little information available on the subject of transient flow simulation, and no team members were aware that it was an option in SWFS prior to this project. After some additional research to comprehend the options available for arranging transient simulation in SWFS, including some relevant YouTube videos, the appropriate flow scenarios were arranged. A simple test was set up with a model of the intake designed by the 2016 team, but no new information had been gained about flow behavior in the real intake. Answering this question was the main purpose of the Excel component of the intake simulation methodology.

Getting Started with SolidWorks Flow Simulation

The first step of developing the intake simulation method was to determine the boundary conditions required for accurate modeling, including the numerical output method required. Since the primary purpose of a well-designed intake is to improve volumetric efficiency (VE), and therefore torque and power, volume flow rate data would be the primary output of the simulation.

The first condition set was the entrance of the intake, which for the 2016 model was a plane across the entrance of the restrictor. To emulate ambient air conditions, this plane was set as an “Environment Pressure” boundary with a temperature and pressure of 298 K, 101325 Pa. The next boundary condition defined was the internal surface of the intake, which was set to behave as a “Real Wall.” The settings used for this condition throughout testing were a temperature equivalent to the ambient air, and a roughness value of 1 micrometer as an approximation of a smooth finished surface. Since the exit boundary condition had not yet been given any formal definition, an interim solution to get started with SWFS was to use the exit plane of the intake as a variable pressure boundary (where the intake mounted to the engine). In Excel a simple half-sine wave pressure drop was arranged as a crude approximation of the pressure pulse from the engine. For the pressure values input to the SWFS exit boundary condition, an interval of 0.000125 seconds was used for all tests, a value arbitrarily chosen to be on the same order of magnitude as the calculation time steps preferred by SWFS. To calculate the volumetric flow rate that resulted, a “Surface Goal” was used on the same face as the exit pressure boundary and set to track the volume flow rate of air into what would be the engine. Once a preliminary test was run for the purpose of gaining familiarity with the SWFS user interface, the results were discarded, and work resumed on determining the currently unknown model conditions.

The first step after this preliminary attempt was to create a SolidWorks model of the portion of intake runner integral to the cylinder head of the WR450F. Since the intake valves would form a convenient physical boundary between the intake flow handled by SWFS and the cylinder conditions imitated by the exit pressure boundary, modeling the intake runner extension would reduce the number of assumptions made in calculating the pressure pulse profile at the intake exit. Characterizing the internal geometry of the cylinder head proved quite difficult due to its complex shape and tight confines, but it was eventually approximated. What was ultimately used to dimension this integral runner was the diameter of the valve seats, which could be found from the owner’s manual; the diameter of the inlet, which had been manually measured; and some rough measurements of the internal surface of the runner. Figure 48 is a picture of this integral runner and illustrates the difficulty of measuring the cavity. Using a protractor, the angle of the inlet port was also measured relative to the square sides of the engine.



Figure 48. WR450F Integral Intake Runner Extension and Intake Valve Stems

In SolidWorks, assembling even a skeletal model of this runner required several hours of iterative dimension adjustment, but once its form was figured out it produced a valuable result. Using a 3D sketch, the valve faces were located within an approximation of the cylinder bore, the inlet orifice was located at the origin using the angular measurements of its position relative to the engine body, and the relative positioning of the bore and inlet was determined by iteration, with the linear measurements to the valve positions as a guide. The completed 3D sketch made some approximations of the real shape, such as the assumption of coplanar valve faces when they are in fact slightly angled, and the true shapes of the runner sections leading to each valve. Where measurements could not be taken, their values were approximated from pictures, and the completed model appeared to resemble the actual integral runner to an acceptable degree. Figure 49 shows the completed integral runner model from a similar angle to the above picture.

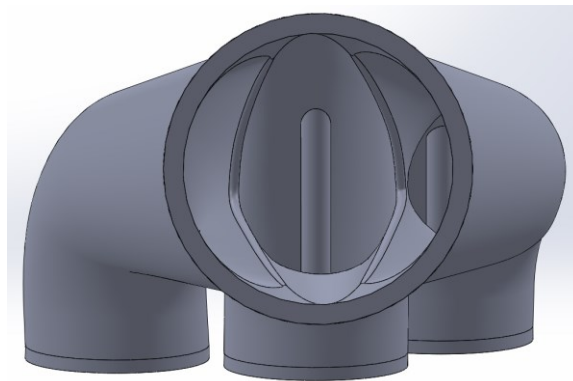


Figure 49. Interior of Model of Integral Runner Extension

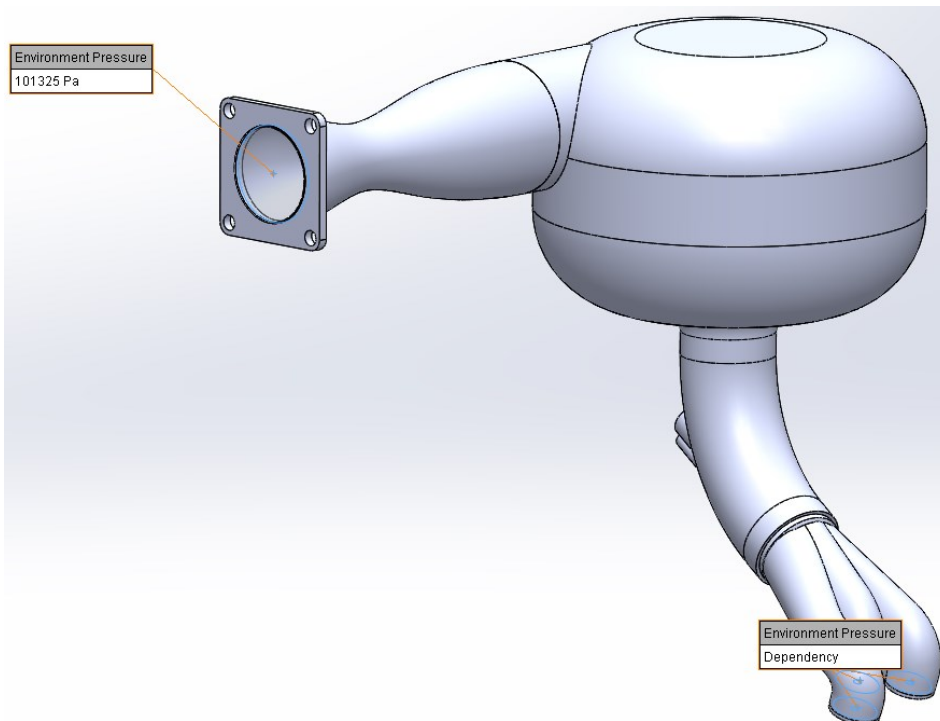


Figure 50. 2016 Intake Model with Integral Runner and SWFS Boundary Conditions Set

Once the integral runner model was mated to the outlet of the 2016 intake model, the exit pressure boundary condition was redefined to the three valve faces of the integral runner, as shown in Figure 50. After this, focus shifted to adding to the pressure wave calculation spreadsheet to account for additional physical aspects of the situation. The spreadsheet was completed prior to any additional simulation runs in SWFS from which numerical results were collected.

Pressure Wave Simulation Spreadsheet

The completed pressure wave calculation spreadsheet is a somewhat complex set of calculations designed to approximate the static pressure at the valves of one cylinder of a four-stroke engine at a specific steady-state condition. It outputs pressure data as a function of time, with an option for user control of the output time step, and manual control of the total output time period. The spreadsheet takes in user inputs of:

- Bore and Stroke of Cylinder (millimeters)
- Compression Ratio
- Engine RPM
- Intake Valve Duration (crank degrees where lift is at or greater than 1 mm)
- Intake Valve Lift (millimeters)
- Plenum/Ambient Air Pressure (Pascals)
- Plenum/Ambient Air Temperature (Kelvin)
- Volumetric Efficiency Guess (decimal percentage)

The spreadsheet also uses some other constants and thermodynamic data that are not intended to be user-controlled:

- Universal Gas Constant $R = 8.314 \text{ J/mol-K}$
- Exhaust Gas Initial Temperature
- Simplified Chemical Composition of Gasoline Exhaust Fumes
- Molar Mass, Specific Heat C_p of Nitrogen (N_2)
- Molar Mass, Specific Heat C_p of Carbon Dioxide (CO_2)
- Molar Mass, Specific Heat C_p of Water Vapor (H_2O)
- Molar Mass, Specific Heat C_p of Carbon Monoxide (CO)
- Molar Mass, Specific Heats C_p and C_v of Air

These thermodynamic properties were included in some aspects of the pressure calculation process by creating curve fits of tabulated data with temperature as the independent variable.

With all of the above information entered, the spreadsheet goes through several steps of calculation to characterize the current situation, finally outputting total pressure in the cylinder. As the spreadsheet is designed to be dragged to the desired length, each column includes only a formula for its particular variable which references either specific values or values calculated in other columns. An excerpt of the pressure wave data this spreadsheet produces is shown in Figure 51. The physical characteristics taken into account, which represent the different steps of the calculation, include:

- Crank Angle of Engine – Repeats at intervals of 720 degrees, for each four-stroke combustion cycle
- Piston Position and Velocity – Determined by sinusoid functions
- Total Cylinder Volume – Displacement at current time stamp, including cylinder volume remaining at TDC due to finite compression ratio
- Propagation (Mach) Delay Time, Delay Adjusted Stroke, and Delay Adjusted Displacement – Accounts for delay between changes in Piston Position and Velocity and response of air in intake runner
- Intake Valve Position – Percentage openness of intake valves at current time; used to control approximate air flow rate into cylinder
- Volume and Mass of Air Ingested – Assumption of some airflow into cylinder to create more realistic pressure wave profile; includes coefficient for model calibration
- Mixed Gas Temperature – Current temperature of exhaust gas and air mixture; found from mass fractions of air and exhaust gas in cylinder at current time
- Total Moles of Gas in Cylinder – Including residual exhaust gas at beginning of intake stroke and air ingested during stroke, allows static cylinder pressure calculation with Ideal Gas Laws
- Gas Mixture Density – Average density of air and exhaust gas mixture in cylinder, for determination of dynamic pressure; determined by mass proportions of exhaust gas and air in cylinder
- Dynamic Pressure at Piston – Pressure created exclusively by motion of piston
- Static Pressure in Cylinder – Pressure created by the imperfect flow of air into the cylinder; also by the cooling, and therefore volume reduction, of the residual exhaust gas in the cylinder
- Total Pressure in Cylinder – Combination of Dynamic and Static pressures in cylinder

Excerpt of Total Pressure vs. Time Output Data at 6000 RPM

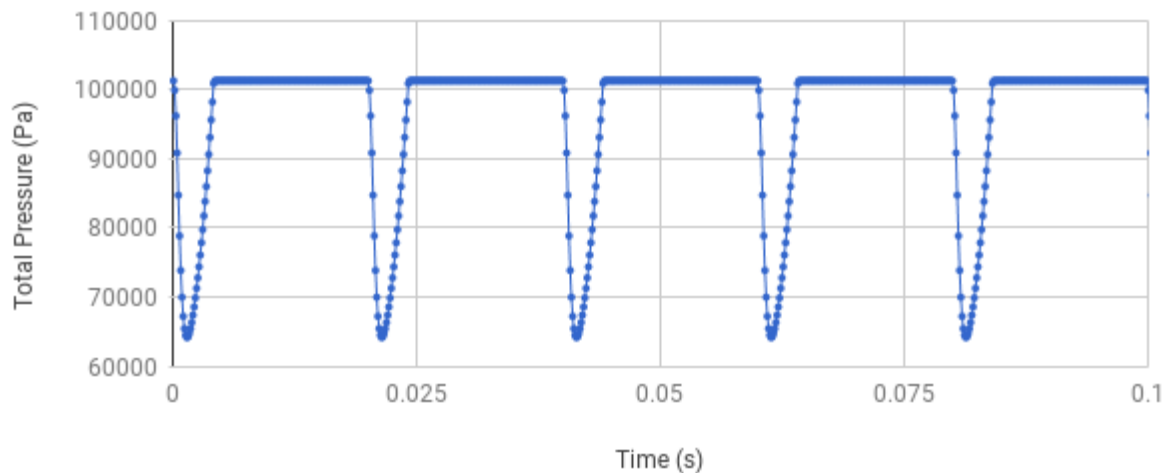


Figure 51. Excerpt of Pressure Output Data from Pressure Wave Spreadsheet

This model also makes several assumptions to simplify calculations for the available data and one-dimensional nature of spreadsheet calculations. These assumptions are acknowledged to potentially have significant effects on the output of these calculations, but have been excluded due to a lack of information or inability to sufficiently characterize these phenomena with the current form of the simulation model. All known or intentional assumptions are listed below:

- Piston stroke follows sinusoidal pattern
- Intake valves open exactly at TDC
- 1 mm lift is minimum for valve to be “open”
- Intake valves open and close exactly according to sinusoid (cam profile unknown)
- Airflow into cylinder is proportional to piston stroke, excepting propagation delay
- Due to the time scale of the intake stroke, propagation delay is non-negligible
- Propagation delay is primarily governed by temperature and specific heat ratio of air, not exhaust gas (to avoid circular dependency with Mixed Gas Temperature formula)
- Airflow into cylinder is restricted proportional to intake valve openness
- Heat transfer between intake air and exhaust gas is instantaneous
- Intake air density is constant for purposes of mass flow determination
- Intake air has constant specific heat (C_p) for determination of Mixed Gas Temp.
- Exhaust valves are fully closed throughout intake stroke
- Some exhaust gas remains in cylinder at beginning of intake stroke, volume equal to TDC cylinder volume
- Residual exhaust gas is at 1atm pressure, 1100K temperature (mid-high temp for exhaust gas temp sensor)
- Fuel injection is ignored; intake air is assumed pure
- Due to assumed flow conditions, pressure in the cylinder rises above atmospheric pressure for a non-negligible portion of the intake stroke, and the total pressure formula includes a cutoff to compensate for this and only allow cylinder pressures at or below atmospheric pressure. This has the effect of shortening the pressure pulse for certain simulation conditions.
- Simulation is calibrated only for Wide Open Throttle, with the 2016 WPI Formula SAE intake. Accuracy is unknown for other intakes, engines, and throttle positions

Due to the sheer quantity of different steps involved in the pressure wave calculations, it is unfeasible to include a full description of each of these formulas and their interdependencies here. Appendix D describes the simulation setup used for the intake design iteration process in more detail. All formulas not related to the physical operation of engine components rely upon ideal gas laws or simple thermodynamic formulas regarding the mixture of different gases and can be found in the textbook *Fundamentals of Engineering Thermodynamics* (Moran & Shapiro, 2004).

Model Calibration

Once the pressure wave calculation spreadsheet was complete, engine tuning data from the 2016 car was used to calibrate the volumetric efficiency calculation model by adjusting the pressure wave model spreadsheet. This was done using a coefficient left in the spreadsheet specifically for this purpose, named the “Volume Air Moved Coefficient” (VAM). This coefficient is included in the

formula for “Volume Air Moved,” which determines the rate at which air is drawn into the cylinder, and due to its placement in the formula essentially scales the volumetric efficiency guess to compensate for errors in the calculation method. Since the determination of cylinder pressure is a complicated problem and requires the assumption of many characteristics of the flow entering the cylinder, this coefficient was included in the spreadsheet as a simple way to scale the pressure response as necessary. The VAM Coefficient was calibrated by comparing the volumetric efficiency calculated by the simulation method to the values calculated for the 2016 intake, the only test item that had been set up to test in SWFS at that point.

The data file used for comparison was a spreadsheet of engine tuning data left by the 2016 team. This data seemed to have been exported from the ECU controller software and included calculated values for volumetric efficiency determined by sensor readings during dynamic engine testing. Team members present around the time this data would have been taken were contacted, and they confirmed that this data file does correspond to tuning data from the 2016 intake.

To gather comparable data from the simulation results, data was exported using the Surface Goals set to monitor the simulated airflow into the cylinder. Using the “Goal Plot” function in SolidWorks, volume flow rate data was exported from the Surface Goals to Excel. On opening the data files, it was noted that charts of volume flow rate across the target surfaces showed continuous flow throughout the simulated time span rather than intermittent flow only when the intake valves would be open, as shown by Figure 52.

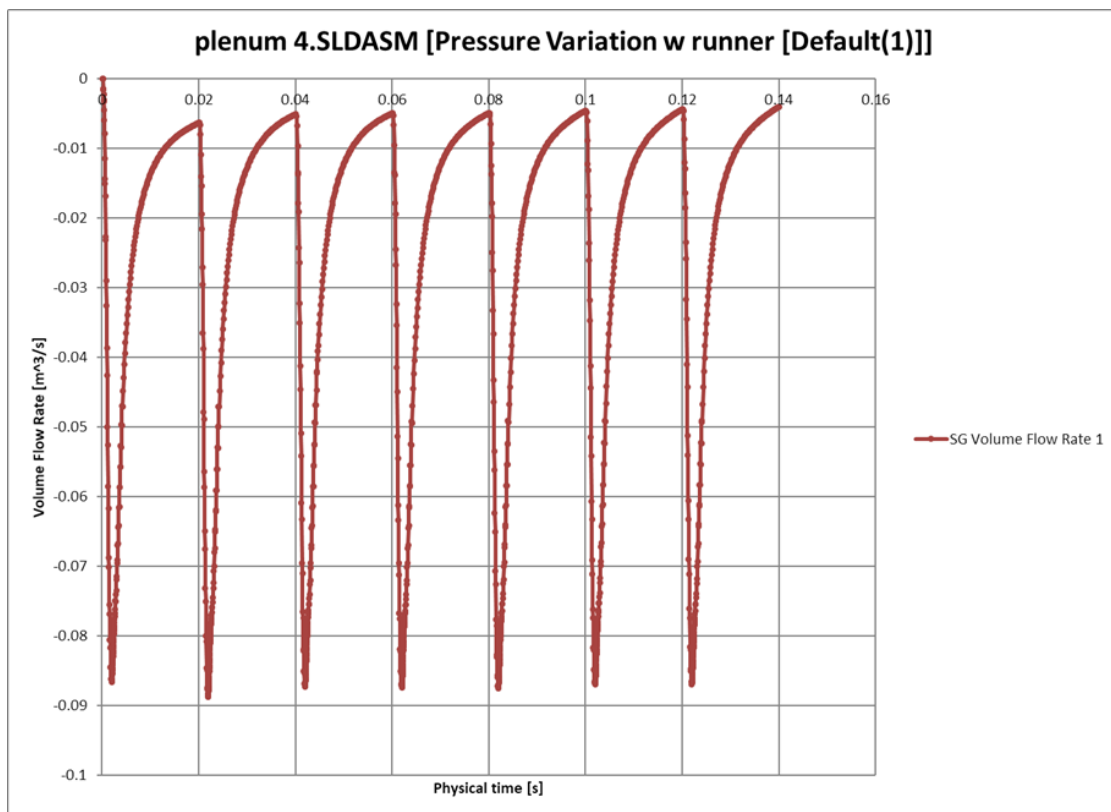


Figure 52. Goal Plot Result for a 6000 RPM Calibration Run

Research into the problem found that it was impossible to temporarily block pressure boundaries in SWFS, making it impossible for the simulation to match the behavior of a real intake valve. Although this issue may have affected the accuracy of the simulated volumetric efficiency results throughout calibration and testing due to the effects of valve closure on airflow, the calibration process should have compensated for any such error. As the volumetric efficiency output by this model is also used for comparison rather than specific values, this issue should ultimately have little effect on the validity of the model for its intended purpose.

To extract volumetric efficiency data from the exported volume flow rate data, simple Excel formulas were used to numerically integrate the total volume transferred into the cylinder over the simulation period. Using formulas used prior to determine valve openness in the pressure wave spreadsheet, periods when the intake valves would be closed were excluded. The first cycle of the data was then manually removed to exclude any startup transients, as well as the last cycle if it was incomplete. The number of complete combustion cycles in the simulation period was then manually counted by observing the result graphs and was used to find the average volume flow per intake stroke. This average volume transfer per cycle was then divided by the displacement of the engine to determine the volumetric efficiency of the simulated intake. If this simulated volumetric efficiency differed from the Volumetric Efficiency Guess entered into the pressure wave calculation spreadsheet by more than two percent, the Guess value in the spreadsheet was changed to the average of the previous Guess and simulated values. This process was repeated until the results converged on one Volumetric Efficiency, which was then compared to the corresponding value for that RPM from the 2016 tuning data. If the two differed by more than two percent, the VAM Coefficient was adjusted, and iterative testing was repeated until the modeled result matched the physically estimated value.

This lengthy process of simulation, comparison, and convergence was repeated for 2000, 4000, 6000, 8000, and 10000 RPM, to provide five VAM Coefficients across the RPM range that would later be used for intake design testing. For the many simulation runs required, time was a key constraint, so a time period of 0.14 seconds was used for all runs during the calibration process aside from the 2000 RPM runs, which used a period of 0.25 seconds. Despite their brevity, these periods were deemed acceptable as simulated volumetric efficiency was averaged over four combustion cycles for the 4000 RPM runs, or three cycles for the 2000 RPM runs, which was adequate for the degree of accuracy sought. Additionally, for the 2000 and 4000 RPM test runs, the resulting data varied little between cycles, so the averaging aspect of the calculation method was not essential to the accuracy of the resulting volumetric efficiency figure. For the 8000 and 10000 RPM tests, the volume transferred in each cycle varied more, but the large number of cycles simulated countered this issue. With these time periods, each simulation run took between 20 and 40 minutes to run.

Once values were determined for the VAM Coefficient for the five RPM levels tested, the curve fitting function in Excel was used to create a polynomial fit, and this formula was then entered into the cell in the spreadsheet where VAM coefficient had previously been entered manually. With this step, the volumetric efficiency simulation model was considered complete and calibrated from 2000 to 10000 RPM. The behavior of the model between the calibrated RPM values has not been characterized, but calibrating the model at finer intervals would take an excessive amount of time,

and allowing for the use of intermediate RPM values should provide additional opportunities for simulation comparison. The team also acknowledges the fact that the accuracy of this method may not hold for intake models other than that of the 2016 car, as the one it was calibrated for. This simulation model seems to produce error within plus or minus two percent with the intake it was calibrated for, so it should produce data well within a usable degree of accuracy for comparisons of different intake designs at the same RPM ranges.

Prototype Intake Design

Once the simulation method for comparing the volumetric efficiency of different air intake designs had been completed, the process of designing the first prototype intake could begin. At this point in the development process, the team had almost fully prepared the engine for benchtop testing, so the prototype intake had to be designed and manufactured on a tight time budget. To make this possible, only two major designs were modeled and simulation tested, with specific RPM ranges in mind and a heavy reliance on “ideal” component proportions derived from earlier research.

The first component modeled after completing the simulation model was the throttle body, an electronically controlled Bosch unit with a 40mm throttle blade diameter. This throttle model was completed in two pieces, the body and the vane, to allow for simple adjustment of throttle vane angle via an assembly constraint if desired during flow simulation testing. After checking the effect of the throttle vane on flow conditions with some test runs and finding its effect to be negligible when over 60 degrees open, the angle adjustment functionality has not yet been used again, with all testing simulating “wide open throttle” (WOT). When testing the 2016 intake, the throttle body had not yet been modeled due to negligence of its potential to affect flow patterns in the intake, but after seeing this result confidence in the simulation model was renewed. Using WOT as the test case for simulation also allowed for direct comparison to the WOT column of the VE table output by the ECU during engine tuning.

After completing the model of the throttle body, the bellmouth was modeled next, following the “optimized” profile found in research. After completing the bellmouth, the restrictor was modeled next, again using the optimized values found during earlier research. There was some confusion when choosing an exit diameter for the restrictor as, unlike the entrance which mates to the throttle body, the exit of the restrictor does not need a specific exit diameter since it vents directly into the plenum. A diameter of 41mm was chosen for the restrictor exit to match the measured diameter of the integral intake runner, and to thus allow the restrictor to be directly attached to the integral runner to test the effect of zero plenum volume on volumetric efficiency (63% at 6000 RPM, 46% at 8000 RPM).

Since no conclusive evidence had been found for the advantages of any particular plenum shape, it was difficult to decide where to begin with the plenum design. In previous years the WPI team had used several different plenum shapes and volumes, and due to their varying success, no trends could be easily determined. In the absence of any clear idea for how to proceed, plenum design began with the two simplest shapes that came to mind; a sphere and a cylinder. For each of these shapes, plenum volumes of 1, 5, and 10 times the displacement of the engine were modeled.

Each plenum included a bellmouth leading to the runner for each using the same optimized elliptical proportions used for the entrance bellmouth. For the spherical plenum, this meant tapering from the runner and restrictor until the bell profile became tangent to the sphere. For the cylindrical plenum, the elliptical profile was raised into the plenum volume slightly to include the radius on the outside of the bellmouth entrance, as research had shown that this slight alteration could offer additional benefits to airflow through the plenum. The cylindrical plenum was also given a protruding radius where the restrictor entered, to smooth the entrance of air into the plenum. These design choices were made primarily through arbitrary intuition about what looked “streamlined” due to a lack of concrete information about plenum design. All plenum designs were also given a “zero-length runner” by directly attaching the elliptical bell taper at their exit to the integral runner model, since there was not yet a clear concept for the shape the runner would need to be to package the intake properly on the car. Figure 53 shows cross sections of the spherical and cylindrical plenum designs at 5x displacement volume.

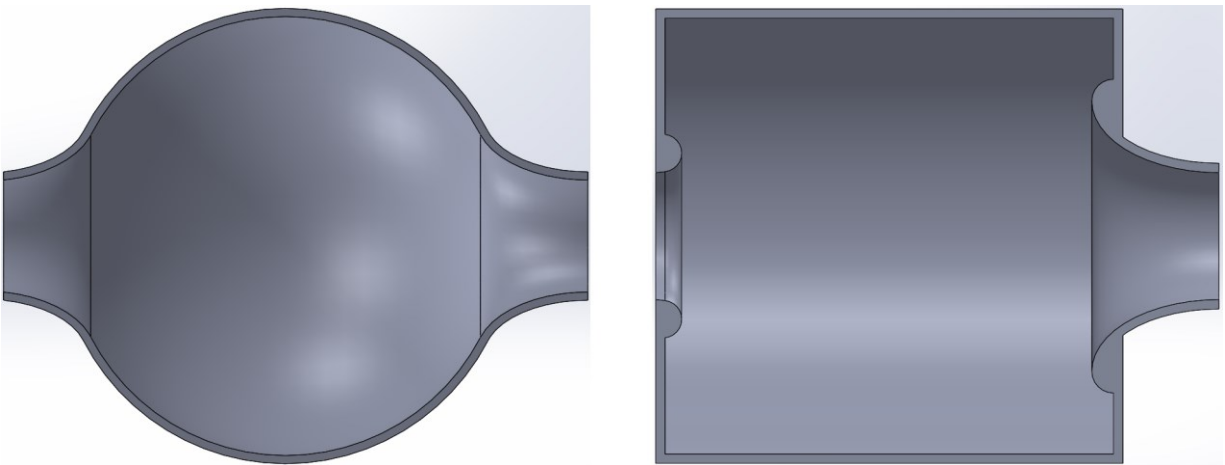


Figure 53. Plenum Prototype Design Cross Sections, 5x Engine Displacement Volume

To vary the volume of the spherical plenum, a model was made to represent the volume contained by the plenum, and the SolidWorks “Mass Properties” tool was used to check the volume as the radius of the spherical portion was varied. For the cylindrical plenum a similar process was followed, but only the length of the cylinder was varied to change its volume.

In addition to these components, another model was made of an arbitrarily shaped volume to place around the intake bellmouth. In SFWS, the inside surface of this volume was set as an environment pressure boundary to simulate unrestricted airflow from the atmosphere. Setting this surface as the entrance pressure boundary instead of a plane across the entrance of the intake is the only major difference between the SWFS setup for plenum testing relative to the configuration used for model calibration. Figure 54 shows the SWFS test configuration for plenum design, including the free air bubble.

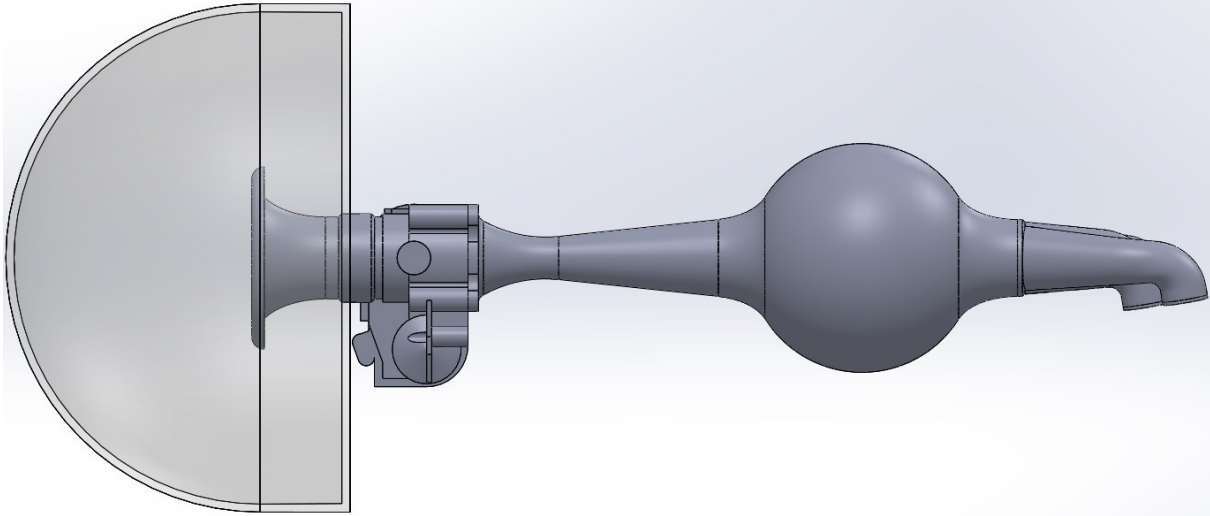


Figure 54. Plenum Design Simulation Assembly, Including Free Air Bubble

After these components were assembled into a continuous intake, simulations were run for all configurations at 6000 RPM, beginning with the 1x displacement spherical plenum and continuing through to the 10x displacement cylindrical plenum. The results observed for the volumetric efficiencies of these configurations proved somewhat confusing, as the spherical plenum design remained nearly constant at 60 percent efficiency for all volumes tested, and the cylindrical plenum produced volumetric efficiencies of 70 percent, 67 percent, and 64 percent for the 1x, 5x, and 10x volumes, respectively. After re-running simulations for the cylindrical plenum designs, the results were confirmed – the smallest of the cylindrical plenum designs was the most efficient. While the conclusions of research on the subject had shown that a larger plenum volume was preferable for volumetric efficiency, the simulation results had shown the opposite, with proportionally equivalent drops in efficiency from the 1x to 5x displacement volumes, and from the 5x to 10x volumes. Testing the cylindrical plenums again at 8000 RPM only confirmed these results, with volumetric efficiencies of 66 percent, 60 percent, and 58 percent for the 1x, 5x, and 10x volumes. Above all, it was clear that the spherical plenum design was not competitive, with consistently low efficiencies for all volumes, but the team was still hesitant to follow through with a plenum design that ran counter to the theoretical and research-corroborated trends, even at a prototype level. Nonetheless, work continued to prepare the prototype for manufacturing, to allow for some physical testing of the new plenum concept.

Prototype Manufacturing

To ensure the intake designs would be completed as quickly and inexpensively as possible, 3D printing was chosen as the means for making the prototype intake. Brief consideration was given to the possibility of machining some of these parts from aluminum, or molding them from fiberglass, but due to the complexity of these processes, 3D printing would likely be the simplest and fastest way to build prototypes. To make sure the parts would fit into the build volume of the printers that would be used, those being the Ultimaker 3 and MakerBot Replicator 2, the intake prototypes were broken down into 6 parts, which would later be assembled and fastened with epoxy resin:

- External Bellmouth
- Restrictor Top Half (from bolt flange for throttle body, to just past the choke point)
- Restrictor Bottom Half (exit cone)
- Plenum Top
- Plenum Body Bottom
- Runner Bellmouth

These components were produced by modifying and segmenting existing models used for simulation testing. As it was preferable to attach a standard air filter over the bellmouth entrance instead of constructing a filter, the entrance bellmouth was modified to provide space for the cylindrical flange and hose clamp of a standard filter. The restrictor was split into two pieces to allow it to be printed standing upright, and thereby increase the accuracy of the print. The plenum was split into top and bottom, with both parts gaining thicker walls for reinforcement against the pressure waves they would experience, as well as another flanged joint to locate the top and bottom together. Two versions of the plenum bottom piece were modeled, one for each of the two volumes made. The internal bellmouth leading from plenum to runner was also made into a separate part from the plenum body. The end of the bellmouth that had previously attached directly to the integral runner was replaced by an extension with a 30-degree angle to allow for further fine tuning of its position in the vehicle. Attached to this extension by way of another silicone coupler is the only portion of the intake not 3D printed, that being the lower runner section.

Compared to the rest of the intake, the lower portion of the runner, which makes the last 90-degree bend to enter the intake port of the engine, is far closer to both the engine and the exhaust, and it must also include the fuel injector mount. Due to the fragility of 3D printed plastic when faced with the chemical and thermal stresses this part would face, it made more sense to construct this lower portion of the intake runner out of thick-wall aluminum tubing, and to weld the fuel injector mount in place. Thick-wall tubing was chosen to ensure a good fit in the existing intake gasket on the engine, and to reduce the chance of accidentally melting through the tube while welding the injector mount in place. The injector mount was designed similarly to the design used in previous years, with a hole for the injector and two parallel threaded holes for small bolts to hold the injector in place. Figure 55 shows a cross section of the assembled model, sectioned for 3D printing.



Figure 55. Cross Section of Prototype Intake Design with 1x Volume Plenum (colors as manufactured)

With the full intake assembly modeled in SolidWorks prior to manufacturing, an additional set of SWFS simulations was run to verify that the changes made to the design for manufacturing, particularly regarding the runner extension, would not significantly alter the volumetric efficiency of the plenum design. Simulation runs were done for 6000 and 8000 RPM, resulting in volumetric efficiencies of 77 percent and 72 percent, respectively. Despite still not having any simple way to verify the results of the simulation model, these results seem reasonable relative to each other, with higher RPM reducing the efficiency of the intake similarly to earlier tests.

Following the 3D printing of the prototype intake components, a significant amount of sanding was required to fit the various component joints together for assembly due to the shrinkage inherent in 3D printed parts. For some components, reprinting with modified tolerances was required for assembly, and some components suffered from layer delamination due to droop in the prints. Assembling the parts once tolerances had been modified was simple, and the same epoxy

used for fiberglass and carbon fiber lamination was used to hold the joints together. To avoid chemical damage from gasoline or other automotive fluids, the inside and outside of all plenum components was coated with a layer of epoxy to form a protective shell.

To satisfy Formula SAE rules requiring rigidly mounting the intake to the engine, a bolt plate was welded to the aluminum runner extension, and extended bolts through the intake gasket were used to hold the intake in place. At the interface between the throttle body and the runner, gasket paper was used to seal any gaps produced by the slight flex in the 3D printed face. A hole was also drilled into the plenum to accommodate a hose fitting for the MAP sensor.

Before any testing could be done with the 5x volume plenum, it was dropped and broken, and since it had already been glued together and fiberglass wrapped, it would require a complete reprint to be functional. Due to this failure, as well as the re-tuning that would be required once the intake was exchanged, the 5x intake prototype was never installed or tested.

Physical Testing and Refinements

During the first starts of the engine, before any tuning had been done, a particularly bad backfire caused the restrictor to unseat from its joint with the plenum top, causing some delamination and cracking in the plenum top. Due to this damage, and significant visible flex in the plenum body observed during testing, the entire intake was wrapped with a layer of fiberglass to improve rigidity and reduce the likelihood of any catastrophic damage to the intake. This nearly eliminated flex in the intake plenum, but also increased its weight. Figure 56 shows the intake mounted to the car prior to frame painting. In this picture the intake does not appear green and white as in the above image, as after it was wrapped with fiberglass it was sprayed with black plasti-dip. The sensor protruding from the top of the air filter is the Intake Air Temperature sensor, which was glued into the air filter for convenience.



Figure 56. Intake Prototype Mounted in Car

After these initial modifications, the intake prototype remained attached to the engine for several months of intermittent tuning, as well as one trip to the dynamometer. The resulting dyno curves, as well as the VE table calculated during the prior tuning validated the high efficiency of the small intake plenum despite its counterintuitive configuration. Although the VE table produced by the ECU is subject to multiple variables in the tuning software, the values observed at the time of writing showed less than 10 percent error of the simulation model at worst, with the physical intake producing somewhat higher efficiency than the model in most comparable cases. This result was deemed to be a great success for the intake design by the team, since no prior data had been available to validate the strange plenum shape produced by the hasty design process. Given the success of the prototype, and the failure of several subsequent plenum concepts to surpass its performance in simulation testing, the prototype design was carried forward to the final design.

Three manufacturing methods were considered for the final intake: 3D printed molds to produce a carbon fiber intake, carbon fiber reinforced 3D printing for the final intake, and 3D printing as with the prototype. After discussing the potential options, ordinary 3D printing was chosen to build the final plenum primarily because of its lower cost and complexity compared to the alternatives, since carbon impregnated printing would cost several thousand dollars and an entirely new manufacturing method would need to be designed to use a carbon laminate construction.

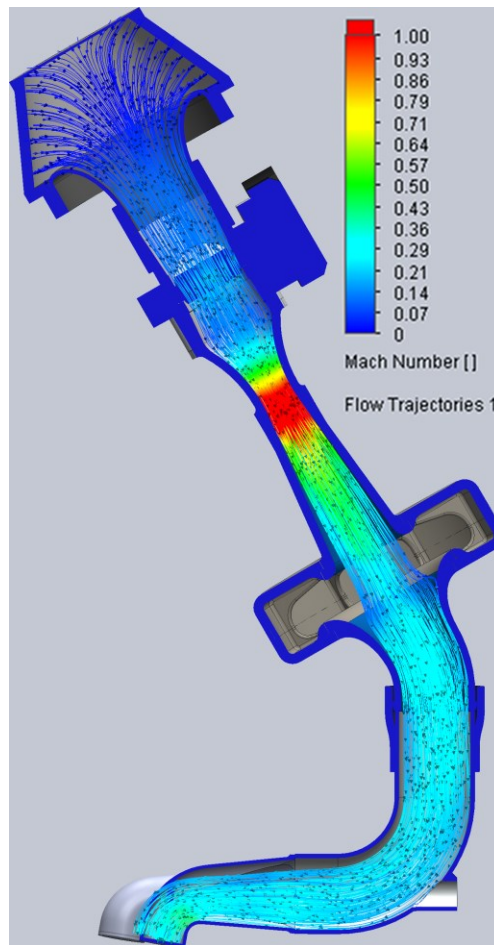


Figure 57. Screen Capture of Flow Simulation of Final Intake Design, Showing Mach Number and Flow Trajectories

To compensate for the fragility, unwanted flexibility, and poor tolerance of the restrictor choke point observed with the prototype intake, the final intake required some minor modifications. Since, as previously discussed, the exact diameter of the restrictor choke point can have a significant impact on the behavior of the intake plenum, a metal restrictor was manufactured to ensure dimensional stability and accuracy of the restrictor choke point. To counter the excessive flex observed in the prototype plenum body during intake suction events, the plenum was modified to include internal ribs to reinforce both halves. The plenum body was also extended slightly to accommodate for the internal volume occupied by the ribs, while the restrictor was shortened slightly to maintain the same overall length. Simulation in SWFS showed negligible differences in volumetric efficiency between the prototype plenum and the revised design. Figure 57 above shows a representative screen capture from the resulting data visualization. To assist with the flex problem, as well as the durability issues encountered with both prototypes, the infill percentage of the new plenum body halves was increased from 15 percent to 50 percent, and the wall thickness of the components was increased to three print layers from two. To eliminate some issues with drooping during printing encountered with the prototype components, the joints between the plenum body and the restrictor and runner were segmented further, and all unsupported overhangs were eliminated from the designs. Additionally, a fiberglass wrap was applied to reinforce the joints between plenum components as a preventative, rather than reactionary measure. Figure 58 & Figure 59 below show the final intake design in SolidWorks, and the 3D printed components of the final intake prior to assembly. The different material colors are due to the different printers that were used, due to differences in availability.



Figure 58. Cross Section of Final Intake Design



Figure 59. 3D Printed Components of Final Intake

The completed intake design used on the 2018 WPI Formula SAE vehicle represents an extensive and thorough design process that lasted for nearly the entire year-long vehicle design process. The highly unconventional design resulting from these efforts has allowed for equal or better performance when compared to previous designs, while occupying far less space.

Intake Mounting

Due to a lack of information about the exact position of the intake in the frame, resulting from a poor-quality 3D scan of the engine, the mounting solution used for the 2018 air intake was largely determined ‘on the fly.’ Since the Formula SAE rules dictated that the intake needed to be rigidly mounted to the engine and soft mounted to the frame, two rubber sandwich mounts were purchased to offer some degree of vibration attenuation for the upper intake mount near the throttle body. This upper mount system was initially designed to place the two sandwich mounts on opposite sides of the throttle body to minimize the moment delivered to the soft rubber mounts, but this design was reworked to reduce the weight and complexity of the system after the intake design was completed. The new design, shown below in Figure 60 and Figure 61, uses a modified shaft collar originally intended for side-mounting the radiator, along with a hand-finished piece of aluminum L bracket, and a machined 0.25 inch thick aluminum adapter plate to span between the sandwich mounts and the throttle body bolt pattern. This mount design is effective in both providing support to the intake and absorbing some vibration transmitted to the throttle body, but could certainly be simplified and lightened. Since the exact vibration attenuation performance and strength of this mount is not critical, it was not analyzed in detail.



Figure 60. Top View of Upper Air Intake Mount to Frame



Figure 61. Side View of Upper Air Intake Mount to Frame – Throttle Body at Left, Main Roll Hoop Brace at Right

At the engine side of the intake, the aluminum runner section was fitted into the existing intake gasket that was supplied with the engine, and no additional sealing was required. To hold the metal runner section to the engine, the three-bolt pattern used to mount the intake gasket was repurposed with longer bolts to hold the intake in place. After measuring the dimensions of the bolt pattern, a simple flange was machined and welded to the metal runner section, and longer bolts were run through this bolt flange and the intake gasket into the threaded holes in the cylinder head. This engine-side mount was also not analyzed in detail since very minor loading was expected for this joint. The bolts used for this joint were cross-drilled, and safety wire was used to ensure they would

not vibrate loose during driving. Figure 62 below partially shows the engine-side mount flange, at top, as well as the fuel injector mount, at bottom.

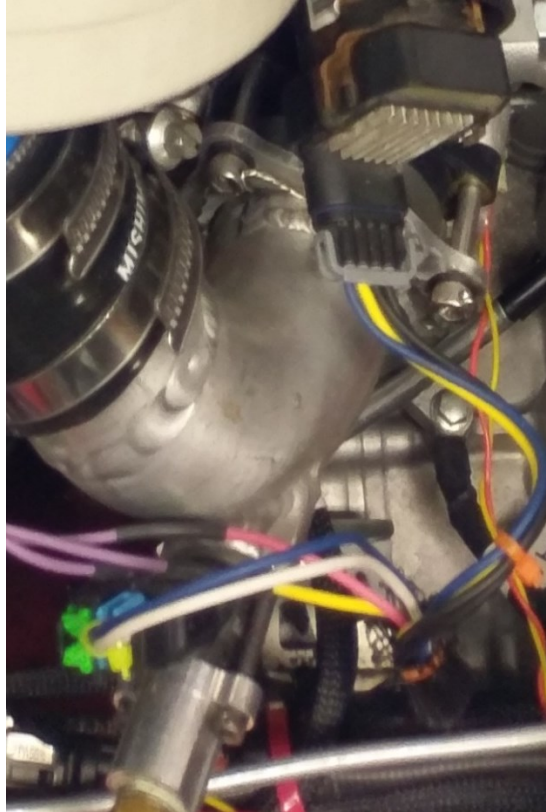


Figure 62. Metal Lower Runner Section – Bolt Flange to Engine at Top; Fuel Injector Mount at Bottom

Future Recommendations

In future WPI Formula SAE vehicles, this team recommends that intake design be approached using a similar method to the one used for the 2018 vehicle, if the exact simulation process is not entirely carried over. Compared to previous intake design efforts, the simulation process designed this year offered an unprecedented level of design validation, enabling the team to determine the approximate behavior of an intake design without the expense and time required to manufacture and tune a physical prototype. This also allowed for iterative design as a reinforcement of the rules of thumb and general design theories available to previous design efforts. While the simulation data produced for the prototype design only aligned to the tuning VE table within approximately 10 percent, this is far more accurate than the steady-state analyses used previously, and with the intake performance data produced by the 2018 car, future WPI teams may be able to improve the accuracy of the model and design future intake designs for even greater performance.

With regard to the manufacturing methods used for the 2018 intake, the 2018 team highly recommends future use of 3D printing for this application. Although some durability issues were encountered with the prototype designs, most damage to the 3D printed structures was remarkably easily repaired with epoxy and fiberglass. Even with minimal infill in the prints, the prototype intakes held up well to the forces of the application, with the damage rendering the larger prototype

unusable being a result of careless handling prior to installation rather than any of the stresses encountered during use. While certain designs may be difficult or expensive to print, the degree of design control afforded by 3D printing is generally only matched by relatively complex machining or composite layup processes, making the process invaluable to both prototyping and final production.

The 2018 team also recommends a reconsideration of intake mounting with the goal of reducing the bulk of the mounting system. Due to the inaccuracy of the first 3D scan of the engine, and the resulting uncertainty about the exact location of the intake in the frame, the 2018 car uses a shaft collar to attach to the frame, which could be replaced with a welded tab if its position could be more accurately fixed. Since it is difficult to work around packaging issues like this without an accurate 3D scan of the engine, the 2018 team recommends making such a scan a high priority to aid drivetrain packaging in general, and especially intake packaging.

Exhaust Tuning

Exhaust tuning was the third avenue for optimization discussed, and one eventually deemed as similarly important to intake design. As with the intake, exhaust tuning has the potential to greatly impact engine performance due to airflow concerns, and like the intake it faces issues of restriction. Outside the realm of Formula SAE, many high performance vehicle designs use large diameter exhaust pipes and cleverly shaped headers to minimize the physical confinement of exhaust gases, and the back pressure at the exhaust valves as a result. As addressed in the Cal Poly engine development report, reduction of back pressure due to exhaust gas stagnation is a key contributor to improved engine performance. Similarly to the intake runner, resonance tuning is one way that exhaust efficiency is typically increased, and some companies such as FMF have built a business around providing precisely engineered exhaust headers for to improve the performance of motorcycle engines. Once the team learned that professionally designed aftermarket exhaust headers were available for the WR450F, one was ordered almost immediately. Purchasing this pre-made part significantly reduced the design and manufacturing demands placed on the team, thus halting research into exhaust tuning to allow the team to allocate manpower elsewhere.

Header Pipe Modifications

The header pipe and silencer purchased for the engine were manufactured by FMF a well known company in the dirtbike and atv exhaust market. A stainless steel PowerBomb header (pn# 1046930030 and Hex Q4 Silencer (pn# 1401380017). The Q4 was purchased because it is the top of line quiet performance muffler for the motor, and the although a lighter titanium header pipe was available, the stainless one was purchased for ease of welding. While the engine was running on the engine stand, the header pipe and silencer worked in their stock form. However, upon creating a SolidWorks model of the header pipe and inserting it into the full car assembly, it became apparent that there would be a clearance issue between the pipe and the firewall. Section T.4.3.2 of the 2017-2018 Formula SAE rules states that heat transfer by convection must be addressed by a minimum 1in air gap between the pipe and any surface that the driver could touch, eg. the firewall. With its factory dimensions, the header pipe had a mere half inch clearance between the pipe and the firewall. The solution was take one inch out the straight section right after the the exhaust port flange and add that section to the section right before the expansion chamber. This solution allows the exhaust to remain the same overall length, without drastically changing the bend radius at the exhaust outlet. The welded joints can be seen bellow in Figure 63.



Figure 63. Header Pipe Modification

From the factory, the silencer came with an extended section of pipe that formed a slip fit with the header pipe. This extended section of pipe was designed to package in the dirtbike and route the exhaust past the rear fender. For the purpose of an Formula SAE vehicle, this section makes the entire system much too long. Based on packaging CAD models of both the silencer and the header pipe, the simplest solution was to move the slip directly between the silencer and the header pipe, shown below in Figure 64.



Figure 64. Exhaust Slip Fit

This configuration places the mounting point for the silencer almost directly above the rear most cross member of the frame, which made for relatively simple mounting via a small tab and two bolts. The O2 sensor, from Innovate Motorsports, was mounted as far downstream from the exhaust port as possible, about 16-18 inches, which is as close to the recommended 24 inches as possible.

Fuel system

Fuel system design was primarily based around frame packaging and engine constraints. The system was designed to be a recirculating system, as most suitable off the shelf components are designed for this type of system, and because it would allow for a simple, constant flow rate pump to be used (also because that is what has been used in the past, so it is what is most familiar). 5/16 ID fuel line was chosen because it had been used in the past and obtaining fuel fuel filters and other components for that tubing size was easy. In the future, fuel hose size could most likely be reduced to save weight. A Walbro 255 Fuel pump was selected due to its reliability, because the team had used it in the past, and it was convenient. For the next car build, a smaller, more lightweight pump may be able to be used, as a 255LPH (liter per hour) can typically support builds over 500HP.

An Aeromotive adjustable bypass fuel pressure regulator was selected, as in the past the team has encountered issues with custom fabricated or modified regulators. This regulator was originally selected because it had the number of inlets and outlets needed (it was thought that three would be needed, and the regulator selected had 4), as well as because it was adjustable within the pressure ranges needed. However, it was later realized that less fuel inlets/outlets were needed, so in the future a smaller and lighter regulator may be able to be found.

The second portion of the fuel system design was the fuel tank. The 2016 car had roughly a one gallon capacity tank, and nearly ran out of fuel during the endurance portion of the Formula SAE competition. This was the basis for a new fuel capacity goal of 1.5 gallons, as this would give the car enough fuel to complete the endurance race without adding excessive weight. Due to packaging, there was limited space to achieve this, meaning that one side of the tank had to protrude backwards next to the engine (see Figure 65). One disadvantage to this design was that there was no space to mount the battery behind the firewall, hence the fuel tank should be redesigned to accommodate the battery if at all possible.

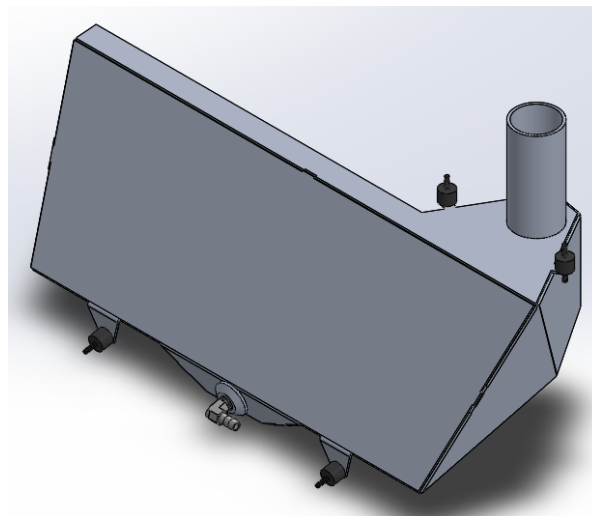


Figure 65. Fuel Tank Isometric

Additionally, the 2016 car experienced fuel starvation issues during endurance, despite having a fuel sump tasked with keeping fuel near the fuel inlet. To correct this, the new fuel tank design incorporates baffles, as well as a sloped bottom, to help ensure the fuel pickup will always be able to intake fuel (see Figure 66)

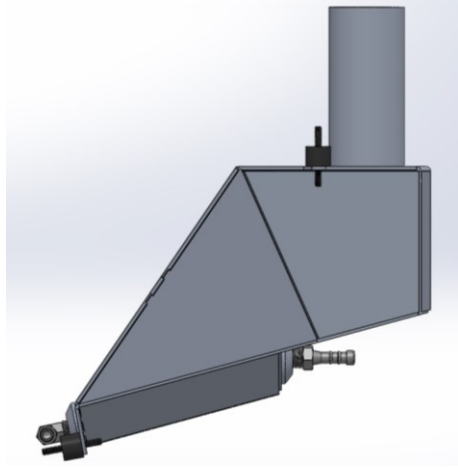


Figure 66. Fuel Tank Side View

The tank was built out of 0.09in thick 5052 Aluminum, as this was the thinnest material able to be welded (in addition, most fuel cells are made from 0.09in thick aluminum). It was important that 6061 Aluminum was not used, due to the fact that it cracks when bent (the tank is constructed out of multiple 2D pieces that are then bent and welded together). Bungs were welded in to easily thread fittings into the tank, and the inlet bung was trimmed to lower the inlet hole as close to the bottom of the frame as possible.

Cooling System

The cooling system of the vehicle was one area ripe for improvement over previous years' designs, as both the 2015 and 2016 WPI Formula SAE cars used dual, side-mounted radiators. In the absence of any coherent method for predicting the thermal behavior of certain radiator and engine combinations, motorcycle radiators designed to match the chosen engine were used; i.e. a pair of Yamaha WR450F motorcycle radiators were purchased to cool a Yamaha YFZ450R engine in the 2016 vehicle. The theory behind these purchases was that, since the dual radiators were designed for the specific engine they were meant to cool, they would have sufficient cooling capacity regardless of the performance alterations needed to accommodate the intake restriction and custom exhaust. The dual radiator setup also allowed for side-mounting of the radiators, assumed to be beneficial due to the free airflow access this position provides, as well as the potential for a lowered center of gravity.

In practice, the dual radiator setup introduced no significant problems, but did clarify some areas for improvement. Due to the separation of the radiators, the dual core arrangement required a large amount of hose to connect the two to each other and the engine, adding mass and complexity by forcing three separate tubing runs when ordinarily only two would be necessary. The outboard mounting of the radiators also forced the installation of thick aluminum mesh around the radiator cores to prevent road debris from punching holes in the radiator cores, further increasing the weight of the system and obstructing airflow. This mesh was required on both the forward and rearward faces of the radiators due to their position between the front and back wheels on either side of the car, exposing them to any debris thrown from any of the wheels. Due to the airflow restriction caused by the mesh, and the fact that the radiator fans had to be mounted outside this mesh nearly half an inch away from the radiator core, the car also displayed some symptoms of overheating during summer driving.

The goal of the revisions for this year was primarily to reduce the mass and complexity of the cooling system while ideally improving thermal performance. The original intent for this was to use SolidWorks Flow Simulation to simulate heat transfer from the radiator and use iteration to determine the ideal combination of airflow and radiator core size. This method ultimately proved to be unfeasible, as did a method based on comparisons between the stock WR450F and the engine as configured on the car. Radiator sizing was also approached via heat transfer calculations, but again a lack of information limited the value of calculating the total heat transfer coefficient. Ultimately, radiator sizing was determined by applying a nominal percentage oversize relative to the stock radiator pair, with the assumption that this would compensate for any increase in heat output caused by the configuration of the engine on the car. Fan selection was also limited by this lack of information as well as the severe power limitations faced by the car, and fan choice was dictated by experimental experience. At the time of writing, the cooling system has shown full functionality, but future WPI teams should attempt to improve the validation behind radiator and fan selection.

Testing

The first step in the design process was to calculate the coolant flow rate and temperature drop across the radiator so that these numbers could provide a baseline for simulation and hand calculations. Once the engine was running with a basic tune on a test stand, a simple physical test was designed to gather this information.

This test involved running the engine on the test stand with the exhaust and prototype air intake attached, although no mechanical resistance was provided to the engine output. The cooling system on the test stand included a radiator from a Yamaha YFZ350 ATV and a 7.5 inch generic cooling fan. To provide points of reference for coolant temperature on the “hot” and “cold” sides of the loop, a Delphi TS10075 coolant temperature sensor was installed via a T fitting into the coolant line leading from the radiator outlet back to the engine. This secondary temperature sensor supplemented the coolant temperature sensor integrated into the WR450F engine block. The secondary sensor was monitored via a multimeter since routing it to the ECU would require modifications to the test bench wiring harness, while the temperature sensor in the engine block was monitored via ECU output. Figure 67 shows the radiator and fan used on the test bench.



Figure 67. Test Bench Radiator and Fan

Testing was completed in two steps, the first being a measurement exclusively of the coolant flow rate through the engine, and the other being a measurement of the hot and cold coolant temperatures. To measure the coolant flow rate, the coolant lines were disconnected from the radiator, and each was manually held into a five-gallon bucket. One bucket held coolant water while the other received, and markings were made on the side of the coolant supply bucket to find the volume of coolant used by the engine during testing. The time span of coolant flow rate testing was determined by the volume of the bucket, and testing was stopped before the water level reached the

bottom of the bucket to prevent the coolant pump from ingesting air. To compensate for coolant usage before the engine stabilized at the desired RPM, the supply bucket was filled above the “start” line of the test. For the coolant temperature test, the coolant lines were reconnected to the radiator and the system was bled of air by briefly running the engine and topping off the radiator. The engine was then run and held at the desired RPM until the coolant temperature stabilized, usually taking about 30 seconds, followed by recording of the temperature values at either end of the coolant loop. The radiator fan was run during the coolant temperature testing, and the ambient temperature at the time of testing stayed between 6 and 7 C, as found from the Intake Air Temperature sensor. The results of this testing are shown in Table 6 below.

Table 6. Cooling System Test Results

Engine RPM	Coolant Hot Side Temp. (C)	Coolant Cold Side Temp. (C)	Coolant Displaced (L)	Time (s)	Coolant Flow Rate (L/s)
2500	77	69			
3000			14.75	28.0	0.526
5000	72	63	12.9	17.3	0.747
7000	73	63	13.8	12.8	1.08

The discrepancy between 2500 and 3000 RPM is listed for thoroughness, but both test runs were completed at idle. Throughout testing, similar variations in RPM were observed to a lesser extent and have been attributed to the crude engine tune available at the time. The exact coolant volume values were calculated from the height reduction of the water level in the supply bucket. Using this data, along with values for the enthalpy and density of water gathered from the Fundamentals of Thermodynamics textbook, the heat dissipated by the cooling system was calculated (Moran & Shapiro, 2004). The heat transfer rate in kW was calculated using the simple formula $Q = \Delta h \cdot \dot{m}$, where h is enthalpy in kJ/kg and \dot{m} is mass flow rate of coolant, found from the average density of water at the temperatures encountered during a test run, and the volumetric flow rate of that test run. A summary of the heat transfer calculations is shown in Table 7 below.

Table 7. Cooling System Heat Dissipation Calculations

Engine RPM	Coolant Hot/Cold Temp. (C)	Coolant Δh (kJ/kg)	Coolant Avg. Density (kg/m ³)	Coolant Flow Rate (m ³ /s)	Coolant \dot{m} (kg/s)	Heat Dissipated (kW) (hp)
Idle (2300-3000)	77/69	33.5	976	0.000526	0.513	17.2 23
5000	72/63	37.7	979	0.000747	0.731	27.6 37
7000	73/63	41.9	979	0.00108	1.06	44.4 60

The large heat transfer values produced by the test surprised the team, and although these values may be normal, not enough is known about the engine to determine whether this is true. Assuming that these heat transfer values are anomalously high, one potential cause is that the only resistance to the engine's rotation was the internal friction of its own piston and transmission, so any power the engine would have made under load was instead output as waste heat. The other potential cause for the large heat output is the extremely crude engine tune at the time of testing, which barely allowed the engine to maintain a steady idle. If this tune caused the engine to run more lean than ideal, i.e. with a higher air-fuel ratio, the engine would theoretically produce more waste heat. Regardless of uncertainty about the meaning of the results, these testing results were then used to begin the development of a simulation of heat transfer through the radiator.

Simulation Method

Flow Simulation of the radiator was the first method pursued to validate certain combinations of fan configuration and radiator size, to determine an ideal solution for the car. This simulation method was later dropped in favor of simple hand calculation and approximation due to the unfeasibly large time required to run each simulation.

Measurements of the test bench radiator were used to create a watertight model of its core. The Flow Simulation model was configured to include two separate chambers for air and water, with equivalent inlet and outlet volume flow rate conditions set at either end of each chamber to control each medium. Goal Plots were arranged to monitor the outlet temperatures of the air and water, and the results from physical testing were used to set the flow rates and temperatures of the inlet conditions. Figure 68 below shows a cross sectional view of the smaller model arrangement attempted for the flow simulation, where coolant flows vertically through the radiator core segment and air flows horizontally. For simulation of the radiator as a whole, this configuration was scaled to fit a test section representative of the entire radiator core.

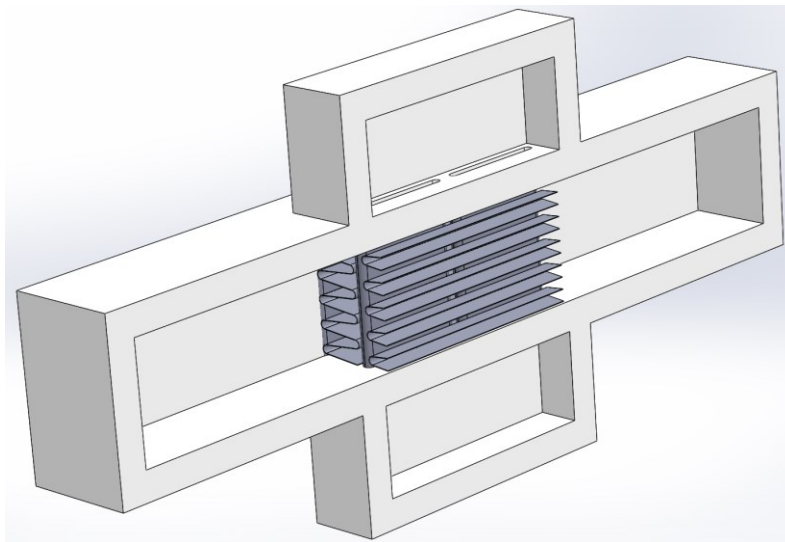


Figure 68. Section View of Radiator Segment Simulation Setup

For this smaller scale test, the coolant flow rates of the full radiator were scaled down to match the number of cooling channels included in the radiator surface area under test, with the air and coolant inlet temperatures set to equal the real test results. Exact airflow output for the radiator fan was not known, so a nominal flow velocity of 2 meters per second was assumed instead. This flow rate is also not necessarily representative of the real test, since the fan was not shrouded to produce even airflow through the entire radiator core.

Although this simulation method was believed to be valid, upon running a simulation of the full radiator core for the first time, SolidWorks gave an estimated time to completion of several days, which is anomalously long considering the simulation was steady state and not time-dependent as with the intake. A test case run with a small 20x20mm segment of the radiator core, shown above, was also attempted, but would still take several days to complete according to the estimate output by SolidWorks Flow Simulation at the start of calculation. Unlike the air intake simulations, which could be run in a matter of hours or minutes, each iteration of the cooling system would require days to analyze, making this method useless in the tight time frame available for cooling system design. Instead of continuing to attempt to optimize the simulation model, this method was discarded in favor of finding a simpler approach. Due to the futility and likely inaccuracy of this method, the details of this simulation setup have not been described in detail in this report, although the relevant SolidWorks files have been saved.

Comparison Method

Since the simulation model had proven unfeasible, a simpler method was considered to find the correct radiator size, primarily based on the stock WR450F from which the car takes its engine. Although this method also proved to be unfeasible, this method would likely work if more information were available about the engine in its stock configuration, and its behavior as installed on the car. Assuming that the most cooling-limited scenario for either the stock WR450F or the car in normal operation would be at high RPM in first gear due to the low travel speed, both vehicles would encounter nearly the same worst-case conditions due to their similar gearing. Due to the different wheel diameters and final drive ratios, the 36:13 final drive ratio chosen for the 2018 WPI Formula SAE car produces speed ranges for each gear that are very similar to those of the 2015 WR450F. Since the WR450F also does not come fitted with radiator fans as standard, a comparison of the waste heat output by the two vehicles could be used to determine the approximate radiator size required for the car as a function of its increased waste heat output. This method would rely on some assumptions about the waste heat output of each vehicle, particularly the test data gathered earlier, as well as the obvious assumption of competence on the part of the Yamaha engineers that decided on the radiator configuration for the WR450F.

According to the radiator core dimensions included in the 2015 WR450F owner's manual, the stock radiators have a total core volume of 116 cubic inches. According to a dyno test run by Motorcycle USA on the 2012 WR450F, which is identical to the 2015 model, the maximum power output of the WR450F is roughly 30 kW at 8500 RPM, although values from some other debatably trustworthy websites are 10 to 12 kW higher (Hilderbrand, 2012). To compare the test data to this performance figure, research was done on the thermal efficiency of gasoline-powered, single-

cylinder, four-stroke engines like the WR450F, but what little information was found on the topic was either too generic or poorly cited to be of use. What would be necessary to compare the stock WR450F power output to the bench test results would be a relation between load and thermal efficiency, and a further comparison of waste heat output via exhaust gas versus the cooling system. The only seemingly reputable result found on the topic stated a single efficiency of 20 percent (Mirani et al., 2008). Some of the more poorly cited results showed engine efficiency at 30 percent under moderate load, with a drop to less than 5 percent efficiency under 10 percent load, although these values varied. No relation between coolant system heat transfer and exhaust heat loss was found, making the intended comparison effectively impossible to achieve.

Due to a lack of information about engine efficiency in general, the WR450F engine in its current configuration, and most critically the assumed efficiency reductions incurred by the restricted intake and heavier vehicle, radiator selection could not be validated by this method. If these efficiency values could be found, this method would consist of first calculating the waste heat output of the engine based on its efficiency and maximum power output. This heat output would then be compared to the test results to determine the degree of excess heat output by the engine in its restricted configuration, and a radiator would then be selected which was oversized compared to the stock radiators by the required percentage.

Radiator Selection

Since the deadline for radiator selection was fast approaching at this point in the design process, and little progress had been made in determining an accurate method for calculating the required radiator size, a final method was created, partially using qualitative measures for the final decision. While a method using heat transfer calculations was investigated, the persistent lack of information made this effort moot. For future reference, Chapter 11 of *Fundamentals of Heat and Mass Transfer (7th ed)* was used as reference for this research, and this textbook would likely contain all necessary formulas to make this method work. The new, and final method for radiator selection involved a review of commercially available options in approximately the correct size for the WR450F, a comparison based on core volume, and selection based on the potential mounting options for each model on the car.

A thorough review of available options on Summit Racing and some other online automotive supply stores showed that generally, only ATV radiators came in small enough sizes, and with reasonable enough prices for the application. Radiators intended for peripheral additions to drag racing cooling systems and limited-run radiators for shifter kart racing were also available in appropriate sizes, but would all cost several hundred dollars more than comparable ATV radiators. A spreadsheet was created to compare each radiator to the stock WR450F, expressing this comparison as a multiple of the volume of the WR450F radiators. The radiators were also compared on the basis of their flow orientation, as a preliminary investigation of available radiator mounting positions on the frame heavily favored wider crossflow radiators over taller downflow radiators. An excerpt of the comparison spreadsheet is shown in Table 8.

Table 8. Radiator Option Comparison

Radiator Model (Intended Vehicle)	Layout	Core W/H/D (in)	Core Volume (in ³)	% Oversize vs. WR450F Stock	Ease of Mounting (out of 5)
WR450F Stock	Dual, Downflow	4.78/11.02/1.1	115.9 (both radiators)	N/A	1
Yamaha YFZ450R	Crossflow	11.97/7.24/1.57	136.1	17	3
Yamaha YFZ350 (Test Bench)	Downflow	7.625/12/1.57	143.7	24	1
Suzuki LTZ400	Crossflow	12/7.4/1.65	146.5	26	2
Kawasaki KFX450R*	Crossflow	11.97/8.19/1.57	153.9	33	4
Suzuki LTR450	Crossflow	14.88/6.77/1.57	158.2	36	2
Yamaha YXR450	Crossflow	9.37/14.96/1.65	231.3	100	5

Looking specifically at radiators between 20 and 40 percent oversized brought the field of options down to three, all designed to fit different ATV models: Suzuki LTZ400, Kawasaki KFX450R, and Suzuki LTR450. These radiators all had crossflow configurations, core volumes between 25 and 40 percent oversized versus the WR450F, and all cost exactly \$150, making their only clear functional distinction being their mounting flexibility. Since uncertainty about the exact needs of the cooling system persisted, this size range was selected to provide a moderate margin of safety for the cooling system. Figure 69 shows the chosen Kawasaki KFX450R radiator.



Figure 69. Kawasaki KFX450R Radiator (Mishimoto, n.d.)

Due to the fragility of their aluminum construction, an important factor in the choice of a radiator was the avoidance of any welding or other modifications to the radiator for the purpose of mounting. Mounting hardware integrated into the radiator thus became the final criterion. Although a specific mount position on the car had not yet been established at the time the radiator was chosen, the KFX450R radiator was selected for its large mounting tabs, running the full length of the top and bottom of the radiator core, offering twelve mounting holes. Due to the availability of mount holes in plane with both sides of the core, this radiator offered several options for mounting the radiator to the frame, as well as mounting fan shrouds or brackets.

The KFX450R also provided a reasonable core volume of 133 percent that of the stock WR450F radiators, reducing the prospective need for any active fans while remaining small enough to package in the frame. The overall mixture of valuable traits has made the KFX450R model an easy radiator to work with, and at the time of writing it has seemed well suited to the car.

Radiator Mounting

After selecting a radiator, two main mounting locations were considered, one being on the side of the car next to the engine, perpendicular to the long axis of the car, and the other being on the jack point at the rear of the car. Figure 70 below shows these two positions on the frame. The location on the side of the car was investigated first, with mounts created in SolidWorks to attach to the main roll hoop and roll hoop supports. These mounts would be somewhat complicated and difficult to make due to the odd angles of the frame tubes relative to the radiator. As this position placed the radiator perpendicular to the direction of travel, a simple shroud would also be necessary to funnel air into the radiator. Due to Formula SAE rules restrictions on aerodynamic devices at the vertical height of this radiator position, the intake area of the radiator shroud had to be relatively small compared to the area of the radiator core, meaning that this location would result in less-than-ideal cooling performance while in motion. More specifically, the largest possible dimensions for the inlet of a shroud for a radiator in this position would be about 5.5 by 8 inches, only 45 percent of the total core area of the radiator. This position would also place the mass of the radiator and coolant high and off-balance, potentially affecting the center of gravity of the car enough to harm its performance in the tilt-test. Further, the proximity of the engine to the radiator in this position would limit the space available for inboard, or “pull” radiator fan mounting. One advantage of this position is the short coolant lines required, since the radiator is immediately next to the engine. Also due to its inboard, perpendicular positioning, the radiator is less likely to be impacted by debris than the outboard dual radiators of the 2015 and 2016 vehicles, making the restrictive and heavy protective mesh unnecessary. Despite this, the disadvantages to center of gravity and cooling performance outweighed the advantages in the opinion of the team, and this radiator position was not chosen.

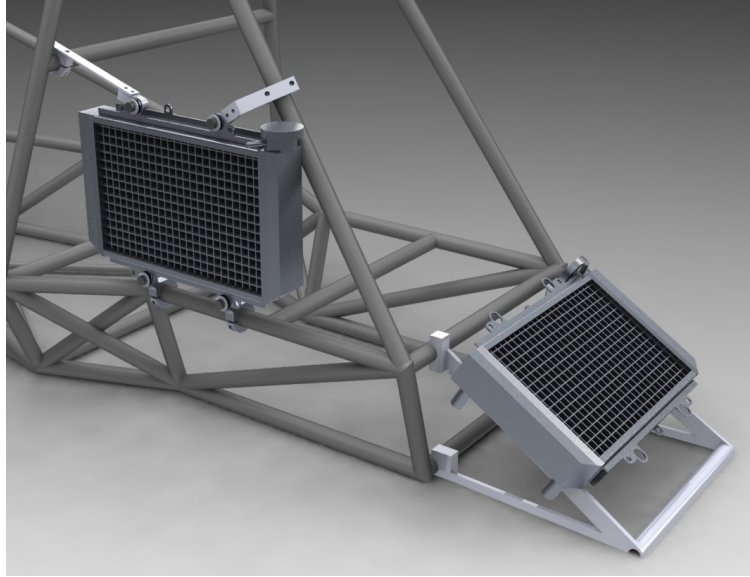


Figure 70. Two Proposed Radiator Positions

The second mount position considered, and the one chosen for the car, is far to the rear of the vehicle on the jack point support structure. The jack point supports are one area of the frame that is low to the ground, is not occupied by any other components, and is well proportioned to fit the radiator core with minimum obstruction. This position requires the use of long coolant hoses to reach the coolant inlet and outlet at the front of the engine, but the low and centered location is beneficial to the center of gravity of the vehicle. Since the radiator is also somewhat protected from flying debris by being beside rather than in plane with the wheels, as with the side mount location, protective mesh is not required for this mount position.

Despite the high angle between the radiator and the direction of travel due to the angle of the jack point supports to which it is mounted, this mount position offers the potential for better airflow than the side position first discussed. In this position, the angle between the direction of travel and the plane of the radiator is 35 degrees, which makes the turn angle of air entering the radiator core 55 degrees. Assuming cosine loss is the only result of this turn angle, the radiator still has $\cos(55) = 57$ percent access to a perfectly horizontal incoming airstream, far more than the 45 percent for the side mount position. Additionally, since the radiator is not shrouded in this position, any upward turn in the incident airstream caused by aerodynamic interactions between the car and ground will allow the radiator to perform even more efficiently. The combined benefits to center of gravity, mounting complexity, and airflow made the jack point the preferred mounting position for the radiator.

To mount the radiator to the jack point, some simple cross braces were bolted between the two sides of the jack point supports, and the radiator was bolted directly to these using some of the mount holes integrated into the radiator design. Anti-vibration mounting using rubber grommets was considered, but an inability to assess the effectiveness of this solution caused it to be discounted. Figure 71 shows the radiator in place on its mounts. Despite the apparent proximity of

the exhaust muffler in this position, this portion of the muffler does not get as hot as the exhaust header, and does not radiate a significant amount of heat into the radiator.



Figure 71. Radiator Mounted to Jack Point on Car

Fan Research and Selection

To provide airflow through the radiator while the car is stationary, different fan options were considered, mainly focusing away from fans specifically designed for automotive use due to the often vague information available about their performance and power characteristics. Fan selection was tightly constrained by the 160-watt maximum output of the WR450F stator, so whichever fan was selected would need to either be highly efficient and run consistently, or push a large amount of air through the radiator to minimize its active time and allow the battery to recover its charge. A 40-watt power limit imposed by the ECE team as a result of other power demands codified this part of the fan selection process.

Using the filter tools on websites such as DigiKey and Mouser Electronics, fan selection was narrowed by a couple of key criteria in addition to the power limit, leaving only a limited set of options. Within the realm of non-automotive electric fans, the selection was narrowed to those requiring 12-volt DC power, since any other voltage would require active circuitry to convert the power supply accordingly. Fans were also filtered to those with IP68 ingress protection ratings to minimize the risk of fan damage due to rain or dust. While some of the fans meeting these criteria stated relatively high airflow compared to their power draw, particularly fans under the Sanyo Denki San-Ace brand, all of the fans which combined high airflow and low power draw also had prices over \$100. These fans also stated low static pressure capability, and even the highest output fan would only produce 100-200 CFM under the approximately 100-150 Pa loads typically expected for radiator applications, far less than the 400 CFM estimated for the test bench fan (Flex-A-Lite, 2010; Sanyo Denki, n.d.). This top performer also stated a power draw of 32 watts, while the test bench fan was measured to draw only about 40 watts in spite of the 80-watt label on its motor housing. Additionally, despite their relatively small 140mm square frame, the Sanyo Denki fans weighed nearly the same as the larger fan on the test bench radiator due to their aluminum frame. Due to this

difficult combination of traits, the prospect of spending over \$100 per fan for the Sanyo Denki fans was unfavorable. Figure 72 and Figure 73 below show one of the Sanyo Denki fans considered, and the fan used on the car, respectively.



Figure 72. Fan Considered (Sanyo Denki, n.d.)



Figure 73. Radiator Fan Used (Auto Dynasty, n.d.)

Due to the unfavorable traits of the Sanyo Denki fans and similar alternatives, the team instead chose to work with the inexpensive seven-inch radiator fan currently used on the engine test bench. During the prior bench testing used to determine the cooling performance required for the WR450F, the test bench radiator and fan combination had been shown to be sufficient, if not excessive, to cool the engine in low temperatures. Since the radiator used for testing had a radiator core similar in volume to the chosen KFX450R radiator, and the power draw of the fan was known via testing to fit within the necessary limit, the team decided that the combination of this fan and the new radiator would essentially be an already proven design, and would thus not require any further testing or simulation to validate the configuration. This fan was also known to be inexpensive, at less than \$30, and was designed to be water and dust resistant due to its automotive specific design. This combination of low cost and high performance made this fan well suited to the purpose, as it would be easily replaced in the event of a failure and would provide plenty of airflow to rapidly cool the engine if passive airflow was not sufficient.

As installed on the car, the cooling fan is oriented in a “push” configuration with the radiator, and is turned on and off by a temperature monitoring circuit. When the engine runs above a certain temperature threshold, either when driving or idling, the fan is turned on and held on until the engine returns below the threshold. The threshold for this system is adjusted through testing, and allows some degree of control over the amount of power drawn by the fan during driving, helping to alleviate potential power draw issues. Due to the high airflow output by the fan, this system results in only brief fan power events, and a majority of quiescent time where the ambient airflow over the radiator is sufficient. At the time of writing, the fan threshold temperature is set to 195 F, just above the 158-194 F idle temperature range stated in the WR450F manual.

Future Recommendations

For future WPI Formula SAE vehicles, the 2018 team recommends attempting more quantitatively based design processes for the cooling system. While driving results have shown that the 2018 car’s cooling system is plenty sufficient for cold weather driving, or even stationary dyno testing, this system has not, at the time of writing, been validated in warmer weather. The insistence on clear validation is also essential to performance in the Formula SAE design judgment if nothing else. Recommendations for future improvement include:

- Physical testing in broader range of air temperatures and engine performance conditions, covering both bench and drive testing as well as hot ambient temperatures
- Simulation validation in lieu of physical testing, if sufficiently high-performance computing resources become available - simulation of radiator heat transfer would require the inclusion of radiative heat transfer, as well as full-scale radiator simulation rather than small subsections.
- Simulation or physical testing of different radiator positions on the vehicle, and consideration of radiator placement in overall vehicle design - positioning for this year was mostly decided by weight distribution concerns rather than thermal performance.

Suspension

Overview

The purpose of a vehicle's suspension is to maintain each tire's maximum contact patch with the ground over bumps and during cornering. For road going vehicles, both driver comfort and vehicle performance need to be considered, meaning that all road cars are a compromise between a soft comfortable suspension, and a firm and responsive suspension. In order for a suspension system to achieve this, suspension geometry, along with spring and damper rates, need to be optimized (1). Additionally, parameters such as vehicle weight, center of gravity, tire selection, and road surface must be considered.

For road racing applications, such as in this project, driver comfort is only marginally considered, and only to the extent as to mitigate driver fatigue while racing. Additionally, as road racing usually occurs on smooth surfaces, large ground clearances and soft, bump absorbing suspension are not needed. Aerodynamic factors also play an important role in suspension design, as under trays must remain as close to the ground as possible without bottoming out, and because increased downforce will change the effective weight applied to the suspension.

The vehicle's chassis is also a key factor in suspension design, as chassis design determines possible suspension mounting points. Additionally, any chassis flex will affect how the suspension works as a system. While this project worked with a previously designed frame, this section covers some best practices to suspension and frame design, while pointing out some issues with the current way the WPI Formula SAE club designs these systems.

Design Formulation

In order to design a well performing suspension, one must determine the conditions that the suspension will be subject to, as well as the key characteristics one would want the suspension to exhibit. Suspension design is often a balancing act, as if one changes a parameter to increase one set of characteristics (ex. Steering feel) it can negatively affect another characteristic (instability under braking). By listing the most important characteristics needed, and the factors that affect them, it will allow for a better understanding of the ideal way to set up the suspension. Furthermore, in an ideal case, suspension design should happen in parallel with the vehicle's frame design, as where the suspension mounts to the frame is extremely important. Figure 74 shows the differences in frame designed in parallel with the suspension and all other car components, and a frame that was not.

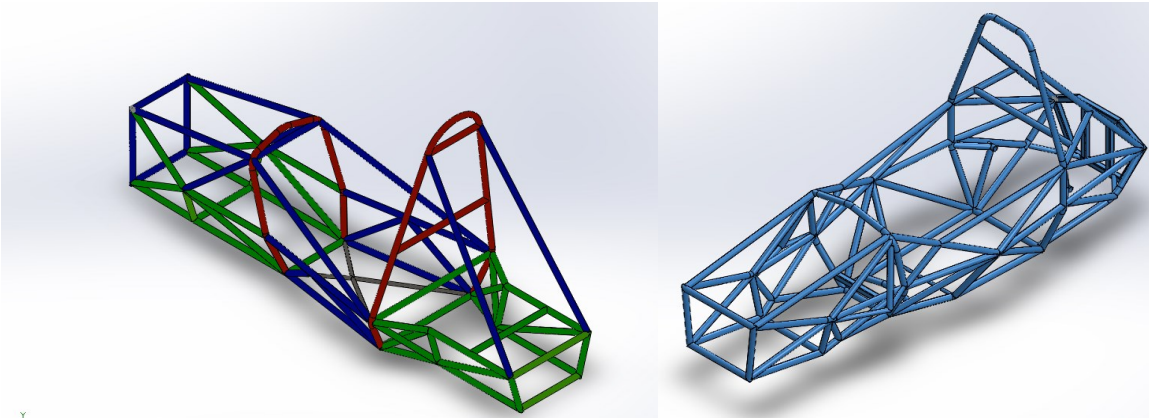


Figure 74. WPI Frame designed before Suspension (left), competitor frame designed in parallel with subsystems (right)

While the WPI frame is easy to manufacture while being simple and lightweight, in order to attach the differential, engine and other components, more complicated and heavy mounts needed to be manufactured. For future redesigns, wheel size, suspension type, differential, etc. should be chosen before frame design starts, and all assemblies should be designed in parallel.

How to Choose Suspension Geometry

Since each suspension parameter affects multiple aspects of the suspension geometry, it is often beneficial to start a suspension design using key parameters to define suspension geometry. For this project, multiple 3D sketches were created in SolidWorks to determine suspension geometry based off of specified parameters (see Figure 75). While this project was to design an unequal length double wishbone suspension, the same principles can be applied to any kind of suspension setup.

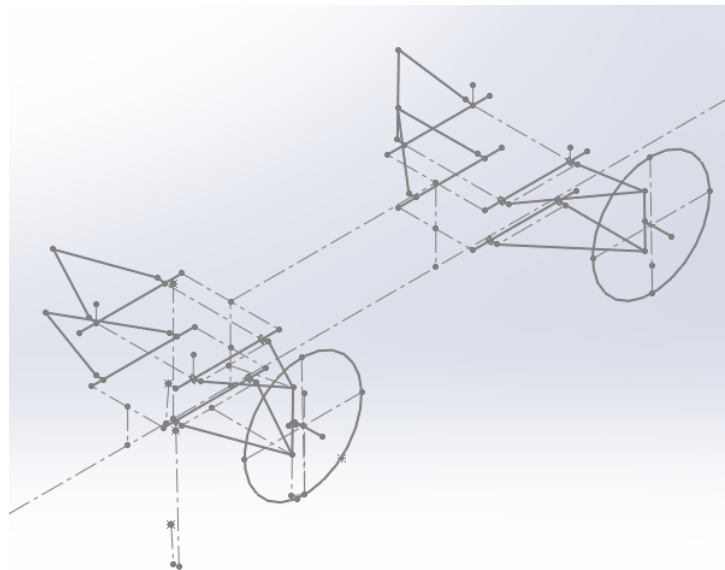


Figure 75. Wireframe model of suspension geometry

The most difficult part of suspension design is choosing which parameters or characteristics are ideal. The key is to keep this one thing in mind:

The suspension's job is to give each tire the maximum amount of grip possible in any scenario (braking, turning, accelerating, corner turn in, slaloms, etc)

While this is much easier said than done, it always needs to be kept in mind during the entire design process. For Formula SAE, the place to start is **TIRE DATA** from Milliken Research Associates (Milliken, 2001). Without tire data there is no way of knowing what half of the suspension values should be (besides comparing to past years and using general rules of thumb). Without this data, the suspension will be entirely guesswork and validating designs to the judges will be very difficult. On top of this, the suspension will most likely not be an ideal design, and dynamic event scores will show this.

Furthermore, suspension and frame simulation is key to understanding how a given suspension and frame will work in the real world. While movable sketches in solidworks will help in determining suspension geometry, it should not be used to conduct dynamic analysis (just use suspension simulation software).

This suspension was designed without tire data or suspension simulation due to time constraints. All values were formulated by analysing the handling characteristics of the 2016 Formula SAE car, and adjusting various suspension values to improve any sub-par characteristics exhibited. Due to this, all values chosen for this project should be checked over and optimized using the appropriate tire data. **Do not make changes until you fully understand the suspension design, geometry, and have simulated the suspension design for this car. Do not make changes just for the sake of making a change.** As of now, the suspension is close to being optimized to the point that without using tire data and suspension simulation software, there is an equally good chance of ruining the suspension as there is of improving it. One of the key areas of improvement that requires suspension simulation software to fully understand and simulate are understanding the dynamic parameters of the suspension, such as roll camber and roll centers (and movement of roll centers during cornering). **Read the parameters that you must fill out and understand in the Design Spec Sheet** that you must submit for competition, all of these factors are important, and if not accounted for, you will be torn apart during the design judging.

As noted before, the vehicle frame and suspension should be designed in parallel. This will allow the suspension mounts to be placed in more ideal locations, and the frame can be designed to comply with all rules at an ideal ride height. This was not done for this project, hence the suspension mount points were for the most part already determined. Ride height was also pre-determined, due to Formula SAE rule T3.24.3, which forced the car to have an excessive ride height of 5.3in.

Design Process

Suspension geometry

Since the frame was already designed, the first step in this project was to create a 3D sketch of the suspension mounting bars on the frame, and determine where on these bars the suspension should mount, shown in Figure 76 below.

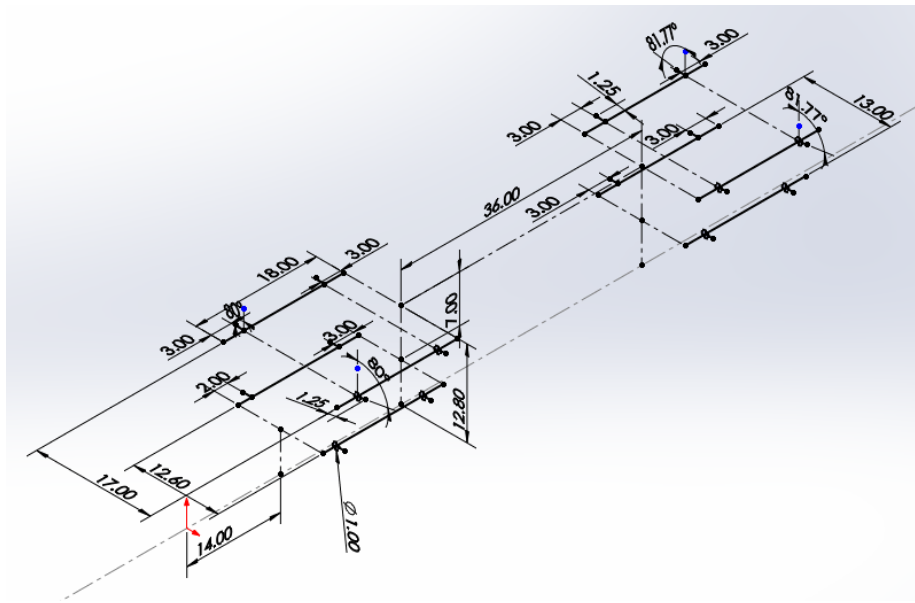


Figure 76. Suspension mounting bars with tab locations

At this stage, any mount locations on these tubes were not necessarily final, as things like wheel clearance during cornering and A-Arm forces could cause these locations to change. As an initial location, mounts were placed close to the ends of the suspension mounting tubes to ensure that the tubes would flex as little as possible when loaded by the suspension. In addition, the mount length, shown in Figure 77 below, was initially guessed at, but was chosen to be 1.25in so that any A-Arm mounting that was used (rod ends, weld cups, etc.) would not contact the frame.

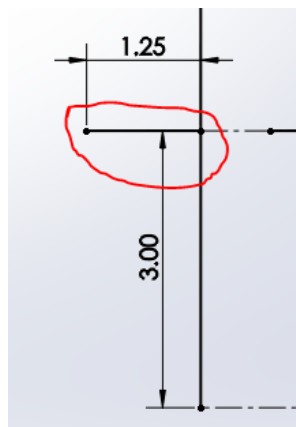


Figure 77. Wireframe sketch of suspension mount point on frame (mount is circled in red)

Once mount points were defined, a 3D “static suspension” sketch was created for the left front and left rear suspension (the final sketch was mirrored to the Right side). At this point a rough suspension shape was defined (see Figure 78), which included A-Arms, Uprights, and wheels (diameter of wheels circled in purple, with a line normal to the wheel diameter to denote the location of the outer wheel face, Track Width (outside to outside) Circled in Blue, Static camber circled in green, caster angle in red, kingpin inclination in pink, wheel diameter in purple).

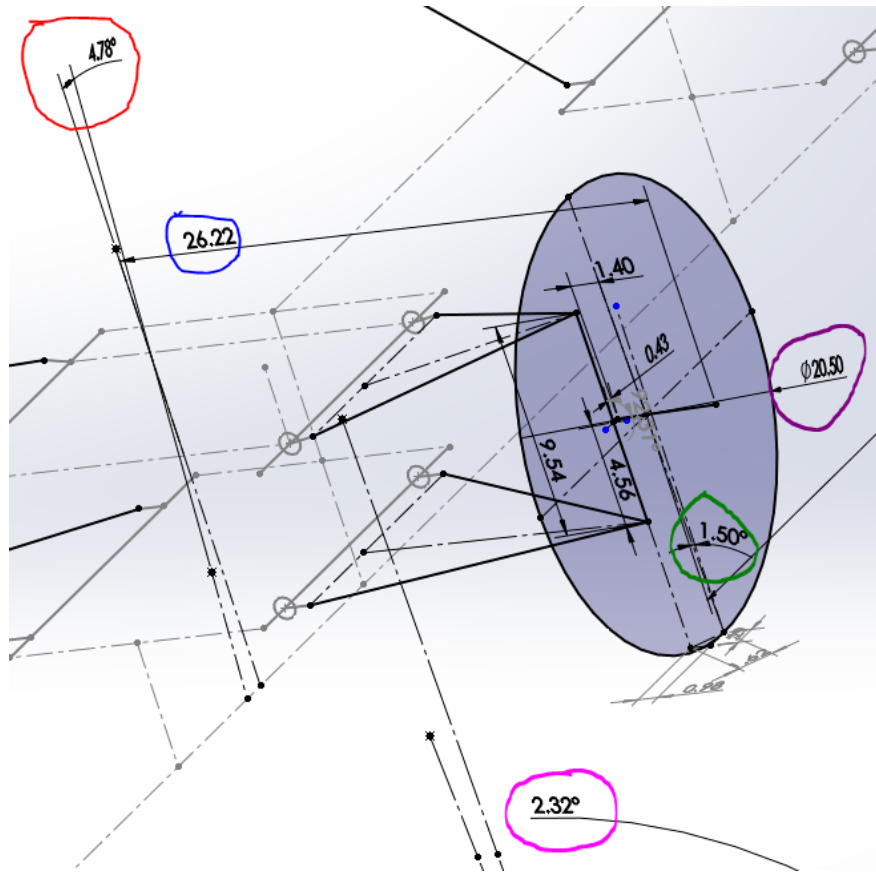


Figure 78. Front suspension wire frame

From there, reference lines were created to make dimensioning easier, and any known dimensions were added (wheelbase, wheel/tire diameter, wheel width, upright height, and track width). Wheelbase was chosen as 61 inches (close to last year), as this would allow for the shortest car possible (the Formula SAE rules specifies a wheelbase of 60 inches or more). The reasons for wanting the shortest car possible is that it allows for a tighter turning radius compared to a longer car with an identical maximum front turning angle. Additionally, a shorter car will allow for the rear wheels to follow the front wheels more closely, meaning that the car will have to turn less to get around a cone during competition. One downside of a short wheelbase is that it will make the car more twitchy, and oversteer will be more sudden (think of the speed of a long pendulum compared to a short one). Front and rear track width was initially chosen to be 26.22in (rolled over from 2016), with the justification being that it is as wide as possible while still fitting into the shop and into the back of a standard pickup truck bed. However, the 2016 cars track width was measured from the

wheel centerlines, and in this project track width was measured from the outside of the wheel. Due to this, the new suspension design was 7" narrower than the 2016 car. This changed the design goal from insuring the car would fit into the bed of a pickup truck, to ensuring that the car would be able to pass the tilt test. the A wide car is beneficial because it means the car will roll less during cornering (less weight transfer from left to right), making the car more stable and allowing the tires to maintain maximum contact patch. However, the wider a car is, the more it will have to move left to right in a slalom, and will not be able to move side to side on course to maximize corner radius. By having a narrow car, it will allow us to better minimize the amount of cornering needed during competition, which is important as the course is extremely narrow. Rim diameter selection is mainly chosen due to packaging. The rims currently used are 13in diameter by 7in wide and the tires are 20.5in tall and 7in wide (same as last year as it is what is available). This was rolled over from 2016 as the packaging constraints would be similar. Aside from packaging and insuring that the car's brakes are big enough to stop the car, the smaller the rim the better. Smaller rims and tires mean less unsprung weight and less rotational inertia (less unsprung weight and rotational inertia is more important than less sprung weight because unsprung weight means the suspension will be slower to react due to increased inertia. Furthermore, less rotational inertia means the engine will have to work less to accelerate the rotating drivetrain components and can work on accelerating the car.), and also means that the tires will heat up to the ideal temperature faster as there is less surface area to heat up. Upright height was directly taken from 2016, and was chosen due to packaging and time constraints.

From there, variables such as kingpin inclination, rim offset, spindle (hub) length (from steering axis), and caster angle were defined (see Figure 78 above). These variables affect multiple suspension parameters, and so their final variables will result in a balancing act that will create an optimized suspension. Rim offset (see Figure 79) was 22mm, as that was the available offset for OZ racing magnesium wheels. These wheels were chosen because they were thought to be the nearly the same as the OZ racing aluminum wheels (used on the 2016 car) from a packaging standpoint (but with an 8 mm offset difference), while being 2 pounds lighter per wheel (reducing both unsprung mass and rotational inertia).

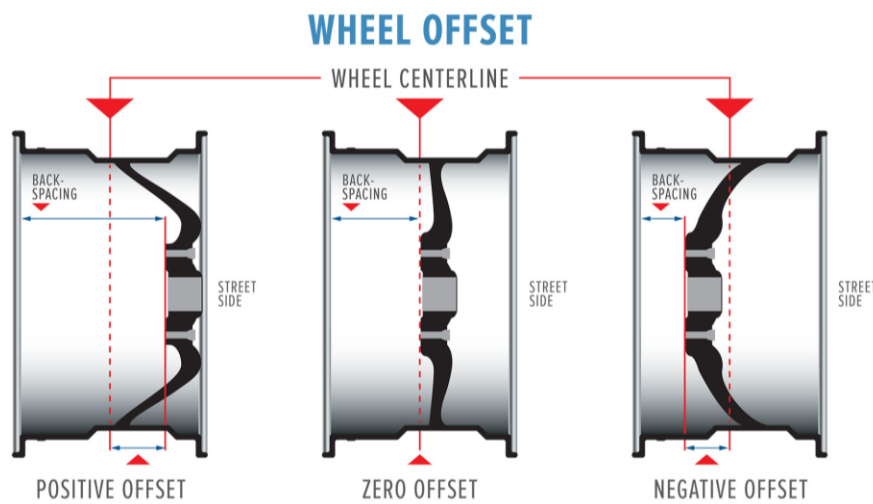


Figure 79. Wheel offset

After purchase it was realized that the magnesium spokes were thicker than on the aluminum wheels, and even with a spacer to make the two offsets identical, the Magnesium wheels would not clear the front brake calipers on the 2016 car. After some design meetings it was determined that brakes would remain the same, and an additional 15 mm would be added to the hub compared to the 2016 car (see Figure 80).

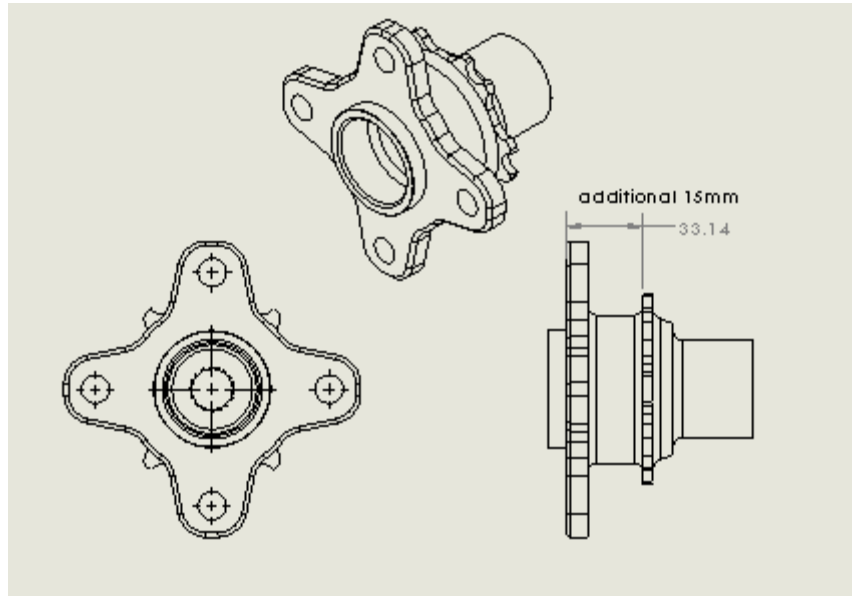


Figure 80. Modified Hub Dimension

Special precaution were taken when manufacturing the hubs because of the fact that they rotate at high rates of speed it is very important that they were well balanced and aligned, any error here could result in vibration and adverse handle characteristics. Every time a part is fixture or moved there is an opportunity for the center axis to be misaligned. This could lead to vibration in the wheel, causing poor driver feeling and decreasing stability it speed. With all this in mind, an effort was made to produce the hubs in as few operations as possible. With the implementation of advanced CNC machines, this was found to be two. The first operation took place in a Hass ST30-SSY, this is a large lathe with live tooling and fourth axis capabilities. With this machine the part was able to be roughed to size by turning, have the board drilled through the middle, and have the geometry milled in for the brake rotor. In the rear hubs, a spline was also cut into the inner diameter, that would later match up with the outer CV joint. The second operation took place in a Hass VM-2 mill. This operation cut off the excess material that was used to hold the part in the jaws on the lath, and cut the clover pattern that would hold the wheel studs. After machining the wheel studs where pressed in and the wheels there fit.

Kingpin inclination was set as 2.32 degrees, and caster angle was set at 4.78 degrees (see Figure 78 for dimensions, and Figure 81 for definitions). These values were based off research and driver feedback from the 2016 car.

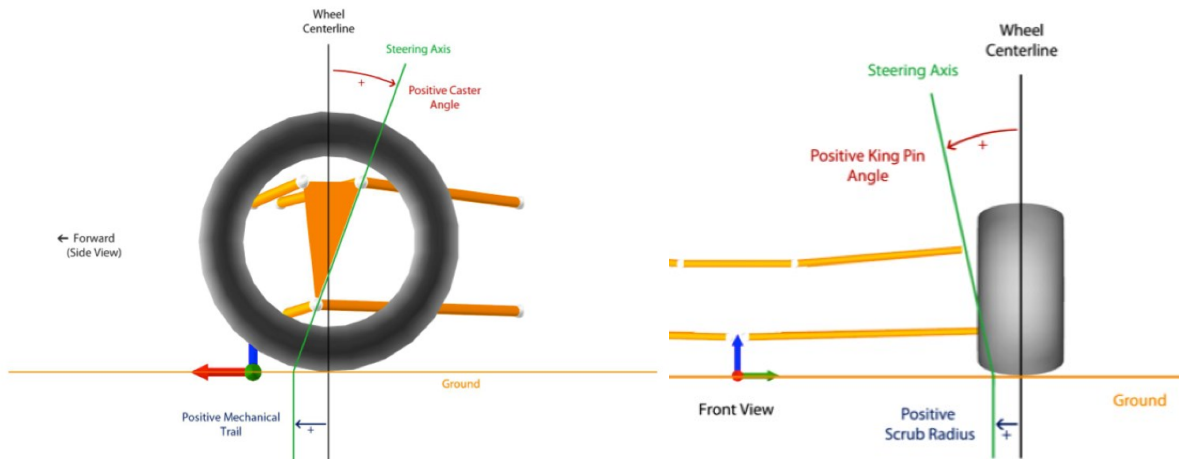


Figure 81. Caster angle and mechanical trail (left), Kingpin inclination and scrub radius (Right)

Both caster angle and kingpin inclination effect steering feel and steering effort (mainly due to scrub radius but also due to other factors) (Kojima, 2011). As the 2016 car was very easy to turn, but had minimal steering feel, it was decided that steering feel should try to be increased at the cost of increased steering effort. Additionally, increased kingpin inclination will result in increased positive camber gain on the cars outside wheel (bad), and increased caster angle will result in negative camber gain on the cars outside wheel (good to an extent). There are also other factors that are affected (Kojima, 2011). Tire data will make it easier to choose these variables, as the best camber gain for the tires used will be clearer.

Once these variables were roughly defined, reference dimensions were created to show dependent variables such as static camber, scrub radius, roll centers, etc. to help with the selection of the best suspension parameters. Static camber is important for initial corner turn in, and for high speed corners where there is minimal steering induced camber gain, however it will reduce straight line traction as the tire contact patch is reduced (especially important for rear wheels, as traction while accelerating is important). Static front camber is 1.5 degrees, and static rear camber is 1 degree. The rear static camber is lower than the front, but in the future the rear static camber should be further minimized (may reduce turn in grip) and replaced with more camber gain due to suspension compression (depending on tire data and testing). Scrub radius (see Figure 81) is a function of kingpin angle and wheel center point relative to the steering axis when viewed from the front plane. The bigger (more positive) the scrub radius, the more steering effort will be required, but will result in increased stability and steering feel. You do not want negative scrub radius.

Mechanical Trail is a function of caster angle and wheel center point relative to the steering axis in the vehicles side view. The bigger (more Negative) the Mechanical Trail, the more steering effort, but the more self-centering and steering feel. Positive scrub radius is bad as it makes the car want to wander and will not self-center.

Once the static suspension sketch is fully defined, a “dynamic suspension” 3D sketch can be created that will allow suspension parameters to be looked at through the suspension’s range of motion, such as camber gain due to suspension movement. Additionally, a “dynamic steering”

sketch can be created, that allows the front wheels to turn (see Figure 82). This will allow for parameters such as camber gain through turning to be roughly determined. As noted before, suspension simulation is crucial at this point in the design process, as it allows evaluation of suspension movement under real world scenarios. Without this simulation, there is no way of knowing how the frame (hence the suspension mount points and the suspension) will rotate and move during a corner.

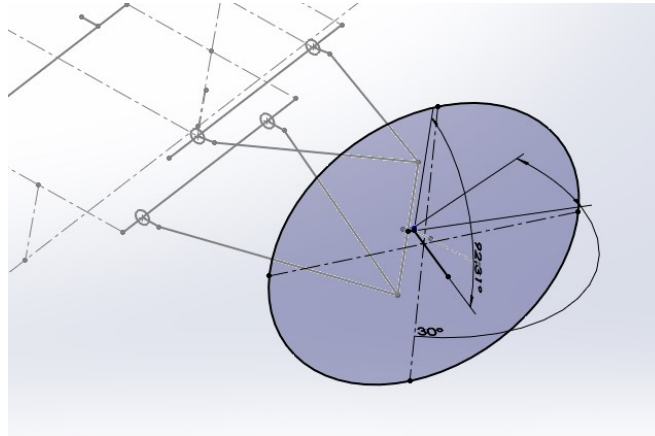


Figure 82. Dynamic Steering and Suspension Sketches

At this point in the design, once the suspension was roughly defined, the “suspension mockup” part, containing all the suspension sketches, can be inserted into an assembly, and wheels, uprights, etc. can be mated to the dynamic suspension and steering sketches to ensure that there are no collisions with any parts (see Figure 83).

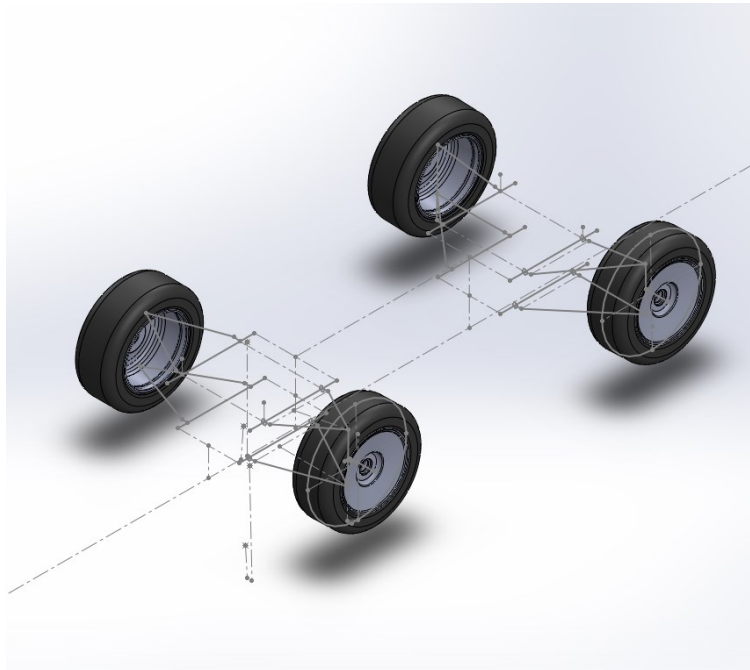


Figure 83. Suspension assembly with “suspension mockup” and “wheel” parts

Once all suspension has been nearly finalized, an “A-Arm tube” sketch can be created that references the static suspension sketch (in some cases the new sketch isn’t necessary, but in this case they were needed to make the A-Arms line up properly with the mounting method chosen) (see Figure 84).

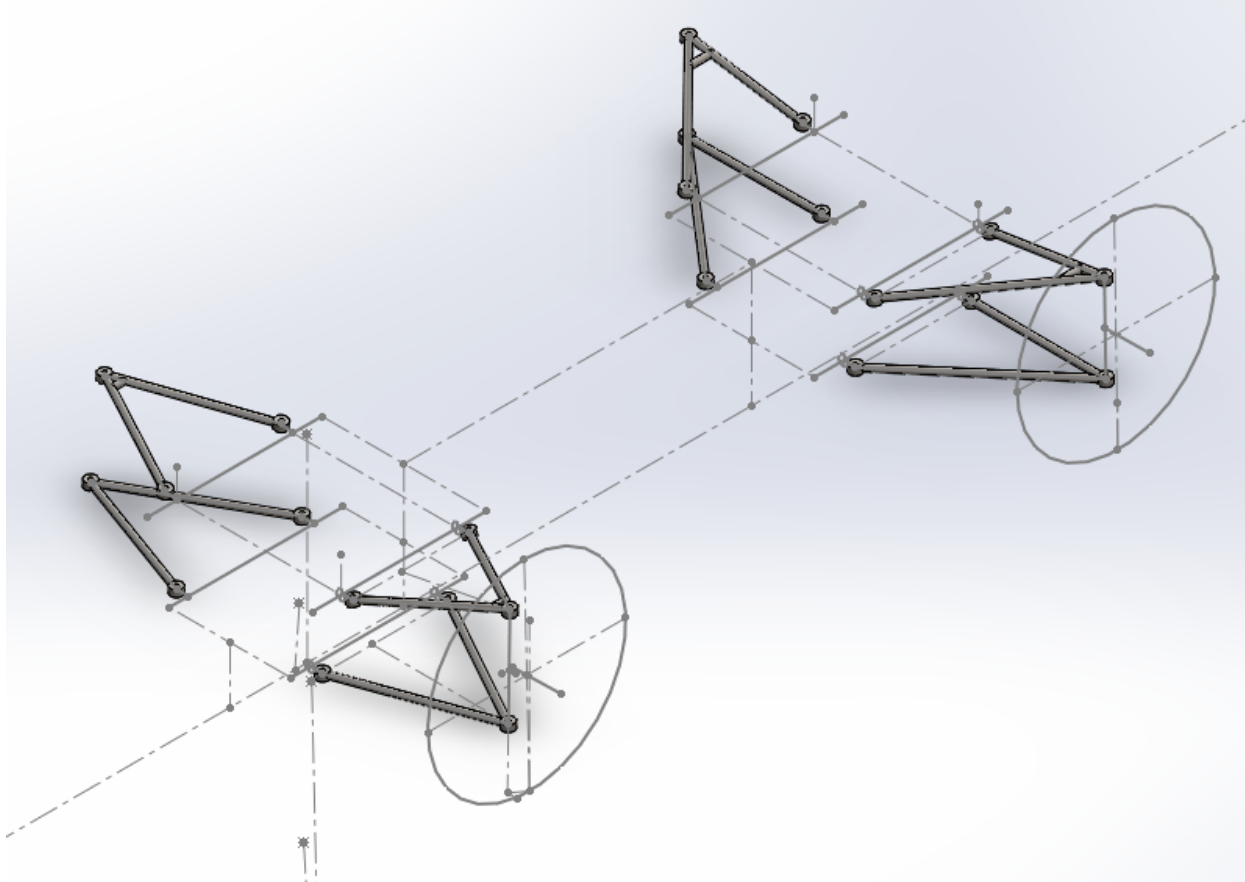


Figure 84. A-arm tube profiles in “suspension mockup” part

A-Arm Design

A-Arm design involved both figuring out needed geometry to match the wireframe suspension, and determining needed strength properties. By using the design process outlined in the above section, the geometry portion of A-Arm design was already mostly finished, however there are a few factors that still needed to be determined.

The first step in A-Arm design was determining what type of spring and damper actuation would be used (Pullrod, Pushrod, Direct acting, ect.). It was decided that a pullrod design would be ideal as it would allow for the weight to be lower down than a comparable pushrod design, which was critical to insuring the car would pass the tilt test (also because it was used on the 2016 car and worked well). A direct acting suspension was not chosen, as when it had been used in the past the long rod connecting the spring to the A-Arm created a bending moment that fatigued the threads in the end of the damper (see Figure 85).

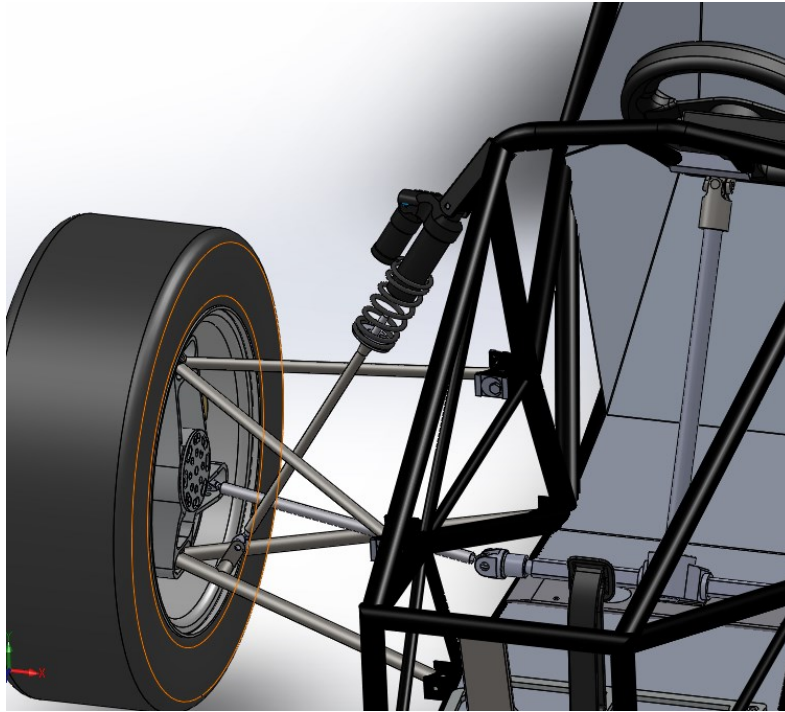


Figure 85. 2015 Front Suspension (long pushrod created bending moment and wore out shock absorber)

Once this was determined, it was clear that a pullrod tab needed to be mounted to the upper A-Arms. The easiest way to mount the tab was with a crossbar across the A-Arm, which was made as short as possible (while still allowing for it to be easy to weld) to make the bending moment applied to the A-Arm as small as possible (see Figure 86).

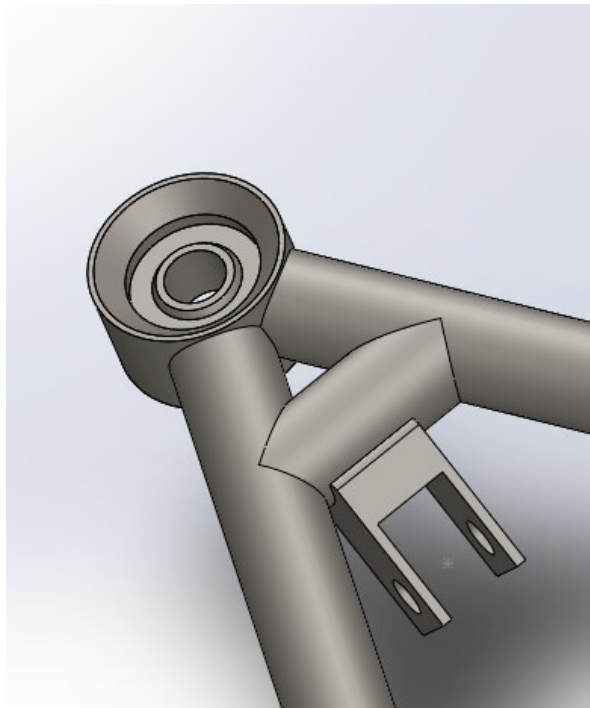


Figure 86. Pullrod Tab and Crossbar (front suspension)

Once this was done, the forces that would be applied during use needed to be calculated, including forces due to Braking, accelerating, cornering, and bump effects. Most teams use 1.5G for the braking, acceleration, and cornering forces, and 3G for a bump force. To calculate A-Arm forces, weight transfer was determined for the 1.5G forces to determine the force on each wheel. From there, the force on each A-Arm where it attaches to the upright was calculated (simple statics problem). Additionally, forces applied due to the pullrod can be calculated (also simple statics problem).

The material for the A-Arms was then chosen to be 4130 steel tubing (carbon fiber tubes would have been ideal, but were too expensive. They were also ruled out as attaching them to the metal threaded ends can be difficult to do correctly, causing them to fail). 4130 tubing was chosen because of its high strength to weight properties, and because tubing has a high resistance to bending. One thing that must be considered when welding 4130 is that it must be TIG welded (due to needing to be preheated), and can only be welded to other 4130 (welding to any other kind of steel will make the connection extremely brittle). Once the material was determined, the team had to determine how they would be made. For tube profiling VR3 Engineering was chosen, which restricted tube selection to the sizes offered by VR3. To determine an appropriate tube size, the proposed design of the A-Arms were modeled in SolidWorks. This was done by first creating an A-Arm sketch in the “suspension mockup” part file, creating extrusions to recreate weld cup placement, and then using custom weldments to create the A-Arm tubes. Each A-Arm was exported to a new part file by selecting the tubes and extrusions for each A-Arm, right clicking, and then selecting “export into new part” (see Figure 87). Once each A-Arm has been exported to its own part, FEA was run using the forces calculated previously by hand. The Frame side of the A-Arms are fixed with spherical fixtures (see Figure 88), and the crossbar was fixed from translating in the Y direction (see Figure 89). The forces calculated are applied to the upright side of the A-Arm (see Figure 90).

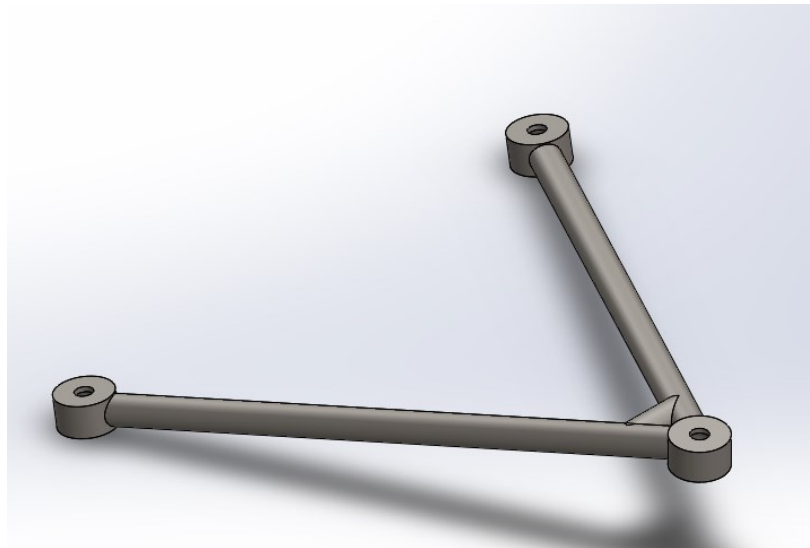


Figure 87. A-Arm part

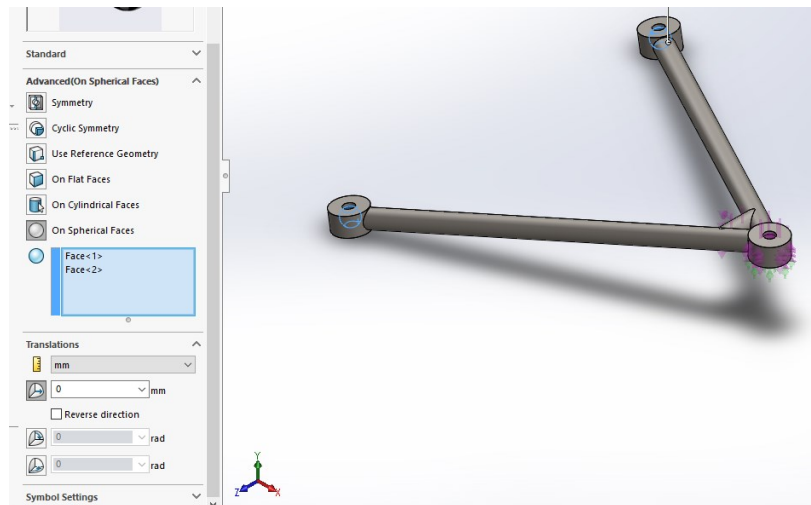


Figure 88. Spherical A-Arm fixtures

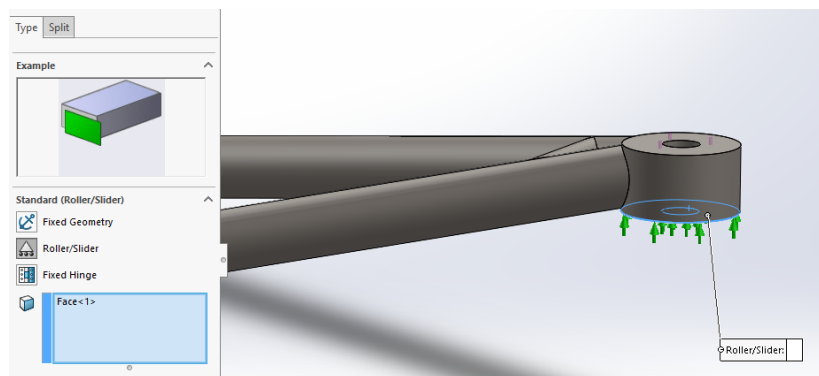


Figure 89. Slider A-Arm Fixture

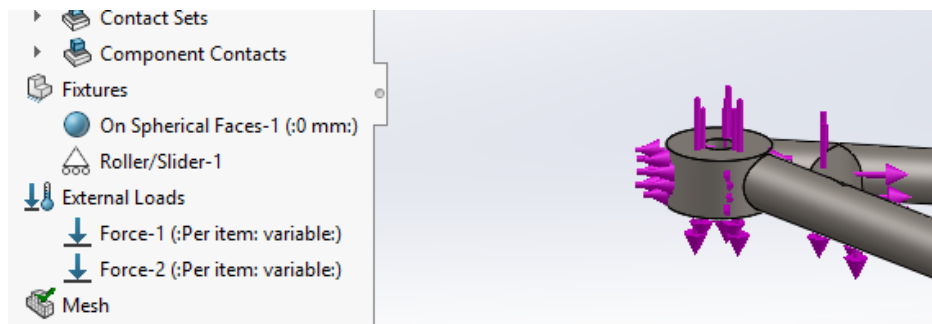


Figure 90. Forces applied to A-Arm

Tube selection was a trial and error procedure, with the goal to find the lightest tube size that would have a factor of safety of 2 or higher. Ultimately, a tube size of 0.625OD x 0.058Wall was chosen, as it seemed to be a good compromise between strength and weight (was also a slightly smaller size than the 2016 car). Running the FEA was especially difficult, as the tube profiles had issues meshing. To solve this the mesh element size was made very small (.1057in for the front, and for the rear), and a Blended curvature mesh type was used for the front, and a standard mesh was used for the rear (see Figure 91).

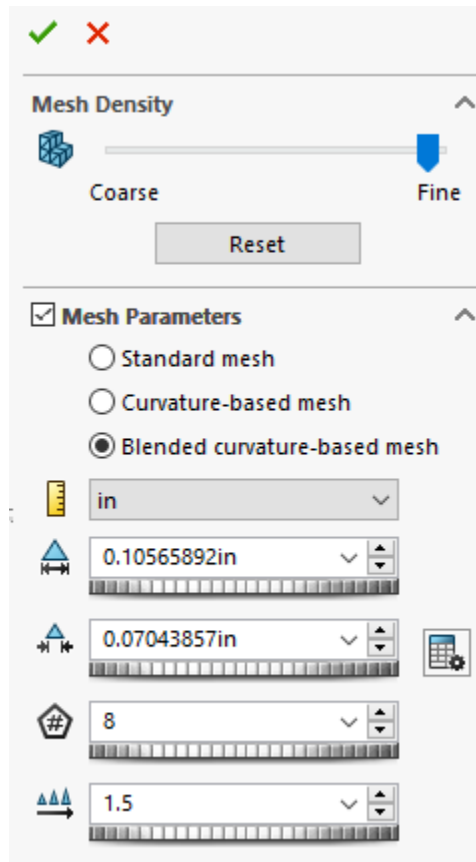


Figure 91. Mesh Parameters for Rear A-Arm

In the future this meshing should be validated for accuracy, as the results may have a large error. Another issue that was encountered was that there were a few points where the stress seemed to be unreasonably high. After looking it over and looking more into stress concentrations, it was decided that the high stress must be an error in the FEA, and so would be ignored (however a slightly thicker tube size was chosen than than the FOS goal required to account for potential errors in setting up the FEA).

Rocker Design

The goal of the rocker is to translate the motion of the spring and damper into movement of the wheel. This can be done in a multitude of ways, but the two primary styles are pullrod type and pushrod type. Pushrod actuated rockers, as the name implies, are actuated by a rod that is pushed by the suspension as it compresses, actuating the rocker and spring. Pushrod designs are usually simple, and linear, however the rockers are usually placed above the suspension, meaning that the majority of the systems weight is placed relatively high up on the car. Pullrod actuated rockers are similar to pushrod activated, except as the suspension compresses it pulls the pullrod, rotating the rocker and compressing the spring. The benefits of this style of actuation is that because the suspension pulls the pullrod, the rocker and spring are usually below the suspension, meaning the majority of the systems weight is near the bottom of the car.

For this project, the rocker was designed such that all motion was as linear as possible. This was done because the rocker design for the 2016 (see Figure 92) car had binding issues, as the rockers were not loaded linearly throughout suspension travel.

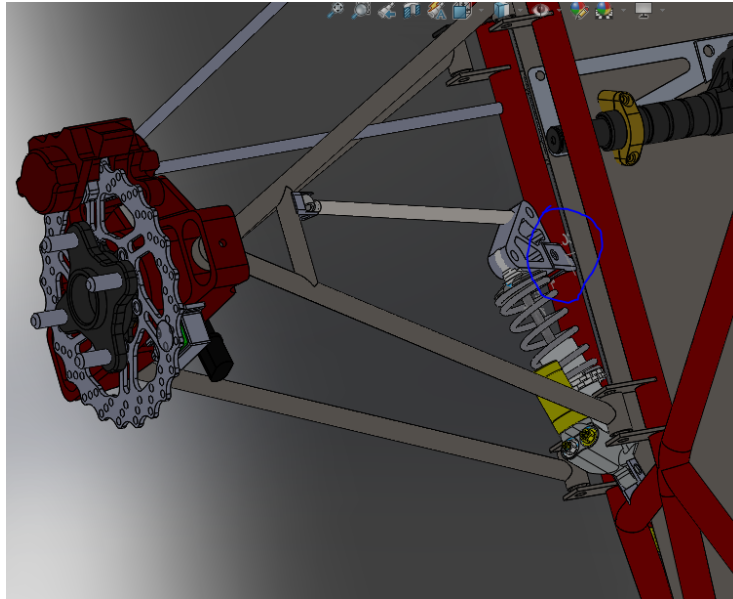


Figure 92. 2016 Front suspension (Experienced binding and excessive tab wear at tab circled in blue)

The initial design was purely linear, with the frame, damper, and pullrod mounts all being on the same plane (see Figure 93).

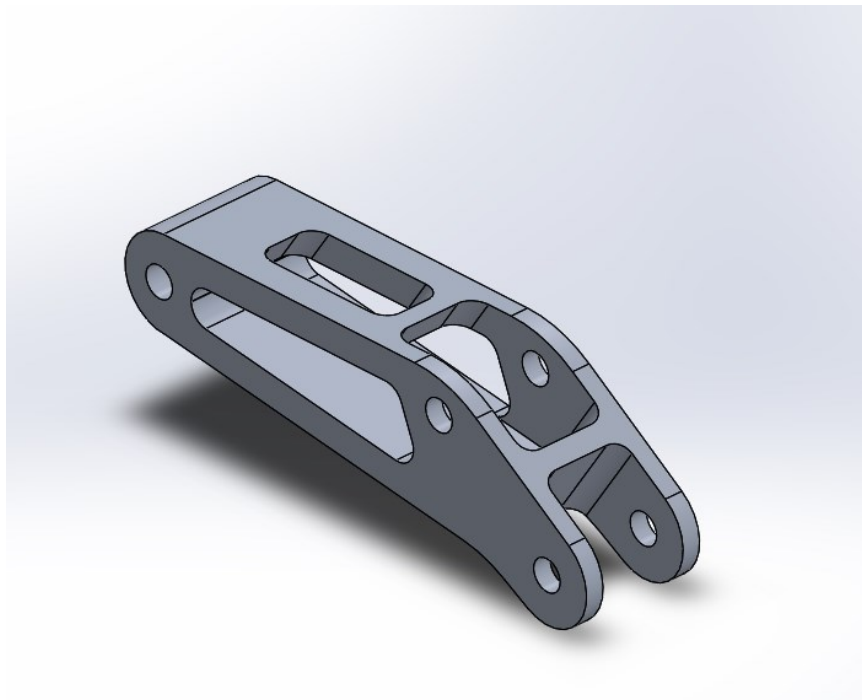


Figure 93. First Iteration of Rocker Design

However, the chosen shock absorbers had 2in of travel, which was also the amount of wheel travel desired. Because of this, the initial rocker idea was discarded, as it would provide 4in of wheel travel or more depending upon the geometry. A new design was created, that allowed the pullrod to be mounted closer to the frame than the spring and damper (see Figure 94).

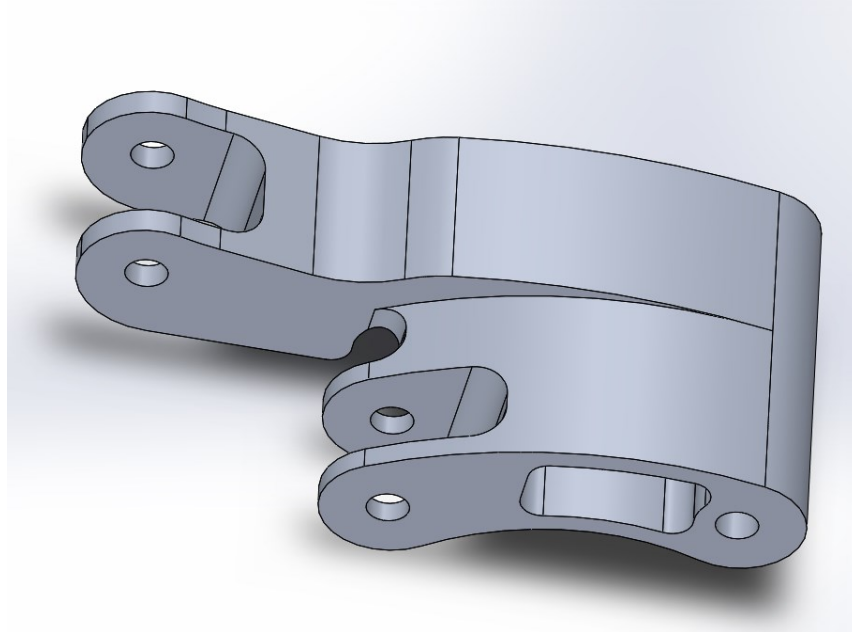


Figure 94. Final Rocker Design

One downside to this design were that because the frame, damper, and pullrod mounts are not in line, creating a moment that could increase the chance of binding. Additionally, this rocker design is slightly heavier than the 2016 rockers. This rocker design was based around giving the wheel a similar overall travel to that of the shock (2in). This was a very basic approach, and in the future, motion ratio and damper information should be taken into account. The final motion ratio for the front was 1.31-1.41, and for the rear was 1.35-1.45. These values were not 1:1 due to the placement of the pullrod tabs on the A-Arms, which were not taken into account when designing the rockers. By using suspension simulation this could have been identified and corrected.

The rockers were machined from extruded 7075 aluminum. Although they are small parts and little material removal was actually needed they were intricate little parts. Each rocker took 3 operations to machine. For this part a Hass Minimill was used. The first operation had the block standing vertically on the long end and cut the profile of the lobe that would be used to connect the pull rod. Then the block was flipped over and held in a set of soft jaws, while the profile of the lobe that would hold the shock was machined, during this operation a through hole was drilled to mount the rocker to the frame. The last operation was to lay the parts flat in the vise and cut out the notches where the pull rod and shock would attach. In order to hold the part flat in the vise custom profiled parallels that matched the contours of the rocker were used.

Spring and Damper Selection

Selecting the appropriate spring and damper combination often involves using some baseline assumptions, testing, and then making any needed changes. This process may be able to be streamlined using suspension simulation, however, this project did not attempt this. For this project, many of the assumptions and equations used in determining the initial spring and damper setup were obtained from either the Optimum G website (Technical papers, 2017), or from “Race Car Vehicle Dynamics”(Milliken, 1995). The dampers selected were Ohlins TTX25 with C12/R12 valving, as these are a common choice for Formula SAE teams, and because the WPI team had experience with them in past years. To adjust the damper to match the damper rates chosen, the damper graph for these dampers was found on the Ohlins Formula SAE website and the dampers were adjusted to the desired settings (Ohlins TTX25 MkII Product Page, (n.d.)).

The first step in this process was to determine key vehicle specs, such as center of gravity, sprung mass per wheel, and motion ratio, which should have already been calculated and factored into all designs. Once this is done, a sprung mass natural frequency must be chosen. Based off Optimum G’s website, a value of 3Hz was chosen for the front suspension, and 2.7Hz was chosen for the rear. The spring rate could then be calculated using the below equation (Technical papers, 2017).

$$K_s = 4\pi^2 f_r^2 m_{sm} MR^2$$

K_s = Spring rate (N/m)
 m_{sm} = Sprung mass (kg)
 f_r = Ride frequency (Hz)
 MR = Motion ratio (Wheel/Spring travel)

After converting the spring rate to Lb/in, the front spring rate was calculated to be 240Lb/in, and the rear spring rate was calculated to be 193Lb/in.

The next step was to determine the damping ratio (percent of Critical Damping), which was chosen to be .7 for both the front and the rear, as this is a common starting point for race cars (Technical papers, 2017). The high and low speed damping values were determined in a similar manner, and all equations can be found either in the Optimum G articles, or in a spreadsheet in the WPI Formula SAE google drive, labeled “2018 (Initial) Spring, wheel rate, Damping Ratio, and roll rate Calculations”. These values are only rough initial guesses, and the values should be further refined based off of skid pad, slalom, and autocross testing, as well as off of driver feedback.

Steering

The steering system of any vehicle is extremely important because it controls changes in direction of the vehicle. This is useful because there's almost no point during the competition that the car will not need to turn. Weight transfer is another important function of the steering system as well as other car systems.

To be able to optimize the performance of the car at competition, there were a few design parameters that had to be considered. These parameters included steering weight and feel as well as steering wheel angle and tire and rim angles.

The steering system itself is composed of many different parts from the driver input to the movement of the wheels. The steering wheel is the portion that the driver touches and moves to provide input. This then turns the upper steering shaft into the steering box. The purpose of the steering box is to change the direction of the force from nearly horizontal to nearly vertical. From the steering box comes the lower steering shaft which sends force down to the steering rack. The steering rack changes rotational motion into linear motion. The ends of each side of the steering rack are connected to the uprights inside each wheel via a tie rod. The uprights make the wheels and tires turn, thus turning the car.

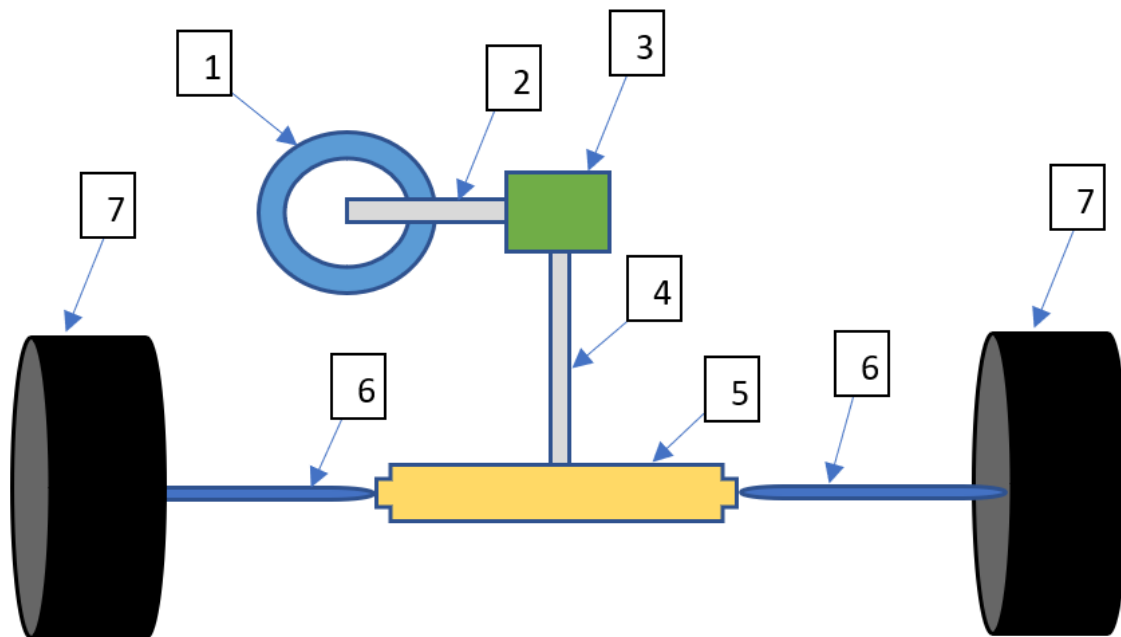


Figure 95. Simplified steering system diagram.

(Steering wheel (1), upper steering shaft (2), steering box (3), lower steering shaft (4), steering rack (5), tie rods (6), wheels/tires (7))

The steering wheel, being the part that is touched by the driver, is a very important part of the steering system. There are a few parts that were incorporated into the steering wheel because of the rules of the competition as well as making the car easier to use. The first component is the quick release spline on the back of the wheel. This is required to meet the competition rules as having a detachable wheel makes it much easier to get out of the car quickly in case of an emergency. Another design that was incorporated are the pogo pins inside of the quick release spline. These pins are used to connect the electronics in the steering wheel to the rest of the car. The electronics on the wheel include the paddles for the shifting as well as backup buttons in the event a paddle fails. Besides these components, some other considerations for the steering wheel are the size and shape. The conventional shape of a steering wheel is a circle but a more common shape for racing purposes is an oval or a circle with a flat bottom. These shapes save on vertical size when the wheel is in the straight position as well as providing more space under the wheel for driver legs. The wheel used employed a circular shape with the exception of the flat bottom.

From the steering wheel there is a steering shaft into the steering box. This shaft has a few features that are needed for it to function properly. The first part is the spline on the steering wheel side so it can connect to the wheel. After the spline there is a washer welded on that will keep the roller bearing in place against the bearing race. moving towards the center of the box, there is a keyway cut in to allow the connection of a gear.



Figure 96. Steering shaft from the steering wheel to the steering box.

The steering box is the portion of the system that redirects the rotational motion from the steering wheel down towards the steering rack. The way that the steering box works is with a set of spiral miter gears that are made to transfer motion 90 degrees.

The design of the steering box in the previous car was good but had a lot of room to improve. Overall it was quite complicated, and seemed overbuilt for the forces that it would be facing. There were some portions that were able to be kept though.

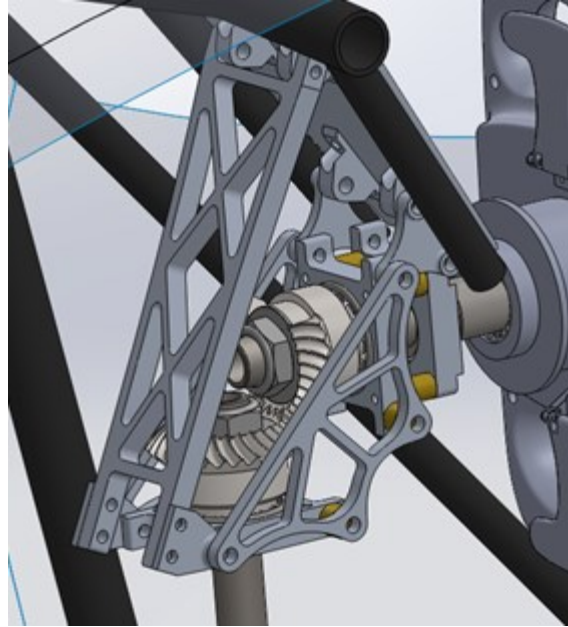


Figure 97. Old Steering Box Design

The miter gears that were used in the previous design were one of the strongest parts of the previous design. While most teams use universal joints, and have success with those, using miter gears gives much less play in the overall system and is also much stronger. Regular miter gears had been shown, in the previous design process, not to have smooth operation as well as having a lot of backlash. The gears that were used before and will be used in this car are spiral miter gears. The spiral cuts allow for much smoother operation as well as backlash mitigation.



Figure 98. Spiral Cut Miter gears

Along with the gears, the bearings used in the previous car will also work well in the new design. The tapered roller bearings that had been selected were chosen to handle the axial and radial forces applied to the steering system during the use of the steering system. The bearings that were used before had no issues, so the same ones will be used again.



Figure 99. Tapered Roller Bearings

Because the steering box design will be overall similar to previous years, the pieces that hold the bearings can remain very similar to the way they were in the previous car. The only change that has been made to them has been making them one eighth inch wider to avoid the need for spacers on the side. The reason for getting rid of the spacers is to reduce the number of overall pieces in the system.

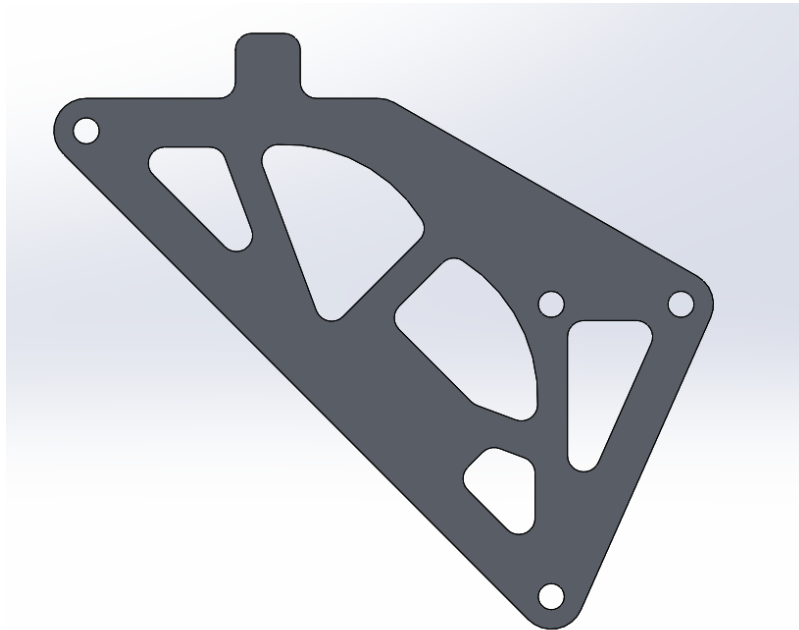


Figure 100. The new side panel design

While there were a few good parts of the old version of the steering box, there are also many things that could be improved. The most prevalent is that the overall design is too complex. There are many pieces that are not really needed. There are spacers on each side that add unnecessary pieces as well as a cover plate that is not really justified. As well as being too complex, the mounting points are quite spread out. While this was not a problem for the previous car because of the higher roll hoop, the new car does not have space for spread out mounting points.

The first problem that was addressed while redesigning the steering box was the height relative to the front roll hoop. In the old car, the steering box hung quite far below the roll hoop. Because the roll hoop is lower in the new car, the steering box needed to be raised as much as possible. This was first done by changing the setup of the mounting points from using a top cover with high mounting points to close mounting points on the front most bearing mount. This alone was not enough to pass the template through as it needed. To move the steering box even higher up, the gears had to be flipped over.

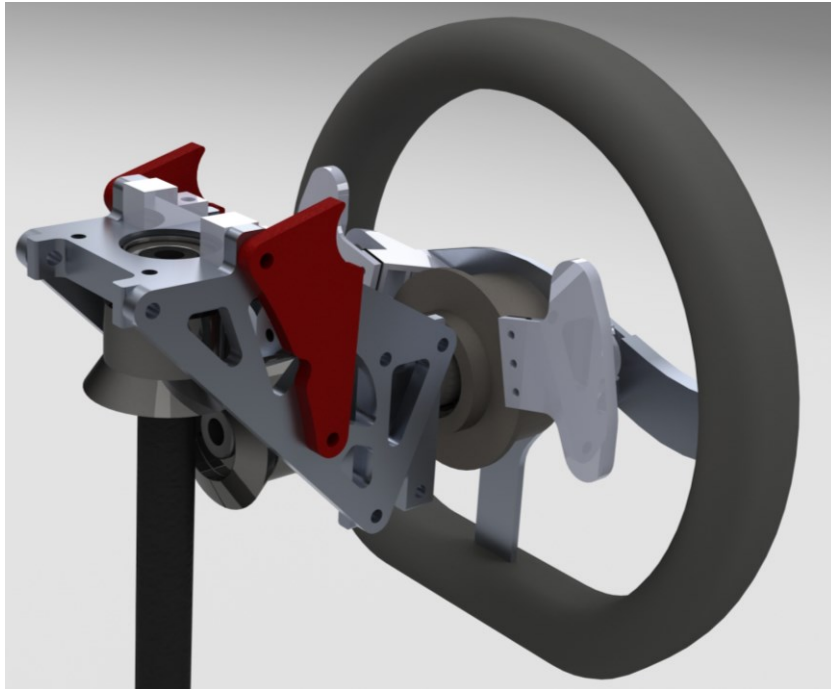


Figure 101. SolidWorks model of the new steering box design

Flipping the gears allowed the template to pass through under the box and still have the steering wheel be below the front roll hoop.

As mentioned before, the steering box of the previous car was overcomplicated. To simplify the box, the sides were completely simplified to be only one piece. There are cuts to allow for screws as well as larger ones to save weight where possible. The sides are $\frac{1}{4}$ inch thick aluminum. This flat piece was possible because of the widening of the bearing mounts. This extra width negated the need for spacers on the sides.

Another major change to the steering box was the method of mounting to the frame itself. The old steering box mounted to the frame using pipes welded on with a sheet of steel in between. The box mounted via screws through this steel sheet. The new way that the steering box was attached was with vertically oriented steel tabs. These tabs were positioned so the steering box fits nicely in between them and mounts with screws to the side plate. The reason this mounting style was chosen over the previous method was because the previous method was too wide to work with the lower roll hoop. The template that must pass forward through the car has a small cutout in the

top that allows for things that are hanging down. The pipes would have to be much wider than the steering box itself. This caused interference in this template and the car would not have passed.

The steering box with the new mounting style and simplified sides was much simpler to machine. There were only three different parts that had to be made. There were the two side plates, the three bearing mounts, and the spacers between the two front bearing mounts. The two side plates were able to be laser cut because they are only a 2d design. They are also made of quite thin material. The finish on the edges was not very good after getting cut so they had to be gone over with a deburring tool. The bearing mounts were CNC machined because they were a more complex design with 3d features. These parts also needed to have a high level of precision to ensure a pressed fit of the bearing cups into the mounts themselves. To make sure this was the case. The bearing mounts were not machined until after the bearings came in to confirm the dimensions of the parts.



Figure 102. Old bearing mount

The steering column, the shaft from the steering box to the steering rack, is composed of three segments. The topmost portion is one inch of 3/8-inch thick steel tubing. This section has threads cut into it for the securing the bolt as well as the keyway for the gear. The middle section is a thinner 1/16-inch walled tube. This middle portion is thinner because there are no cuts in it and some weight was saved with this lighter shaft. The bottom piece is the splined connector to the steering rack. This part is welded onto the bottom of the thinner tube.

The steering rack was a very important decision for the car. The rack that was used in the previous car was the second choice for the team and was only used because the KAZ steering rack was unavailable at the time. Luckily the KAZ was available for purchase for the new car. The KAZ was decided upon using a decision matrix. The matrix from the previous car is shown in Table 10 below. This matrix was used again this year. It was looked over and was the same as it had been. Table 9 compares the two steering racks, and Figure 103 shows the chosen KAZ rack.

Table 9. Steering rack specifications

	Kaz Technologies	Pro-Werks Stiletto
Specification	Value	Value
Weight	3 lbs	2.74 lbs
Materials	Gear: Steel, Case: Aluminum	Gear: Steel, Case: Aluminum
Rack Travel	3.25 in	4.5 in
Pinion Rotation	246 degrees	315 degrees
Rack Travel/Rotation	4.75 in/rotation	5.14 in/rotation
Mounting System	Outboard Collar Mounts	Inboard Bolt Holes
Sensor Integration	Yes	No
Cost	\$670	\$328

Table 10. Steering rack decision matrix

		Kaz Technologies		Pro-Werks Stiletto	
Decision Factor	Weight	Score	Value	Score	Value
Steering Range (Angular)	7	10	70	8	56
Linear Motion Range	9	6	54	8	72
Cost	8	4	32	9	72
Durability	10	10	100	4	40
Weight	4	7	28	10	40
Totals			284		280



Figure 103. Kaz Technologies steering rack

The tie rods are the link between the steering rack and the uprights. They need to be strong enough to not break yet remain light to keep the total weight of the car down. Hollow steel tubing was selected to fulfill this role. On the ends, there are nuts welded on to allow connection to the tie rod ends as well as providing adjustability. The ends closest to the uprights will have left hand threaded hardware to allow the tube itself to be rotated to adjust the toe angle of the wheels. The rod ends on both sides are steel spherical joints. Both ends will be secured in their position on the threads with jam nuts.

Once the steering measurements had been finalized, the steering ratio, c-factor and steering arm length could be calculated. The steering ratio is the ratio of the angle that the steering wheel is turned to the angle that the wheels turn. The c-factor is the amount the actual rack part of the steering rack moves with one turn of the pinion. It is completely defined by the steering rack itself. The steering arm length is the distance between the axis of rotation of the upright and the connection point of the tie rod to the upright. The steering ratio is 4.6:1, the c-factor is 120.8mm and the steering arm length is 92.4mm.

Once a steering rack and implementation method had been chosen, it was necessary to determine the max output angle needed at the tires to be able to navigate the course. The Formula SAE rules state that the minimum radius for the outside of a corner will be no less than 14.75ft through an angle of no more than 135 degrees. Figure 104 is taken from the 2015 Formula SAE MQP report and shows that when optimized for the best driving line the minimum turning radius needed is 16.5ft. The minimum turning radius of the 2015 was set to 15ft. With this in mind and driver feedback from the last car it was determined to that a goal of 14ft would be set for this year.

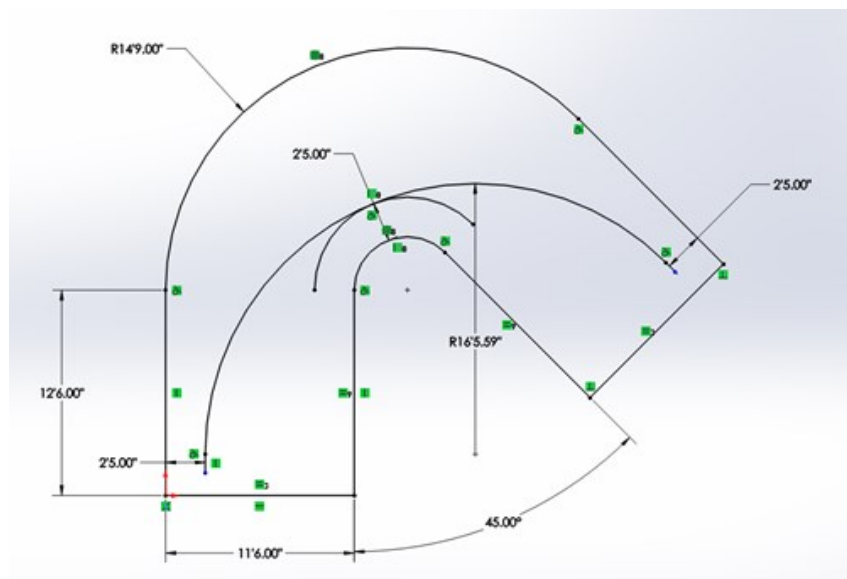


Figure 104. Optimized driver line through minimum radius corner

The next step was to determine the maximum steering angle of both the inside and outside wheel. From the model of the suspension and wheel assembly, it was determined that the maximum turning angle of the wheels with clearing was 27 deg for the inside wheel and 33 for the outside wheel.

Implementation of Ackermann Geometry

When going around a corner the inside and outside tire travel different paths around the same axis of rotation. These paths have different radiuses and require different amounts of angle for the wheels to travel these paths. When the steering wheel is turned both tires don't turn the same amount. For example in going around a left hand corner your inside tire could be turned 22 degrees while your outside tire will only have to be turned 18 degrees. This is displayed in Figure 105. The amount of different in the two angle is determined by your track width, wheelbase and desired radius of curvature.

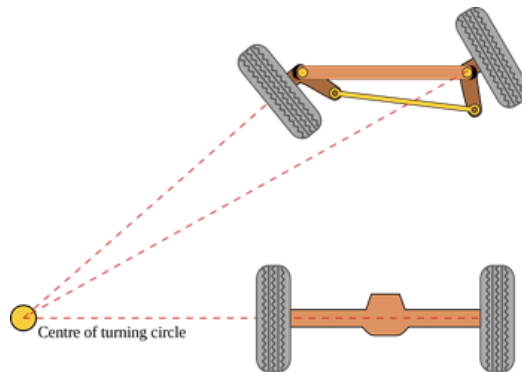


Figure 105. Example of perfect Ackermann steering geometry

However full Ackermann steering is best used in low speed, high grip corners because it eliminated tire scrub reducing rolling resistance. This changes significantly in high lateral acceleration corners, because there is already a significant amount of wheel scrub. In a high-speed corner with Ackermann steering the inside tire has a minimal load and is forced to a much higher slip angle than effective, creating drag and slowing the car. Parallel steering geometry is when both tires turn the same amount, in this scenario the inside tire is turning less thus leading to less drag. A lack of tire data makes it hard to tell exactly how much slip angle is needed on the inside tire to achieve maximum cornering force, because of this the decision was made to have an adjustable Ackermann setup. With driver experience from the 2015 car, which ran 90% Ackermann for the majority of its driving, and the recommendation from the book *Race Car Vehicle Dynamics* the two positions that were chosen where parallel steering and 50% Ackermann.

After the decision was made for parallel and 50% Ackerman geometry, the uprights had to be redesigned in order to implement this. Some other considerations when redesigning the front uprights where, manufacturability and weight. The resign started by determining where relative to the steering axis the connection point for the uprights should be. This was done by using a simple sketch of the vehicle characteristics with the know parameters. The Kaz rack has a total travel of 1.63 in either side from center, it is 15.25in long and is placed 3.53in behind the steering axis. These parameters are shown in red in Figure 106 below. With these parameters determined values were chosen for trail, shown in black and offset shown in green. The output angle of the inside and out wheel was then determined, show in blue. In order for perfect parallel steering, it was determined, that the trail should be 3.53in and the offset should be 0. For 50% Ackerman steering it was determined that the trail should again be 3.53in and the offset should be 0.65in.

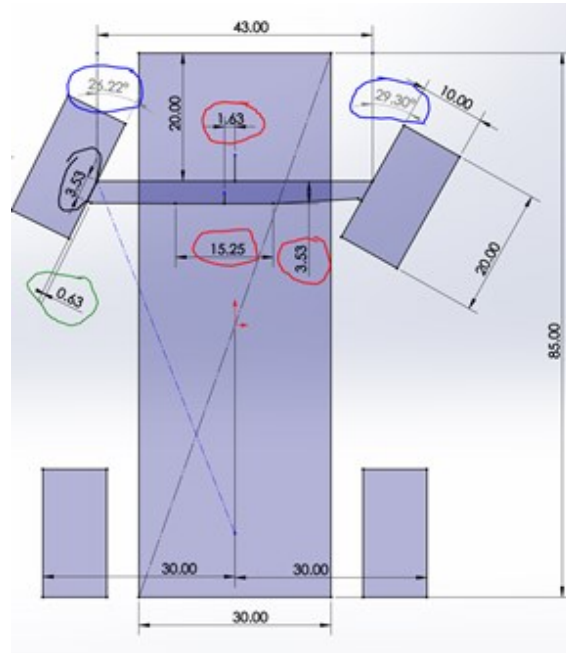


Figure 106. Sketch used to determine steering geometry

Once these values were determined, the first step to redesigning the old front uprights was to delete the original steering pickup and plot the location of the two points needed. Then create a boss that could easily support this location, while being easier to manufacture. Figure 107 shows the redesigned front upright.

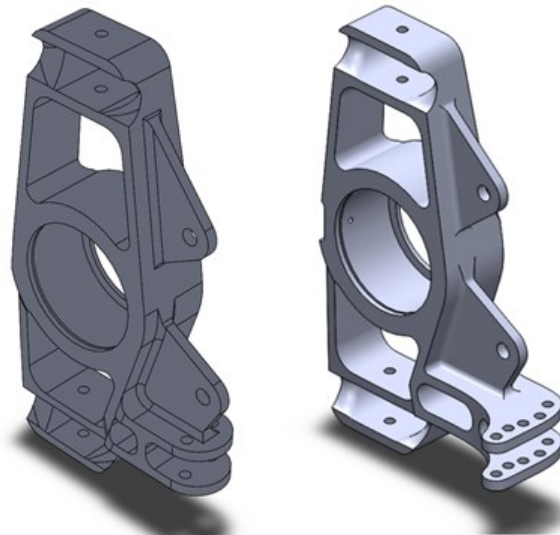


Figure 107. Redesigned front upright (left) next to old upright (right)

Manufacturing of the uprights was done on a Hass VM-2. The raw material was a 12in by 7in by 2.5in block of 6061 T6 aluminum. In order to have all the required features the machining took place in four distinct fixture orientations. The first two were used to drill the vertical holes in the piece that would later be used to fixture the A-arms. These were quick operations however due to

the limited high available in the machine the machine could not safely complete a tool change with the block under the spindle. In order to avoid this the g-code was modified by hand to move the block into a safe position so that it could complete a tool change safely. This was not a problem once the block was layer flat in the next two fixtures. The third operation was to rough out most of the major geometry while leaving excess at the bottom so that it could be properly fixture in a vise. For the majority of the roughing a half inch three flute roughing end mill was used. This was the longest single operation and took approximately 40 minutes of pure cutting time, because of this the feeds and speed for the tool where optimized for maximum material removal while not pushing the tool to its breaking point. For this the speeds and foods found on mfelabs.org where used as a starting point and slowly pushed faster and faster. The final material removal rate was just over 35 cubic inches per minute. Once the block was roughed to size a final pass was made over all finished surfaces, to give a smooth consistent finish. In order to grip the block in the final position a set of soft jaws or custom shaped aluminum jaws where made for the vise. This last operation just took off the material that was used to hold the block into the vise in the op before and any positions that could not be reached from the other side. While in this configuration the bore the bearing was brought to size, about .001 smaller than the size of the bearing, and a slot was cut in the bore for the snap ring that would hold the bearing from sliding out. After machining some hand finishing was done with a buffing wheel and files and the bearing was pressed in. In order to not damage, the bearing while it was being pressed in heat was used to expand the aluminum in the upright. This would allow the bearing to drop with some retaining compound. Once cooled the snap ring was placed and bearing was securely in place. This same procedure was used for all four uprights, although because the geometry differed, separate CAM programs had to be made.

Redesign and Implementation

During the design process a few issues were encountered. The main issue that had to be resolved was the overlooking of the extent of the lowered front roll hoop. The previous vehicle's front roll hoop was extensively lowered in the designing of the new frame and the amount was not understood during the beginning iterations of the steering box design process. After the first iteration, the template that must pass forwards into the front of the vehicle originating in front of the steering wheel did not come close to fitting. This was the reason the steering box was flipped in comparison to the previous year's mitre gear setup.

For future MQPs there are multiple things that should be revisited to make improvements. The first being the pretensioning of the upper bearing. With the current setup, there is play due to there being no way to preload the bearing against the race other than by forcing the entire steering column up and using a set screw to secure it in place. Another place for improvement is in the mounting of the steering box. The design that was used worked but could be greatly improved upon as it was installed before the steering box was finalized. A very important recommendation is to triple check the direction of the steering rack! The steering box had to be adapted to fit into the already welded mounts which is why for the side plates, the holes had to be drilled post CNC machining. This is also why there are cut tubes. These were a potential mounting solution for the original steering box design.

Brakes

Brake Components

The braking subsystem is one of the most important subsystems in the car. The braking subsystem needs to work in all conditions to ensure the drivers complete safety. This subsystem will be scrutinized during the dynamic competition events and specifically the skid pad event. The major task examined during that event is that the wheels must all lock at the same time when the car is coming to a stop.

The main components that drive the brakes are the calipers, the front and rear master cylinders, and the rotors. In the 2016 Formula SAE car, the team used Wilwood Billet Dynalite Single Calipers for the front and Wilwood PS-1 Calipers for the rear. The team also used Compact Remote Flange Mount master cylinders with a bore diameter of $3/4$ in² for the front and $7/8$ in² for the rear. The master cylinders have reservoirs that are filled with fluid. When the brake pedal is pushed the fluid compresses forcing a pressure on the calipers to squeeze together on the rotors. The rotors are then locked causing the wheels to stop rotating and the car to stop.

As stated earlier, one of the goals for this year's car is for it to be lighter. With this in mind, the team bought new OZ Racing Formula Student Magnesium wheels for the car, which are much lighter than the old OZ Racing Formula Student Aluminum ones. The magnesium wheels weigh 3.4 kg and have a 22 millimeter offset, while the Aluminum ones weigh 2.45 kg and have a 30 millimeter offset. The approximate weight reduction would then be 0.95kg, which is about 2 pounds per wheel, totaling 8 pounds in weight loss for the car.

The brake subsystem in the 2016 car performed and was designed very well. Therefore it served as a model for this current design. The first design choice was to keep the same calipers and master cylinders as the 2016 car, but change the wheels. However, an oversight when buying the wheels was not knowing the width. The manufacturer would not provide the entire dimensions of the wheel so the width was unknown. When research on the brake calipers was conducted, it was found that the wheels would not properly fit on the car due to interference with the hubs and calipers. The width of the magnesium wheel is slightly larger than the previous aluminum wheel causing it not to fit. Additionally, the offset on the magnesium wheels was 8 millimeters greater than the old aluminum wheels meaning there was less room. Since the new magnesium wheels interfered with the brake calipers, the two options were to change the offset of the hubs or get new calipers and redesign the brake subsystem to cooperate with them.

The hubs were redesigned around both the suspension and the brakes. They originally could not have a big offset due to the suspension parameters. The designed offset was 8 millimeters to match the difference between the 30 millimeter offset of the magnesium and the 22 millimeter offset of the aluminum wheels. This offset was in accordance with the suspension parameters and could not increase any more. Since the width of the magnesium wheels was causing interference there

needed to be another 6 millimeters of offset. The hubs could not have a larger offset, so therefore the calipers needed to be smaller.

After examining the hubs and determining that offset cannot be changed, different calipers were explored. As previously mentioned the old calipers were Wilwood Billet Dynalite Single Calipers on the front and Wilwood PS-1 Calipers on the rear. The front calipers were now too big, so smaller ones were needed about 6 millimeters thinner. The following assumptions and equations were used to determine the best calipers and master cylinders to use.

Assumptions:

W_{total} = Total weight of the car including a person = 650 pounds

H_{CG} = Center of gravity height = 14 inches

$F_{braking}$ = Intended Brake Deceleration/ Designed stopping force = 1.5 g's

$L_{wheelbase}$ = Wheel base distance = 60.5 inches

$$W_{transfer} = \frac{W_{total} * H_{CG} * F_{braking}}{L_{wheelbase}}$$

Brake pedal lever ratio, master cylinder pressure, caliper force, clamping force, and brake pad friction were used to solve for the rotor torque. As shown in the appendix, an excel sheet was used to calculate these values. Once again, the 2016 car was utilized as a model for the design and calculations. In the 2016 car, the front wheel rotor torque was about 558 ft*lbs, and the rear wheel rotor torque was about 135 ft*lbs. While trying to keep the 80%-20% distribution, different master cylinder areas and different front calipers were experimented with.

Using the above equation on an excel sheet, calipers with different areas were explored. The main goal was to have the ideal 80% to 20% brake torque ratio front to rear and to keep similar values as the 2016 car. The excel sheet was used as the template for exploring different master cylinders and calipers, as it always displayed the above values. When a different master cylinder area was imputed the affected equations would automatically update. This way the torque front to rear ratio was always known.

The first iteration in attempting to solve the interference was to change the calipers but keep the master cylinders the same. The current rear calipers fit on the car with no interference so those would remain the same. Research on smaller front calipers that had smaller widths was then conducted. However, there were no calipers that had a smaller width with the same area. The same area is important to keep the same brake torque ratio. Calipers with different areas were then explored but different rear calipers must also be adjusted to keep the 80-20 ratio. After many different calipers were investigated, no calipers met the requirement without having to change the master cylinders as well. The decision was then to pick both new calipers and master cylinders that would not interfere with the wheels and keep the same brake torque ratio. After many iterations the best option was to change the front calipers to Wilwood PS-1's with an area of 0.99 in² and to change the front master cylinder from a 3/4" bore diameter to 5/8" and the rear master cylinder

from 7/8" to 1+1/8". This would give a distribution of 81%-19% while allowing the front calipers to properly fit. However, the rotor torque on the front would then be very low at 327 ft*lbs compared the 2016 value of 558 ft*lbs and the rear would be 82 ft*lbs compared 135 ft*lbs. This became the first design iteration and because the rotor torques were significantly lower, other design options were considered.

The next design iteration had a considerable problem. During one of the team meetings it was discovered that the template of Percy would not fit into the car. The frame from the current car is smaller and shorter than the 2016 car, so this was overlooked. Percy's leg was interfering with the brake pedal. This meant that the position of the brake pedal and master cylinders would have to change, or a redesign must be completed. The solution was to redesign the brake pedal and use smaller master cylinders. Changing the current Compact Remote Flange Mount master cylinders to GS Compact Remote master cylinders along with a new brake pedal design allowed Percy to fit. For the size of the master cylinders, the best option was to keep the front bore diameter of 5/8", but change the rear to 13/16". The rear caliper would also have to change in order to keep the ratio. The current PS-1 caliper with an area of 0.77 in² needed to have a slightly larger area, so it was changed to a Wilwood SC3 Single Piston caliper with an area of 0.87 in². The reason for changing the caliper is because when the front caliper was changed, one of the only options that would fit under the wheel size restriction was the DH4 Dual Hydraulic caliper with an area of 1.77 in². However, that caliper has floating mounts instead of traditional lug mounts, which were used on the 2016 car. Therefore, the reasoning was to have the rear calipers also be floating mounts and the SC3 Single Piston is the best option for the size with floating mounts.

The advantages and disadvantages of floating mounts on calipers were then examined. Floating calipers work by having pistons on one side of the disk brakes that move in and out on the bushings like a clamp. When the brakes are applied, the piston forces the inner brake pad against the rotor, while the caliper slides and clamps the outside pad against the rotor. Some of the advantages are the packaging sizes are much smaller, the cost can be lower, and it is easy to build. The size advantage is really important for the team because the old calipers do not fit, and some of the only small enough calipers are floating calipers. The lower cost is also important because the team has a budget and saving money on the brakes allows an increase of funds for other subsystems. Floating calipers can also be easier to build because they have fewer parts. The calipers will be bought pre-assembled, however, fewer parts generally means fewer points of failure.

One of the big disadvantages, however, is that the floating calipers allow a degree of flexibility in the assembly. The brake pads can start to wear over time due to this issue, which means they will need to be replaced more often. This may also change the feel of the pedal when braking.

After reviewing both the advantages and disadvantages the team decided that it is best to purchase the floating calipers. Other Formula SAE teams use floating calipers, so it is not out of the ordinary and an unreasonable decision. The final components selected were the Wilwood DH4 Dual Hydraulic Calipers for the front and Wilwood SC3 Calipers for the rear. The master cylinders would also be changed the Wilwood GS Compact Remote Master Cylinders with a bore diameter of 5/8" for the front and 13/16" for the rear. Using these parts, the car would have a rotor torque of 585

ft*lb in the front, and 171 ft*lb in the rear. This results in about a 77-23% distribution, which is very close to last year's car. This can be seen in the appendix as well as all the values used to find the distribution.

Even though this was mostly finalized the team decided to abandon this idea after a team discussion. The brake assembly on the 2016 car performed very well and the team was very satisfied with the design. Therefore, this year's team wanted to follow a very similar design. The original plan was to add a spacer to the hub to gain more offset. This would make zero interference between the caliper and the new wheel. However, this would affect the suspension parameters such as camber gain, kingpin angle, and scrub radius. Therefore, the team decided to explore the option of getting new calipers. After iterating and finding a solution, the team determined that it might be just as effective to add a spacer for more offset. The suspension was redesigned and as a result, adding more offset was proved to not greatly negatively affect the suspension. Adding an extra 15 millimeters to the hub would decrease the camber gain, which is already very high, and will not greatly increase steering effort. Therefore the team added a spacer of 15 millimeters to the hub. This made no interference between the wheels. The suspension was already redesigned and made sure that adding the additional offset was not an issue. This was the final decision on the brakes and the team was able to order two Wilwood Billet Dynalite Single Calipers with a piston area of 2.4 in^2 for the front, two Wilwood PS-1 Calipers with a piston area of 0.79 in^2 for the rear, a Wilwood Compact Remote Flange Mount Master Cylinder with a bore diameter of $3/4$ " for the front and $7/8$ " for the rear, and four RCV 220 rotors that fit with the brake calipers. Shown in Figure 108 below are the front and rear calipers.

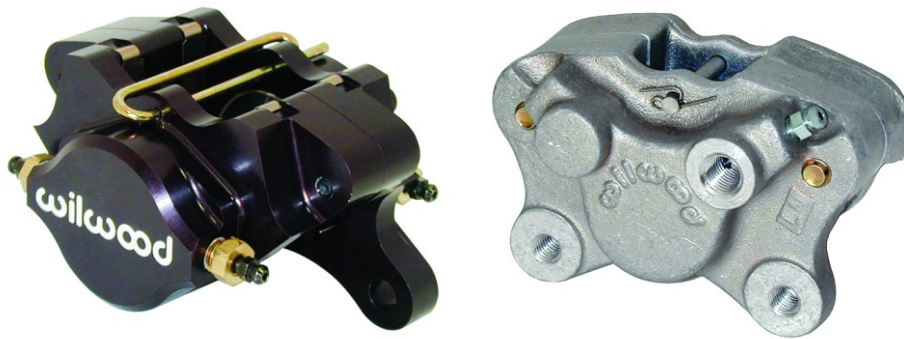


Figure 108. Wilwood Billet Dynalite Single, on the right, and Wilwood PS-1, on the left

Pedal Assembly

Background Information

In a Formula SAE car, the brake and throttle pedal assemblies must be designed for ease of use by the driver, to be lightweight, package easily and allow the for the placement of a template representing the relative size of a 95th percentile male into the cockpit of the vehicle, the size of the template is shown below in Figure 109.

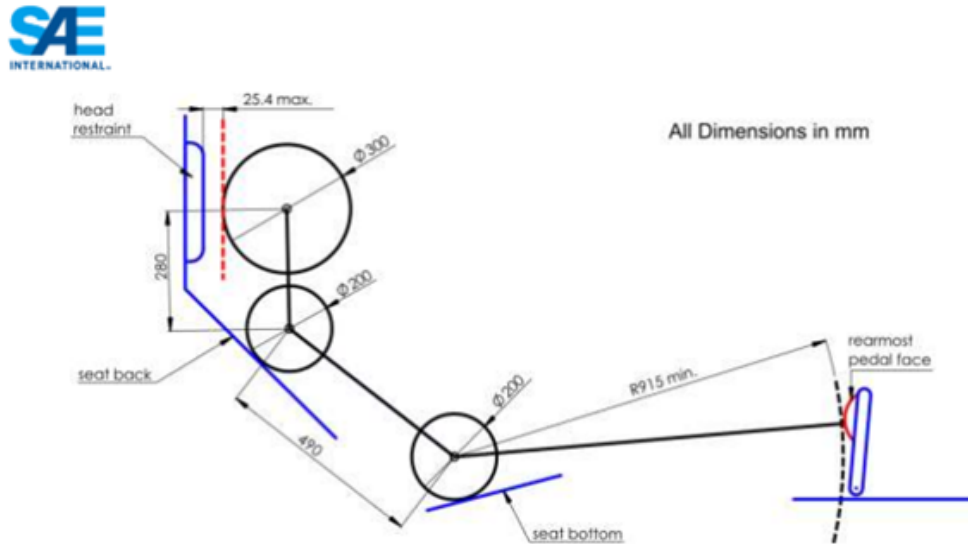


Figure 109. 95th Percentile Male Template Dimensions

As seen above, pedal placement is critical to the fitment of this template in the chassis of the vehicle, there can be a minimum radius of 915mm between the “torso” of the template, which rests in the seat bottom and the rear most pedal face. Failure to meet this minimum requirement or any other requirement related to the template results in failure of technical inspection, thus the vehicle will not be allowed to complete in any dynamic events.

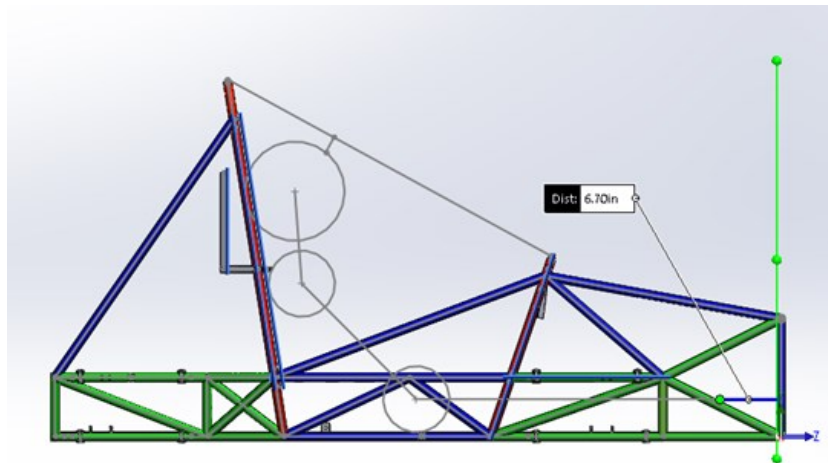


Figure 110. Sketch of 95th Percentile Male Template place in 2017-2018 Frame

Figure 110 above shows the frame design for this upcoming competition, with a sketch of the 95th percentile male template, aptly nicknamed “Percy”. Between the end of Percy’s foot and the plane defined by the rearmost surface of the tubes constructing the front bulkhead, there is but 6.7” of space to fit the entire pedal box.

Design Process

In the previous two cars built by WPI, for the 2016 Formula SAE competition and the 2014 Formula SAE competition, a Wilwood brake pedal/master cylinder assembly has been used. This assembly packaged both master cylinders, the pedal and a balance bar in a relatively small space, with four simply spaced mounting points. This assembly traditionally gets mounted to a large aluminum pedal plate, which also serves as a mount for the throttle pedal, the Wilwood assembly is shown below in Figure 111.



Figure 111. Wilwood Brake Pedal Assembly used in Previous Years

Initially, the same brake pedal assembly was to be used, it is relatively inexpensive, easy to source and requires no validation as it is a pre-designed component; the only task is to package the assembly in the front of the vehicle. After some searching on Formula SAE forums, it was determined that would be advantageous to have an adjustable (fore and aft) pedal assembly, instead of changing seat inserts based on the driver, which has been done in the past. The pedal assembly weighs much less than a fully outfitted driver, moving the pedals a few inches fore or aft would have much less of an effect on vehicle C.G. versus moving the driver. A pedal plate, like that of previous years was designed and mounted on sliding rail system in the frame (in SolidWorks) as a proof of concept, this first iteration of a pedal box is shown below in Figure 112.

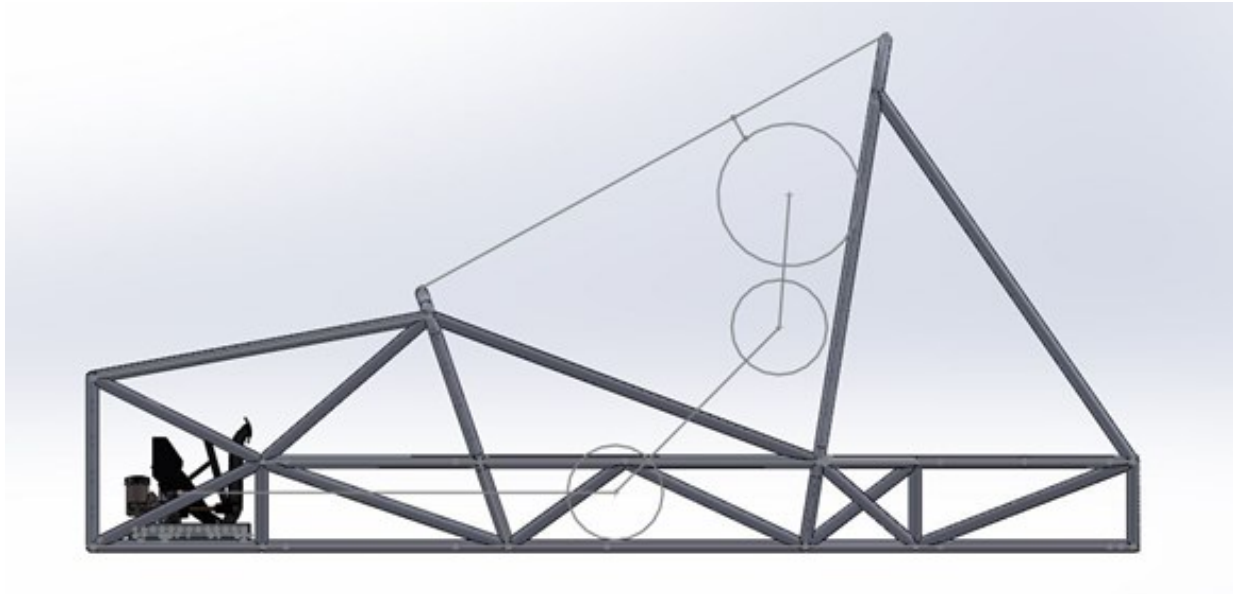


Figure 112. First Pedal Box Iteration

Difficulties arose due the front section of the frame tapering towards the front of the vehicle, this made it difficult to prototype mounting tabs because any tab would have to mount at a specific point on the tapered frame tubes. As seen above, with the Wilwood assembly mounted on the adjustable plate, even in its most forwards position, the template for the 95th percentile male interfered with the entire system.

At this point two options were considered, shorten the Wilwood bracket by 1.25in, which would still allow for the function of the adjustable pedal tray. Or source a reverse mount hanging pedal assembly shown in Figure 113, where the master cylinders mount rearward of the pedal and its associated mounts



WILWOOD P/N: 340-13832

Figure 113. Wilwood Hanging Pedal Assembly

The issue with shortening the Wilwood bracket is that it moves the pedal much closer to the master cylinders, which means the master cylinder pushrods must deal with more vertical misalignment as the pedal is in motion. That, and this would also have to be an entirely custom/complicated piece that would require a significant amount of machine time. The hanging pedal option also came with its own set of issues, due to the required pedal length to achieve a 5:1 mechanical advantage (used for braking torque calculations), the whole assembly would have to mount to the top of the frame, putting the master cylinders and reservoirs outside the envelope of the frame, undesirable in a rollover situation and against the rules, the hanging pedal also did not allow for an adjustable pedal tray.

In a team meeting, someone suggested that the master cylinders might be able to mount underneath the floor. The idea was to lay the master cylinders on their side, mount them underneath the floor, behind the brake pedal and design a custom brake pedal and mounting arrangement. The pivot point for the pedal would have to be above the connection point to the master cylinder pushrods so that as the driver pushes on the pedal, the pushrods are compressed into the master cylinders. Although this would eliminate the possibility of an adjustable pedal assembly, it was seen as the best option as the team has considerable experience with using removable seat inserts based on the driver.

The master cylinders would be mounted to a bracket traveling across the length of the frame, another similar bracket would be mounted forward of the rear bracket. The distance between the two brackets was determined from the uncompressed length of the master cylinders and the Wilwood brake balance bar that would be used, in the end, 6.125" ended up being the optimal distance between the two. The front bracket was placed in the model first, as close to the front of the frame as possible, then the rear 6.125" behind it, the arrangement is shown below in Figure 114.

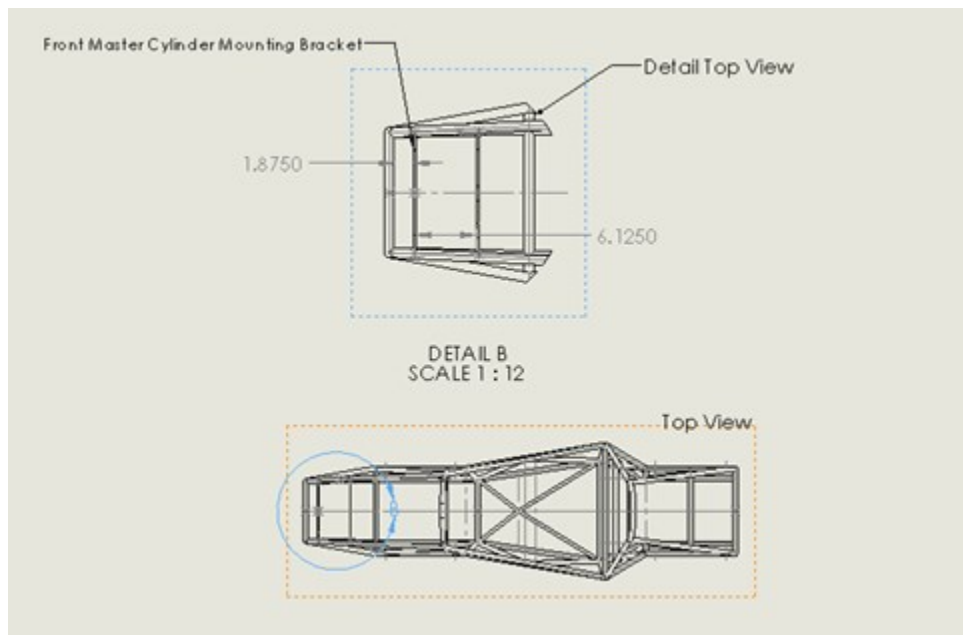


Figure 114. Placement of Master Cylinder Mounting Brackets in Frame

Initially, shaft collars would have been the method of attachment for the mounting brackets, but due to the proximity of the front bracket to a node on the frame, there might be interference between the welds around the node and the shaft collar, so welding was chosen as the preferred method of attachment. This meant that the brackets would need to be made of AISI/SAE 4130 steel, the same material as the frame tubes. To start, .25" was chosen the initial bracket thickness and the bracket height would be fixed at 1.75", the width of the mounting face of the Wilwood master cylinders that would be used. A bolt pattern was created on the rear bracket and the previously created models of the Wilwood GS remote master cylinders were placed in assembly with the pushrods located such that the overall length of the master cylinders was the uncompressed length of 7.99". Next a model of the Wilwood balance bar was inserted into the assembly and mated to both master cylinder pushrods, this ideally should place the balance bar in the general location where it will rest with the brakes bled and without any input from the driver (of course the pushrods thread into clevises on the balance bar so there will be some fore and aft adjustment.

The master cylinders were placed favoring the left side of the frame, as to keep the brake pedal to the left of the centerline of the car, the left master cylinder was placed as close to the frame rail as possible, while still allowing room for the hard brake line and the soft line to the reservoir. The master cylinders were initially placed as close together as possible, but had to be moved to 3.75" centerline to centerline, the reasoning is explained below.

Using the sketch of the 95th percentile male template in the model of the frame in SolidWorks, the pedal face was placed 1 inch forward of the template (1.75" rearward of the vertical centerline extending through the balance bar, which should provide a buffer in case of any manufacturing inaccuracies or differences between the model and physical frame; Due to the style of clevis on the balance bar, the pedal can be further moved forward by threading in the master cylinder pushrods. The pedal face was angled back 10 degrees (80 from horizontal ccw) and based on physical measurements taken of a size 10 human foot, the center of the pedal face should be about 7.5" above the pivot point. In the brake calculation spreadsheet, a 5:1 mechanical advantage for the pedal was assumed when doing all relevant braking force calculations, with the pivot point 1.375in above the centerline of the balance bar, the mechanical advantage ended up being 5.45:1. The pivot point was moved .39 rearward of the vertical centerline traveling through the balance bar, this is an arbitrary number, further refinement could be done to determine an optimal location.

With all the critical points placed, the next step was to sketch a pedal shape, again the shape was arbitrary, the profile was loosely based off a Wilwood pedal, a few profiles were created, the final one, which fulfills all the critical dimensions listed above is shown below in Figure 115.

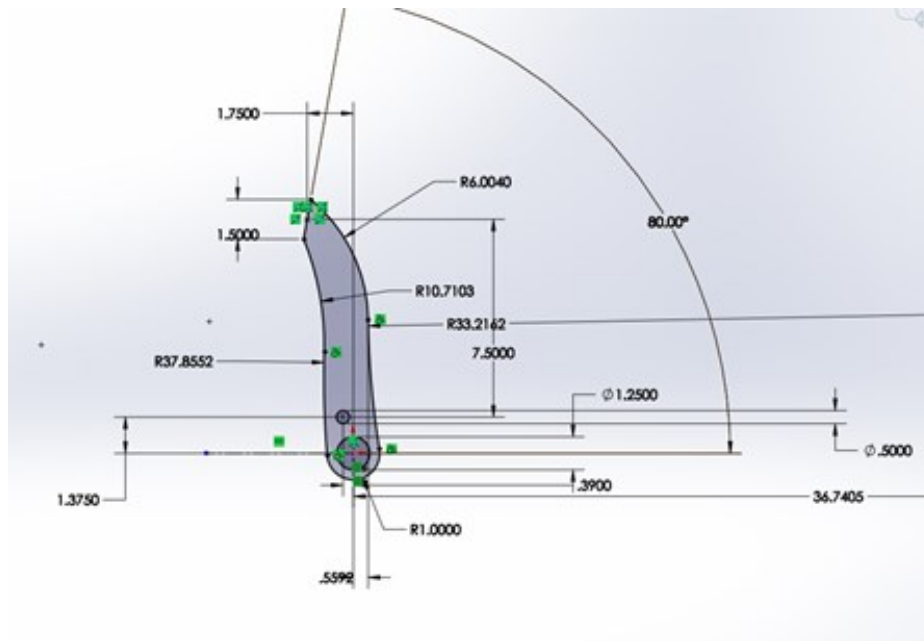


Figure 115. Sketch of Final Pedal Profile

The pedal thickness was chosen to be 1.5", this is the width of the mounting surface for the Willwood balance bar that would be used and it will be machined out of 6061-T6 aluminum due to its availability, strength and low weight.

The next step was to create the bracket that the pedal mounted to, initially, the only constraints were a 6.125" overall length, a bolt pattern on both ends that was the same as the bolt pattern between the two master cylinders, a hole corresponding with the pivot point on the brake pedal and a slot that the brake balance bar would be able to travel inside. As a starting point, the thickness of the bracket was chosen to be .75", half of the thickness of the pedal. Because the master cylinders were mounted so close together, it was not possible to fit any hardware with a positive locking mechanism, thus the master cylinders were moved to 3.75" from centerline to centerline to allow the use of 3/8-24 hardware in conjunction with nylock nuts to attach the pedal mount bracket, the mounting face is .25" thick. The initial pedal bracket was 2.25"x1.75"x6.125" with C-channel style cutouts to allow the use of the above hardware, this was placed in the assembly with the steel mounting brackets, master cylinders, balance bar and pedals. In the assembly, the 1.5" slot and profile for the upper part of the bracket, provision for mounting of the pedal at the pivot point, were sketched and later fully defined in the context of the singular part. The O.D. of the balance bar is 1.25", so the 1.5" slot allows for plenty of fore and aft travel of the pedal, though there should be very little with a properly bled hydraulic system.

On either side of the pedal mount bracket are two brackets that provide additional support to the assembly, they share the same mounting geometry as the pedal mount bracket and share the same outer bolt holes the master cylinders. They are also shaped like a piece of C-channel to allow for the use of a positive locking fastener and are .25" all the way around, the final assembly is shown below in Figure 116. As with the pedal, all three supporting brackets will be manufactured from 6061-T6 aluminum because there was stock available on site.

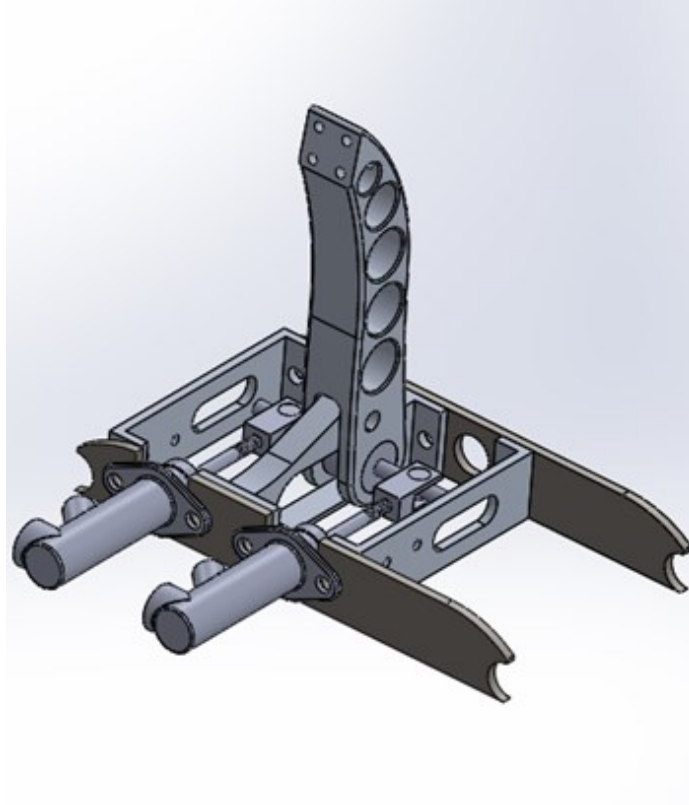


Figure 116. Final Pedal Assembly

Finite Element Analysis

Per the Formula SAE 2017-2018 rules, section T7.1.8 states, “The brake pedal must be designed to withstand a force of 2000 N without any failure of the brake system or pedal box. This may be tested by pressing the pedal with the maximum force that can be exerted by any official when seated normally.” Initially, finite element analysis was going to be conducted on each part, using forces resolved by hand from the 2000N (450lb) pedal force, but as the assembly is statically indeterminate, conducting a simulation of the entire assembly would save time, the selected software was SolidWorks 2017. Appendix H is a simulation report discussing in more detail the FEA setup used for the pedal assembly.

Assumption and Modifications to the Assembly

It was assumed that the pedal box would not fail due to the Wildwood components, as they are designed and tested to perform in some of the toughest automotive racing applications, thus these were taken out of the equation. The master cylinders were removed altogether and replaced with two supports that mount in the same location, they extend to the clevises on the balance bar. These two supports were made rigid, so their only job is transfer load from the pedal to the mounts. The balance bar itself was not removed, however it was also made rigid, again to just transfer load. Finally, a simple 1/2” pin was created and placed in the assembly to mount the pedal to its mounting bracket, the modified assembly is shown below in Figure 117.

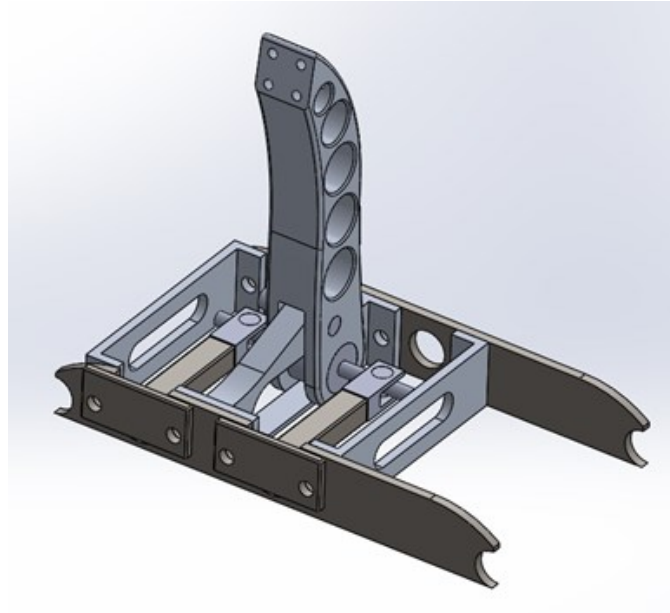


Figure 117. Pedal Assembly Brackets

Fixtures and Loads

The only fixed geometry in the entire assembly are the surfaces where the two steel mounts would be welded to the frame, shown below in Figure 118. The only load on the assembly was a 2000N force applied normal to the pedal face, shown below on the right.

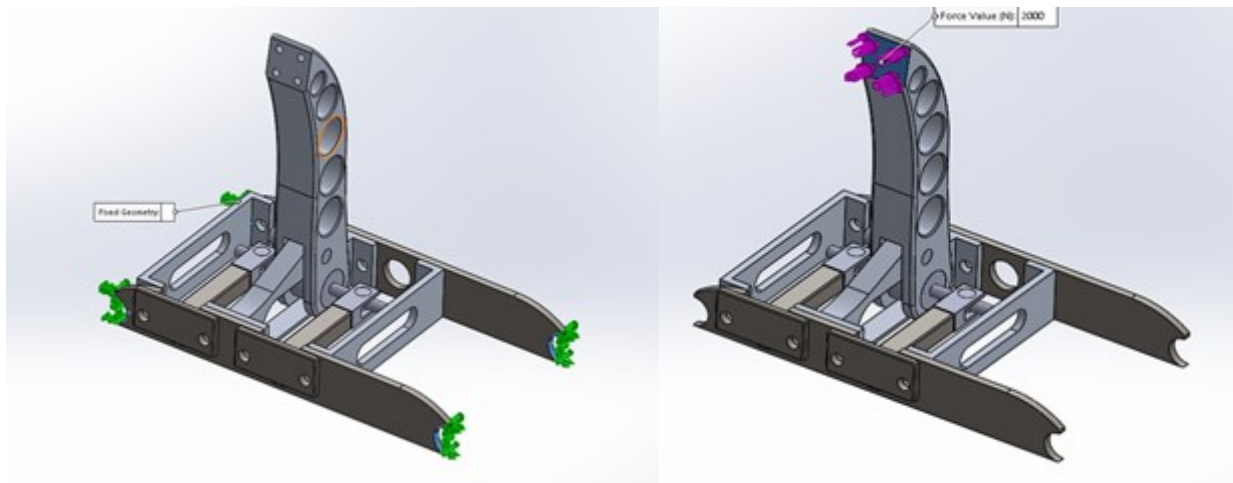


Figure 118. Pedal Assembly Brackets FEA

Connectors and Contact Sets

A simulated bolt was used in all places where an actual bolt would be used, a circular edge must be selected for both the head of the bolt and the nut. The simulate hardware size was 3/8, with a 25 ft*lb preload, the parameters are shown below in Figure 119 and Figure 120.

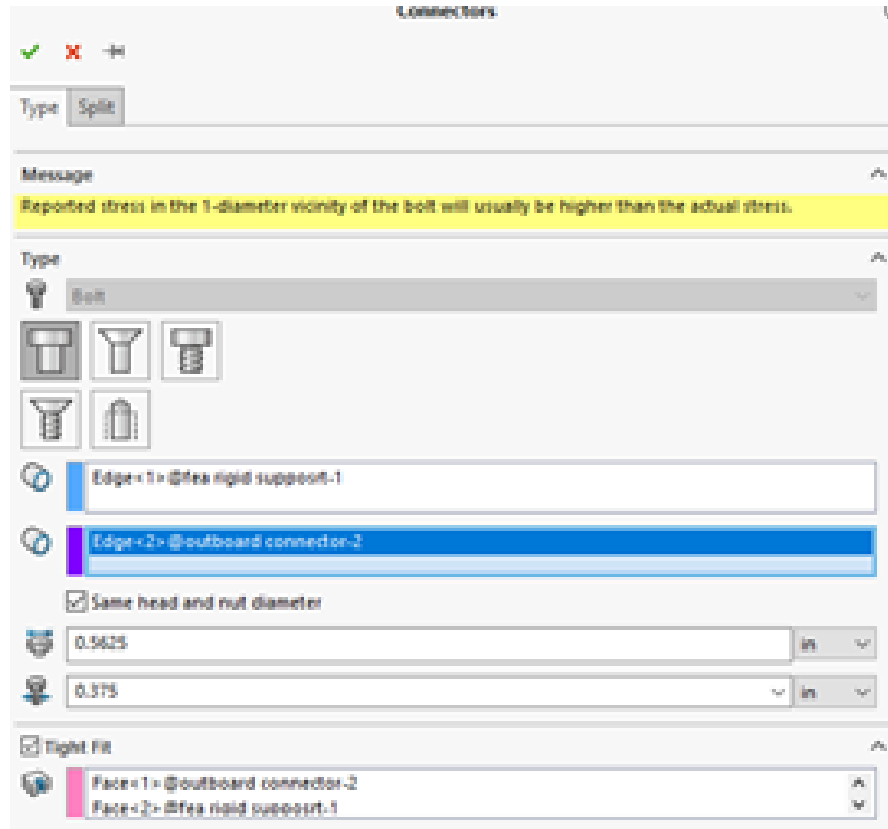


Figure 119. Pedal Assembly Brackets FEA Setup

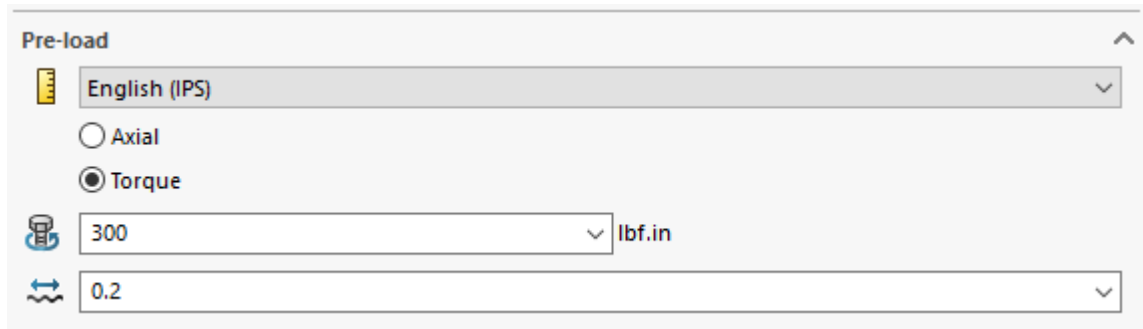


Figure 120. Pedal Assembly Brackets FEA Preload

A no-penetration contact set was used where there was coincident contact between components. This contact set essentially defines a barrier between two surfaces, such that they cannot occupy the same space during the simulation. The other type of contact set is a bonded contact, which is also between two components with coincident contact, this type of contact set permanently bonds the two touching surfaces with a “perfect glue.” The only place bonded contact sets were used was between the supports and the clevises on the balance bar, to keep the two components in contact during the simulation. To assign a contact set, either bonded or no-penetration, the two coincident faces on the corresponding components must be selected individually, shown below in Figure 121, which is the contact set between the pedal mounting pin and bracket.

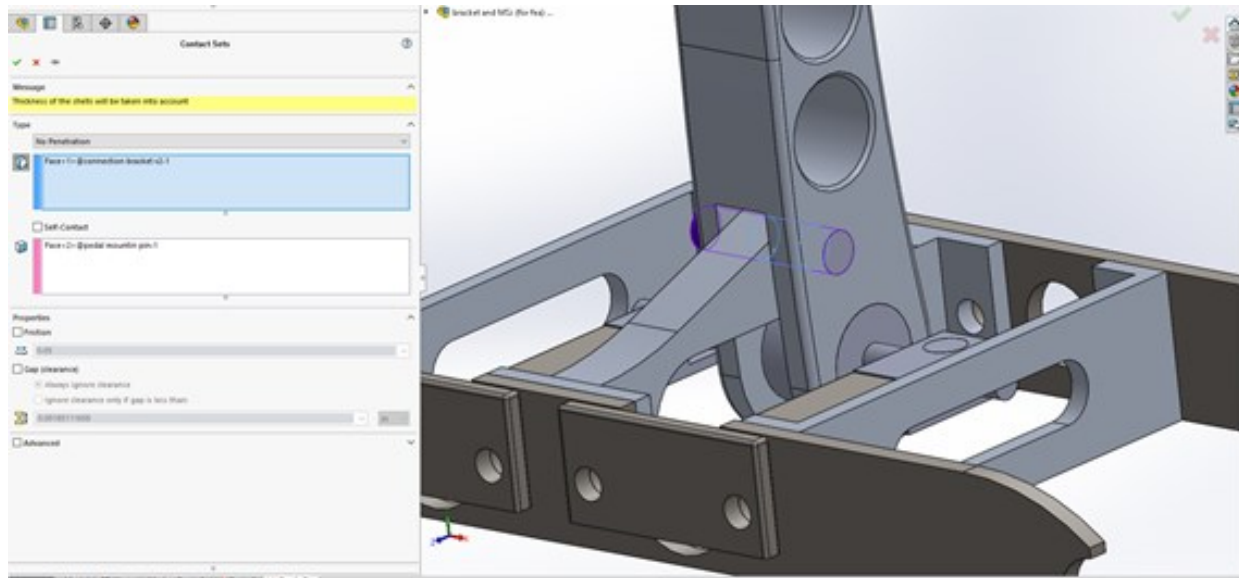


Figure 121. Pedal Assembly Brackets FEA Contact Sets

Because both components contact on faces, it does not matter which is selected first, however it would matter if there was contact between an edge or vertices and a face. It is important to define a contact set between every component that contacts another, without a defined contact set, the simulation will fail because the program will not know how to simulate component behavior relative to one another.

Mesh

To allow SolidWorks to conduct a finite element analysis on the assembly, a mesh must be created. The mesh is essentially a web connecting all nodes of each element in a part/assembly. In the early days of FEA, meshing a part was a huge undertaking, now most CAD programs with simulation packages include an automesh function that will import the part geometry and automatically create the mesh (Norton, 519). For this analysis, this function in SolidWorks was utilized. The user interface for this function is refined to the point where the end user simply must select from a coarse or fine mesh on a gradient, shown below in Figure 122.

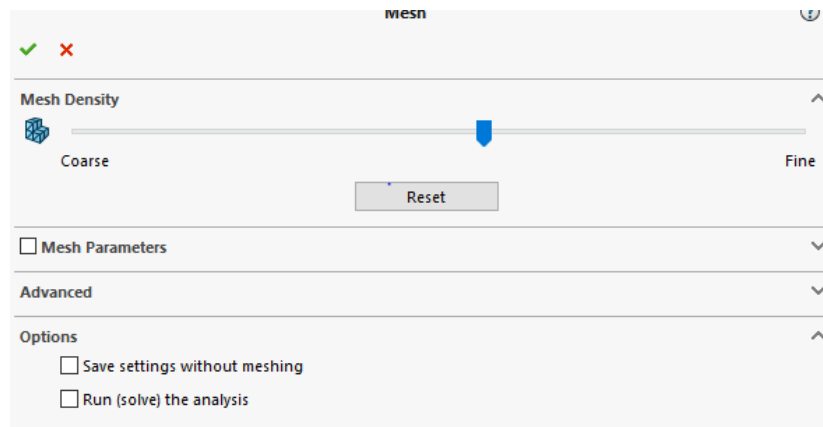


Figure 122. Pedal Assembly Brackets FEA Mesh

A coarse mesh will yield a faster computation time but may not be able to accurately analyze a high stress gradient, a fine mesh will quickly increase computation time, but will also yield the best results, and the key is to find the balance between the two. For this analysis, the best mesh density corresponds the gradient above. A less dense mesh had trouble around some of the complex curves around the pockets in the pedal and a very fine mesh was causing infinite computing time and multiple software crashes.

Results

After a few failed simulations, due to missing contact sets, the first successful simulation yielded the first design issue. The web shown below, indicated by the red arrow in Figure 123, was far too thin, about .125” and was yielding under load, the solution was to increase the radius of the sketch curve that joins the two extrusions that create the part. The radius was extended all the way to the rear edge of the part, resulting in a minimum web thickness of .37” increasing the factor of safety to 4 in that region.

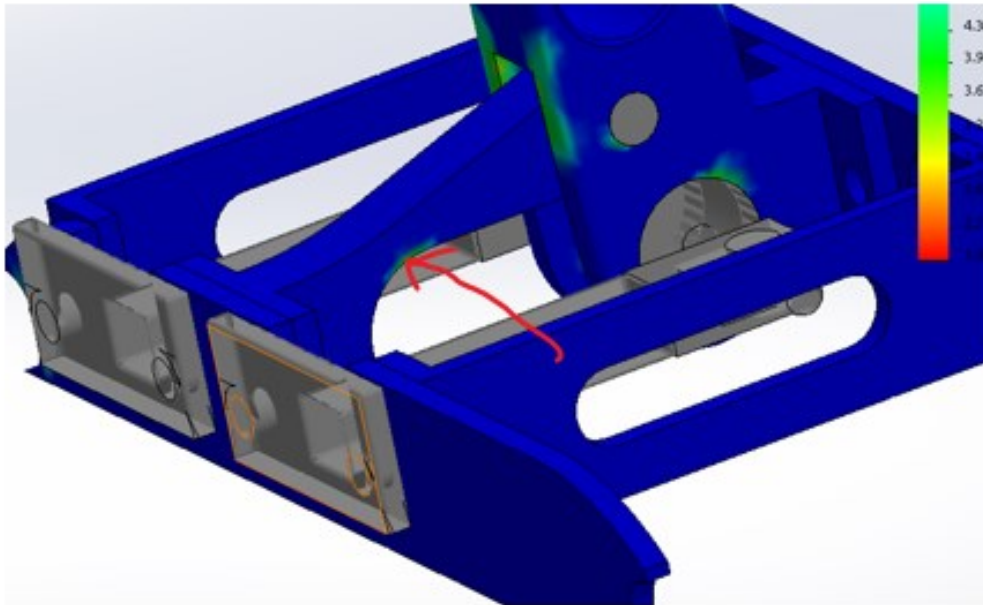


Figure 123. Pedal Assembly Brackets FEA Results 1

As expected, the highest stress in the assembly was in the steel mounting brackets, around the bolt holes where the master cylinders’ mount, as they transfer all the load from the pedal to the surrounding bracketry.

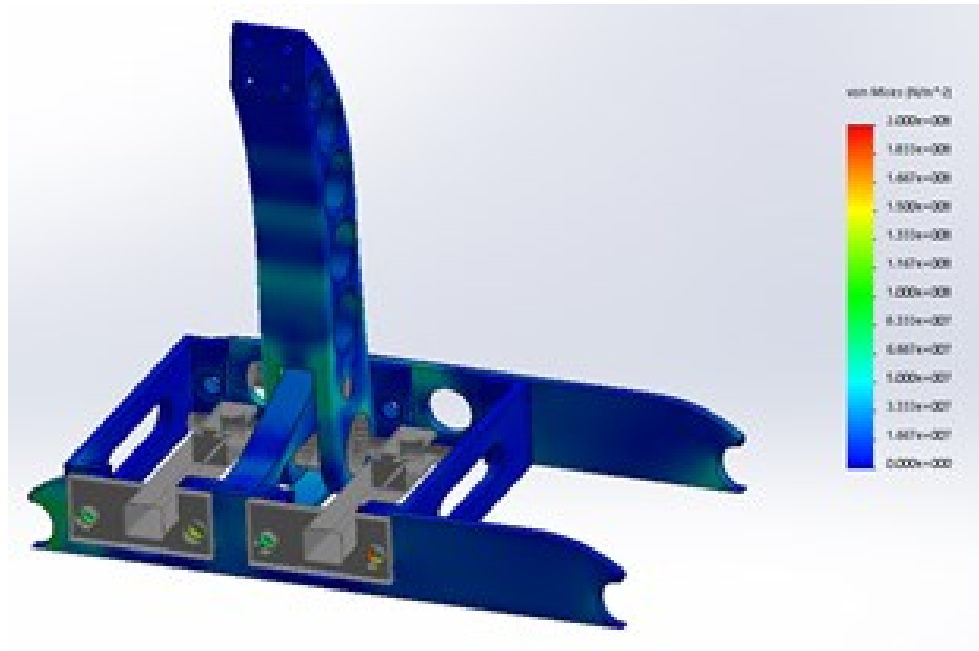


Figure 124. Pedal Assembly Brackets FEA Results 2

Figure 124 above shows the fringe plot of the von Mises effective stress, the maximum stress in the part was $2e+8$ Pa, which in AISI/SAE 4130 steel, yields a lowest factor of safety of ~ 1.9 , as shown below in Figure 125.

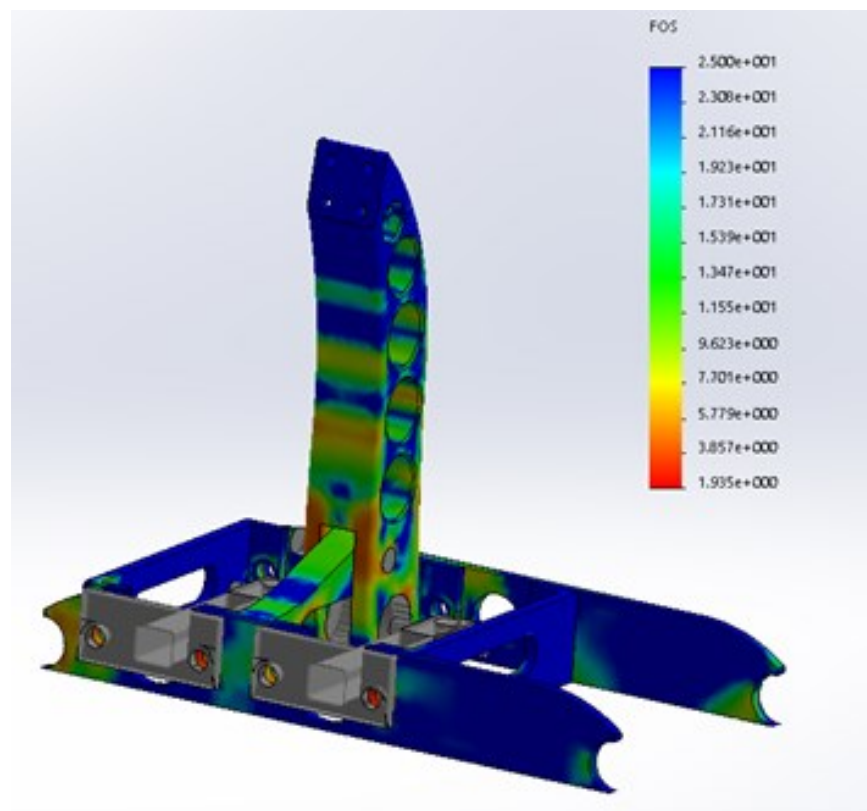


Figure 125. Pedal Assembly Brackets FEA Factor of Safety

As the minimum factor of safety in the steel brackets was ~ 2 , and their height and width were defined by the master cylinders and frame respectively, no further changes were made. A simulation was run where the thickness of the outer support brackets was reduced to .125", however this resulted in safety factors lower than 1.5 around their mounting holes, so to err on the side of caution, the thickness was kept at .25". At this point a considerable amount of time had been dedicated to the design an analysis of the assembly, and with plenty more to do to achieve performing vehicle in 28 weeks, the design was locked and moved to the manufacturing stage.

Post-Manufacturing Design Modifications

After the pedal was manufactured, it was decided that the weight needed to be reduced to be competitive with the weight of pedal assemblies in previous years. Initially, the pedal had 3 pockets on either side that were 1" in diameter and only .5" deep. Due to the way the pedal was machined, there was only one way to fixture the finished product in the vise, meaning all operations must be done on one side of the pedal. The solution ended up being an increase in the diameter of the 3 existing pockets, to 1.25", the addition of two smaller pockets towards the top of the pedal and making it such that all pockets cut through the entire pedal, this would reduce the weight from 2lbs to just a little bit over 1lb.

Because so much material was removed from the pedal, there was concern that the factor of safety would no longer be above 1. A new simulation was done to confirm or deny this theory. This time around the only component in the assembly was the pedal, it was fixtured using fixed geometry in the mounting holes, on the sides that would be forced against the mounting hardware during the loading situation, the fixturing is shown below in Figure 126.

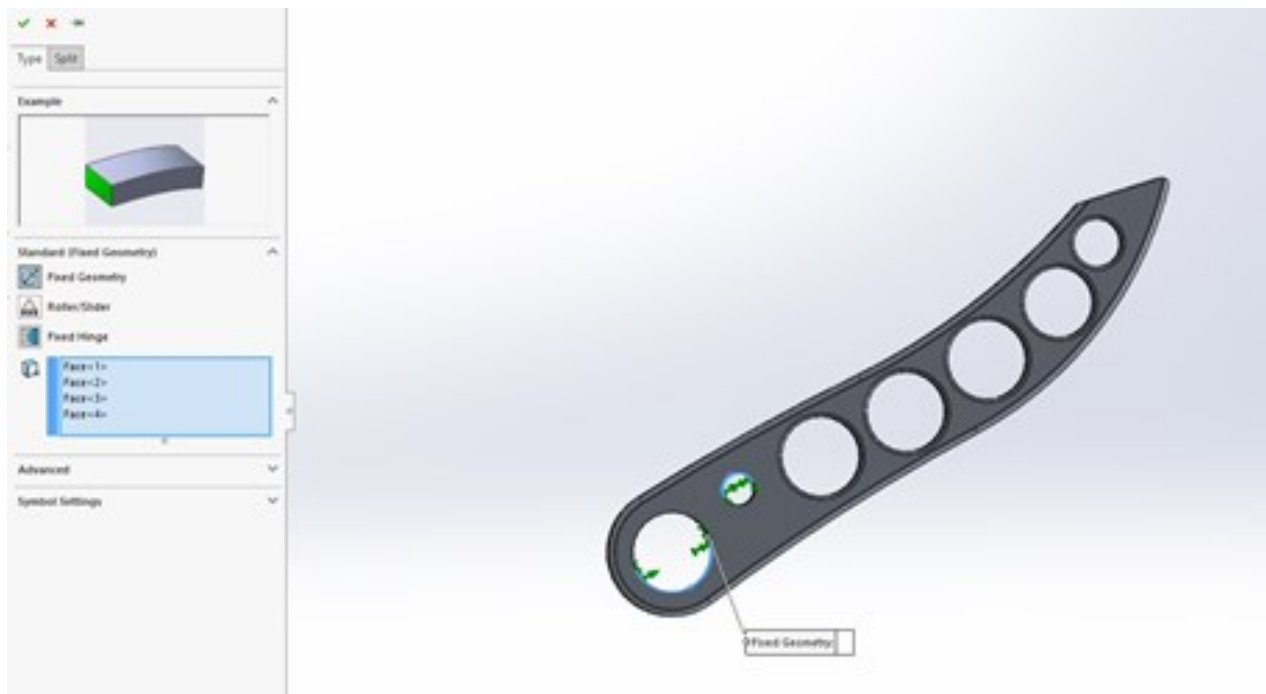


Figure 126. Pedal FEA Setup

With the same load as the previous simulation applied to the face of the pedal, the minimum factor of safety was ~ 2.8 as shown below in Figure 127. The ideal way to reduce the weight of the pedal would have been to pocket out both sides to form an I-beam shape, but this would've required the manufacturing of another set of jaws for the vise to hold the pedal. It was determined that the further weight savings would not be worth the added machine time, so the design was finalized and the pedal went in for its final machining operation.

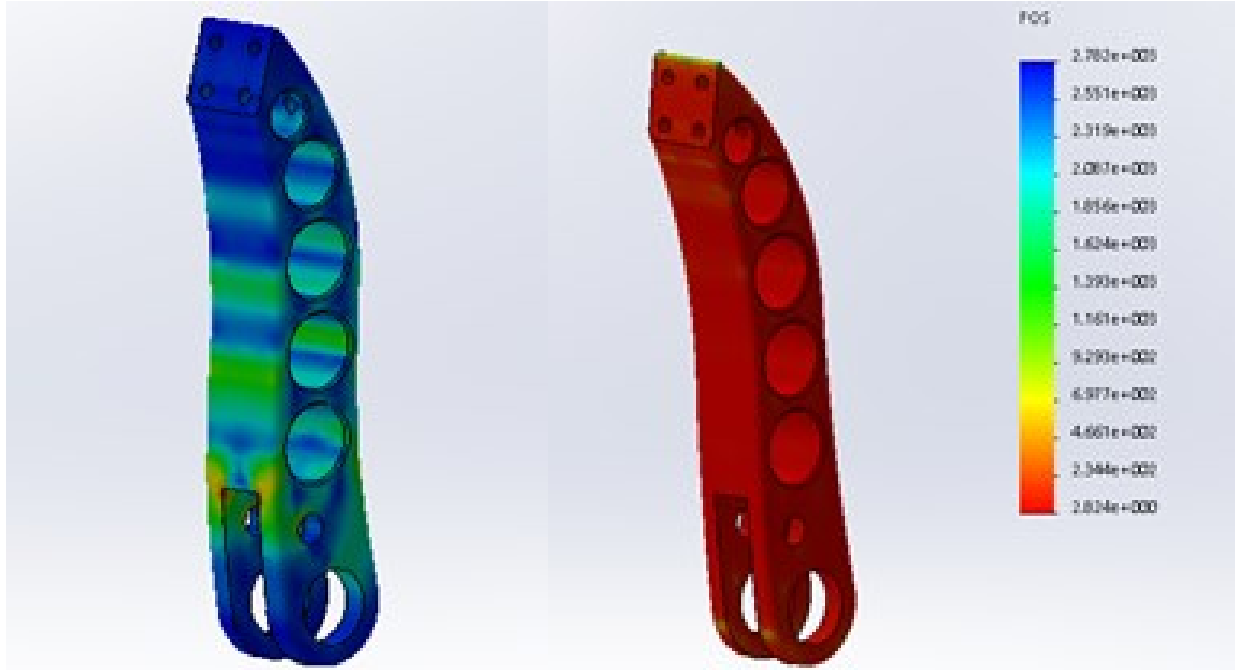


Figure 127. Pedal FEA Results

After the pedal mount bracket was manufactured, and pedal was test fit, there was a noticeable amount of binding during pedal motion due to the aluminum to aluminum contact. To alleviate this binding, $.005''$ was taken of the face of the pedal mounting bracket, indicated by the red arrow shown below in Figure 128, and the corresponding face on the opposite side. Also, a $.0625''$ deep slot with a $1''$ OD, indicated by the blue arrow, was milled around the mounting point for the pedal on both sides of the bracket, to allow for the installation of bronze thrust bearings, which should also help to minimize any binding between the pedal and mounting bracket as the pedal is in motion.

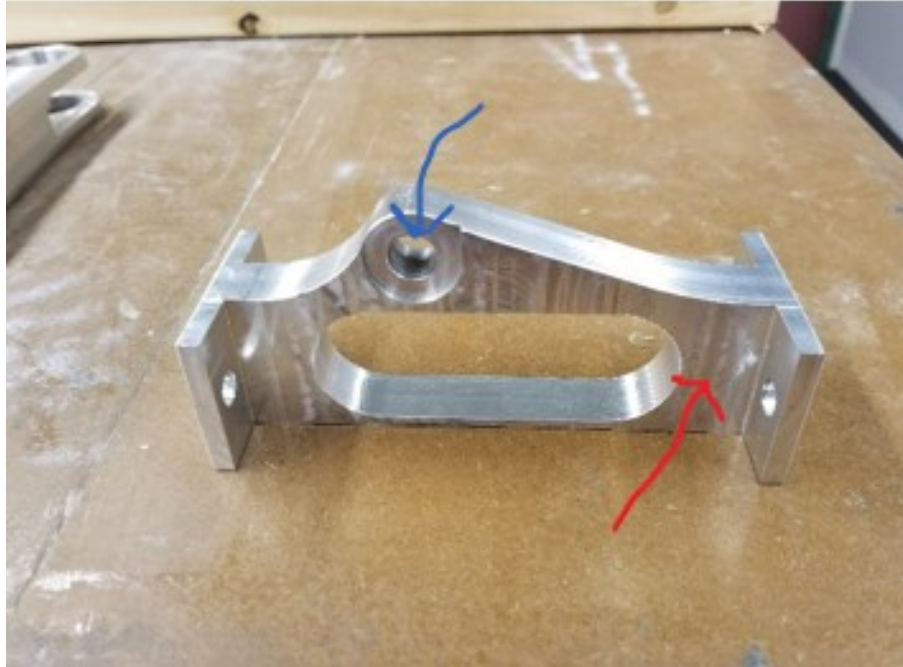


Figure 128. Pedal Bracket

Optimization Recommendations

In theory, when conducting finite element analysis, the mesh size and type should be changed over the course of multiple simulations until the stress gradient converges to one maximum stress value, or at least a very small range (Norton, 520). Due to time constraints, the mesh for this assembly was for the most part kept constant during every simulation, with more time, the mesh could be fine-tuned for each individual part in the assembly, allowing the size/shape and thickness of each individual part to be optimized to further reduce the weight of the entire assembly. Of course, in the future, if a new frame is manufactured that is but 1.5" longer than the existing frame, the need for this custom brake pedal assembly could be eliminated and the team could revert to using the pre-packaged Wilwood assembly, which could free up time for the re-design/optimization of much more critical systems in the vehicle.

Throttle Pedal Mounting and Placement

The mounting of the throttle pedal is far less critical than the mounting of the brake pedal as the driver will not be frantically applying force to the throttle pedal in the event of a panicked driving situation. The pedal that will be used for competition is an OEM BMW part, part number (insert part number here) and is pictured below in Figure 129.



Figure 129. BMW Throttle Pedal

Based on the design of the brake pedal assembly, the easiest way to mount the throttle pedal is a bracket extending from the rightmost aluminum support bracket to the bottom right frame tube in the front section of the frame, the initial design is shown below in Figure 130. The bracket would be bolted to the aluminum support with small hardware and attach to the frame with shaft collars using 6-32 machine screws.

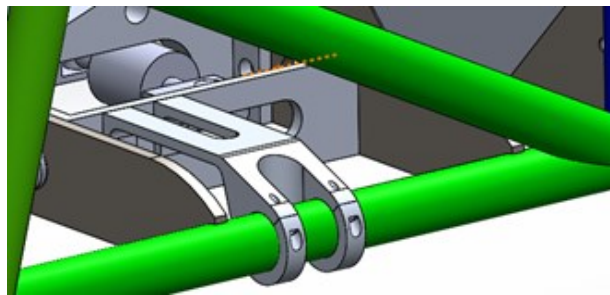


Figure 130. Throttle Pedal Assembly Bracket

The pedal has an overall length of about 8.5” and having the back of the pedal rest up against the impact attenuator anti intrusion plate put the pedal face in the optimal position with respect to the brake pedal face and the “foot” of the 95th percentile male template. However, Section T3.22 of the 2017-2018 Formula SAE rules states that “all non-crushable objects (eg. batteries, master cylinders, hydraulic reservoirs) inside the primary structure must have 25mm (1”) of clearance to the rear face of the impact attenuator anti-intrusion plate.” Based on the above definition, the team assumed that the throttle pedal was a crushable object and the bracket was sent off to be manufactured, however, a later rules clarification revealed that the throttle pedal is in fact a non-crushable object, thus it would have to be moved 1” rearward in the car, luckily the mounting holes have not been drilled in the aluminum support bracket, so this task was easily achieved. Another rules clarification submitted on Formula SAE online verified that if the throttle pedal is the rear most pedal, the “foot” of the 95th percentile male template is placed on the pedal face where the actual driver’s foot would make contact, meaning that the pedal would still fit in the allotted space. The manufacturing of the throttle pedal mounting bracket and associated shaft collars was outsourced to one of the team sponsors, Forgione Engineering, located in Lowell, Massachusetts. They can 3D print using a carbon fiber filament, as the bracket is a small component, it would make a good first test piece to gauge the print quality and strength of this type of rapid prototyping.

Ergonomics

Firewall and headrest

The two main components for the ergonomics of the car are the firewall and the headrest. The seat and the body panels are the other major components but those will be manufactured during C term. According to the Formula SAE competition rules, the firewall must act as a divider between the driver and the fuel tank system. The driver should not be in contact with the fuel, oil, cooling system, or any electrical hardware with high voltage. Four inches above the bottom of the tallest drivers helmet must also not be in direct line of the fuel, oil, or cooling systems. There also may be no holes allowed for the seatbelt to pass through.

The firewall is made of 22 gage 5052 aluminum sheet metal. The design started with the floor pan flat on the bottom of the frame. Then it was bent upwards 45 deg, as shown in Figure 133, in order to make room for the fuel tank. The fuel tank will extend the length of the firewall tucked underneath in the triangular prism. Once the firewall reaches the back of the frame it will be bent up 36 deg more to be flush with the frame. Lastly, the top of the firewall will be bent to sit over the middle bar in the back of the frame. Two holes are cut out and folded out to create space for the seatbelt tabs. A hole is then made in each of those firewall tabs, so it can be bolted to the tabs that are welded to the frame. Four tabs are welded to the frame, which correspond with the same hole locations as the holes cut in the firewall. This allows the firewall to be rigidly mounted to the frame. Six cutouts along the sides of the firewall, shown below in Figure 90.

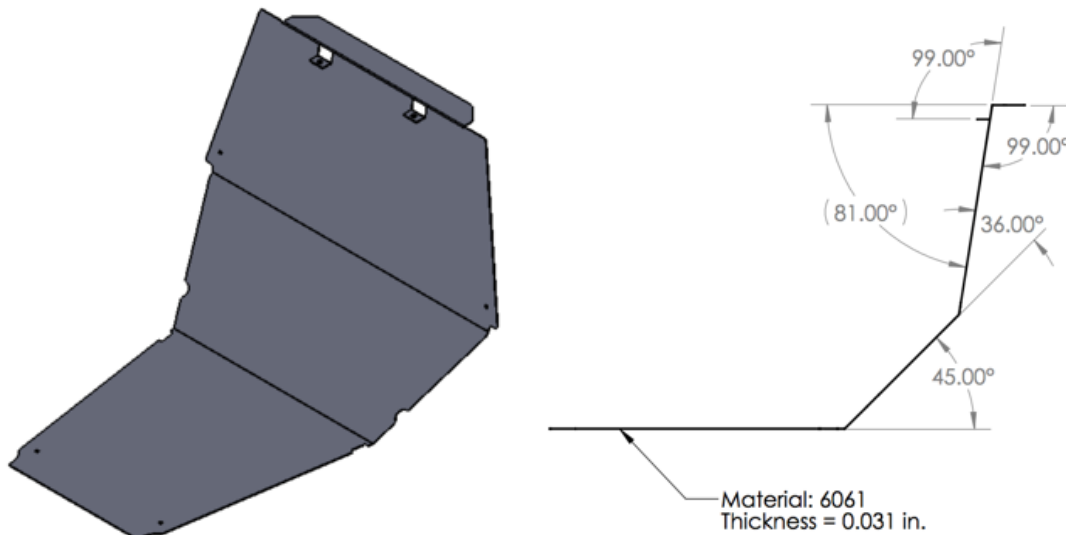


Figure 133. Firewall Sheet Metal

The headrest is the second major component in the ergonomic subsystem. The headrest serves the purpose of constraining the driver's head and not allowing it to move backwards. The same material as the firewall, 22 gage 5052 aluminum, was used for the headrest as well. The headrest had

three bends, shown in Figure 134 below, to make it flush with the frame. The top flap in the firewall will bend over the bottom of the headrest. This will help mount the headrest to the frame.

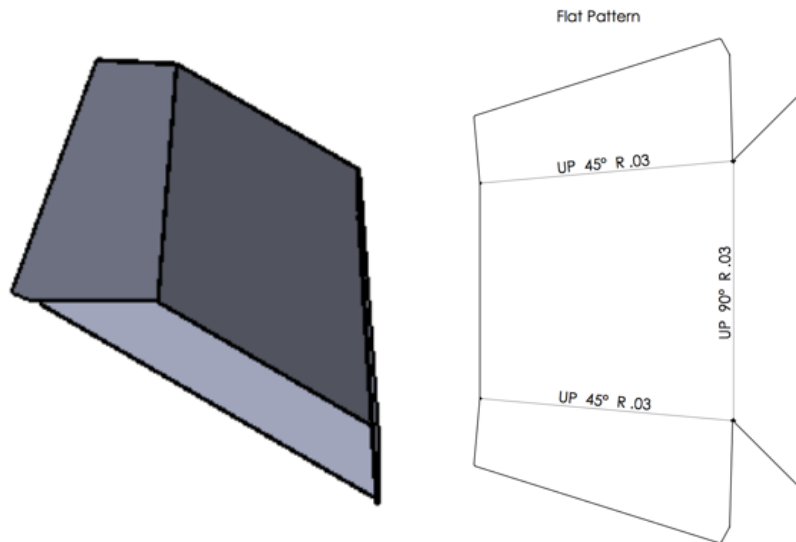


Figure 134. Headrest Sheet Metal

As stated earlier the seat and body panels will be manufactured C term. Fiberglass was laid over a leather seat in order to create a mold. Due to the leather in the seat, the mold had many wrinkles and was not smooth. The decision was to then use bondo to fill in the wrinkles and gaps to smooth the mold. Once the mold is smooth and hardened, carbon fiber will be laid over the mold to create a carbon fiber seat. This will then be used as the car's seat. Expanding foam will then be used behind the seat in order to properly mount it in the car. Wooden molds bought from a previous MQP team are being used to make the body panels for this year. These molds need to be sanded and epoxied multiple times for a smooth surface finish. Carbon fiber will also be laid over these molds and used for the body panels. The product panels of the mold will then be bent over the frame for the proper shape. This will be accomplished during C term.

Electronics

There were several electronic components that were mounted on the firewall. Due to limited space in the frame, the firewall was determined to be the best mounting location available. The largest component on the front side of the firewall is the battery. The battery is not physically mounted to the firewall, but is contained inside a 22 gage 5052 aluminum box bolted to the firewall, as shown in Figure 135 below. Underneath the battery are two clearance holes lined with rubber grommets for the terminal cables to run through the firewall to connect it to the battery. The vehicle's management system is a Haltech Elite 1500, which tells the system when to inject fuel and how much to inject. The Haltech is mounted on the front driver's left side of the firewall for easy accessibility for wiring. These two components are the largest and were the first to be wired in the wiring harness so took priority in mounting locations, as shown below in the left picture.

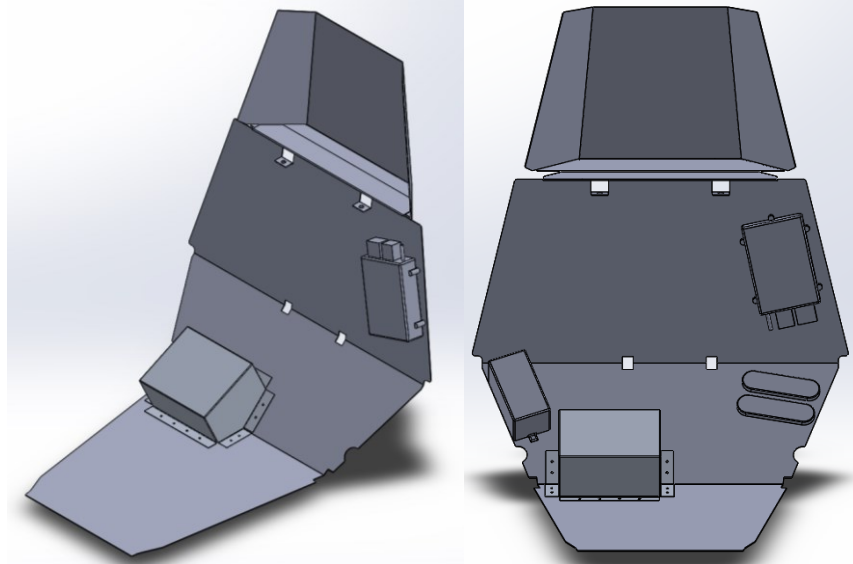


Figure 135. Component mount locations on Firewall

The next component mounted on the front of the firewall was the fuse box, which is on the driver's right side above the battery box, as shown in Figure 135 above. The fuse box is connected to the Haltech and is part of the ECU system. There are two junctions, one is ground and the other is 5 volts, that are mounted on the driver's left side of the firewall underneath the Haltech. The battery, Haltech, fuse box, and electrical junctions are all mounted on the front of the firewall underneath the seat. The rectifier, 200 amp circuit breaker, and the starter relay are all mounted on the back of the firewall. Due to tight packaging constraints these electrical components were forced to be mounted to the firewall. The heat from the muffler made mounting to the back of the firewall more difficult due to less space available.

Seat

There were a few different methods that were used to make the seat in the vehicle. The first method was to use the leather seat from the previous MQP vehicle and make a mold out of fiberglass. The fiberglass mold had a rough finish with too many bumps and wrinkles. Therefore, bondo was then used to fill in the gaps and crevices and make the mold smooth. However, the mold was not perfectly symmetric was still rough around the edges. The goal of the smooth fiberglass was to then lay carbon fiber over it and have a nice carbon fiber surface finish. The carbon fiber mold would then be padded and used as a final seat. This idea was not followed through after it was determined the fiberglass was not well suited to be layered in carbon fiber.

The second method was to use a plastic go-kart seat and expanding foam to create a mold. A sixteen pound kit of two pound density urethane foam was used from US Composites. A bag covered the go-kart seat and the mixed urethane foam was poured into the bag and expanded into the seat shape. Once the foam hardened the seat was removed and the mold was sanded and cut in order to fit into the frame. This mold was better than the previous fiberglass mold in terms of the shape and surface finish. After creating this mold, epoxy was then used to cover the outside in order

to lay up carbon fiber. The goal was to similarly use carbon fiber as the seat and cover it in padding for the driver. However, the epoxy did not sit well over the expanding foam and in some areas ate away at and ruined the foam. This foam mold was not created to be the seat itself so another iteration was completed for the seat.

The last iteration for the seat was also using the sixteen pound kit of two pound density urethane foam. Although the method to create this seat was slightly different. A bag was laid in the frame and the go-kart seat was placed over it. A team member then sat in the seat in the best position for a driver. The position was determined by having the member hold onto the wheel, properly place his foot on both the throttle and brake, and having the member pass the driver's restraint system rule. The driver's restraint system rule states that a driver's helmet must be at least two inches apart from the straight line from the top of the main hoop to the top of the front hoop. When the member was in position his helmet was more than two inches from that line and he was comfortable with his hands on the wheel and his foot on the pedal. After the member was properly positioned, the expanding foam was poured into the bag and conformed to the seat and the firewall. After the foam hardened the seat and bag were removed and the foam was taken out of the bag. The foam mold was then cut and sanded to a desirable shape. This goal with this last foam mold was to cover it with leather and use it for the seat. After cutting holes in the back for space for the electronics, as described in the electronics section above, the seat was covered in leather. The final seat is shown below in Figure 136.



Figure 136. Leather Seat

Scheduling Overview

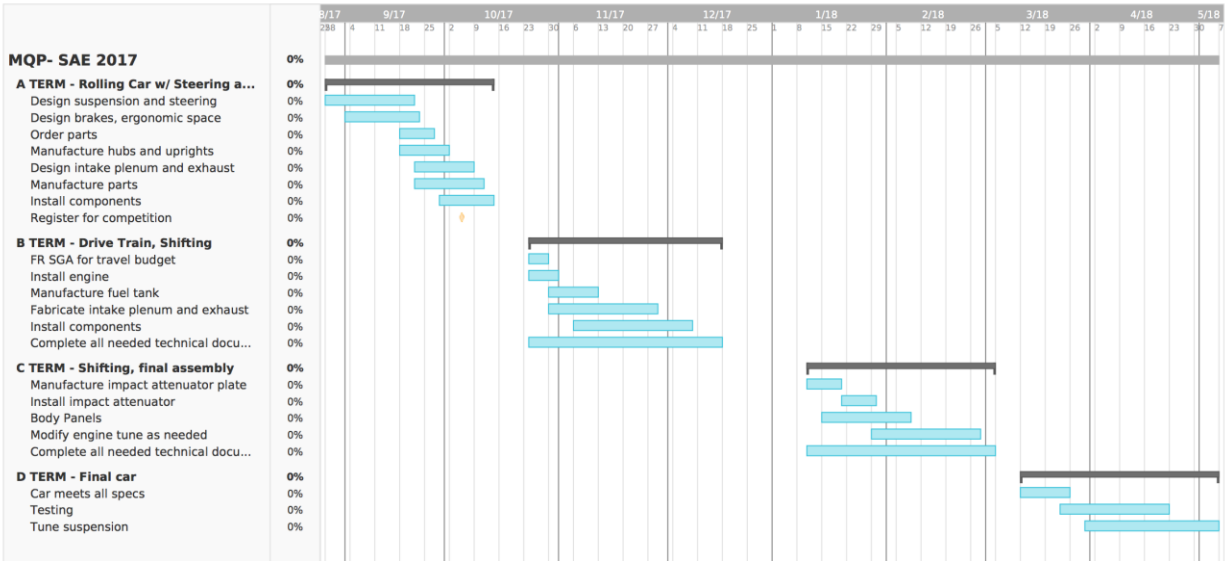


Figure 137. Beginning of Year Gantt Chart

Shown above, in Figure 137, is the Gantt Chart that was used at the beginning of the year. The team’s goal for A term was to have a rolling car with steering. This was a very ambitious goal that the team did not believe they would reach but was put in place to make great progress. The goal for B term was to then have a rolling car, with the drivetrain and shifting done. The majority of design work was done during A term. Initial design concepts were ruled out and several designs were finalized. During B term most of the manufacturing was done. The frame was sent to a few welders so the tabs and a-arms could be welded. Due to time constraints and not getting the frame back, the team was unfortunately not able to have a rolling car at the end of B term. However the drivetrain and shifting were finalized and the car was built and started being tested in C term. The team finished most of the design work early in the process and did a lot of the manufacturing all at once afterwards.

In C and D term, the team validated designs and made sure all the parts fit properly on the vehicle. After the vehicle was tested once or twice the team took apart the whole vehicle to paint the frame. Then the vehicle was put back together and everything fit properly without any issues. Testing was then performed for the rest of D term until competition.

Bibliography

- Ales, M., Mendoza, R., Thomas, M., & Vinokurov, L. (2010). Cal Poly Formula SAE Engine Development. San Luis Obispo: California Polytechnic State University. Retrieved from: <http://digitalcommons.calpoly.edu/mesp/32/>
- Auto Dynasty. (n.d.) *7 Inch High Performance Black Electric Radiator Cooling Fan Assembly Kit* [Photograph]. Retrieved from: <https://www.amazon.com/Performance-Electric-Radiator-Cooling-Assembly/dp/B00H29LGXM?th=1>
- Bergman, T. L., Lavine, A. S., Incropera, F. P., and Dewitt, D. P. (2011). Heat Exchangers. In *Fundamentals of Heat and Mass Transfer* (7th ed.) (pp. 705-766). Hoboken, NJ: John Wiley & Sons, Inc.
- Blair, G. P. & Cahoon, W. M. (2006, September). Best Bell: Design of an Intake Bellmouth. *Race Technology Magazine*, 34-41. Retrieved from: http://www.proflairandassociates.com/pdfs/RET_Bellmouth_Sept.pdf
- Deshpande, O. N., & Narappanawar, N. L. (1-3 July, 2015). Space Advantage Provided by De-Laval Nozzle and Bell Nozzle over Venturi. *Lecture Notes in Engineering and Computer Science: Proceedings of The World Congress on Engineering 2015* (pp. 1165-1168). Retrieved from <http://www.iaeng.org/publication/WCE2015/>
- Flex-A-Lite. (2010). *The Truth About Airflow and Amperage*. Retrieved from: <https://www.flex-a-lite.com/blog/the-truth-about-airflow-and-amperage/>
- Formula SAE Forum Thread. (2013, October). Retrieved February 05, 2018, from <http://www.fsae.com/forums/showthread.php?11652-Roll-rates-in-RCVD>
- Moran, M. J., & Shapiro, H. N. (2004). *Fundamentals of Engineering Thermodynamics* (5th ed.). John Wiley & Sons, Inc.
- Hamilton, L., Cowart J. (2010). Modeling the Effects of Intake Plenum Volume on the Performance of a Small Naturally Aspirated Restricted Engine. *ASME 2010 Internal Combustion Engine Division Fall Technical Conference*, 893-901. doi:10.1115/ICEF2010-35023
- Harris, W. (2005, May 11). *How Car Suspensions Work*. HowStuffWorks. Retrieved February 05, 2018, from auto.howstuffworks.com/car-suspension.htm.
- Hilderbrand, J. C. (2012). *2012 Yamaha WR450F Shootout*. Retrieved from: <http://www.motorcycle-usa.com/2012/05/article/2012-yamaha-wr450f-shootout/>
- Hot Cams, Inc. (n.d.). *Camshafts, Part Number 4023-1IN*. Retrieved from: http://www.hotcamsinc.com/ProductInfo.aspx?item_id=559
- Hot Cams, Inc. (n.d.). *Camshafts, Part Number 4044-1E*. Retrieved from: http://www.hotcamsinc.com/ProductInfo.aspx?item_id=574

- Kasprzak, J. (2011, May 13). *Damping Calculations*. Retrieved February 5, 2018, from <http://www.kaztechnologies.com/wp-content/uploads/2014/03/FSAE-Damping-Calculations-Seminar.pdf>
- Kojima, M. (2011, December 26) *The Ultimate Handling Guide Part 8: Understanding Your Caster, King Pin Inclination and Scrub*. MotoIQ. Retrieved October 05, 2017, from www.motip.com/MagazineArticles/ID/1982/The-Ultimate-Handling-Guide-Part-8-Understanding-Your-Caster-King-Pin-Inclination-and-Scrub.aspx.
- Mariucci, V., Selamet, A., & Miazgowicz, K. D. (2007). *Effect of Primary Intake Runner Tapers and Bellmouths on the Performance of a Single Cylinder Engine* (No. 2007-01-0382). SAE Technical Paper. Retrieved from: <http://engine.osu.edu/ASJP/JP/J72.pdf>
- Miller, J. (2008). *Turbo: Real World High-performance Turbocharger Systems*. North Branch, MN: CarTech. Print.
- Milliken, Douglas. (2001). *Formula SAE Tire Test Consortium*. Milliken Research Associates, Inc, Milliken Research Associates, Inc.. Retrieved February 01, 2018, from www.millikenresearch.com/fsaettc.html.
- Milliken, W.F., Kasprzak, E. M., Milliken, D. L., & Mets, L. D. (1995). *Race car vehicle dynamics*. Warrendale: SAE International
- Mirani, A. A., Khan, J., Solangi, S. A., and Channar, A. A. (2008). Performance Evaluation of a Single Cylinder Four Stroke Petrol Engine. *ARPJN Journal of Engineering and Applied Sciences* (vol. 3, no. 4). Retrieved from: http://www.arpnjournals.com/jeas/research_papers/rp_2008/jeas_0808_1211.pdf
- Mishimoto. (n.d.) *Kawasaki KFX450R Aluminum Radiator, 2008-2014* [Photograph]. Retrieved from: <https://www.mishimoto.com/kawasaki-kfx450r-aluminum-radiator-08-11.html>
- Moser, Tyler, et al. (2015). *DESIGN AND OPTIMIZATION OF A FSAE VEHICLE*. Web.
- Norton, R. L. (2014). *Machine Design an Integrated Approach* (Vol. V). Boston, Mass.: Prentice Hall.
- Ohlins TTX25 MkII Product Page. (n.d.). Retrieved February 5, 2018, from <https://www.ohlinsusa.com/suspension-products/Automotive/Auto Racing/Shock Absorber/70/TTX25 MkI>
- Pingel Enterprise, Inc. (n.d.). *Electric Speed Shifters*. Retrieved from: <http://www.pingelonline.com/prodcat/electric-speed-shifters.asp>
- SAE International. (2017). *2017-2018 Formula SAE® Rules - September 13, 2017*. Retrieved from: <https://www.fsaeonline.com/page.aspx?pageid=e179e647-cb8c-4ab0-860c-ec69aac080a3>
- Sanyo Denki. (n.d.) *San Ace Splash Proof Fan 140x140x51mm*. Retrieved from: <https://products.sanyodenki.com/en/contents/hp0094/list.php?CNo=94&ProCon=1315>

Sutton, G. P., and Biblarz, O. (2017). Nozzle Theory and Thermodynamic Relations. In *Rocket Propulsion Elements* (9th ed.) (pp. 45-98). Hoboken, NJ: John Wiley & Sons, Inc.

Taylor Creative Inc. (n.d.). *BTL Series Inner Hub / Pressure Plate Kit Yamaha WR450F 2003-2009, 2011-2016*. Retrieved April 08, 2018, from <http://hinsonracing.com/product/btl-series-inner-hub-pressure-plate-kit-yamaha-wr450f-2003-2009-2011-2016/>

Technical Papers. (2017). Retrieved February 05, 2018, from <http://www.optimumg.com/technical/technical-papers/>

Updated: YFZ 450R - Model Review. (2013, November 08). Retrieved April 08, 2018, from <http://www.atvriders.com/atvreviews/yamaha-2014-yfz450r-review-p2.html>

Vertex Pistons, Inc. (n.d.). *Performance Piston Kit, Part Number 22896C*. Retrieved from: http://www.na.vertexpistons.com/ProductInfo.aspx?item_id=325

Appendix A. WR450F Clutch Retrofit Forum Posts

<http://supermotojunkie.com/showthread.php?200073-Factory-Yamaha-Slipper-Clutch>

<https://thumpertalk.com/forums/topic/1201436-slipper-clutch-for-2012-wr450f-yzf450-atv-adige/>

Appendix B. Brake Force Calculations

Below are the equations used for the brake system calculations shown in Figure 138 and Figure 139 on the following pages.

$$\text{Brake pedal output force } F_{out} = R_{pedal} * F_{in}$$

$$\text{Master cylinder output pressure } P_{line} = \frac{F_{out}}{A_{mstercylinder}}$$

$$\text{Brake caliper clamping force } F_{clamp} = P_{line} * A_{caliper}$$

$$\text{Friction force of brake pads } F_{friction} = F_{clamp} * \mu_{pad}$$

$$\text{Brake torque } T_{brake} = F_{friction} * r_{rotor}$$

Car with 5/8" front and 13/16" rear master cylinders			
Front		Rear	
GS Compact Remote Master Cylinder (5/8 bore)		GS Compact Remote Master Cylinder (13/16 bore)	
DH 4 Dual Hydraulic Caliper		Wilwood SC3 Single Pistons	
Brake Peddle Lever Ratio (lbs)			
pedal force (lbs)	37	pedal force (lbs)	37
Linkage Length (in)	1	Linkage Length (in)	1
Pedal length (in)	5.2	Pedal length (in)	5.2
	192.4		192.4
Master Cylinder Pressure (psi)			
Area Master Cyl (in ²)	0.31	Area Master Cyl (in ²)	0.52
	620.6451613		370
Line Pressure = at both ends			
Caliper Force (lbs)			
Area Caliper (in ²)	3.54	Area Caliper (in ²)	1.74
	2197.083871		643.8
Clamping Froce (lbs)			
	4394.167742		1287.6
Brake Pad Friction (lbs)			
Friction Coef Pads	0.4	Friction Coef Pads	0.4
	1757.667097		515.04
Rotor Torque (ft*lbs)			
Rotor radius (in)	4	Rotor radius (in)	4
	585.89		171.68
Brake Torque %		Required Torque %	
Front	77.3	Front	81
Rear	22.7	Rear	19

Figure 138. Brake System Design for Original Values.

Front		Rear	
GS Compact Remote Master Cylinder (5/8 bore)		GS Compact Remote Master Cylinder (13/16 bore)	
Wilwood Billet Dynalite Single		Wilwood PS-1 Calipers	
Brake Peddle Lever Ratio (lbs)			
pedal force (lbs)	25	pedal force (lbs)	25
Linkage Length (in)	1	Linkage Length (in)	1
Pedal length (in)	5.2	Pedal length (in)	5.2
	130		130
Master Cylinder Pressure (psi)			
Area Master Cyl (in ²)	0.31	Area Master Cyl (in ²)	0.52
	419.3548387		250
Line Pressure = at both ends			
Caliper Force (lbs)			
Area Caliper (in ²)	4.8	Area Caliper (in ²)	1.58
	2012.903226		395
Clamping Froce (lbs)			
	4025.806452		790
Brake Pad Friction (lbs)			
Friction Coef Pads	0.4	Friction Coef Pads	0.4
	1610.322581		316
Wilwood 15E-6083K PolyMatrix E Compound		Wilwood 150-4091K Sintered Metallic Compound	
Rotor Torque (ft*lbs)			
Rotor radius (in)	4	Rotor radius (in)	4
	536.77		105.3333333
Brake Torque %		Required Torque %	
Front	83.6	Front	70
Rear	16.4	Rear	30

Figure 139. Brake System Design with Final Values.

Appendix C. Simulation Study for Differential Mount FEA

This appendix describes the procedures and settings used to run FEA on the final version of the differential mounts. This process was repeated after any modifications to the design to verify the integrity of the mounts. Assumptions are listed throughout, as appropriate. The table below shows the overall settings used for the FEA simulation.

Table 11. Overall Settings for Differential Mount FEA

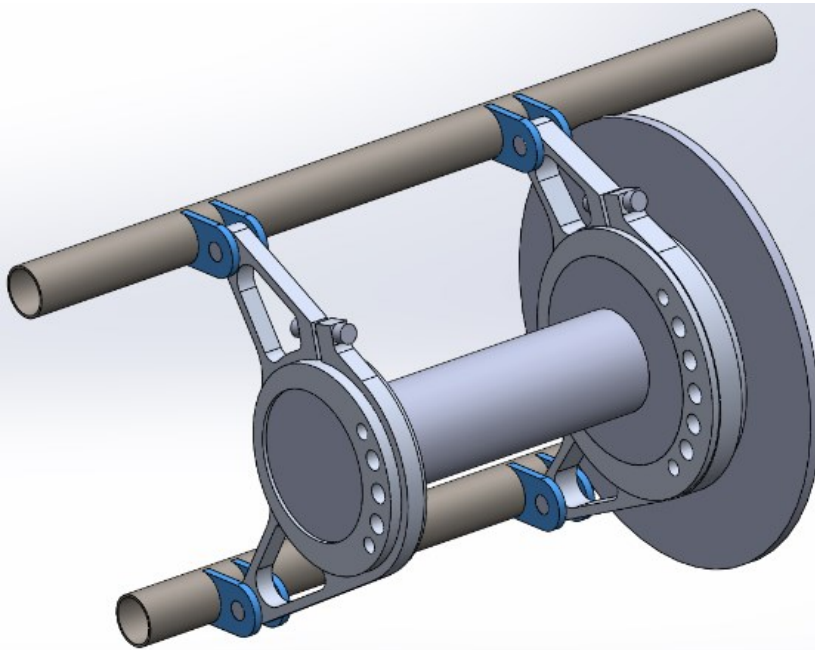
Study name	Static 1
Analysis type	Static
Mesh type	Mixed Mesh
Thermal Effect:	On
Thermal option	Include temperature loads
Zero strain temperature	298 Kelvin
Include fluid pressure effects from SOLIDWORKS Flow Simulation	Off
Solver type	FFEPlus
Inplane Effect:	Off
Soft Spring:	Off
Inertial Relief:	Off
Incompatible bonding options	Automatic
Large displacement	Off
Compute free body forces	On
Friction	Off
Use Adaptive Method:	Off

Components and Assembly

The assembly used for this FEA simulation included all custom designed components of the differential mounts, including the bearing cups, mount brackets, and frame tabs. The tab bolts and pinch bolts used to hold the mounts in place were substituted by simplified representations constructed from basic geometric shapes. The table below lists the file names of each of the parts and the material assigned to each. The images below also show the complete assembly, with each part highlighted.

Part File Name(s) and Position(s)	Notes
Frame Mount Tabs	<ul style="list-style-type: none"> • 8 Places, positioned as on

F18_DT_DiffMountTab_v100417.SLDPRT



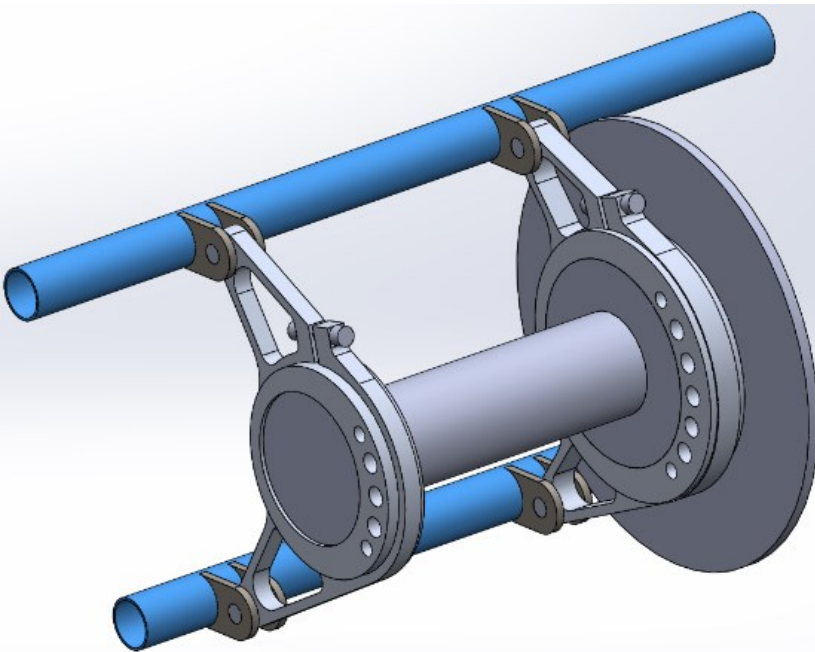
actual frame

Material:

- AISI 4130 Steel, Normalized at 870 C
- Based on assumption at time of design that frame would be normalized after tab welding.

Frame Tube Substitutes

F18_DT_FrameBotTubeFEA.SLDPRT
F18_DT_FrameTopTubeFEA.SLDPRT



- Lengths taken from actual tube lengths, ignoring tube joint miters for simplicity
- ID/OD taken from actual frame tubes

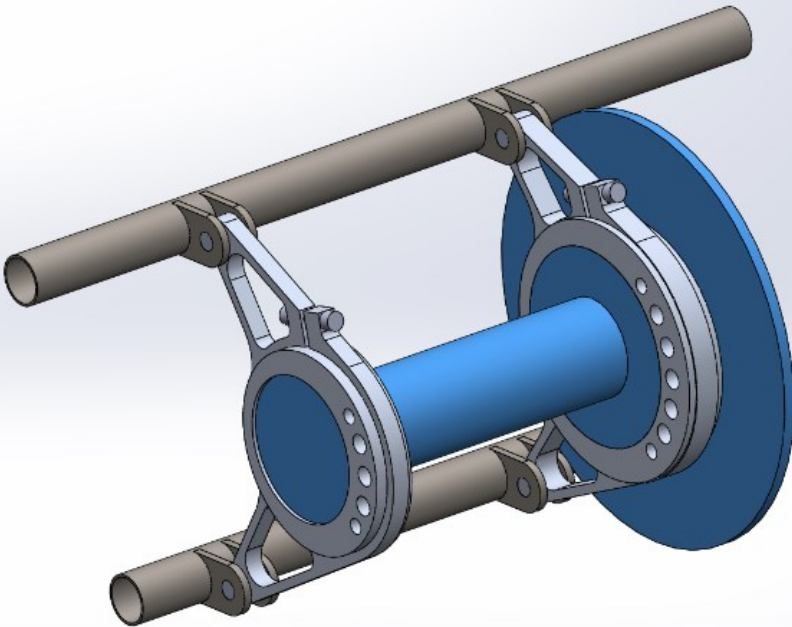
Material:

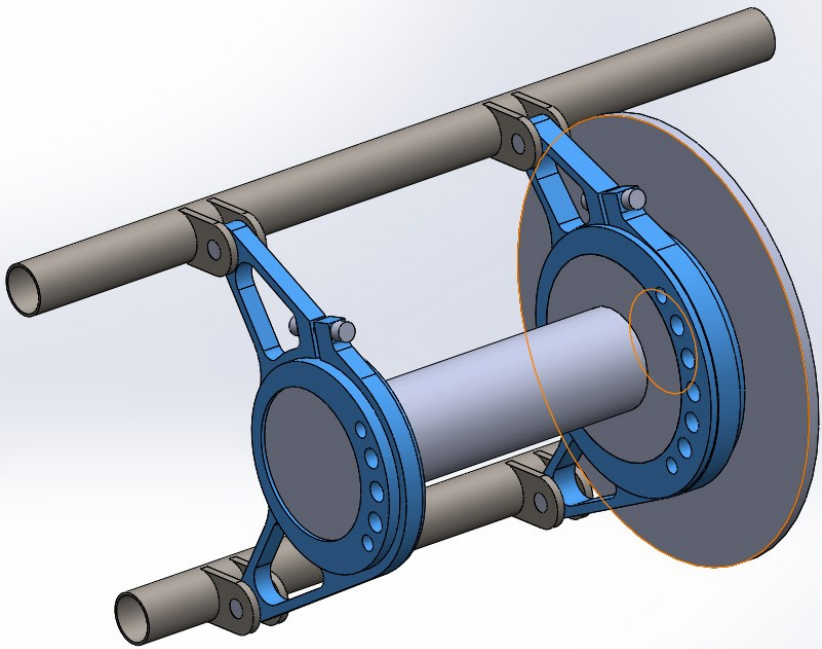
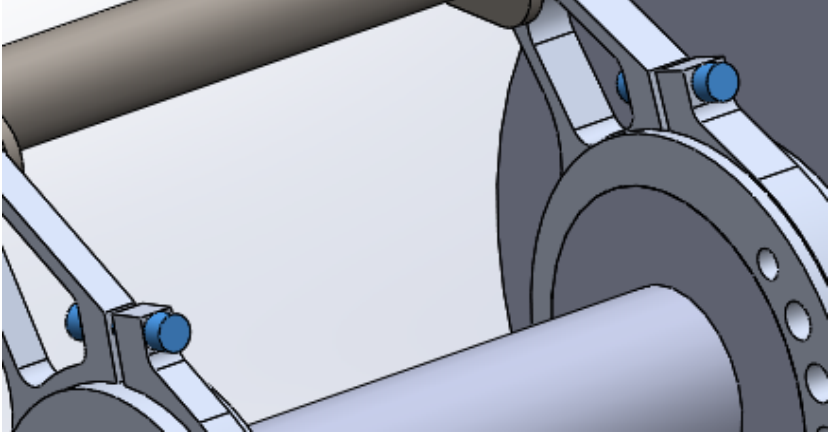
- AISI 4130 Steel, Normalized at 870 C
- Based on assumption at time of design that frame would be normalized after tab welding.
- Not made rigid to allow observation of effect of tabs on frame tubes

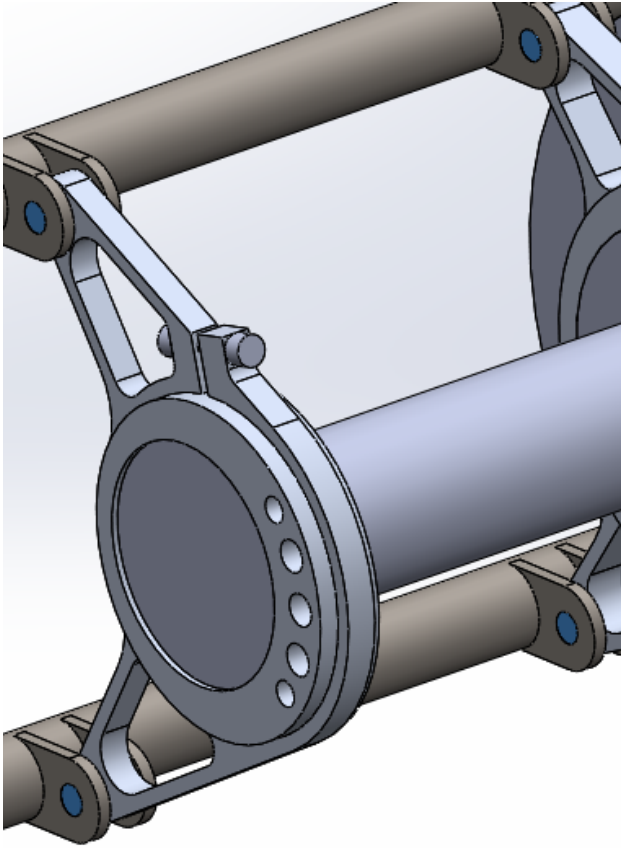
Differential Assembly Blank

F18_DT_DiffBlankFEA.SLDPRT

- Simplified model representing only bearing

	<p>and sprocket outer diameters where the differential assembly contacts the mounts and receives force from the chain</p> <ul style="list-style-type: none"> • Effects of axles on differential assembly assumed to be purely in torsion about axis of differential, allowing the axles to be omitted • Sprocket assumed to be 38 tooth, diameter of blank uses pitch diameter • Sprocket horizontally positioned up against inboard plane of splined interface on Drexler differential due to lack of information about sprocket carrier at time of simulation <p>Material:</p> <ul style="list-style-type: none"> • Made Rigid for Analysis • Based on lack of information about material composition of Drexler differential and bearings, and to simplify analysis
<p>Differential Mount Brackets and Eccentric Cups F18_DT_DiffMountV2_DriveSideEccCup_v100417.SLDPRT F18_DT_DiffMountV2_DriveSideMount_v100417.SLDPRT F18_DT_DiffMountV2_NonDriveSideEccCup_v100417.SLDPRT F18_DT_DiffMountV2_NonDriveSideMount_v100417.SLDPRT</p>	<ul style="list-style-type: none"> • Differential mounts, using current design for each simulation run • Assembled with differential in farthest rearward position, i.e. maximum chain tension <p>Material:</p> <ul style="list-style-type: none"> • Al 6061 T6 (SS) • At time of simulation Al 6061 was used as the most likely material for the finished mounts • Al 7075 was used for mount brackets in final design, as it was readily available, but

	<p>simulation was assumed superfluous due to the overall higher strength of Al 7075</p>
<p>Pinch Bolts F18_DT_DiffMountV2_PinchBolt.SLDPRT</p> 	<ul style="list-style-type: none"> • Simplified pinch bolts, with cylindrical sections representing the bolt head, bolt shank, and nut • Bolt tension when clamped was overlooked <p>Material:</p> <ul style="list-style-type: none"> • Alloy Steel • Alloy steel fasteners would be used on the car, and using the material assumed to allow for more realistic stretching and flexing
<p>Tab Bolts F18_DT_DiffMountV2_Bolt.SLDPRT</p>	<ul style="list-style-type: none"> • Simple cylindrical models simulating the shoulder bolts used for these joints • Head and nut sections assumed to be superfluous due to the perpendicular load application <p>Material:</p>

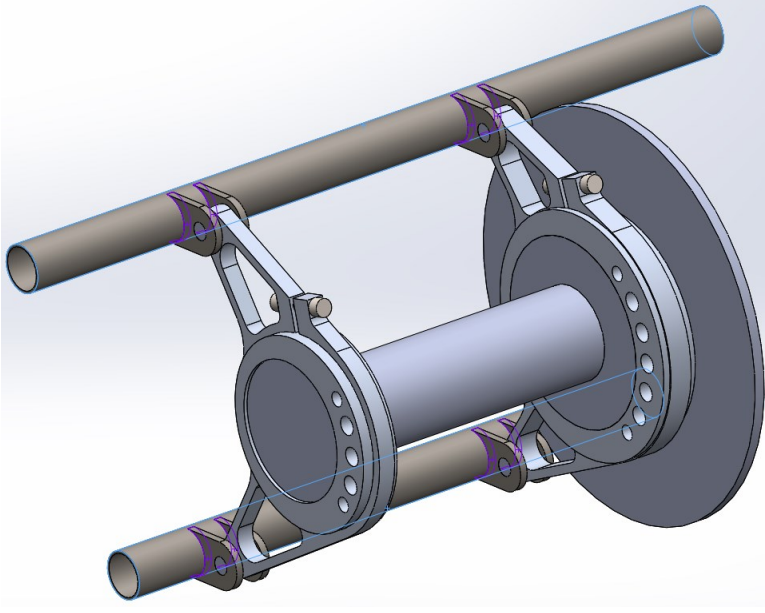
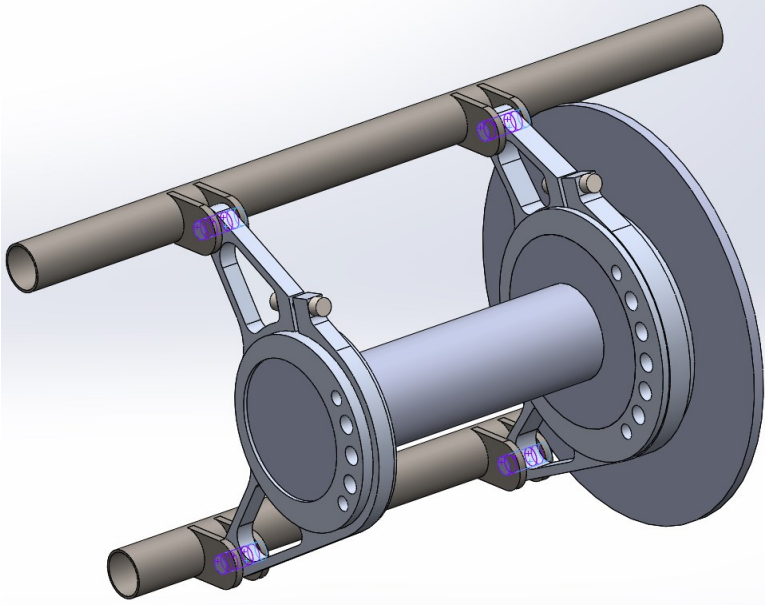


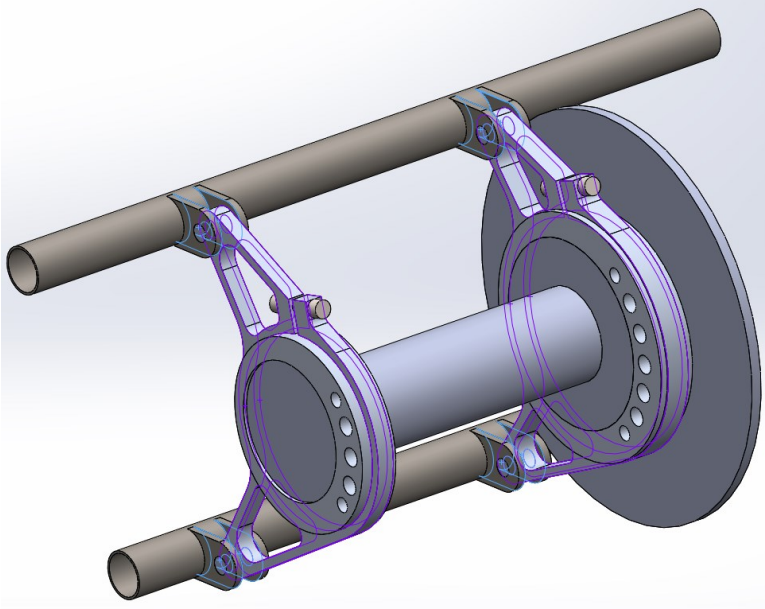
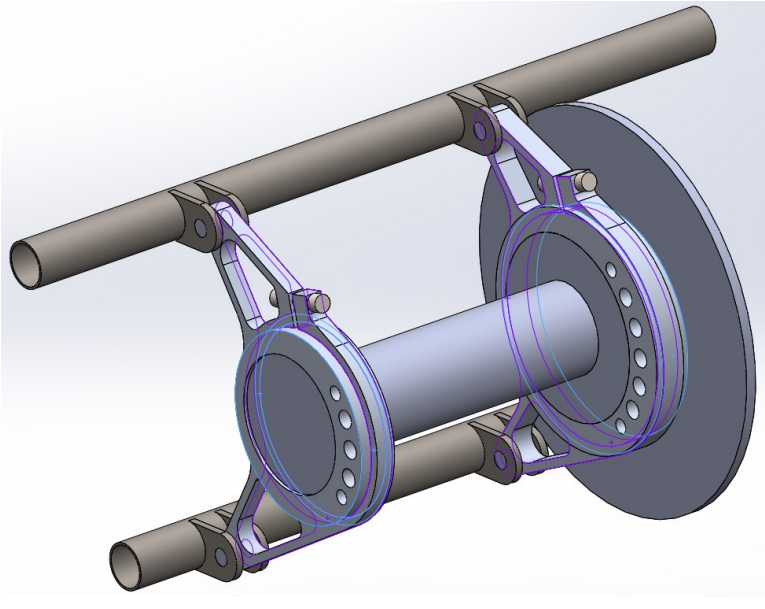
- Made rigid for analysis
- Due to large shoulder diameter, tab bolts assumed to be effectively rigid, and were made so to simplify the simulation

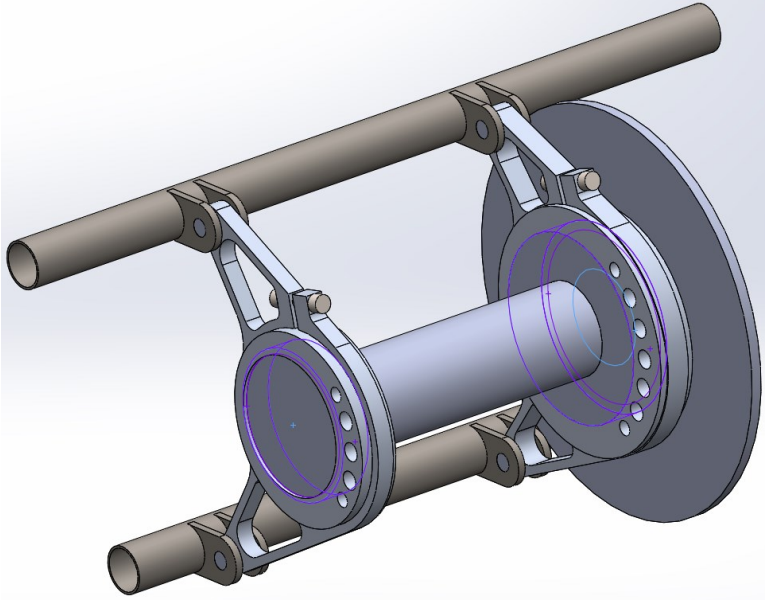
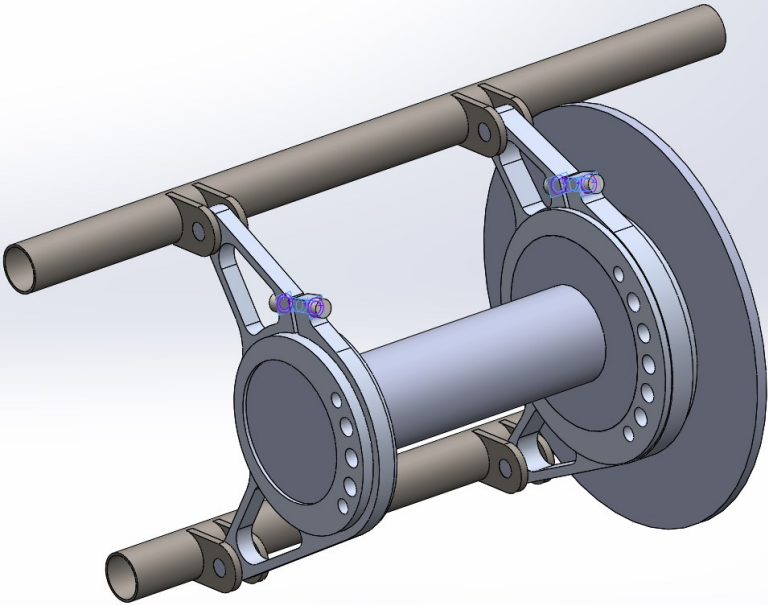
Contact Sets

Several contact sets were used to constrain the behavior of the model. The table below describes the implementation and reasoning of each contact set.

Contact Set, Parts Involved	Description
Contact Set 1 Frame Mount Tabs, Frame Tube Substitutes	<ul style="list-style-type: none"> • 10 Faces • Bonded Contact • All faces where mount tabs contact frame tubes • Simplified representation of welds between the tabs and frame tubes, assuming the tab contact area is equal to the contact area of the weld

	
<p>Contact Set 2 Frame Mount Tabs, Tab Bolts, Differential Mount Brackets</p> 	<ul style="list-style-type: none"> • 16 Faces • No Penetration Contact • Friction ignored • Gap Ignored • No Advanced options used • Handles the bearing loads of the tab bolts on the tabs and mount brackets at the shear joints between the tabs and brackets • Friction, gaps, and advanced contact options assumed to be unimportant
<p>Contact Set 3 Frame Mount Tabs, Differential Mount Brackets</p>	<ul style="list-style-type: none"> • 12 Faces • No Penetration Contact • Friction ignored • Gap Ignored • No Advanced options used • Handles any horizontal loads between the tabs and mount

	<p>brackets</p> <ul style="list-style-type: none"> • Friction, gaps, and advanced contact options assumed to be unimportant
<p>Contact Set 4 Differential Mount Brackets, Differential Mount Eccentric Cups</p> 	<ul style="list-style-type: none"> • 8 Faces • No Penetration Contact • Friction ignored • Gap Ignored • No Advanced options used • Handles interactions between the differential mount cups and brackets, to keep the cups and brackets from intersecting • Friction, gaps, and advanced contact options assumed to be unimportant
<p>Contact Set 5 Differential Assembly Blank, Differential Mount Eccentric Cups</p>	<ul style="list-style-type: none"> • 8 Faces • No Penetration Contact • Friction ignored • Gap Ignored • No Advanced options used

	<ul style="list-style-type: none"> • Handles any load transfer between the bearing representative cylinders and the eccentric cups • Friction, gaps, and advanced contact options assumed to be unimportant
<p>Contact Set 6 Pinch Bolts, Differential Mount Brackets</p> 	<ul style="list-style-type: none"> • 14 Faces • No Penetration Contact • Friction ignored • Gap Ignored • No Advanced options used • Keeps the pinch bolts aligned with the holes, and prevents them from sliding in the holes by contacting the mount brackets • Friction, gaps, and advanced contact options assumed to be unimportant

Fixtures & Loads

This simulation uses a simple fixturing arrangement, in which the frame is assumed to be held fixed in space. The four end faces of the frame tube substitutes are held fixed, with no translation or rotation permitted. This assumes that these tubes are held fixed similarly in the real frame, only

allowed to bend and stretch about their fixed ends. The green arrows in the image below represent these fixtures, with one obscured by the sprocket representation.

The load is 1406 pounds-force, applied to the cylindrical face representing the pitch diameter of the sprocket. This load was calculated via the worst-case assumption discussed in the Differential Mount section of the report, in which the engine or transmission locks up at speed and the wheels break traction at 1.5 G of deceleration. This scenario results in 1406 pounds of tension in the chain, and it is assumed that this force acts exclusively linearly forward on the differential mounts. The pink arrows in the image below represent this force. In SolidWorks, this force is applied only to the one face as shown, with a uniform distribution and oriented directly forwards.

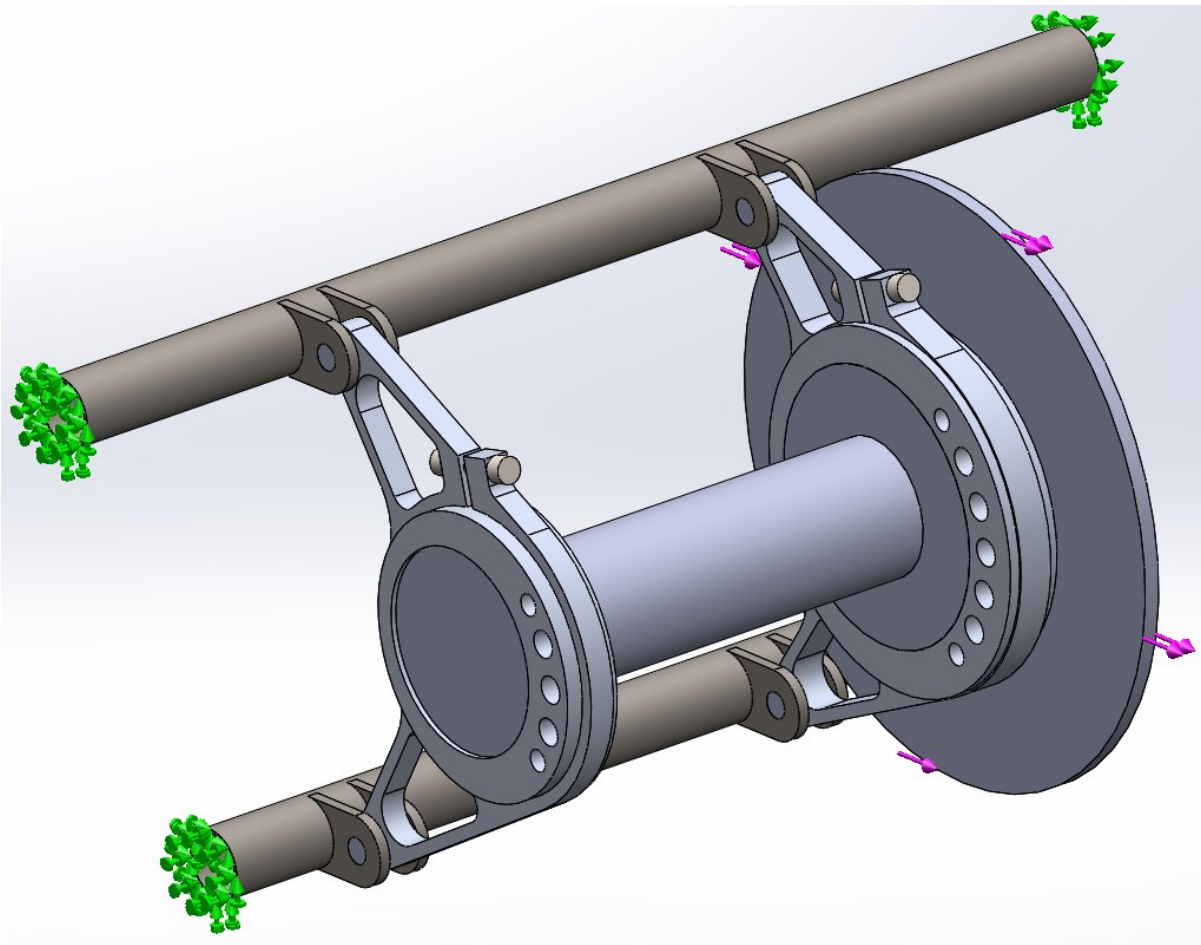


Figure 140. Fixtures and Loads for Differential Mount FEA

Mesh

The table below shows the details of the settings used to create the mesh for this study. Since this study was not extremely resource intensive to run, a high quality mesh was used to ensure accuracy of the results. The figure below shows the completed mesh with the fixtures and loads applied. Rigid components generally appear orange in this mesh, and components with materials assigned appear in their usual color.

Table 12. Mesh Settings and Output for Differential Mount FEA

Mesh type	Mixed Mesh
Mesher Used:	Standard mesh
Automatic Transition:	Off
Include Mesh Auto Loops:	Off
Jacobian points	4 Points
Jacobian check for shell	On
Element Size	6.077 mm
Tolerance	0.30385 mm
Mesh Quality Plot	High
Remesh failed parts with incompatible mesh	Off
Total Nodes	61018
Total Elements	30062

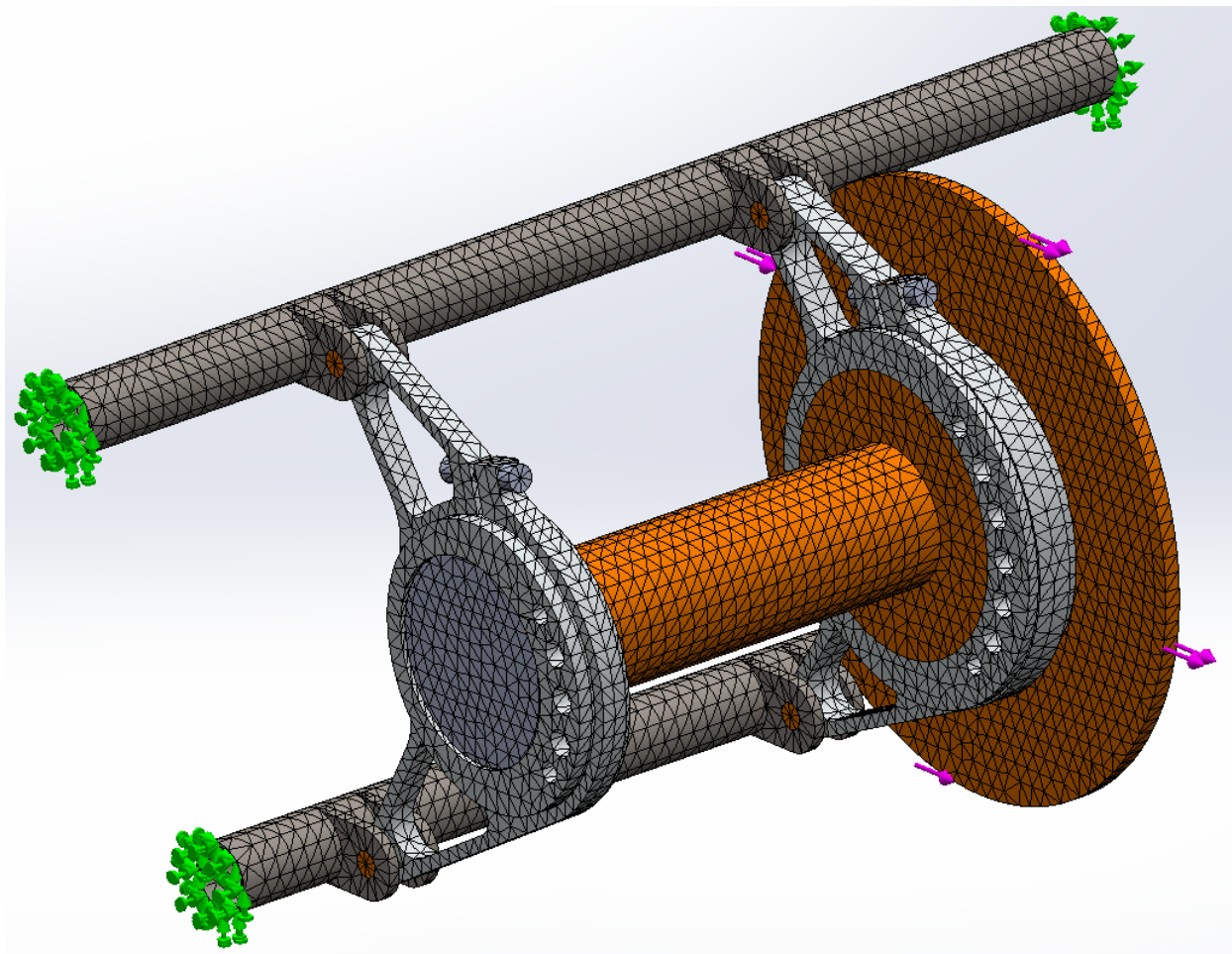


Figure 141. Mesh for Differential Mount FEA

Results

The results from this simulation were primarily reviewed with respect to the Factor of Safety output, as the most important design statistic for the purpose. The figures below show the result plots for Von Mises stress and Factor of Safety, with the rigid components hidden for visual clarity. A second image is provided for Factor of Safety to show only the components newly designed for the differential mounts, on which this study focuses.

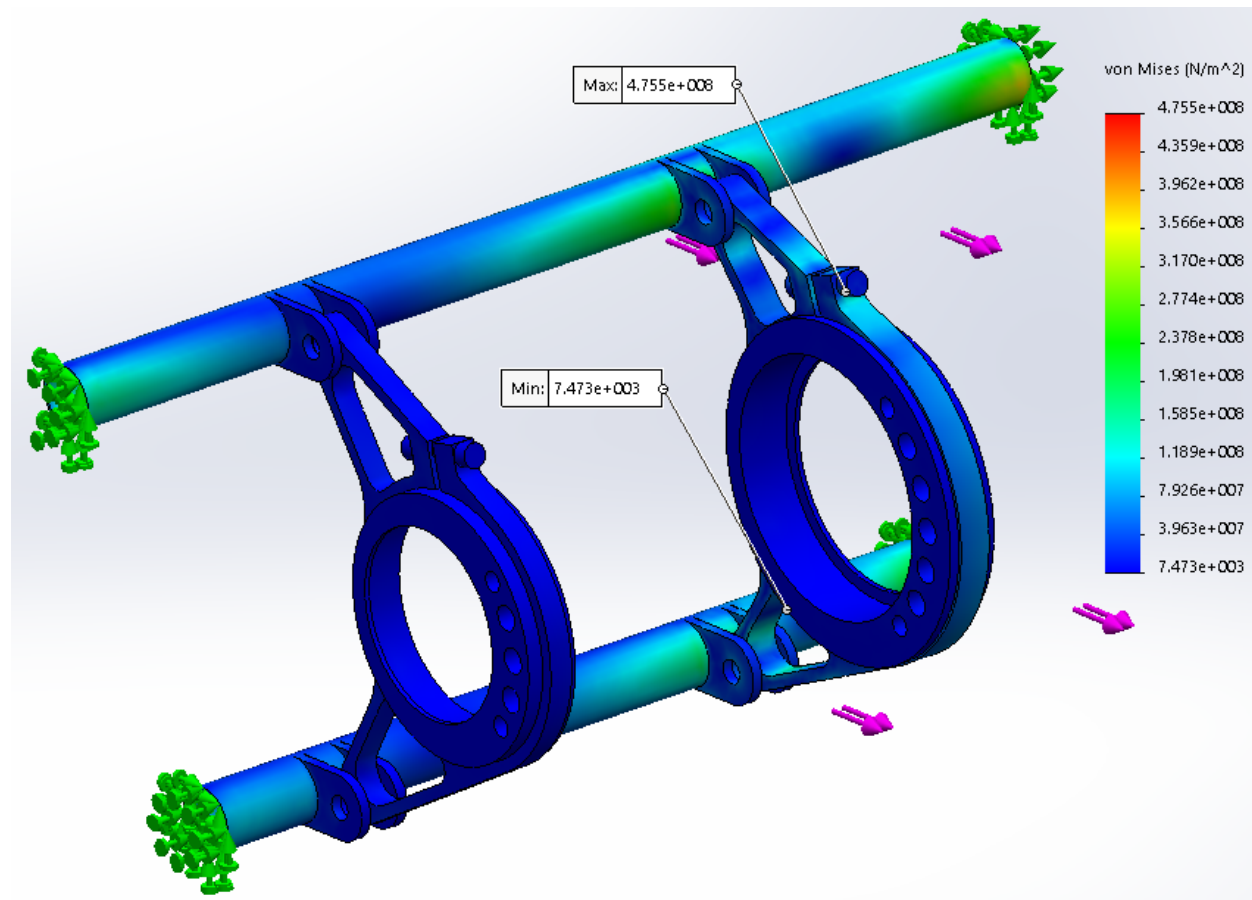


Figure 142. Von Mises Stress Plot of Differential Mounts, Including Frame Tube Substitutes

Although the images below show a minimum Factor of Safety of only 1.3, using the Probe tool to check the FOS at other locations on the part shows a minimum FOS of around 2 to 2.2. The minimum FOS stated by SolidWorks thus seems to be an artifact of the odd loading produced by the pinch bolt model. In practice, the current differential mount design shows a satisfactory FOS of about 2 under even this worst-case scenario, with the failure mode appearing to be ovalizing of the pinch bolt holes prior to failure of the mount proper.

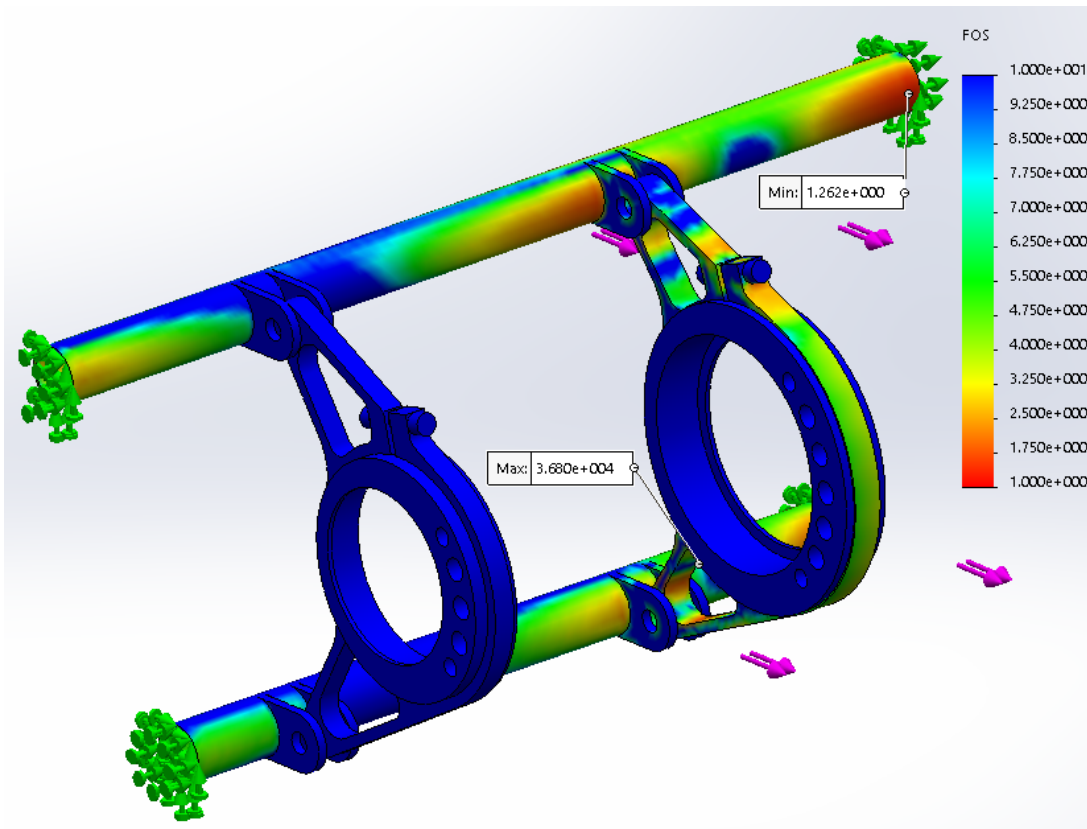


Figure 143. Factor of Safety Plot of Differential Mounts, Including Frame Tube Substitutes

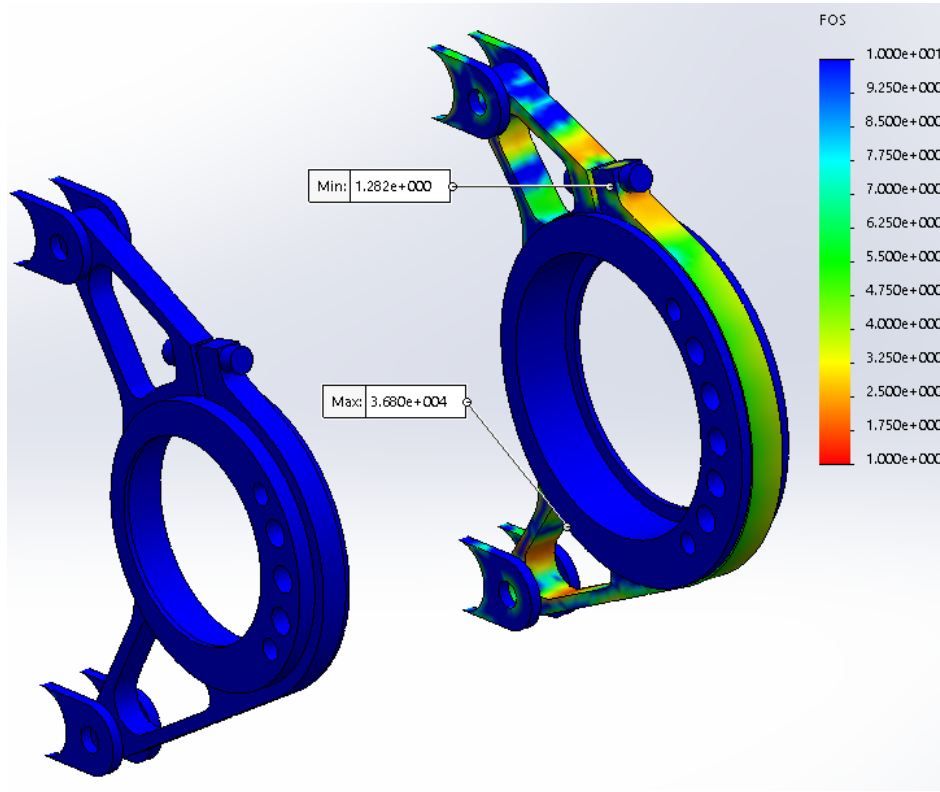


Figure 144. Factor of Safety Plot of Differential Mounts, Only Including Mounts and Tabs

Appendix D. Simulation Study for Sprocket Carrier FEA

This appendix describes the procedures and settings used to run FEA on the sprocket carrier. This process was repeated after any modifications to the design to verify the integrity of the design. Assumptions are listed throughout, as appropriate. The table below shows the overall settings used for the FEA simulation.

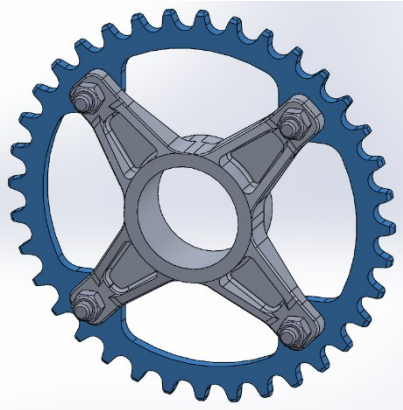
Table 13. Overall Settings for Sprocket Carrier FEA

Study name	Static 1
Analysis type	Static
Mesh type	Mixed Mesh
Thermal Effect:	On
Thermal option	Include temperature loads
Zero strain temperature	298 Kelvin
Include fluid pressure effects from SOLIDWORKS Flow Simulation	Off
Solver type	FFEPlus
Inplane Effect:	Off
Soft Spring:	Off
Inertial Relief:	Off
Incompatible bonding options	Automatic
Large displacement	Off
Compute free body forces	On
Friction	Off
Use Adaptive Method:	Off

Components and Assembly

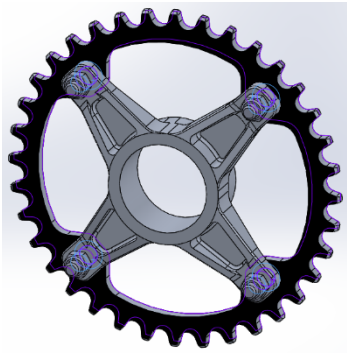
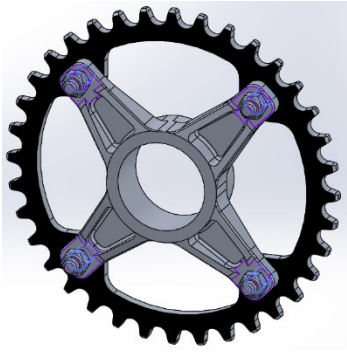
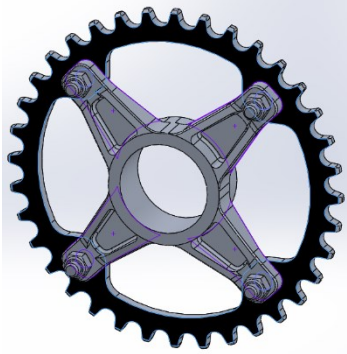
The assembly used for this FEA simulation included an accurate model of the 36 tooth sprocket purchased, models of the shoulder bolts connecting the sprocket to the carrier, and the sprocket carrier itself. The table below lists the file names of each of the parts and the material assigned to each. The images below also show the complete assembly, with each part highlighted.

Part File Name(s) and Position(s)	Notes
Sprocket Carrier F18_DT_SprocketCarrier_v013118.SLDPRT	Material: <ul style="list-style-type: none"> • Al 6061 T6 (SS) • Exact material of sprocket

	<p>carrier blank supplied by Drexler not known, but outward appearance suggested Al 6061 as a common and likely material for the part</p>
<p>Sprocket F18_DT_SprocketActual_36t_520_v013118.SLDPRT</p> 	<ul style="list-style-type: none"> • Bolt pattern dimensions measured manually • Tooth profiles found by researching standard 520 chain dimensions • At this point in design process, 36 tooth sprocket was decided and already bought <p>Material:</p> <ul style="list-style-type: none"> • Made Rigid for analysis • Assuming that sprocket will withstand any forces applied allows focus on sprocket carrier
<p>Sprocket Bolts F18_DT_SprocketBolt.SLDPRT</p> 	<ul style="list-style-type: none"> • Simplified model represents bolt head, shoulder, and nut <p>Material:</p> <ul style="list-style-type: none"> • Made Rigid for Analysis • Assuming the bolts will be strong enough, and are in fact oversized, making rigid simplifies calculation and speeds analysis

Contact Sets

Several contact sets were used to constrain the behavior of the model. The table below describes the implementation and reasoning of each contact set.

Contact Set, Parts Involved	Description
<p>Contact Set 1 Sprocket Carrier, Sprocket, Sprocket Bolts</p> 	<ul style="list-style-type: none"> • 13 Faces • No Penetration Contact • Friction ignored • Gap Ignored • No Advanced options used • All faces where Sprocket Bolts contact Sprocket, and some faces where Sprocket Bolts contact Sprocket Carrier
<p>Contact Set 2 Sprocket Carrier, Sprocket Bolts</p> 	<ul style="list-style-type: none"> • 16 Faces • No Penetration Contact • Friction ignored • Gap Ignored • No Advanced options used • Remaining faces where Sprocket Bolts contact Sprocket Carrier
<p>Contact Set 3 Sprocket Carrier, Sprocket</p> 	<ul style="list-style-type: none"> • 5 Faces • No Penetration Contact • Friction ignored • Gap Ignored • No Advanced options used • Face contact between Sprocket and Sprocket Carrier

Fixtures & Loads

This simulation uses a simple fixturing arrangement, in which the interface between the sprocket carrier and differential is assumed to be held fixed in space. The inside cylindrical face of the sprocket carrier, where the splines would be on the real sprocket carrier, is held fixed, with no translation or rotation permitted. The green arrows in the image below represent this fixture.

The load is 1406 pounds-force, applied to the sides of several teeth on the sprocket as an approximation of the load transfer from the chain with some degree of chain stretch to evenly distribute the load over several teeth. This load was calculated via the worst-case assumption discussed in the Differential Mount section of the report, in which the engine or transmission locks up at speed and the wheels break traction at 1.5 G of deceleration. The pink arrows in the image below represent this force. In SolidWorks, this force is applied as a Total force over the five faces selected and is directed horizontally.

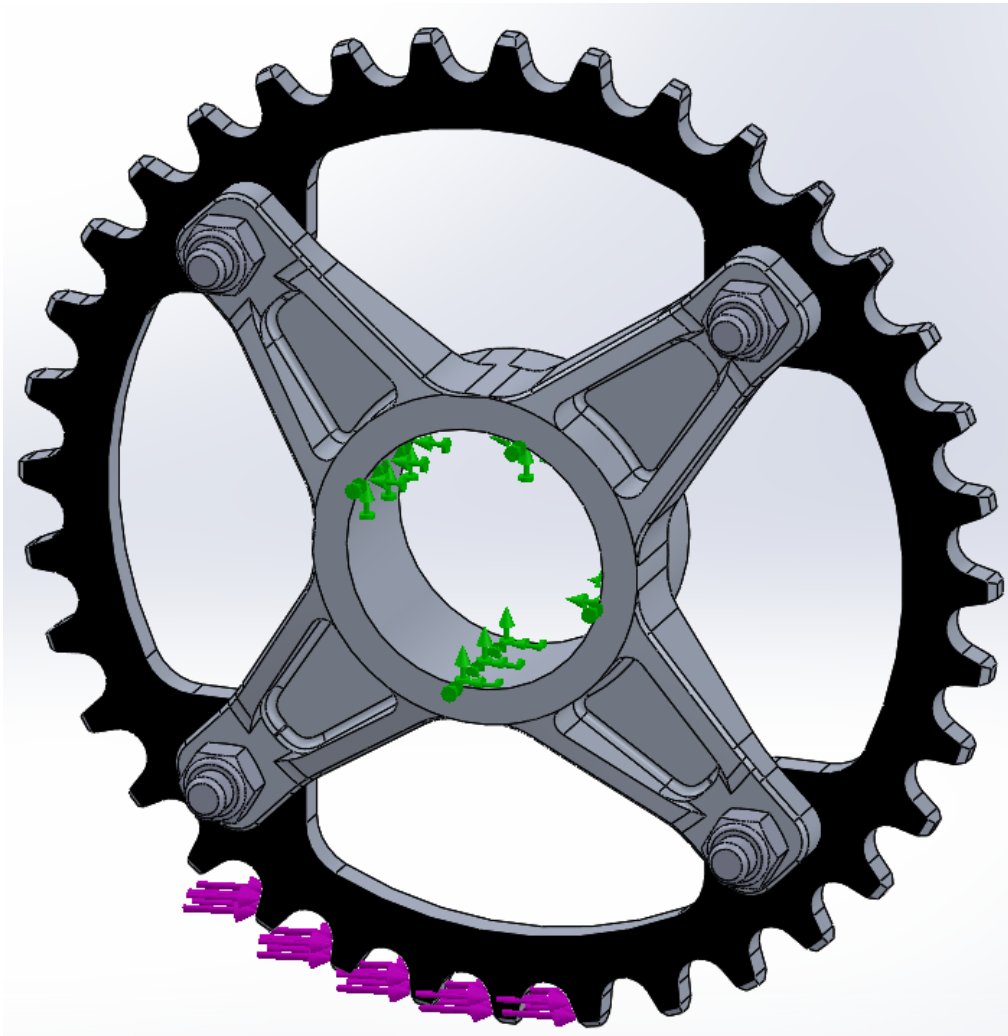


Figure 145. Fixtures and Loads for Sprocket Carrier FEA

Mesh

The table below shows the details of the settings used to create the mesh for this study. Since this study was not extremely resource intensive to run, a high quality mesh was used to ensure accuracy of the results. The figure below shows the completed mesh with the fixtures and loads applied. Rigid components appear orange in this mesh, and the sprocket carrier appears in its normal aluminum color.

Table 14. Mesh Settings and Output for Sprocket Carrier FEA

Mesh type	Mixed Mesh
Mesher Used:	Standard mesh
Automatic Transition:	Off
Include Mesh Auto Loops:	Off
Jacobian points	4 Points
Jacobian check for shell	On
Element Size	3.03925 mm
Tolerance	0.151962 mm
Mesh Quality Plot	High
Remesh failed parts with incompatible mesh	Off
Total Nodes	54905
Total Elements	31344

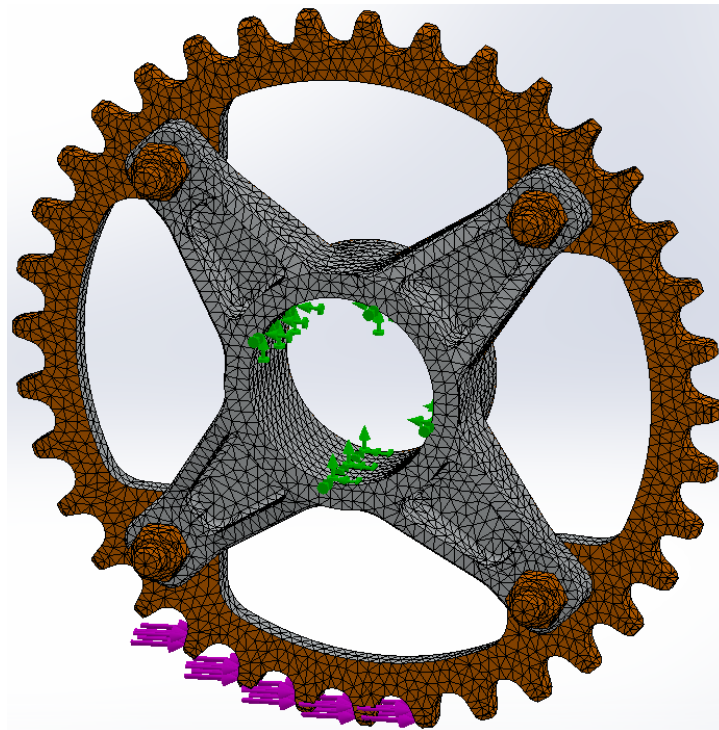


Figure 146. Mesh for Sprocket Carrier FEA

Results

The results from this simulation were primarily reviewed with respect to the Factor of Safety output, as the most important design statistic for the purpose. The figures below show the result plots for Von Mises stress and Factor of Safety, with the rigid components hidden for visual clarity. With a minimum factor of safety of 1.7 under this worst-case load, this sprocket carrier design was deemed strong enough to handle any loads encountered under typical operation, and was carried to completion and used on the vehicle.

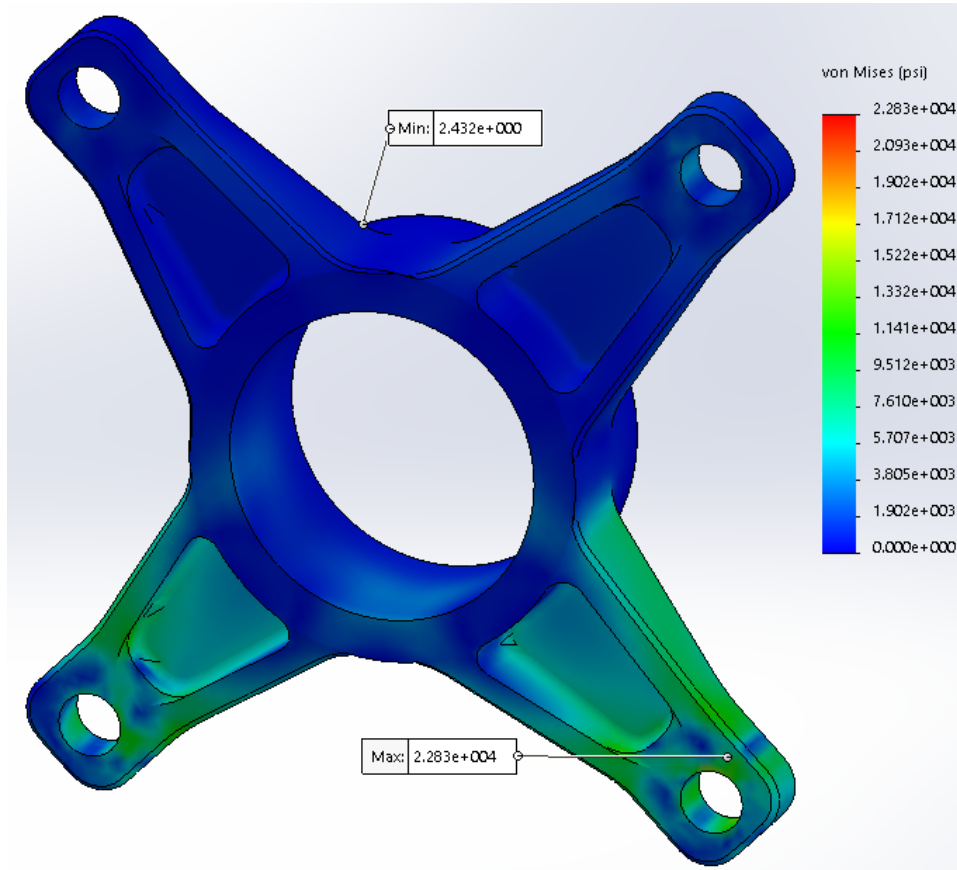


Figure 147. Von Mises Stress Plot of Sprocket Carrier

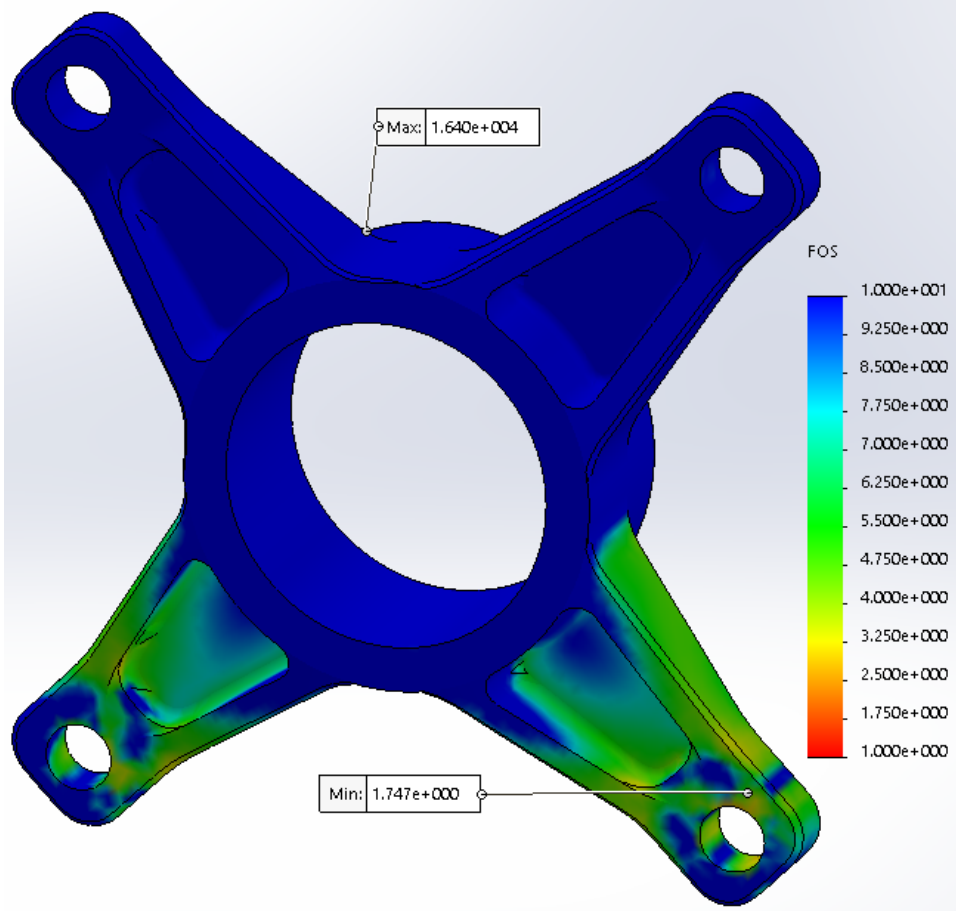


Figure 148. Factor of Safety Plot of Sprocket Carrier

Appendix E. Simulation Method for Air Intake

This appendix describes in greater detail the simulation configuration used for volumetric efficiency calculations on various air intake models. Due to the similarity of the various models used for simulation, this summary will only address the steps taken to simulate the final iteration of the air intake design. This appendix will follow a more instructional tone than one of exacting review.

Components and Assembly

As shown in several images in the Air Intake section of this report, any air intake used for simulation must include a model representing either an air filter or free air bubble around the inlet of the intake. The model must also include a model of the throttle body to be used with the air intake. At the other end, a model of the integral intake runner section for the engine must be attached to the outlet of any designed portion of the intake runner to ensure that the model includes some representation of the intake valves. For the simulation to run properly, the model must also not have any open orifices, such that the Flow Simulation software can treat the air intake as a fully closed volume. If the fuel injector port or some other opening does not have a part to close the gap, the Lids tool in SolidWorks Flow Simulation may be used to generate lids to close the model.

General Settings

In SolidWorks Flow Simulation, the General Settings for a Project can be accessed either in the Wizard when creating a project, or under the General Settings menu. The General Settings define the overall characteristics of the Flow Simulation scenario, and how the analysis will behave overall. The table below lists the settings used in each panel of the General Settings menu.

Tab	Settings	Notes
Analysis Type	<ul style="list-style-type: none"> • Analysis Type: Internal • Consider Closed Cavities: Exclude cavities without flow conditions • Heat Conduction in Solids: No • Radiation: No • Time-Dependent: Yes • Gravity: No • Rotation: No 	<ul style="list-style-type: none"> • Radiation significantly increases simulation time • Gravity is considered to have negligible effect on this simulation • Heat conduction is not important, since the intake constantly takes in ambient temperature air
Fluids	<ul style="list-style-type: none"> • Project Fluids: Air (Gases) – Default Fluid • Flow Type: Laminar and Turbulent • High Mach Number Flow: No • Humidity: No 	<ul style="list-style-type: none"> • Air must be selected from the Gases or Real Gases subsection in the upper portion of the menu, and added to the Project Fluids • High Mach Number Flow

		<p>significantly increases simulation time</p> <ul style="list-style-type: none"> • Humidity varies widely during operation and its inclusion significantly increases simulation time
Wall Conditions	<ul style="list-style-type: none"> • Default Wall Thermal Condition: Adiabatic Wall • Roughness: 5 micrometer 	<ul style="list-style-type: none"> • Adiabatic wall removes thermal issues from the simulation, assuming that the air and intake model are both at ambient temperature • Wall roughness set as guess of roughness of real intake • Roughness has not been observed to significantly affect the outcome of the simulation at normal surface roughness values
Initial Conditions	<ul style="list-style-type: none"> • Parameter Definition: User Defined • Thermodynamic Parameters: Pressure, Temperature • Pressure: 101325 Pa • Temperature: 298 K • Velocity Parameters: Velocity • Velocity in X, Y, Z direction: 0 m/s • Turbulence Parameters: Turbulence Intensity and Length • Intensity: 2% • Length: 0.001545m 	<ul style="list-style-type: none"> • Pressure and temperature set to average atmospheric conditions • Any initial velocity not desired • Turbulence parameters not manually adjusted, left as default

Computational Domain and Boundary Conditions

The computational domain for intake flow simulation has been allowed to be automatically set by SolidWorks for every simulation, but the domain must be checked and ensured to enclose the entire model. If the computational domain does not enclose the complete volume of the intake as set automatically, then the intake model is either not closed, or includes some small internal volume which is closed but does not represent the full air intake assembly.

The boundary conditions of the simulation are the controls that define the simulation being investigated. The image below shows the boundary conditions used for the final air intake simulation. The Static Pressure boundary is set at the inside face of the air filter model, and is set to

identical pressure, temperature, and turbulence settings as the General Settings above. The Boundary Layer option in the Boundary Condition settings for this condition is set to Turbulent.

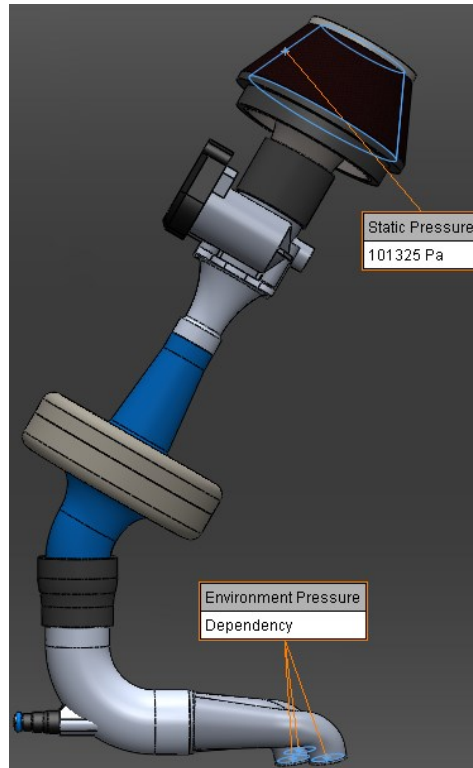


Figure 149. Air Intake Flow Simulation Boundary Conditions

The Environment Pressure boundary condition, set at the three faces representing the intake valves in the WR450F, is where the Excel spreadsheet is used to define the engine performance and cylinder pressure characteristics that drive the simulation. The turbulence and boundary layer settings for this boundary condition are set the same as above. The temperature is set to 298 K, and the pressure is set to a Dependency. This dependency uses the $f(\text{time})$ setting and contains an excerpt of the time - pressure data output by the Excel sheet.

This exit plane boundary condition is used to control and refine the simulation via the Excel spreadsheet. A partial screenshot of the Excel spreadsheet below shows the values entered into the spreadsheet, and where to copy the pressure data for this boundary condition. Note in particular the RPM and Volumetric Efficiency Guess inputs, which are the only two inputs used in normal operation for this simulation method. It is recommended that the RPM be adjusted only in increments of 2000 RPM, since the model has only been calibrated for 2, 4, 6, 8, and 10000 RPM with the WR450F. To add data into the time dependent boundary condition, copy the data from the Copyable Data columns and paste directly into the SolidWorks Dependency window.

	A	B	C	D	E	F
1	VARIABLES AND DATA				COPYABLE DATA	
2	Output Time Step	0.000125	sec		TIME	TOT PRES
3	Bore	95	mm		(sec)	(Pa)
4	Stroke	63.4	mm			
5	Comp. Ratio	12.3	:1		0	101325
6	Cyl Surf Area	0.007088	m ²		0.000125	98881.99217
7	Displacement	0.000449	m ³		0.00025	92629.74597
8	TDC Cyl. Vol.	3.9769E-05	m ³		0.000375	84362.04095
9					0.0005	76129.60391
10	Engine RPM	8000			0.000625	69343.44247
11	Piston Stroke Frequency	133.3333333	Hz		0.00075	64314.33358
12	Piston Ang Vel	837.758	rad/s		0.000875	60872.22006
13	Vol Air Moved Coefficient	2.170			0.001	58681.16889
14					0.001125	57387.44211
15	Intake Valve Lift	7.6	mm		0.00125	56715.73991
16		0.0076	m		0.001375	56485.69322
17	Intake Valve Duration (lift >1mm)	250	crank deg		0.0015	56589.98755
18					0.001625	56969.76124
19	Volumetric Efficiency Guess	0.71			0.00175	57596.72632
20					0.001875	58461.38639
21	Universal Gas Constant	8.3144598	J/mol-K		0.002	59565.33115
22	Plenum Pressure	101325	Pa		0.002125	60916.0857
23	Inlet Air Initial Temp	298	K		0.00225	62523.55293
24	Exhaust Gas Initial Temp	1100	K		0.002375	64397.46168
25					0.0025	66545.46446
26	Calc. Min Pressure	56486	Pa		0.002625	68971.67264
27	Calc. Max Pressure	101325	Pa		0.00275	71675.51312

Figure 150. Excerpt of Excel Spreadsheet Used for Intake Valve Boundary Condition

Surface Goals

The surface goal used to monitor flow through the intake is set at the same three faces as the time-dependent pressure boundary discussed above. This surface goal is used to monitor the Volume Flow Rate across these faces representing the intake valves.

Mesh

Automatic Meshing is used for this simulation. For all simulations, the fineness of the mesh has been set to 3, and Advanced Channel Refinement has been checked.

Calculation Control Options

The Calculation Control Options are another critical control to ensure the flow simulation proceeds as intended, especially since this menu controls the time span of the time-dependent simulation. The table below summarizes the options set in this menu.

Tab	Settings	Notes
Finishing	<ul style="list-style-type: none"> • Criterion to Stop: One Satisfied • Goals Convergence: Not checked • Physical Time: 0.1 s • Iterations: not checked • Travels: not checked • Calculation time: not checked 	<ul style="list-style-type: none"> • Physical Time controls time span of simulation. Typically set to 0.1 to 0.5 seconds, which will span several combustion cycles. It is not recommended to set this to higher than 0.5 seconds due to the time

	<ul style="list-style-type: none"> • Goals Criteria: all set to [auto] • Analysis Interval: [auto] 	<ul style="list-style-type: none"> • required for a longer simulation • Calculation time can be used to limit the time taken to run the simulation, but if set lower than required it will result in a shorter physical time duration being simulated
Refinement	<ul style="list-style-type: none"> • Global Domain: Disabled 	<ul style="list-style-type: none"> • Refinement significantly increases the time required to complete the simulation
Solving	<ul style="list-style-type: none"> • Time Step: [auto] • Nested Iterations: not checked • Time Averaged: not checked • Calculate Local Mean Average (LMA): not checked • Calculate Comfort Parameters: not checked • Results Processing Speed-Up Data: not checked • Freezing Strategy: Disabled 	<ul style="list-style-type: none"> • Solving allowed to use automatically defined time steps for accuracy
Saving	<ul style="list-style-type: none"> • Save Before Refinement: Checked • Save Backup Every: 100 Iterations • Full Results: Periodic, Physical time (s) • Start: 0s • Period: 0.00025 s • Tabular: Not checked • Selected Parameters (Transient Explorer): Not checked 	<ul style="list-style-type: none"> • Saving period set to every other time step in the Excel sheet to reduce the size of the result files, which can be several gigabytes • Saving enabled to allow viewing of partially completed simulation • Adjusting Start of Full Results can be used to remove transient flow development in the first combustion cycle(s)

Results

Once a simulation has been run, the results can be observed in SolidWorks Flow simulation via the various results features, but for purposes of analyzing the Volumetric Efficiency of air intake designs only the Goal Plot feature is used. A goal plot is created to output data gathered by the “SG Volume Flow Rate Outlet” surface goal created earlier. The X axis option underneath the surface goal selection panel is set to Physical Time. If the results are loaded, using the Export to Excel option will create an Excel file containing the surface goal data from all points in the simulation up to and including the current time step loaded. This surface goal spreadsheet includes three sheets, or tabs. The last tab, which includes the Plot Data for the surface goal, is where the Volumetric Efficiency of the simulation result will be calculated.

The image below shows the first formula used to numerically integrate the volumetric flow rate data. This formula is somewhat complicated due to the need to integrate only during actual intake strokes, and the fact that the result data is not spaced at even intervals like the input data. Since the simulation does not include any ability to temporarily close a pressure boundary, flow continues across the intake valve surfaces throughout the simulation, requiring the numerical isolation of time periods when the intake valves would actually be open. In this screenshot, the 0.015 which appears twice in the formula is the total duration of one combustion cycle at the simulated RPM, in this case 8000 RPM. This can be found by observing the spreadsheet that generates the pressure data for the boundary condition. The 0.005125 in this formula is the time span of each intake stroke during which the intake valves are open. This can also be easily found from the input data spreadsheet by observing the Valve Open? column. This formula is applied to the entire length of the data, and then another formula is used to find the volumetric efficiency from this calculation.

D	E	F	G	H	I	J	K	L
Volume Flow Rate [m ³ /s]								
Physical time [s]	SG Volume Flow Rate Outlet							
	Yes							
	11.3							
	0.026749626							
	0.003032798			8000rpm				
	-0.034939618							
	-0.050298751			input 71 ve				
	-0.02249302	=IF(AND(MOD(D12,0.015)<=0.005125,D12>0.015),E12*(D12-D11), "")						
0.00025	-6.93733E-45	IF(logical_test, [value_if_true], [value_if_false])						
0.0005	-2.93571E-44							

Figure 151. Numerical Integration Formula for Flow Simulation Result Data

The image below shows the graph included in the Excel spreadsheet exported from the Goal Plot in Flow Simulation. This graph is used to observe obvious differences between the first cycle and the others, and to determine if the last cycle is complete or partial. This graph is then used to count the number of complete combustion cycles simulated by counting the negative peaks on the graph. The first cycle is exempted from volumetric efficiency calculation due to the startup transients typically observed, and this exclusion is integrated into the above formula. If the last combustion cycle is incomplete, it must be removed manually by deleting the above formula from cells referencing the last cycle. Once this is done, the second formula can be used to find the volumetric efficiency of the simulated intake.

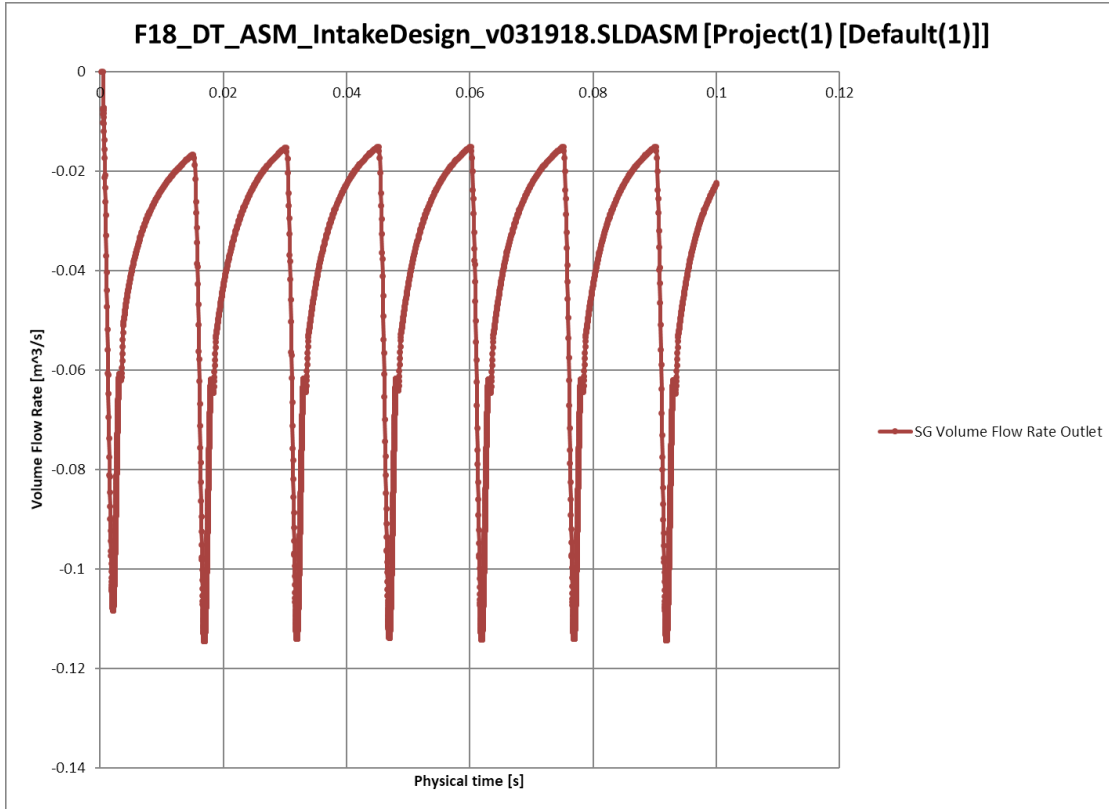


Figure 152. Volume Flow Rate Result Graph for Flow Simulation

A simple formula, shown in the image below, is then used to calculate the volumetric efficiency from the numerically integrated results provided by the above formula. In this image, F is the column over which the above formula was applied, 6 is the number of complete combustion cycles shown on the graph above when the first is omitted, and 0.000449 is the displacement of the WR450F engine in cubic meters.

D	E	F	G	H	I	J
Volume Flow Rate [m³/s]						
Physical time [s]	SG Volume Flow Rate Outlet					
	Yes					
		11.3				
		0.026749626				
		0.003032798		8000rpm		
		-0.034939618				
		-0.050298751		input VE	0.71	
		-0.02249302			0.711634 final	
0.00025		-6.93733E-45		=SUM(F:F)/6/0.000449		
0.0005		-2.93571E-44		SUM(number1, [number2], ...)		

Figure 153. Volumetric Efficiency Calculation from Numerically Integrated Results

To determine whether the simulation has converged to a value for volumetric efficiency, the value resulting from the above calculations is then compared to the Volumetric Efficiency Guess used to generate the input data for the time-dependent boundary condition. If the two do not agree within the desired margin, the simulation must be repeated after modifying the Volumetric Efficiency Guess on the input data spreadsheet to be closer to the calculated result. This process of iterative simulation will, once converged as in the above example, provide an approximation of the Volumetric Efficiency of the air intake model at the set engine RPM.

This simulation method was used to simulate the behavior of the 2016 air intake, the prototype air intakes for the 2018 car, and the final design, with the only major differences being the intake models themselves.

Appendix F. FEA Analysis of Suspension Components



Front Lower A-Arm

Date: Thursday, April 19, 2018

Designer: Solidworks

Study name: max force (Cornering and Braking)

Analysis type: Static

Description

This analysis was used to determine the smallest and lightest tubes that would be able to be used for the given A-Arm design. Forces were applied to simulate the worst case loading scenario to insure that the tube size chosen would be able to withstand any potential forces without failing. Deflection of the A-Arms was also considered to insure that the wheels maintained the optimal contact patch at all times. Any deflections were corrected for by suspension geometry.

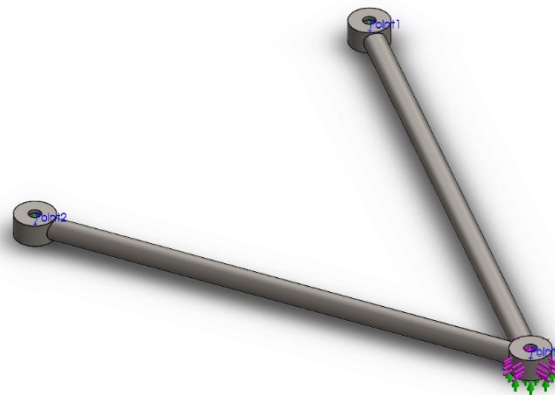
Assumptions

Only 4130 Steel tubes would be considered.

Maximum braking force would be 1.5g

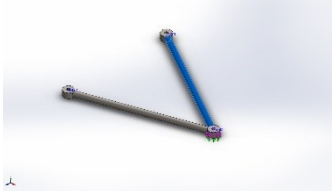
Maximum cornering force would be 1.5g

Model Information



Model name: F18_SU_FrontLeftLowerA-ArmTubes_v101217
Current Configuration: Default

Solid Bodies

Document Name and Reference	Treated As	Volumetric Properties	Document Path/Date Modified
Stock-Suspension Mockup-3 	Solid Body	Mass:0.198872 kg Volume:2.53359e-005 m ³ Density:7849.42 kg/m ³ Weight:1.94895 N	F:\2017-18 FSAE MQP\SolidWorks\F18_ASM_F ullcar_v031218\F18_SU_Front LeftLowerA- ArmTubes_v101217.SLDPRT Apr 18 15:05:21 2018
Cut-Revolve2 	Solid Body	Mass:0.0810222 kg Volume:1.03213e-005 m ³ Density:7850 kg/m ³ Weight:0.794018 N	F:\2017-18 FSAE MQP\SolidWorks\F18_ASM_F ullcar_v031218\F18_SU_Front LeftLowerA- ArmTubes_v101217.SLDPRT Apr 18 15:05:21 2018

<p>Stock-Suspension Mockup-2</p> 	<p>Solid Body</p>	<p>Mass:0.184488 kg Volume:2.35116e-005 m³ Density:7846.7 kg/m³ Weight:1.80798 N</p>	<p>F:\2017-18 FSAE MQP\SolidWorks\F18_ASM_Fullcar_v031218\F18_SU_Front LeftLowerA-ArmTubes_v101217.SLDPRT Apr 18 15:05:21 2018</p>
<p>Cut-Revolve3</p> 	<p>Solid Body</p>	<p>Mass:0.0810222 kg Volume:1.03213e-005 m³ Density:7850 kg/m³ Weight:0.794018 N</p>	<p>F:\2017-18 FSAE MQP\SolidWorks\F18_ASM_Fullcar_v031218\F18_SU_Front LeftLowerA-ArmTubes_v101217.SLDPRT Apr 18 15:05:21 2018</p>
<p>Cut-Revolve1</p> 	<p>Solid Body</p>	<p>Mass:0.0810222 kg Volume:1.03213e-005 m³ Density:7850 kg/m³ Weight:0.794018 N</p>	<p>F:\2017-18 FSAE MQP\SolidWorks\F18_ASM_Fullcar_v031218\F18_SU_Front LeftLowerA-ArmTubes_v101217.SLDPRT Apr 18 15:05:21 2018</p>

Study Properties

Study name	max force (Cornering and Braking)
Analysis type	Static
Mesh type	Solid Mesh
Thermal Effect:	On
Thermal option	Include temperature loads
Zero strain temperature	298 Kelvin
Include fluid pressure effects from SOLIDWORKS Flow Simulation	Off
Solver type	FFEPlus
Inplane Effect:	Off
Soft Spring:	Off
Inertial Relief:	Off
Incompatible bonding options	Automatic
Large displacement	Off
Compute free body forces	On
Friction	Off
Use Adaptive Method:	Off
Result folder	SOLIDWORKS document (F:\2017-18 FSAE MQP\SolidWorks\F18_ASM_Fullcar_v031218)

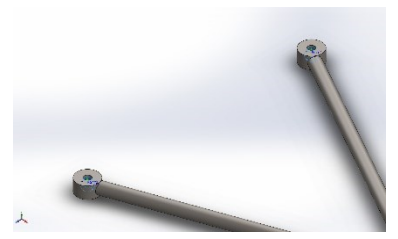
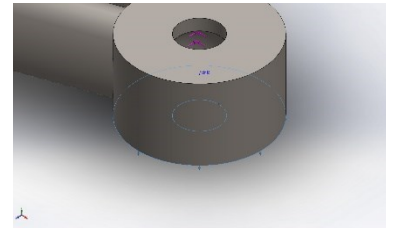
Units

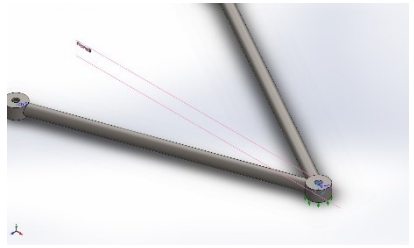
Unit system:	SI (MKS)
Length/Displacement	mm
Temperature	Kelvin
Angular velocity	Rad/sec
Pressure/Stress	N/m ²

Material Properties

Model Reference	Properties	Components
	<p>Name: AISI 4130 Steel, normalized at 870C</p> <p>Model type: Linear Elastic Isotropic</p> <p>Default failure criterion: Unknown</p> <p>Yield strength: 4.6e+008 N/m²</p> <p>Tensile strength: 7.31e+008 N/m²</p> <p>Elastic modulus: 2.05e+011 N/m²</p> <p>Poisson's ratio: 0.285</p> <p>Mass density: 7850 kg/m³</p> <p>Shear modulus: 8e+010 N/m²</p>	<p>SolidBody 1(Stock-Suspension Mockup-3)(F18_SU_FrontLeftLowerA-ArmTubes_v101217),</p> <p>SolidBody 2(Cut-Revolve2)(F18_SU_FrontLeftLowerA-ArmTubes_v101217),</p> <p>SolidBody 3(Stock-Suspension Mockup-2)(F18_SU_FrontLeftLowerA-ArmTubes_v101217),</p> <p>SolidBody 4(Cut-Revolve3)(F18_SU_FrontLeftLowerA-ArmTubes_v101217),</p> <p>SolidBody 5(Cut-Revolve1)(F18_SU_FrontLeftLowerA-ArmTubes_v101217)</p>
Curve Data:N/A		

Loads and Fixtures

Fixture name	Fixture Image	Fixture Details		
On Spherical Faces-1		Entities: 2 face(s) Type: On Spherical Faces Translation: 0, ---, --- Units: mm		
Roller/Slider-1		Entities: 1 face(s) Type: Roller/Slider		
Resultant Forces				
Components	X	Y	Z	Resultant
Reaction force(N)	0	15.2582	0	15.2582
Reaction Moment(N.m)	0	0	0	0

Load name	Load Image	Load Details
Force-1		Entities: 1 face(s), 1 plane(s) Reference: Plane3 Type: Apply force Values: -575, ---, -611 lbf

Contact Information

Contact	Contact Image	Contact Properties
Global Contact		Type: Bonded Components: 1 component(s) Options: Compatible mesh

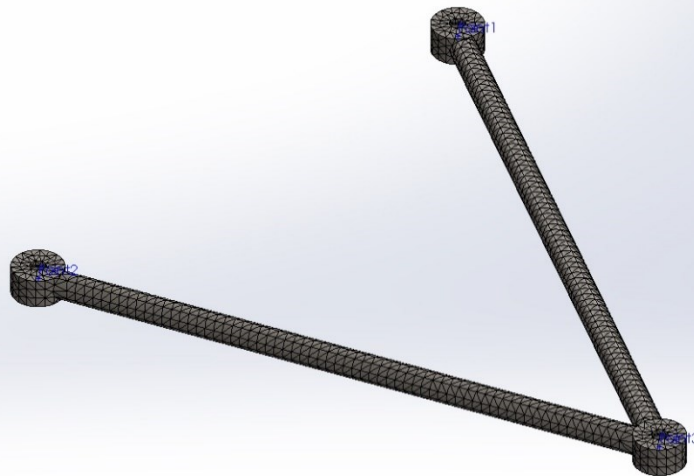
Mesh information

Mesh type	Solid Mesh
Mesher Used:	Standard mesh
Automatic Transition:	Off
Include Mesh Auto Loops:	Off
Jacobian points	4 Points
Element Size	0.210656 in
Tolerance	0.0105328 in
Mesh Quality Plot	High

Mesh information - Details

Total Nodes	19935
Total Elements	10415
Maximum Aspect Ratio	11.746
% of elements with Aspect Ratio < 3	26.7
% of elements with Aspect Ratio > 10	0.096
% of distorted elements(Jacobian)	0
Time to complete mesh(hh:mm:ss):	00:00:03
Computer name:	

Model name:F18_SU_FrontLeftLower-ArmTube_v101217
 Study name:Max Force [Cornering and Braking]-Default
 Mesh type: Solid Mesh



SOLIDWORKS Educational Product. For Instructional Use Only.

Resultant Forces

Reaction forces

Selection set	Units	Sum X	Sum Y	Sum Z	Resultant
Entire Model	N	2557.59	-0.0850184	2717.79	3731.98

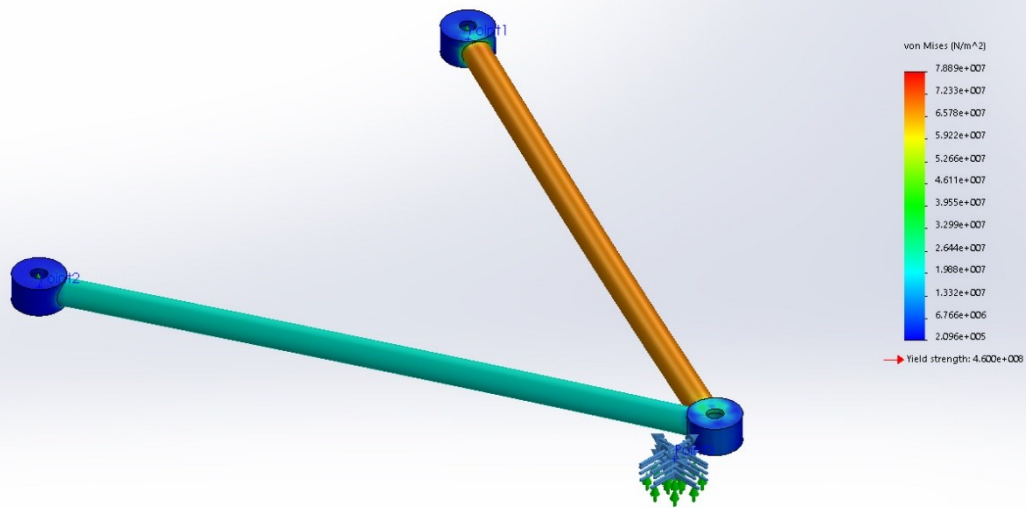
Reaction Moments

Selection set	Units	Sum X	Sum Y	Sum Z	Resultant
Entire Model	N.m	0	0	0	0

Study Results

Name	Type	Min	Max
Stress1	VON: von Mises Stress	2.096e+005N/m ² Node: 19416	7.889e+007N/m ² Node: 7861

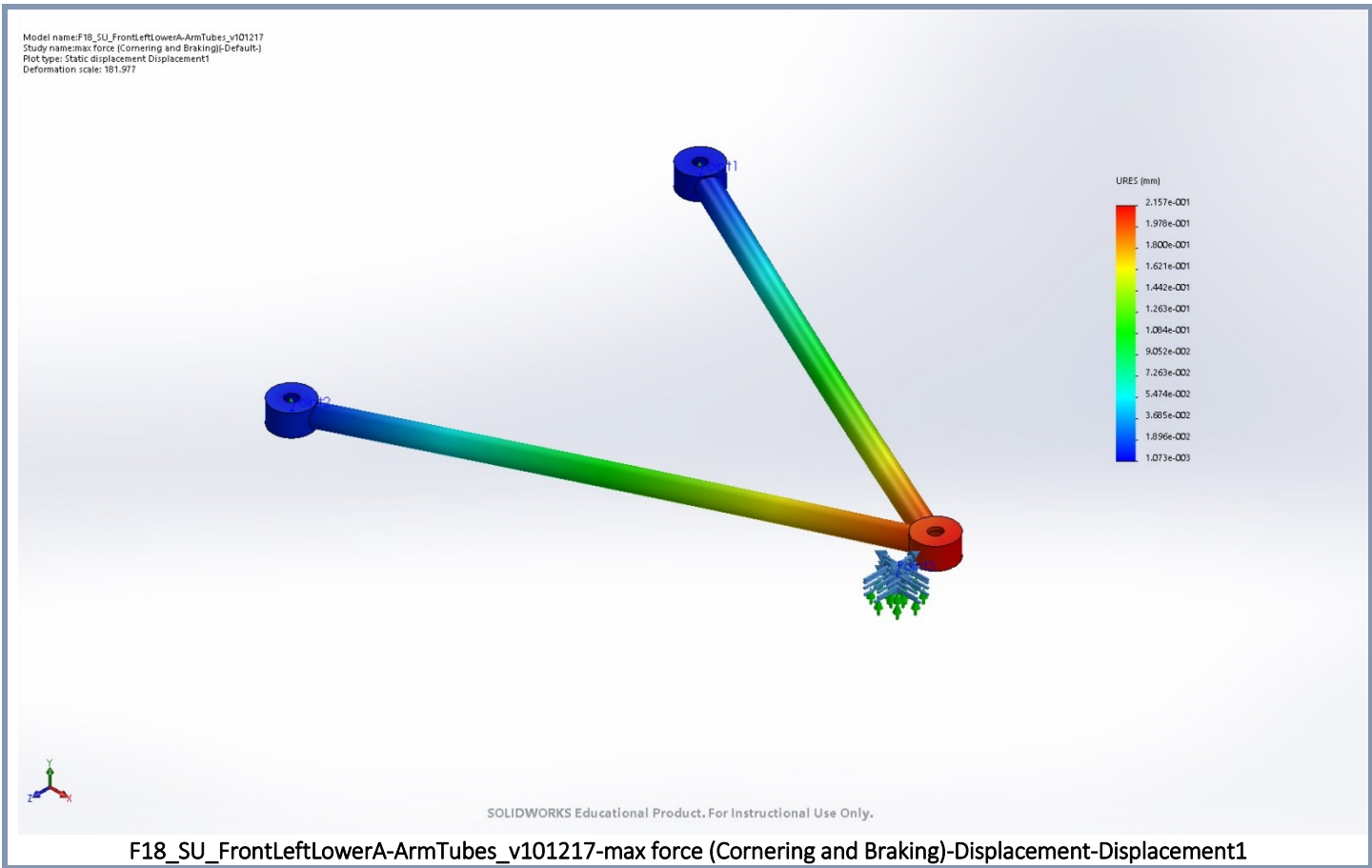
Model name: F18_SU_FrontLeftLowerA-ArmTubes_v101217
 Study name: max force (Cornering and Braking)-(Default)
 Plot type: Static nodal stress Stress1
 Deformation scale: 181.977



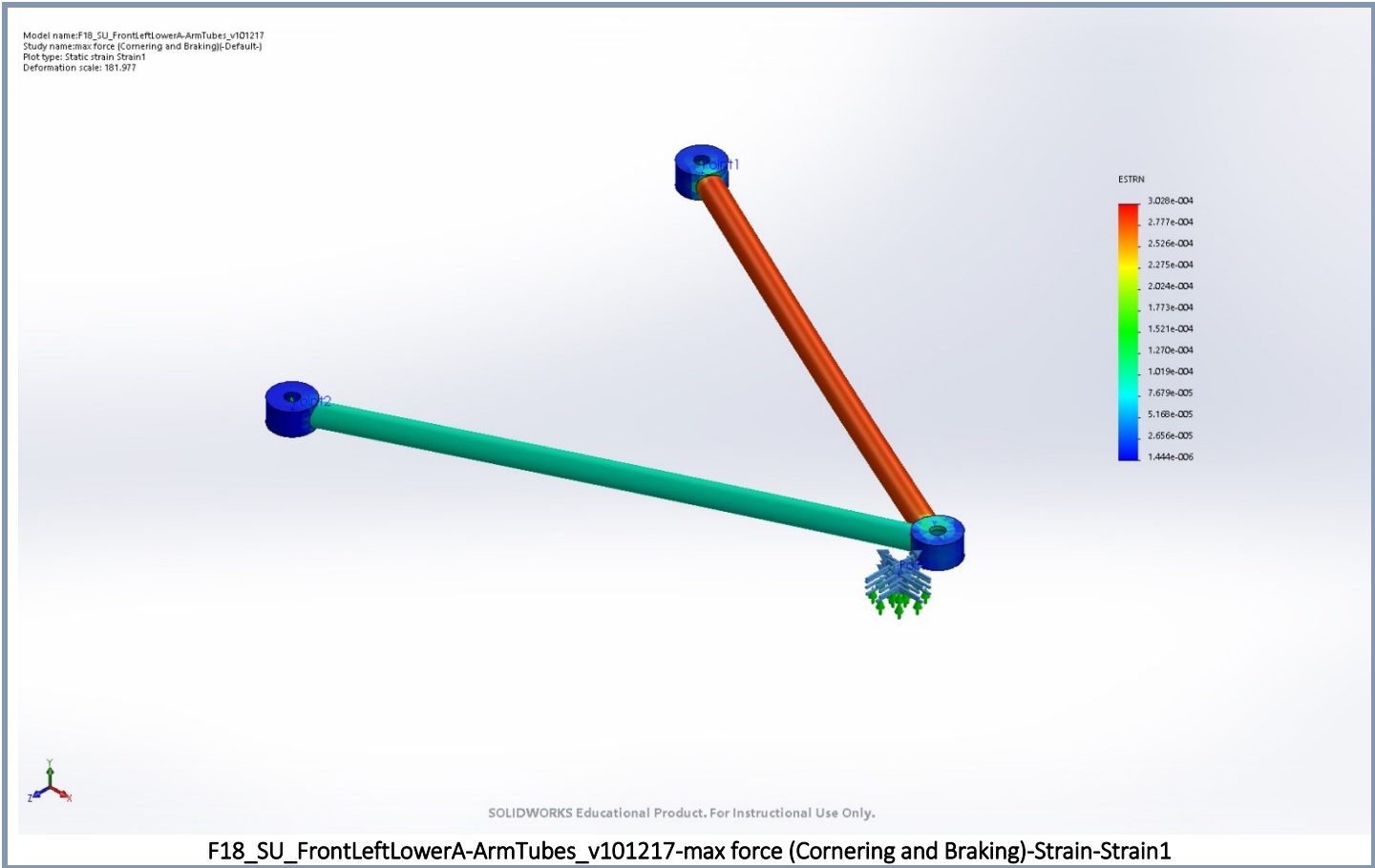
SOLIDWORKS Educational Product. For Instructional Use Only.

F18_SU_FrontLeftLowerA-ArmTubes_v101217-max force (Cornering and Braking)-Stress-Stress1

Name	Type	Min	Max
Displacement1	URES: Resultant Displacement	1.073e-003mm Node: 8006	2.157e-001mm Node: 16807

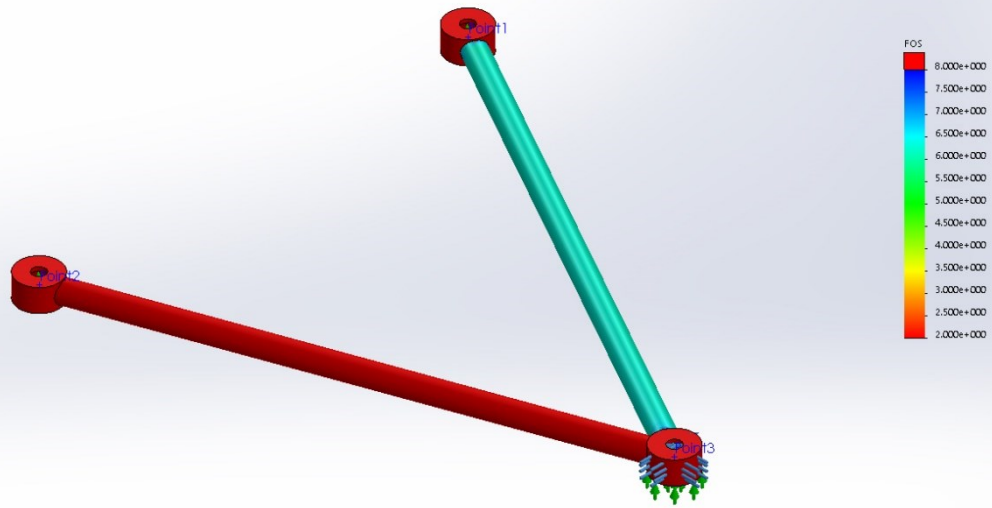


Name	Type	Min	Max
Strain1	ESTRN: Equivalent Strain	1.444e-006 Element: 9631	3.028e-004 Element: 570



Name	Type	Min	Max
Factor of Safety1	Automatic	5.431e+000 Node: 7883	2.195e+003 Node: 19416

Model name: F18_SU_FrontLeftLowerA-ArmTubes_v101217
Study name: max force (Cornering and Braking)-(Default)
Plot type: Factor of Safety Factor of Safety1
Criterion: Automatic
Factor of safety distribution: Min FOS = 5.4



SOLIDWORKS Educational Product. For Instructional Use Only.

F18_SU_FrontLeftLowerA-ArmTubes_v101217-max force (Cornering and Braking)-Factor of Safety-Factor of Safety1



Simulation of Front Upper A-Arm

Date: Thursday, April 19, 2018

Designer: Solidworks

Study name: Max force (Braking and Cornering)

Analysis type: Static

Description

This analysis was used to determine the smallest and lightest tubes that would be able to be used for the given A-Arm design. Forces were applied to simulate the worst case loading scenario to insure that the tube size chosen would be able to withstand any potential forces without failing. Deflection of the A-Arms was also considered to insure that the wheels maintained the optimal contact patch at all times. Any deflections were corrected for by suspension geometry.

Assumptions

Only 4130 Steel tubes would be considered.
Maximum braking force would be 1.5g
Maximum cornering force would be 1.5g

Model Information



Model name: F18_SU_FrontLeftUpperA-ArmTubes_v101217
Current Configuration: Default

Solid Bodies

Document Name and Reference	Treated As	Volumetric Properties	Document Path/Date Modified
Cut-Revolve2 	Solid Body	Mass:0.0810221 kg Volume:1.03213e-005 m ³ Density:7850 kg/m ³ Weight:0.794016 N	F:\2017-18 FSAE MQP\SolidWorks\F18_ASM_F ullcar_v031218\F18_SU_Front LeftUpperA- ArmTubes_v101217.SLDPRT Apr 18 15:05:21 2018
Cut-Revolve1 	Solid Body	Mass:0.0810221 kg Volume:1.03213e-005 m ³ Density:7850 kg/m ³ Weight:0.794016 N	F:\2017-18 FSAE MQP\SolidWorks\F18_ASM_F ullcar_v031218\F18_SU_Front LeftUpperA- ArmTubes_v101217.SLDPRT Apr 18 15:05:21 2018
Stock-Suspension Mockup-3 	Solid Body	Mass:0.151534 kg Volume:1.93065e-005 m ³ Density:7848.86 kg/m ³ Weight:1.48503 N	F:\2017-18 FSAE MQP\SolidWorks\F18_ASM_F ullcar_v031218\F18_SU_Front LeftUpperA- ArmTubes_v101217.SLDPRT Apr 18 15:05:21 2018

<p>Stock-Suspension Mockup-5</p> 	Solid Body	<p>Mass:0.0114988 kg Volume:1.46482e-006 m³ Density:7850 kg/m³ Weight:0.112688 N</p>	<p>F:\2017-18 FSAE MQP\SolidWorks\F18_ASM_F ullcar_v031218\F18_SU_Front LeftUpperA- ArmTubes_v101217.SLDPR T Apr 18 15:05:21 2018</p>
<p>Cut-Revolve3</p> 	Solid Body	<p>Mass:0.0810222 kg Volume:1.03213e-005 m³ Density:7850 kg/m³ Weight:0.794018 N</p>	<p>F:\2017-18 FSAE MQP\SolidWorks\F18_ASM_F ullcar_v031218\F18_SU_Front LeftUpperA- ArmTubes_v101217.SLDPR T Apr 18 15:05:21 2018</p>
<p>Stock-Suspension Mockup-6</p> 	Solid Body	<p>Mass:0.163915 kg Volume:2.08836e-005 m³ Density:7848.96 kg/m³ Weight:1.60636 N</p>	<p>F:\2017-18 FSAE MQP\SolidWorks\F18_ASM_F ullcar_v031218\F18_SU_Front LeftUpperA- ArmTubes_v101217.SLDPR T Apr 18 15:05:21 2018</p>

Study Properties

Study name	Max force (Braking and Cornering)
Analysis type	Static
Mesh type	Solid Mesh
Thermal Effect:	On
Thermal option	Include temperature loads
Zero strain temperature	298 Kelvin
Include fluid pressure effects from SOLIDWORKS Flow Simulation	Off
Solver type	FFEPlus
Inplane Effect:	Off
Soft Spring:	Off
Inertial Relief:	Off
Incompatible bonding options	Automatic
Large displacement	Off
Compute free body forces	On
Friction	Off
Use Adaptive Method:	Off
Result folder	SOLIDWORKS document (F:\2017-18 FSAE MQP\SolidWorks\F18_ASM_Fullcar_v031218)

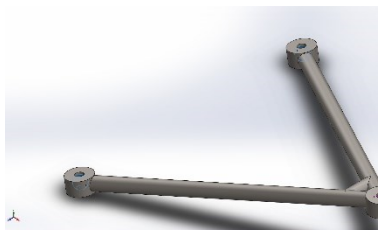
Units

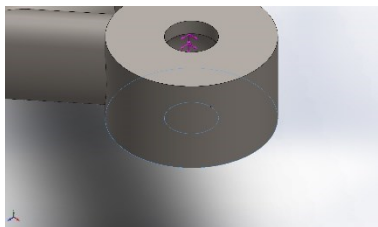
Unit system:	SI (MKS)
Length/Displacement	mm
Temperature	Kelvin
Angular velocity	Rad/sec
Pressure/Stress	N/m ²

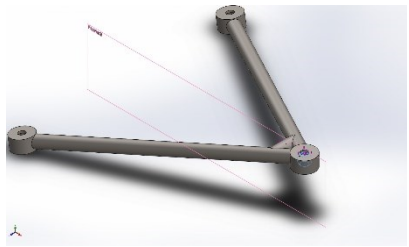
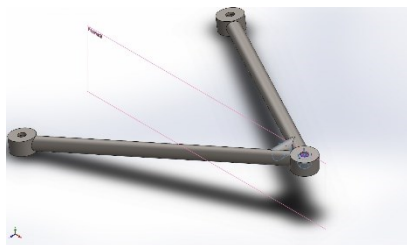
Material Properties

Model Reference	Properties	Components
	<p>Name: AISI 4130 Steel, normalized at 870C</p> <p>Model type: Linear Elastic Isotropic</p> <p>Default failure criterion: Unknown</p> <p>Yield strength: 4.6e+008 N/m²</p> <p>Tensile strength: 7.31e+008 N/m²</p> <p>Elastic modulus: 2.05e+011 N/m²</p> <p>Poisson's ratio: 0.285</p> <p>Mass density: 7850 kg/m³</p> <p>Shear modulus: 8e+010 N/m²</p>	<p>SolidBody 1(Cut-Revolve2)(F18_SU_FrontLeftUpperA-ArmTubes_v101217),</p> <p>SolidBody 2(Cut-Revolve1)(F18_SU_FrontLeftUpperA-ArmTubes_v101217),</p> <p>SolidBody 3(Stock-Suspension Mockup-3)(F18_SU_FrontLeftUpperA-ArmTubes_v101217),</p> <p>SolidBody 4(Stock-Suspension Mockup-5)(F18_SU_FrontLeftUpperA-ArmTubes_v101217),</p> <p>SolidBody 5(Cut-Revolve3)(F18_SU_FrontLeftUpperA-ArmTubes_v101217),</p> <p>SolidBody 6(Stock-Suspension Mockup-6)(F18_SU_FrontLeftUpperA-ArmTubes_v101217)</p>
Curve Data:N/A		

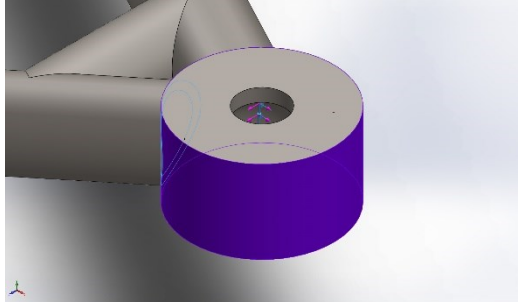
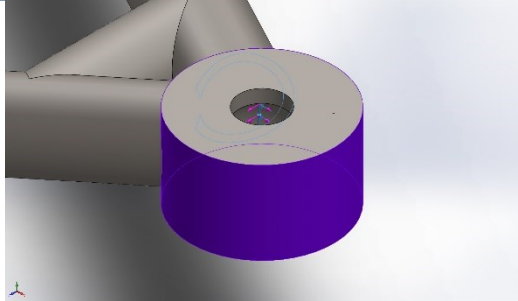
Loads and Fixtures

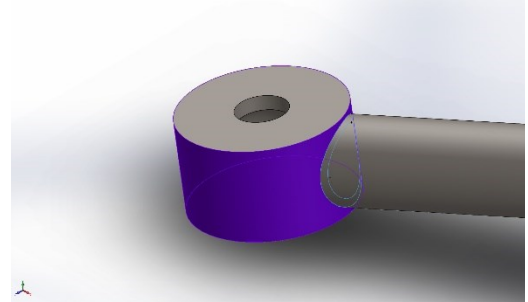
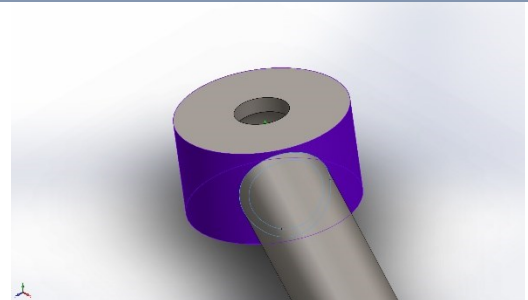
Fixture name	Fixture Image	Fixture Details
On Spherical Faces-1		<p>Entities: 2 face(s)</p> <p>Type: On Spherical Faces</p> <p>Translation: 0, ---, ---</p> <p>Units: mm</p>

<p>Roller/Slider-1</p>		<p>Entities: 1 face(s) Type: Roller/Slider</p>		
<p>Resultant Forces</p>				
<p>Components</p>	<p>X</p>	<p>Y</p>	<p>Z</p>	<p>Resultant</p>
<p>Reaction force(N)</p>	<p>0.00401254</p>	<p>5134.72</p>	<p>0.0167803</p>	<p>5134.72</p>
<p>Reaction Moment(N.m)</p>	<p>0</p>	<p>0</p>	<p>0</p>	<p>0</p>

Load name	Load Image	Load Details
<p>Force-1</p>		<p>Entities: 1 face(s), 1 plane(s) Reference: Plane3 Type: Apply force Values: 215, ---, 229.43 lbf</p>
<p>Force-2</p>		<p>Entities: 2 face(s), 1 plane(s) Reference: Plane3 Type: Apply force Values: -700, -700, --- lbf</p>

Contact Information

Contact	Contact Image	Contact Properties
<p>Contact Set-1</p>		<p>Type: Bonded contact pair Entites: 2 face(s)</p>
<p>Contact Set-2</p>		<p>Type: Bonded contact pair Entites: 2 face(s)</p>

<p>Contact Set-3</p>		<p>Type: Bonded contact pair Entites: 2 face(s)</p>
<p>Contact Set-4</p>		<p>Type: Bonded contact pair Entites: 3 face(s)</p>
<p>Contact Set-5</p>		<p>Type: Bonded contact pair Entites: 2 face(s)</p>
<p>Contact Set-6</p>		<p>Type: Bonded contact pair Entites: 2 face(s)</p>
<p>Global Contact</p>		<p>Type: Bonded Components: 1 component(s) Options: Compatible mesh</p>

Mesh information

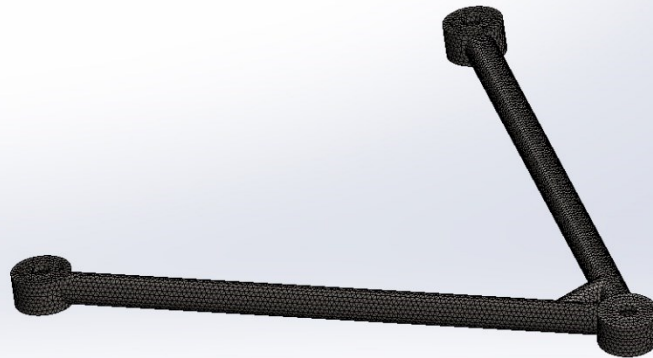
<p>Mesh type</p>	<p>Solid Mesh</p>
<p>Mesher Used:</p>	<p>Blended curvature-based mesh</p>

Jacobian points	4 Points
Maximum element size	0.105659 in
Minimum element size	0.0704386 in
Mesh Quality Plot	High

Mesh information - Details

Total Nodes	80741
Total Elements	44048
Maximum Aspect Ratio	25.564
% of elements with Aspect Ratio < 3	99.5
% of elements with Aspect Ratio > 10	0.025
% of distorted elements(Jacobian)	0
Time to complete mesh(hh:mm:ss):	00:00:04
Computer name:	

Model name: F18_SU_FrontLeftUpperArmTube_v101217
 Study name: Max force (Braking and Cornering)(-Default)
 Mesh type: Solid Mesh



SOLIDWORKS Educational Product. For Instructional Use Only.

Resultant Forces

Reaction forces

Selection set	Units	Sum X	Sum Y	Sum Z	Resultant
---------------	-------	-------	-------	-------	-----------

Entire Model	N	5271.17	6227.51	-1020.54	8222.45
--------------	---	---------	---------	----------	---------

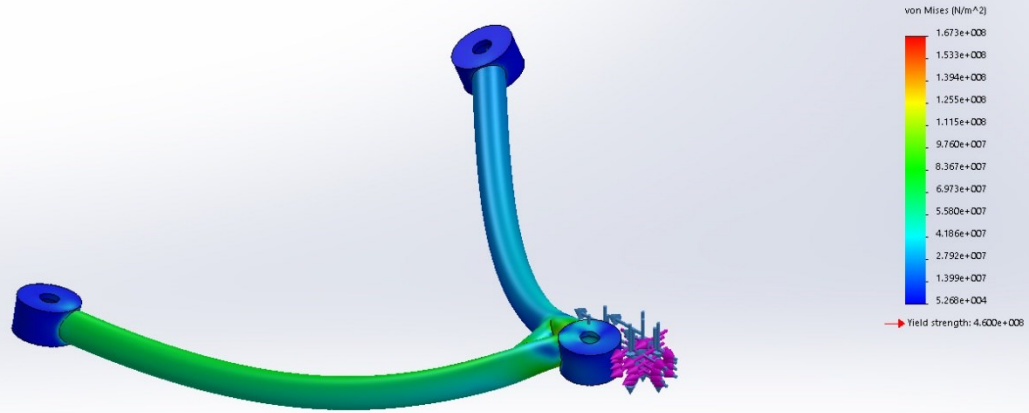
Reaction Moments

Selection set	Units	Sum X	Sum Y	Sum Z	Resultant
Entire Model	N.m	0	0	0	0

Study Results

Name	Type	Min	Max
Stress1	VON: von Mises Stress	5.268e+004N/m ² Node: 10796	1.673e+008N/m ² Node: 27810

Model name: F18_SU_FrontLeftUpperA-ArmTubes_v101217
 Study name: Max force (Braking and Cornering)-Default
 Plot type: Static nodal stress Stress1
 Deformation scale: 269.354

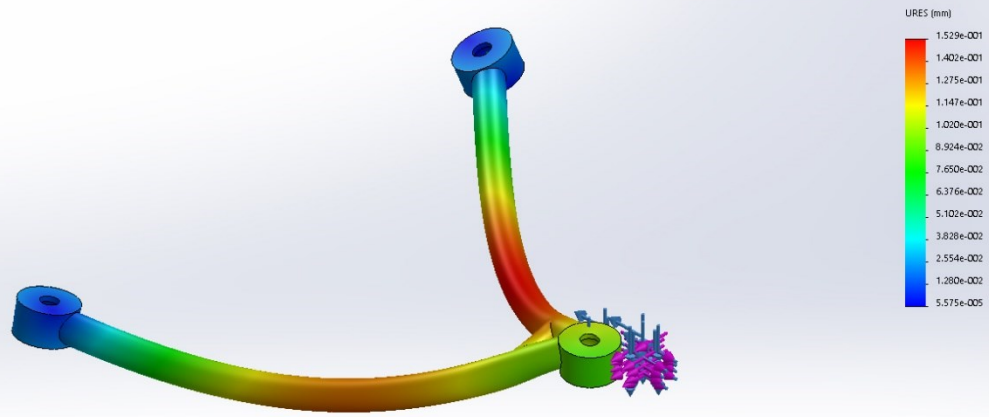


SOLIDWORKS Educational Product. For Instructional Use Only.

F18_SU_FrontLeftUpperA-ArmTubes_v101217-Max force (Braking and Cornering)-Stress-Stress1

Name	Type	Min	Max
Displacement1	URES: Resultant Displacement	5.575e-005mm Node: 16393	1.529e-001mm Node: 69050

Model name: F18_SU_FrontLeftUpperA-ArmTubes_v101217
 Study name: Max force (Braking and Cornering)-Default
 Plot type: Static displacement Displacement1
 Deformation scale: 269.354

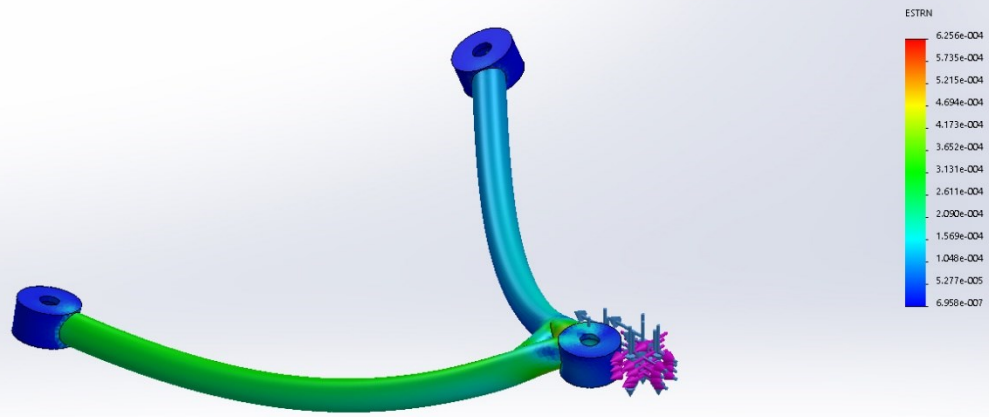


SOLIDWORKS Educational Product. For Instructional Use Only.

F18_SU_FrontLeftUpperA-ArmTubes_v101217-Max force (Braking and Cornering)-Displacement-Displacement1

Name	Type	Min	Max
Strain1	ESTRN: Equivalent Strain	6.958e-007 Element: 8370	6.256e-004 Element: 18411

Model name: F18_SU_FrontLeftUpperA-ArmTubes_v101217
 Study name: Max force (Braking and Cornering)-Default
 Plot type: Static strain Strain1
 Deformation scale: 269.354

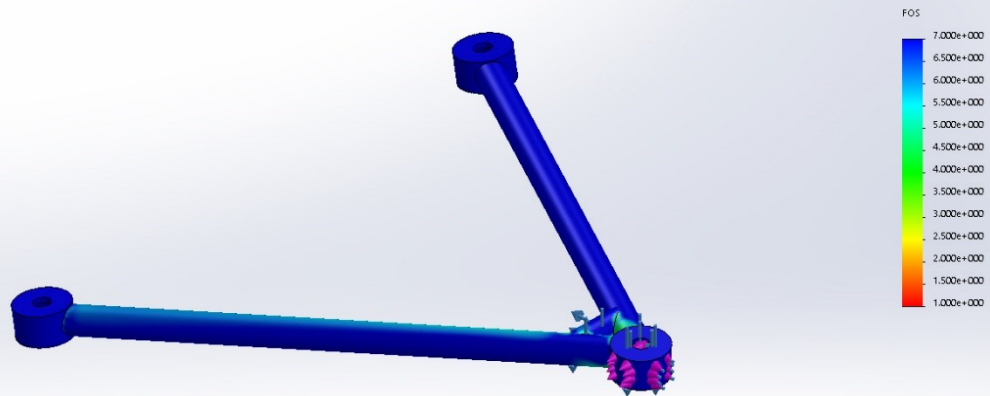


SOLIDWORKS Educational Product. For Instructional Use Only.

F18_SU_FrontLeftUpperA-ArmTubes_v101217-Max force (Braking and Cornering)-Strain-Strain1

Name	Type	Min	Max
Factor of Safety1	Automatic	2.228e+000 Node: 44761	8.732e+003 Node: 10796

Model name: F18_SU_FrontLeftUpperA-ArmTubes_v101217
Study name: Max force (Braking and Cornering)-Default
Plot type: Factor of Safety Factor of Safety1
Criterion: Automatic
Factor of safety distribution: Min FOS = 2.2



SOLIDWORKS Educational Product. For Instructional Use Only.

F18_SU_FrontLeftUpperA-ArmTubes_v101217-Max force (Braking and Cornering)-Factor of Safety-Factor of Safety1

Simulation of Rear Upper A-Arm

Date: Thursday, April 19, 2018

Designer: Solidworks

Study name: Max force (Cornering and breaking)

Analysis type: Static



Description

This analysis was used to determine the smallest and lightest tubes that would be able to be used for the given A-Arm design. Forces were applied to simulate the worst case loading scenario to insure that the tube size chosen would be able to withstand any potential forces without failing. Deflection of the A-Arms was also considered to insure that the wheels maintained the optimal contact patch at all times. Any deflections were corrected for by suspension geometry.

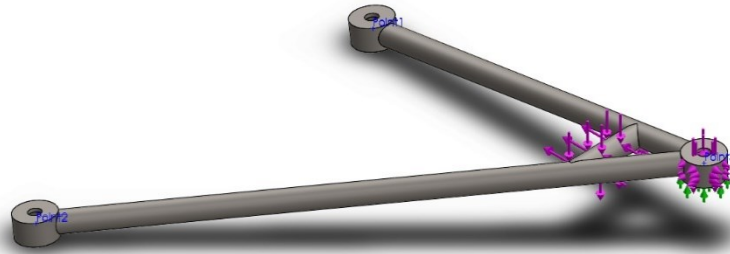
Assumptions

Only 4130 Steel tubes would be considered.

Maximum braking force would be 1.5g

Maximum cornering force would be 1.5g

Model Information



Model name: F18_SU_RearLeftUpperA-ArmTubes_v101217
Current Configuration: Default

Solid Bodies

Document Name and Reference	Treated As	Volumetric Properties	Document Path/Date Modified
Cut-Revolve3 	Solid Body	Mass:0.0810221 kg Volume:1.03213e-005 m ³ Density:7850 kg/m ³ Weight:0.794016 N	F:\2017-18 FSAE MQP\SolidWorks\F18_ASM_F ullcar_v031218\F18_SU_RearL eftUpperA- ArmTubes_v101217.SLDPRT Apr 18 15:05:21 2018
Cut-Revolve2 	Solid Body	Mass:0.0810222 kg Volume:1.03213e-005 m ³ Density:7850 kg/m ³ Weight:0.794018 N	F:\2017-18 FSAE MQP\SolidWorks\F18_ASM_F ullcar_v031218\F18_SU_RearL eftUpperA- ArmTubes_v101217.SLDPRT Apr 18 15:05:21 2018
Cut-Revolve1 	Solid Body	Mass:0.0810221 kg Volume:1.03213e-005 m ³ Density:7850 kg/m ³ Weight:0.794016 N	F:\2017-18 FSAE MQP\SolidWorks\F18_ASM_F ullcar_v031218\F18_SU_RearL eftUpperA- ArmTubes_v101217.SLDPRT Apr 18 15:05:21 2018

<p>Stock-Suspension Mockup-4</p> 	Solid Body	<p>Mass:0.143198 kg Volume:1.82375e-005 m³ Density:7851.85 kg/m³ Weight:1.40334 N</p>	<p>F:\2017-18 FSAE MQP\SolidWorks\F18_ASM_F ullcar_v031218\F18_SU_RearL eftUpperA- ArmTubes_v101217.SLDPRT Apr 18 15:05:21 2018</p>
<p>Stock-Suspension Mockup-5</p> 	Solid Body	<p>Mass:0.0240818 kg Volume:3.06806e-006 m³ Density:7849.18 kg/m³ Weight:0.236002 N</p>	<p>F:\2017-18 FSAE MQP\SolidWorks\F18_ASM_F ullcar_v031218\F18_SU_RearL eftUpperA- ArmTubes_v101217.SLDPRT Apr 18 15:05:21 2018</p>
<p>Stock-Suspension Mockup-3</p> 	Solid Body	<p>Mass:0.209958 kg Volume:2.67499e-005 m³ Density:7848.91 kg/m³ Weight:2.05759 N</p>	<p>F:\2017-18 FSAE MQP\SolidWorks\F18_ASM_F ullcar_v031218\F18_SU_RearL eftUpperA- ArmTubes_v101217.SLDPRT Apr 18 15:05:21 2018</p>

Study Properties

Study name	Max force (Cornering and breaking)
Analysis type	Static
Mesh type	Solid Mesh
Thermal Effect:	On
Thermal option	Include temperature loads
Zero strain temperature	298 Kelvin
Include fluid pressure effects from SOLIDWORKS Flow Simulation	Off
Solver type	FFEPlus
Inplane Effect:	Off
Soft Spring:	Off
Inertial Relief:	Off
Incompatible bonding options	Automatic
Large displacement	Off
Compute free body forces	On
Friction	Off
Use Adaptive Method:	Off
Result folder	SOLIDWORKS document (F:\2017-18 FSAE MQP\SolidWorks\F18_ASM_Fullcar_v031218)

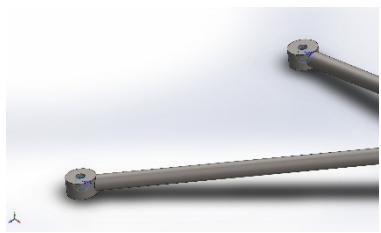
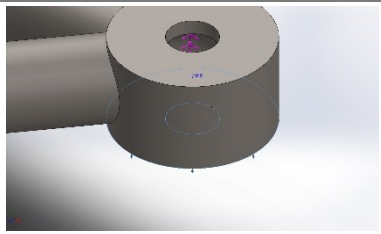
Units

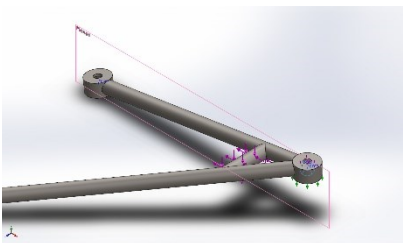
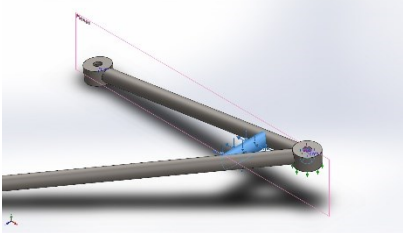
Unit system:	SI (MKS)
Length/Displacement	mm
Temperature	Kelvin
Angular velocity	Rad/sec
Pressure/Stress	N/m ²

Material Properties

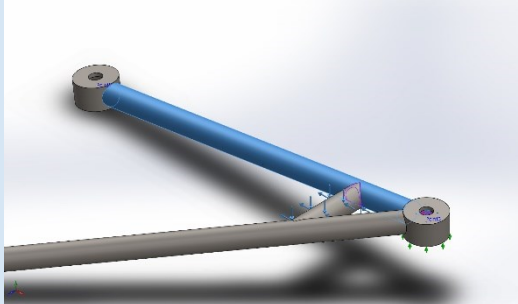
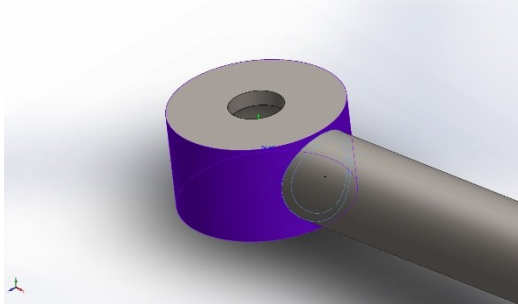
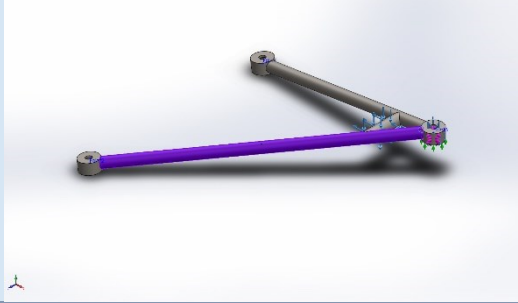
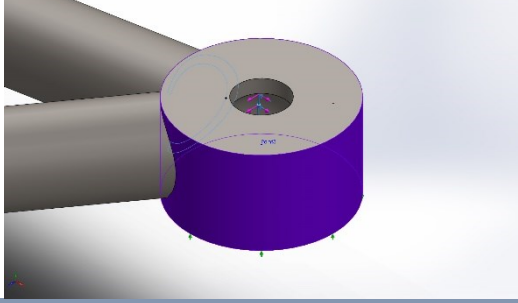
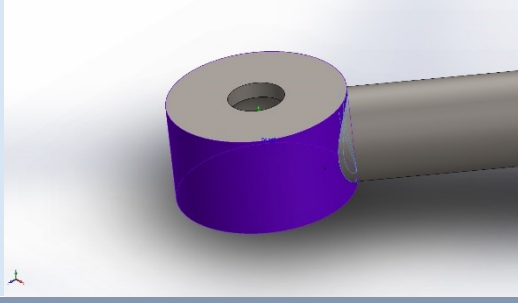
Model Reference	Properties	Components
	<p>Name: AISI 4130 Steel, normalized at 870C</p> <p>Model type: Linear Elastic Isotropic</p> <p>Default failure criterion: Unknown</p> <p>Yield strength: 4.6e+008 N/m²</p> <p>Tensile strength: 7.31e+008 N/m²</p> <p>Elastic modulus: 2.05e+011 N/m²</p> <p>Poisson's ratio: 0.285</p> <p>Mass density: 7850 kg/m³</p> <p>Shear modulus: 8e+010 N/m²</p>	<p>SolidBody 1(Cut-Revolve3)(F18_SU_RearLeftUpperA-ArmTubes_v101217),</p> <p>SolidBody 2(Cut-Revolve2)(F18_SU_RearLeftUpperA-ArmTubes_v101217),</p> <p>SolidBody 3(Cut-Revolve1)(F18_SU_RearLeftUpperA-ArmTubes_v101217),</p> <p>SolidBody 4(Stock-Suspension Mockup-4)(F18_SU_RearLeftUpperA-ArmTubes_v101217),</p> <p>SolidBody 5(Stock-Suspension Mockup-5)(F18_SU_RearLeftUpperA-ArmTubes_v101217),</p> <p>SolidBody 6(Stock-Suspension Mockup-3)(F18_SU_RearLeftUpperA-ArmTubes_v101217)</p>
Curve Data:N/A		

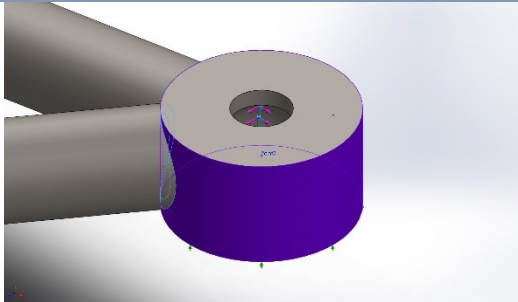
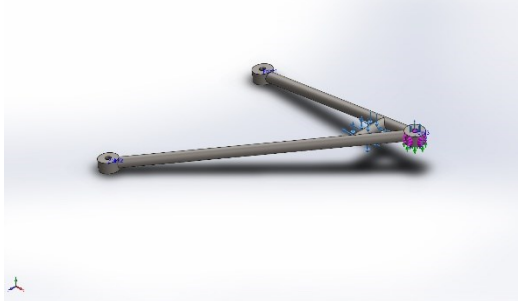
Loads and Fixtures

Fixture name	Fixture Image	Fixture Details		
On Spherical Faces-1		Entities: 2 face(s) Type: On Spherical Faces Translation: 0, ---, --- Units: mm		
Roller/Slider-1		Entities: 1 face(s) Type: Roller/Slider		
Resultant Forces				
Components	X	Y	Z	Resultant
Reaction force(N)	0.054853	4934	0.0703918	4934
Reaction Moment(N.m)	0	0	0	0

Load name	Load Image	Load Details
Force-1		Entities: 1 face(s), 1 plane(s) Reference: Plane1 Type: Apply force Values: 215, ---, 229 lbf
Force-2		Entities: 2 face(s), 1 plane(s) Reference: Plane1 Type: Apply force Values: -650, -650, --- lbf

Contact Information

Contact	Contact Image	Contact Properties
<p>Contact Set-1</p>		<p>Type: Bonded contact pair Entites: 2 face(s)</p>
<p>Contact Set-2</p>		<p>Type: Bonded contact pair Entites: 2 face(s)</p>
<p>Contact Set-3</p>		<p>Type: Bonded contact pair Entites: 2 face(s)</p>
<p>Contact Set-4</p>		<p>Type: Bonded contact pair Entites: 2 face(s)</p>
<p>Contact Set-5</p>		<p>Type: Bonded contact pair Entites: 2 face(s)</p>

<p>Contact Set-6</p>		<p>Type: Bonded contact pair Entites: 2 face(s)</p>
<p>Contact Set-7</p>		<p>Type: Bonded contact pair Entites: 2 face(s)</p>
<p>Global Contact</p>		<p>Type: Bonded Components: 1 component(s) Options: Compatible mesh</p>

Mesh information

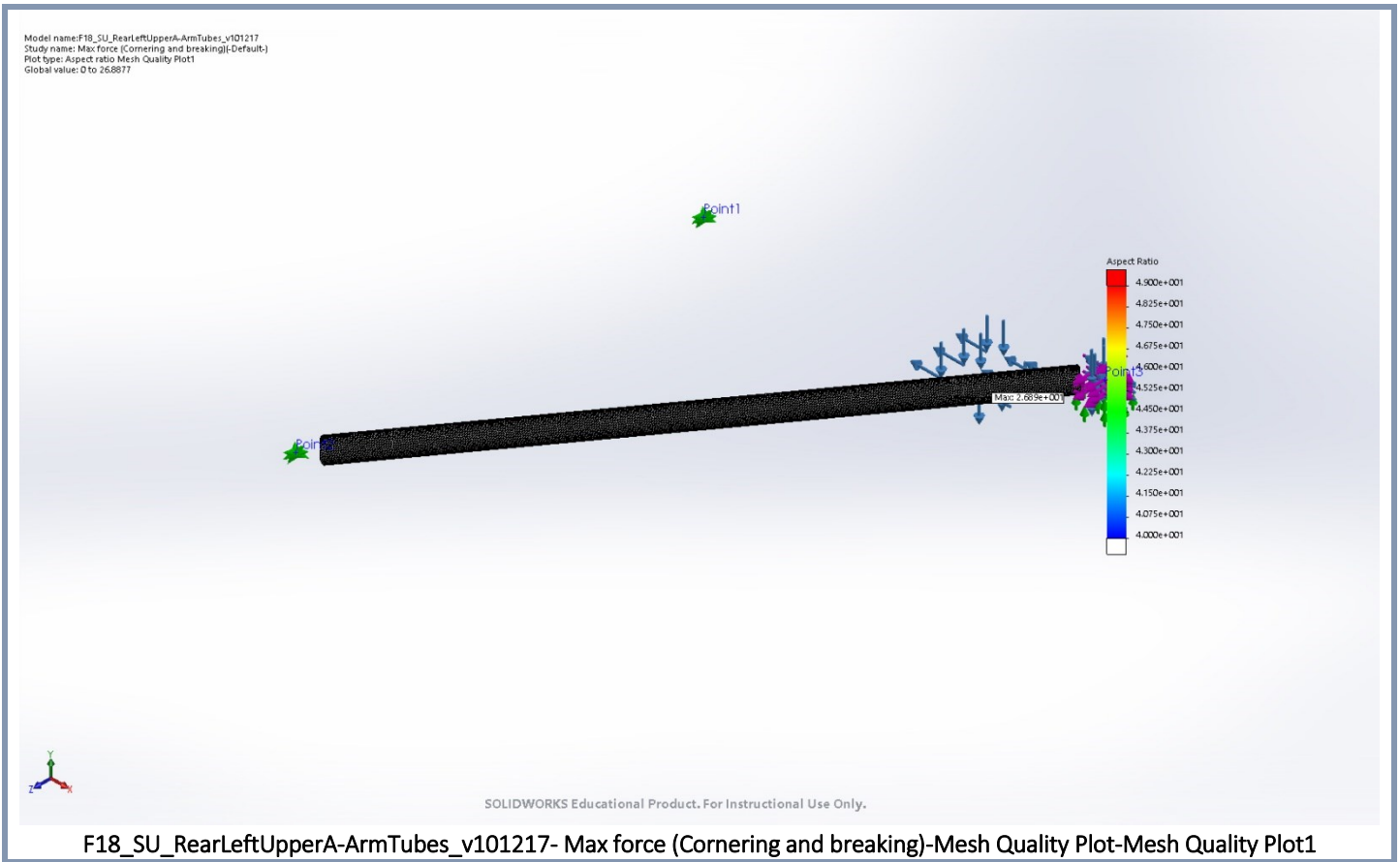
Mesh type	Solid Mesh
Mesher Used:	Standard mesh
Automatic Transition:	Off
Include Mesh Auto Loops:	Off
Jacobian points	4 Points
Element Size	0.05 in
Tolerance	0.0025 in
Mesh Quality Plot	High

Mesh information - Details

Total Nodes	522107
Total Elements	321355
Maximum Aspect Ratio	59.483
% of elements with Aspect Ratio < 3	99.9
% of elements with Aspect Ratio > 10	0.00405
% of distorted elements(Jacobian)	0
Time to complete mesh(hh:mm:ss):	00:00:22
Computer name:	

Mesh Quality Plots

Name	Type	Min	Max
Mesh Quality Plot1	Aspect Ratio	0.000e+000 Element: 1	2.689e+001 Element: 199775



Resultant Forces

Reaction forces

Selection set	Units	Sum X	Sum Y	Sum Z	Resultant
Entire Model	N	4826.33	5782.62	-1018.55	7600.63

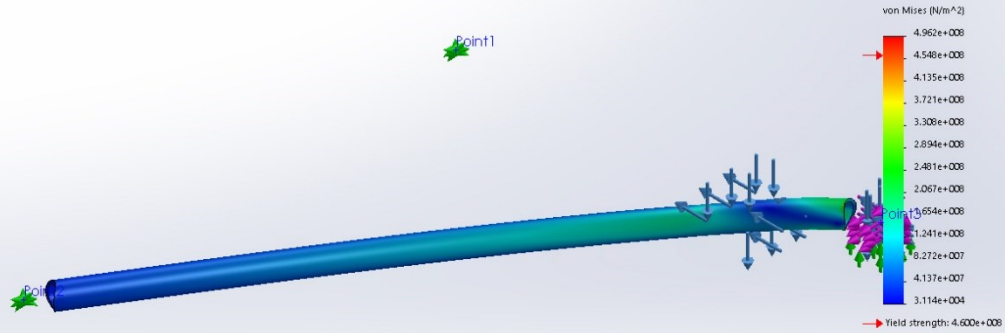
Reaction Moments

Selection set	Units	Sum X	Sum Y	Sum Z	Resultant
Entire Model	N.m	0	0	0	0

Study Results

Name	Type	Min	Max
Stress1	VON: von Mises Stress	3.114e+004N/m ² Node: 155093	4.962e+008N/m ² Node: 268079

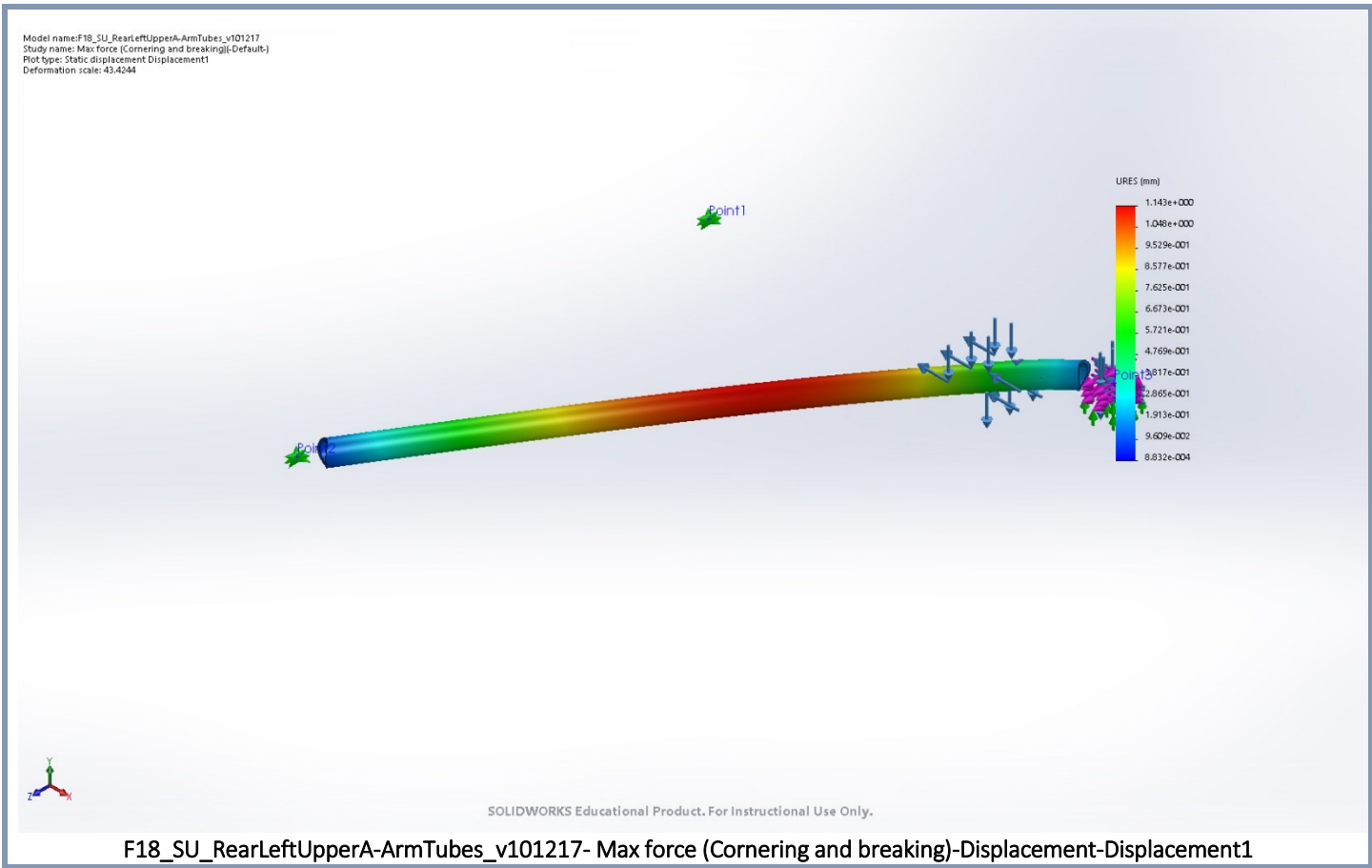
Model name:F18_SU_RearLeftUpperA-ArmTubes_v101217
 Study name: Max force (Cornering and breaking) (Default)
 Plot type: Static nodal stress (Stress1)
 Deformation scale: 43.4244



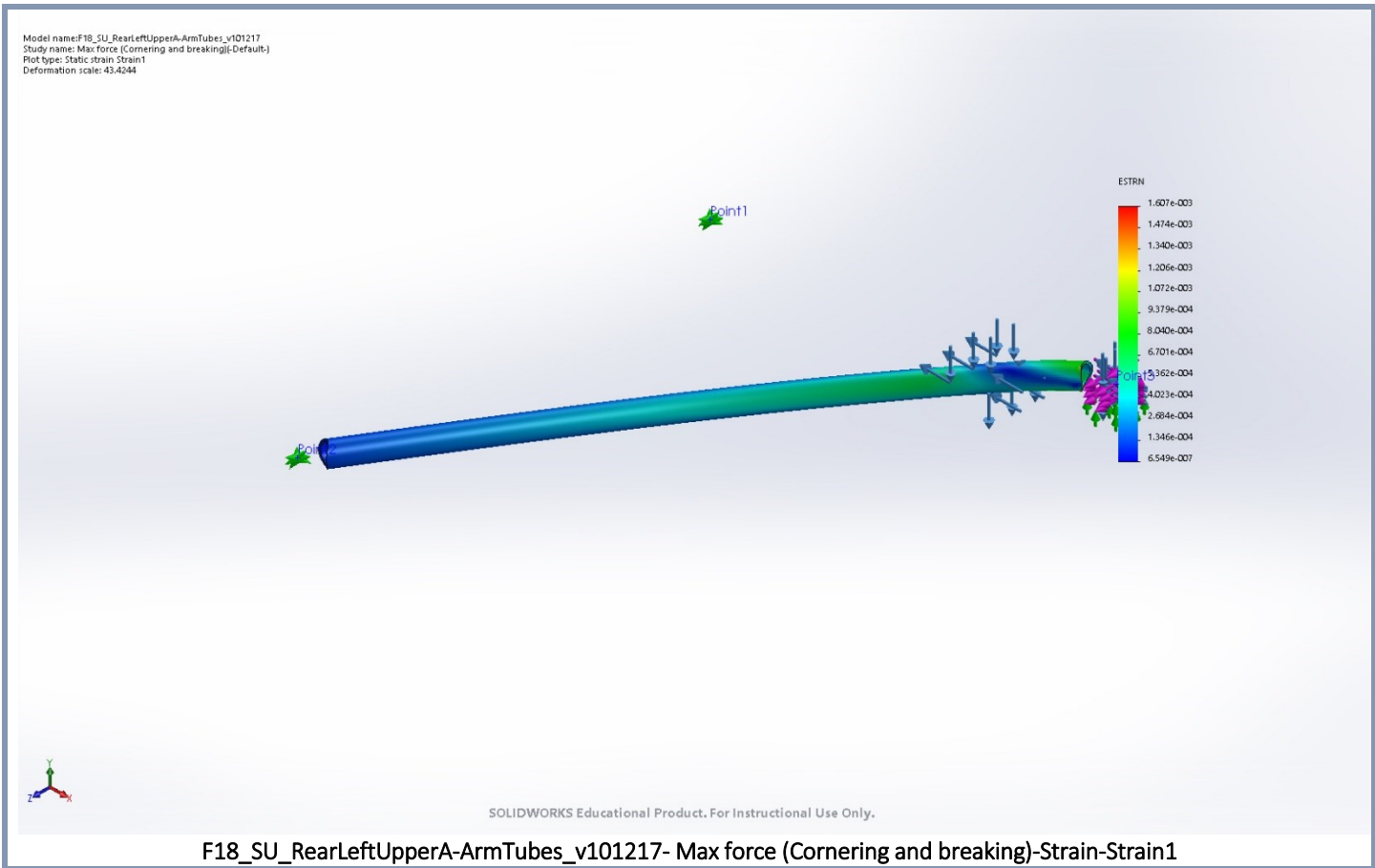
SOLIDWORKS Educational Product. For Instructional Use Only.

F18_SU_RearLeftUpperA-ArmTubes_v101217- Max force (Cornering and breaking)-Stress-Stress1

Name	Type	Min	Max
Displacement1	URES: Resultant Displacement	8.832e-004mm Node: 1483	1.143e+000mm Node: 513878

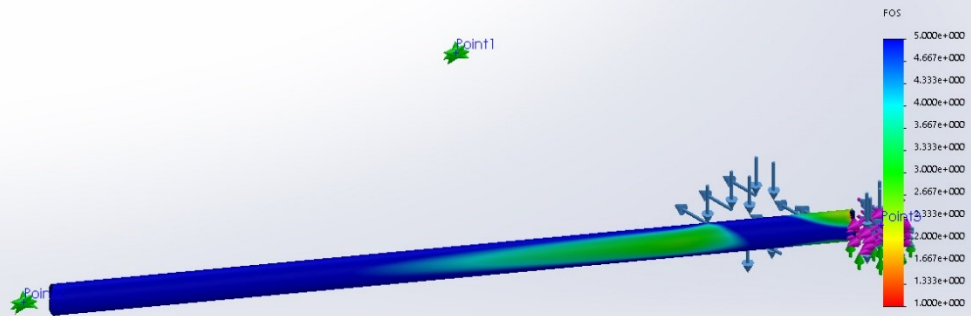


Name	Type	Min	Max
Strain1	ESTRN: Equivalent Strain	1.948e-007 Element: 69555	1.931e-003 Element: 117717



Name	Type	Min	Max
Factor of Safety1	Automatic	1.056e+000 Node: 97885	5.668e+003 Node: 503141

Model name: F18_SU_RearLeftUpperA-ArmTubes_v101217
Study name: Max force (Cornering and breaking)
Plot type: Factor of Safety Factor of Safety
Criterion: Automatic
Factor of safety distribution: Min FOS = 1.1



SOLIDWORKS Educational Product. For Instructional Use Only.

F18_SU_RearLeftUpperA-ArmTubes_v101217- Max force (Cornering and breaking)-Factor of Safety-Factor of Safety1

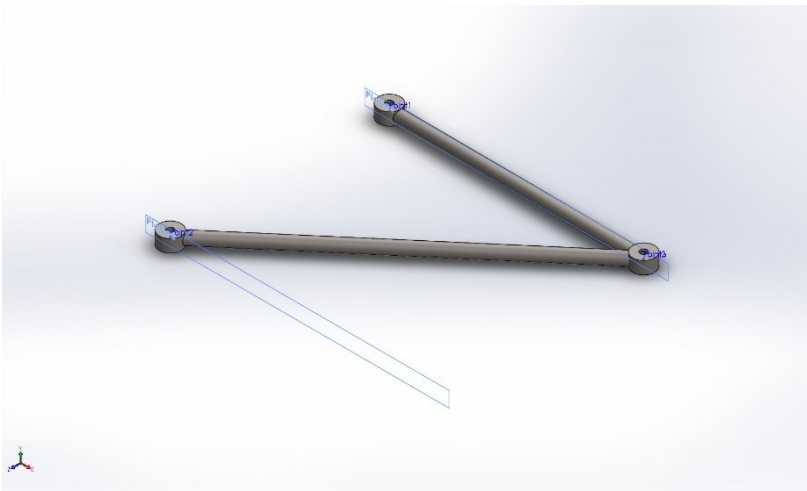
Simulation of Rear Lower A-Arm

Date: Thursday, April 19, 2018

Designer: Solidworks

Study name: Static 1

Analysis type: Static



Description

This analysis was used to determine the smallest and lightest tubes that would be able to be used for the given A-Arm design. Forces were applied to simulate the worst case loading scenario to insure that the tube size chosen would be able to withstand any potential forces without failing. Deflection of the A-Arms was also considered to insure that the wheels maintained the optimal contact patch at all times. Any deflections were corrected for by suspension geometry.

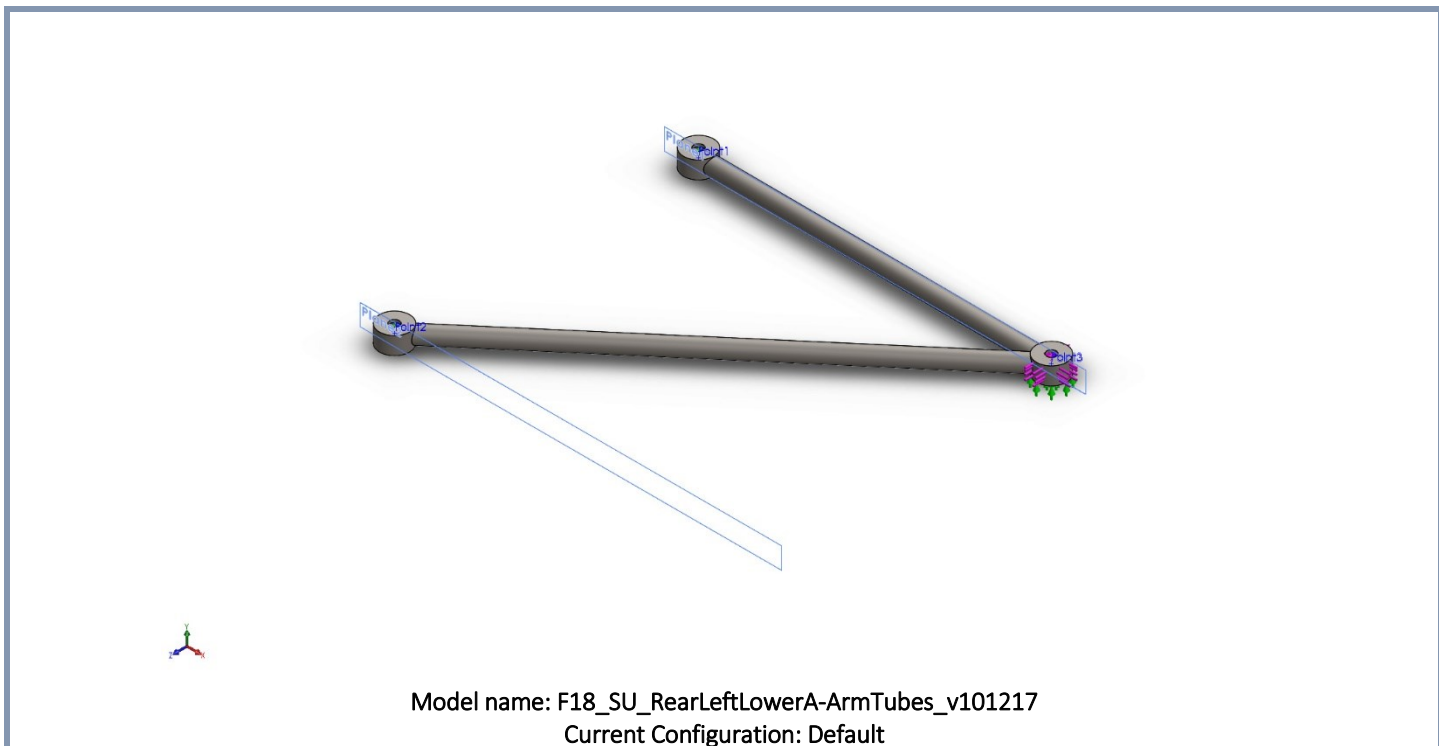
Assumptions

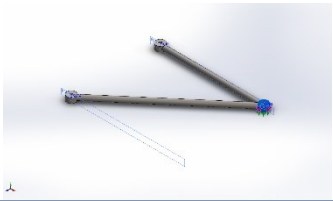
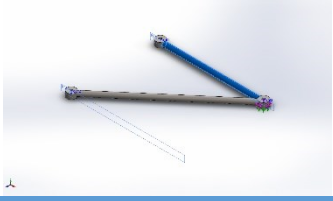
Only 4130 Steel tubes would be considered.

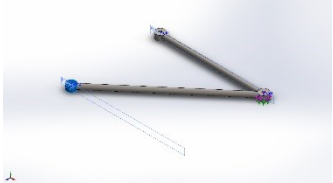
Maximum braking force would be 1.5g

Maximum cornering force would be 1.5g

Model Information



Solid Bodies			
Document Name and Reference	Treated As	Volumetric Properties	Document Path/Date Modified
Stock-Suspension Mockup-2 	Solid Body	Mass:0.229455 kg Volume:2.92347e-005 m ³ Density:7848.73 kg/m ³ Weight:2.24866 N	F:\2017-18 FSAE MQP\SolidWorks\F18_ASM_F ullcar_v031218\F18_SU_RearL eftLowerA- ArmTubes_v101217.SLDPRT Mar 12 11:18:53 2018
Cut-Revolve2 	Solid Body	Mass:0.0810222 kg Volume:1.03213e-005 m ³ Density:7850 kg/m ³ Weight:0.794018 N	F:\2017-18 FSAE MQP\SolidWorks\F18_ASM_F ullcar_v031218\F18_SU_RearL eftLowerA- ArmTubes_v101217.SLDPRT Mar 12 11:18:53 2018
Stock-Suspension Mockup-3 	Solid Body	Mass:0.169542 kg Volume:2.16019e-005 m ³ Density:7848.48 kg/m ³ Weight:1.66151 N	F:\2017-18 FSAE MQP\SolidWorks\F18_ASM_F ullcar_v031218\F18_SU_RearL eftLowerA- ArmTubes_v101217.SLDPRT Mar 12 11:18:53 2018

<p>Cut-Revolve1</p> 	Solid Body	<p>Mass:0.0810222 kg Volume:1.03213e-005 m³ Density:7850 kg/m³ Weight:0.794018 N</p>	<p>F:\2017-18 FSAE MQP\SolidWorks\F18_ASM_F ullcar_v031218\F18_SU_RearL eftLowerA- ArmTubes_v101217.SLDPRT Mar 12 11:18:53 2018</p>
<p>Cut-Revolve3</p> 	Solid Body	<p>Mass:0.0810222 kg Volume:1.03213e-005 m³ Density:7850 kg/m³ Weight:0.794018 N</p>	<p>F:\2017-18 FSAE MQP\SolidWorks\F18_ASM_F ullcar_v031218\F18_SU_RearL eftLowerA- ArmTubes_v101217.SLDPRT Mar 12 11:18:53 2018</p>

Study Properties

Study name	Static 1
Analysis type	Static
Mesh type	Solid Mesh
Thermal Effect:	On
Thermal option	Include temperature loads
Zero strain temperature	298 Kelvin
Include fluid pressure effects from SOLIDWORKS Flow Simulation	Off
Solver type	FFEPlus
Inplane Effect:	Off
Soft Spring:	Off
Inertial Relief:	Off
Incompatible bonding options	Automatic
Large displacement	Off
Compute free body forces	On
Friction	Off
Use Adaptive Method:	Off
Result folder	SOLIDWORKS document (F:\2017-18 FSAE MQP\SolidWorks\F18_ASM_Fullcar_v031218)

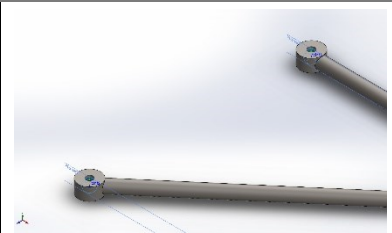
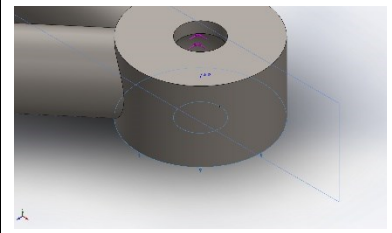
Units

Unit system:	SI (MKS)
Length/Displacement	mm
Temperature	Kelvin
Angular velocity	Rad/sec
Pressure/Stress	N/m ²

Material Properties

Model Reference	Properties	Components
	<p>Name: AISI 4130 Steel, normalized at 870C</p> <p>Model type: Linear Elastic Isotropic</p> <p>Default failure criterion: Unknown</p> <p>Yield strength: 4.6e+008 N/m²</p> <p>Tensile strength: 7.31e+008 N/m²</p> <p>Elastic modulus: 2.05e+011 N/m²</p> <p>Poisson's ratio: 0.285</p> <p>Mass density: 7850 kg/m³</p> <p>Shear modulus: 8e+010 N/m²</p>	<p>SolidBody 1(Stock-Suspension Mockup-2)(F18_SU_RearLeftLowerA-ArmTubes_v101217),</p> <p>SolidBody 2(Cut-Revolve2)(F18_SU_RearLeftLowerA-ArmTubes_v101217),</p> <p>SolidBody 3(Stock-Suspension Mockup-3)(F18_SU_RearLeftLowerA-ArmTubes_v101217),</p> <p>SolidBody 4(Cut-Revolve1)(F18_SU_RearLeftLowerA-ArmTubes_v101217),</p> <p>SolidBody 5(Cut-Revolve3)(F18_SU_RearLeftLowerA-ArmTubes_v101217)</p>
Curve Data:N/A		

Loads and Fixtures

Fixture name	Fixture Image	Fixture Details		
On Spherical Faces-1		Entities: 2 face(s) Type: On Spherical Faces Translation: 0, ---, --- Units: mm		
Resultant Forces				
Components	X	Y	Z	Resultant
Reaction force(N)	2557.7	-13.3497	2717.9	3732.15
Reaction Moment(N.m)	0	0	0	0
Roller/Slider-1		Entities: 1 face(s) Type: Roller/Slider		
Resultant Forces				
Components	X	Y	Z	Resultant
Reaction force(N)	-0.0336852	13.2405	0.0286998	13.2406
Reaction Moment(N.m)	0	0	0	0

Load name	Load Image	Load Details
Force-1		Entities: 1 face(s), 1 plane(s) Reference: Plane1 Type: Apply force Values: -575, ---, -611 lbf

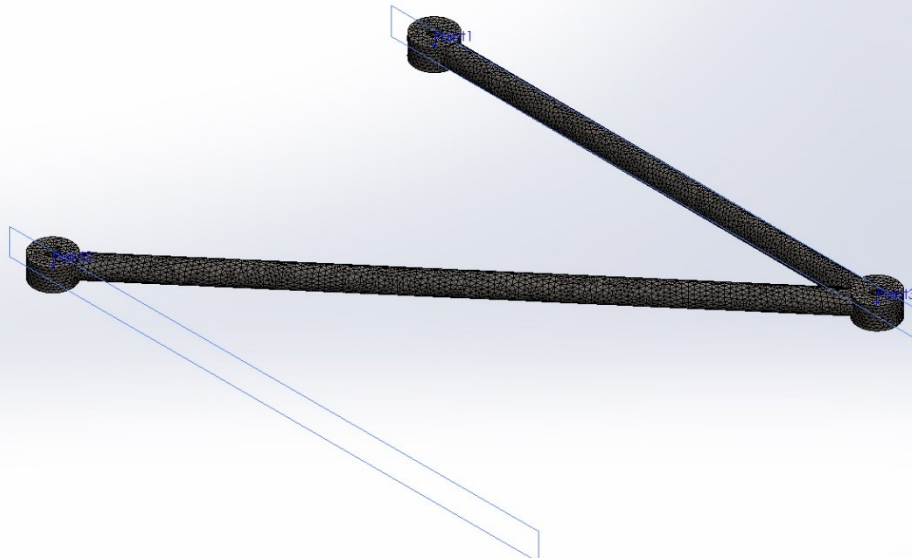
Mesh information

Mesh type	Solid Mesh
Mesher Used:	Curvature-based mesh
Jacobian points	4 Points
Maximum element size	0.113997 in
Minimum element size	0.0379987 in
Mesh Quality Plot	High

Mesh information - Details

Total Nodes	74532
Total Elements	39922
Maximum Aspect Ratio	7.9982
% of elements with Aspect Ratio < 3	98.6
% of elements with Aspect Ratio > 10	0
% of distorted elements(Jacobian)	0
Time to complete mesh(hh:mm:ss):	00:00:04
Computer name:	

Model name: 19_SU_RoarLeftLowerArmTube1_v101217
Study name: Static 1-(Default)
Mesh type: Solid Mesh



SOLIDWORKS Educational Product. For Instructional Use Only.

Resultant Forces

Reaction forces

Selection set	Units	Sum X	Sum Y	Sum Z	Resultant
Entire Model	N	2557.66	-0.109092	2717.92	3732.12

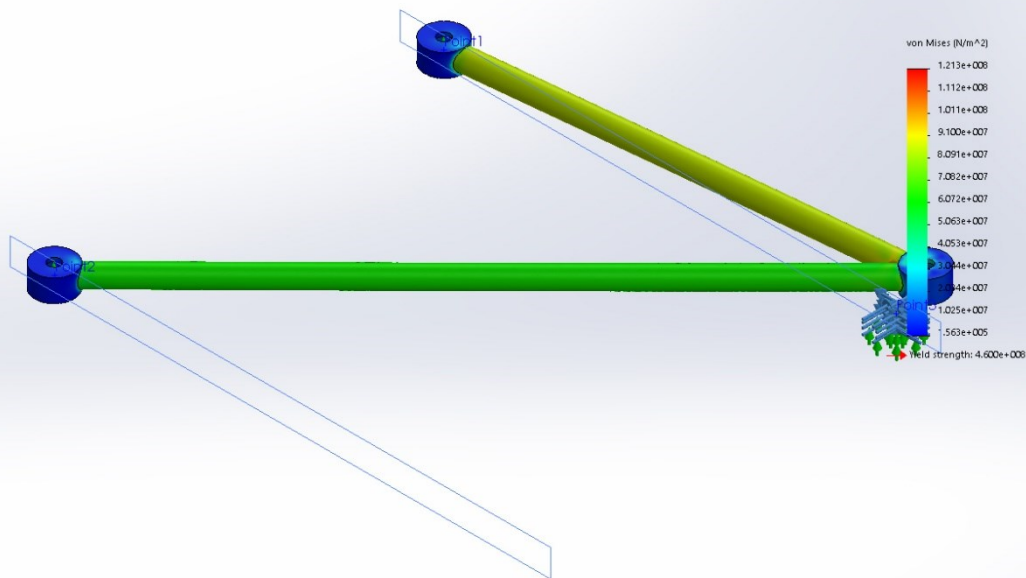
Reaction Moments

Selection set	Units	Sum X	Sum Y	Sum Z	Resultant
Entire Model	N.m	0	0	0	0

Study Results

Name	Type	Min	Max
Stress1	VON: von Mises Stress	1.563e+005N/m ² Node: 70404	1.213e+008N/m ² Node: 5098

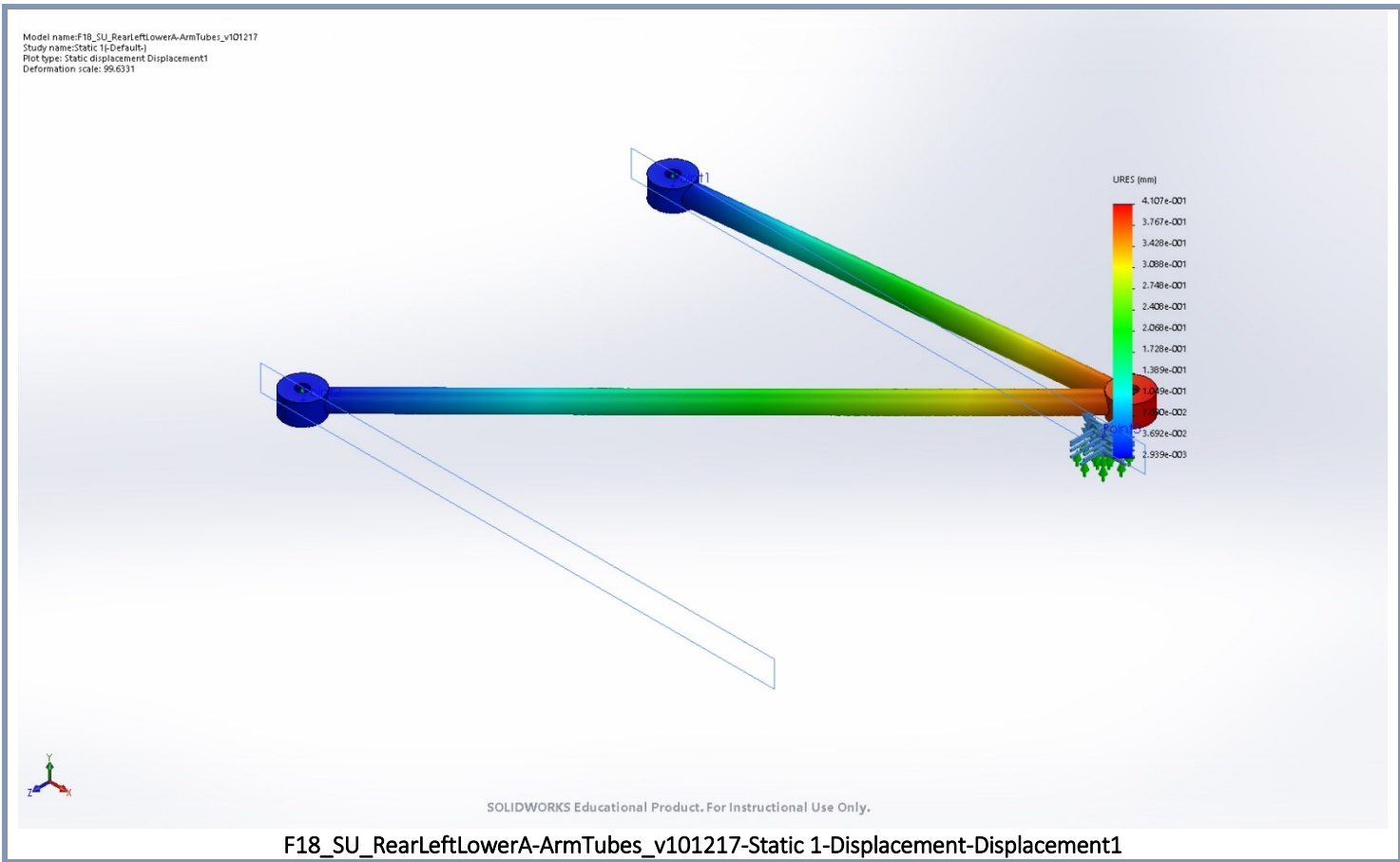
Model name:F18_SU_RearLeftLowerA-ArmTubes_v101217
Study name:Static 1(Default)
Plot type: Static nodal stress Stress1
Deformation scale: 99.6331



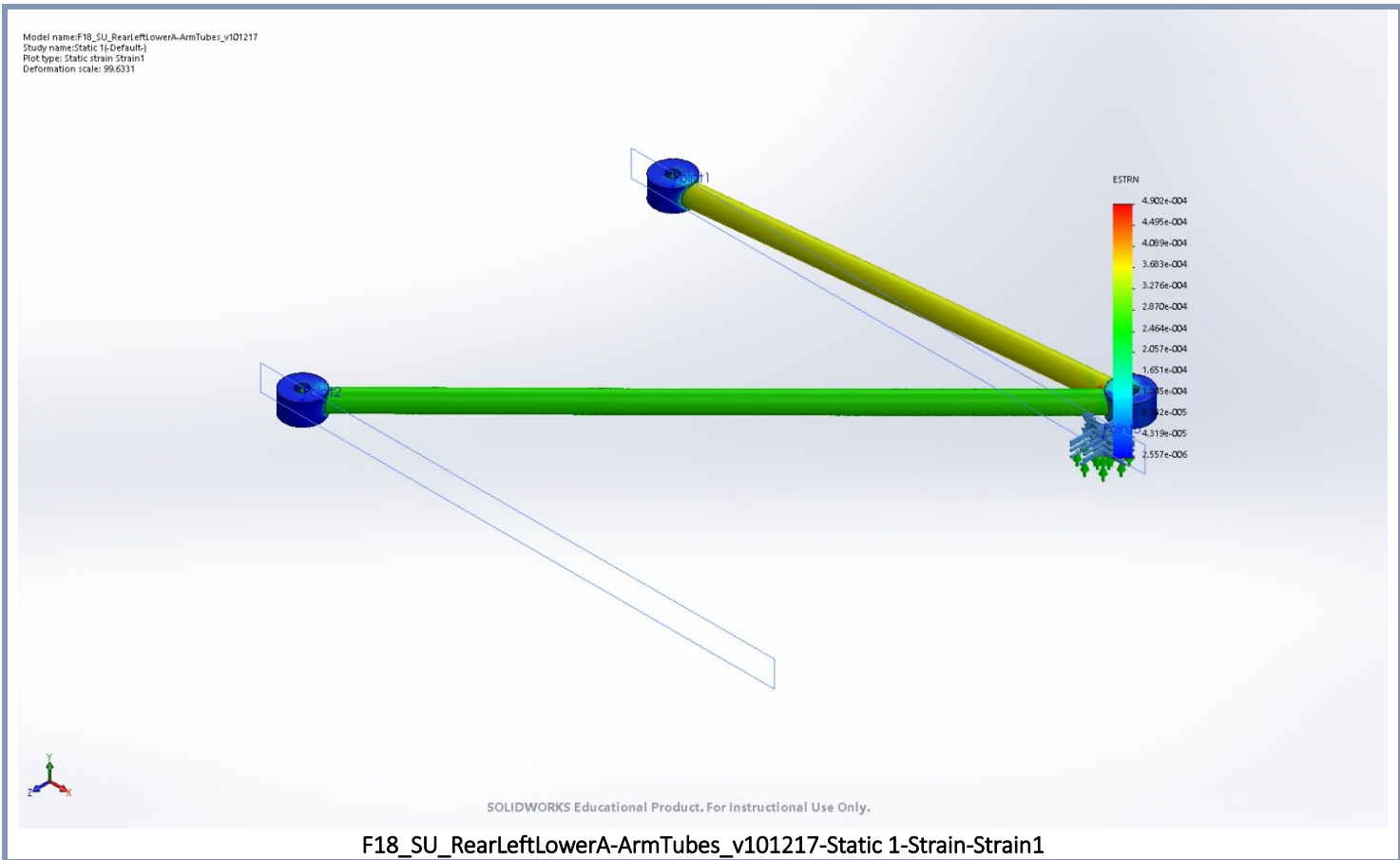
SOLIDWORKS Educational Product. For Instructional Use Only.

F18_SU_RearLeftLowerA-ArmTubes_v101217-Static 1-Stress-Stress1

Name	Type	Min	Max
Displacement1	URES: Resultant Displacement	2.939e-003mm Node: 68546	4.107e-001mm Node: 32583

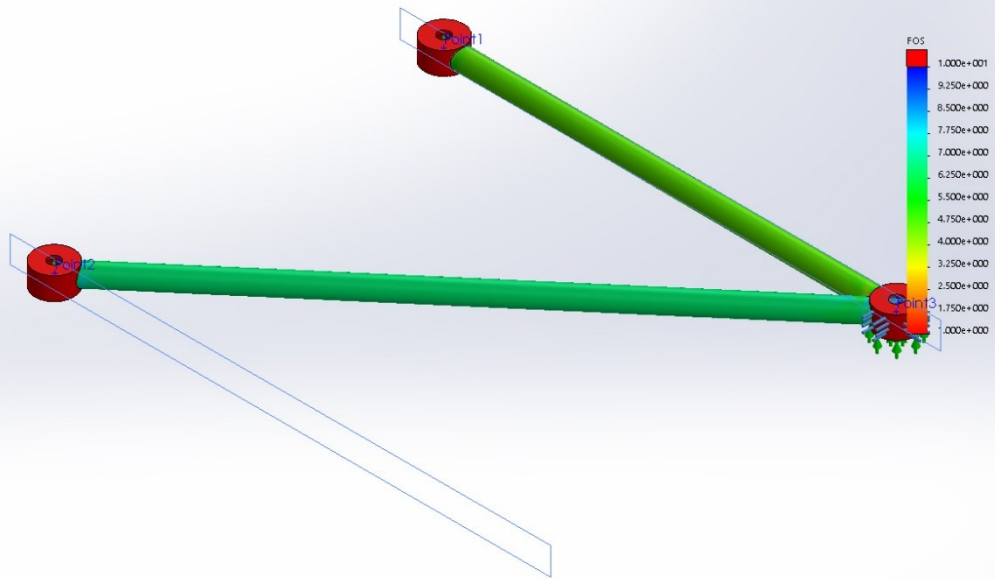


Name	Type	Min	Max
Strain1	ESTRN: Equivalent Strain	2.557e-006 Element: 36241	4.902e-004 Element: 30639



Name	Type	Min	Max
Factor of Safety1	Automatic	3.306e+000 Node: 5098	2.943e+003 Node: 70404

Model name: F18_SU_RearLeftLowerA-ArmTubes_v101217
Study name: Static 1 (Default)
Plot type: Factor of Safety Factor of Safety1
Criterion: Automatic
Factor of safety distribution: Min FOS = 3.3



SOLIDWORKS Educational Product. For Instructional Use Only.

F18_SU_RearLeftLowerA-ArmTubes_v101217-Static 1-Factor of Safety-Factor of Safety1



Simulation of PullRod

Date: Thursday, April 19, 2018

Designer: Solidworks

Study name: Max Tension (Cornering and Braking)

Analysis type: Staticw

Description

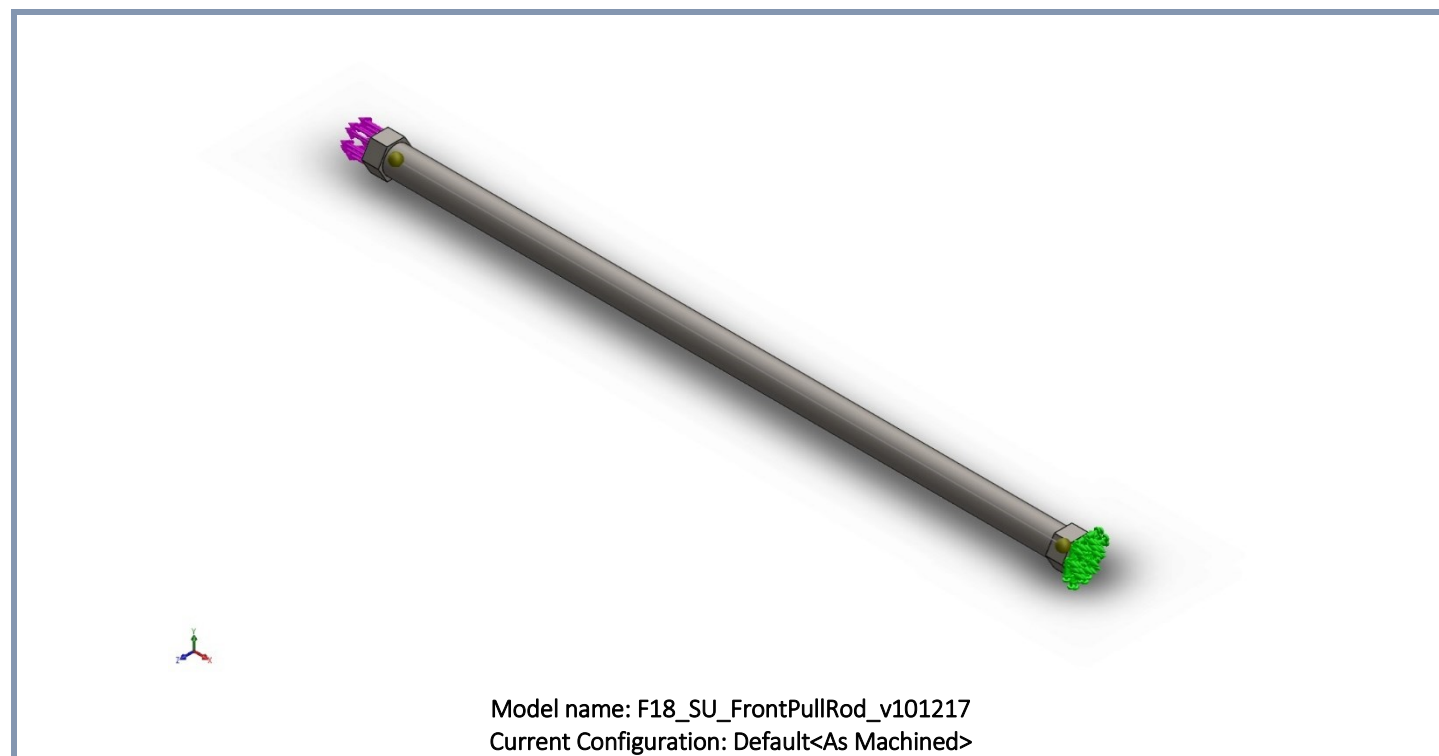
This Analysis was to determine the smallest tubing that could be used for the pull rods.

Assumptions

1.5g cornering force.

1.5g Braking force.

Model Information



Solid Bodies

Document Name and Reference	Treated As	Volumetric Properties	Document Path/Date Modified
5/16 (0.3125) Diameter Hole1[1]	Solid Body	Mass:0.00494576 kg Volume:6.30034e-007 m ³ Density:7850 kg/m ³ Weight:0.0484685 N	F:\2017-18 FSAE MQP\SolidWorks\F18_ASM_Fullcar_v031218\F18_SU_FrontPullRod_v101217.SLDPR Feb 15 12:34:01 2018
5/16 (0.3125) Diameter Hole1[2]	Solid Body	Mass:0.00494576 kg Volume:6.30034e-007 m ³ Density:7850 kg/m ³ Weight:0.0484685 N	F:\2017-18 FSAE MQP\SolidWorks\F18_ASM_Fullcar_v031218\F18_SU_FrontPullRod_v101217.SLDPR Feb 15 12:34:01 2018

Beam Bodies:

Document Name and Reference	Formulation	Properties	Document Path/Date Modified
Beam-1(Tubing 0438ODX034ID(1))	Beam – Uniform C/S	Section Standard- SAE/Tubing/0438ODx034ID Section Area: 3.86334e-005m ² Length:279.4mm Volume:1.07942e-005m ³ Mass Density:7850kg/m ³ Mass:0.0847343kg Weight:0.830396N	F:\2017-18 FSAE MQP\SolidWorks\F18_ASM_Fullcar_v031218\F18_SU_FrontPullRod_v101217.SLDPR Feb 15 12:34:01 2018

Study Properties

Study name	Max Tension (cornering and Braking)
Analysis type	Static
Mesh type	Mixed Mesh
Thermal Effect:	On
Thermal option	Include temperature loads
Zero strain temperature	298 Kelvin
Include fluid pressure effects from SOLIDWORKS Flow Simulation	Off
Solver type	Direct sparse solver
Inplane Effect:	Off
Soft Spring:	Off
Inertial Relief:	Off
Incompatible bonding options	Automatic
Large displacement	Off
Compute free body forces	On
Friction	Off
Use Adaptive Method:	Off
Result folder	SOLIDWORKS document (F:\2017-18 FSAE MQP\SolidWorks\F18_ASM_Fullcar_v031218)

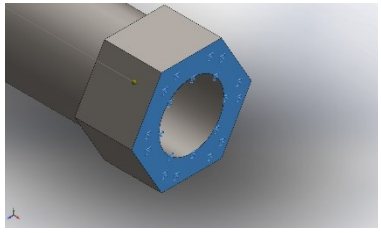
Units

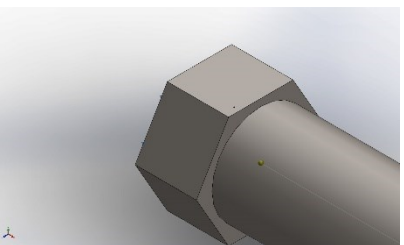
Unit system:	SI (MKS)
Length/Displacement	mm
Temperature	Kelvin
Angular velocity	Rad/sec
Pressure/Stress	N/m ²

Material Properties

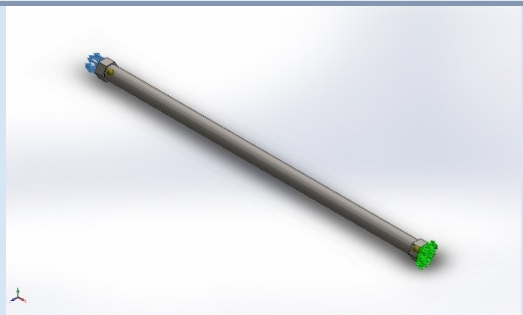
Model Reference	Properties	Components
	<p>Name: AISI 4130 Steel, normalized at 870C</p> <p>Model type: Linear Elastic Isotropic</p> <p>Default failure criterion: Unknown</p> <p>Yield strength: 4.6e+008 N/m²</p> <p>Tensile strength: 7.31e+008 N/m²</p> <p>Elastic modulus: 2.05e+011 N/m²</p> <p>Poisson's ratio: 0.285</p> <p>Mass density: 7850 kg/m³</p> <p>Shear modulus: 8e+010 N/m²</p>	<p>SolidBody 1(5/16 (0.3125) Diameter Hole1[1])(F18_SU_FrontPullRod_v101217),</p> <p>SolidBody 2(5/16 (0.3125) Diameter Hole1[2])(F18_SU_FrontPullRod_v101217),</p> <p>SolidBody 3(Tubing 0438ODX034ID(1))(F18_SU_FrontPullRod_v101217)</p>
Curve Data:N/A		

Loads and Fixtures

Fixture name	Fixture Image	Fixture Details		
Fixed-1		<p>Entities: 1 face(s)</p> <p>Type: Fixed Geometry</p>		
Resultant Forces				
Components	X	Y	Z	Resultant
Reaction force(N)	4546.08	-3.97861e-005	4.19617e-005	4546.08
Reaction Moment(N.m)	0	0	0	1e-033

Load name	Load Image	Load Details
Force-1		<p>Entities: 1 face(s)</p> <p>Type: Apply normal force</p> <p>Value: -1022 lbf</p>

Contact Information

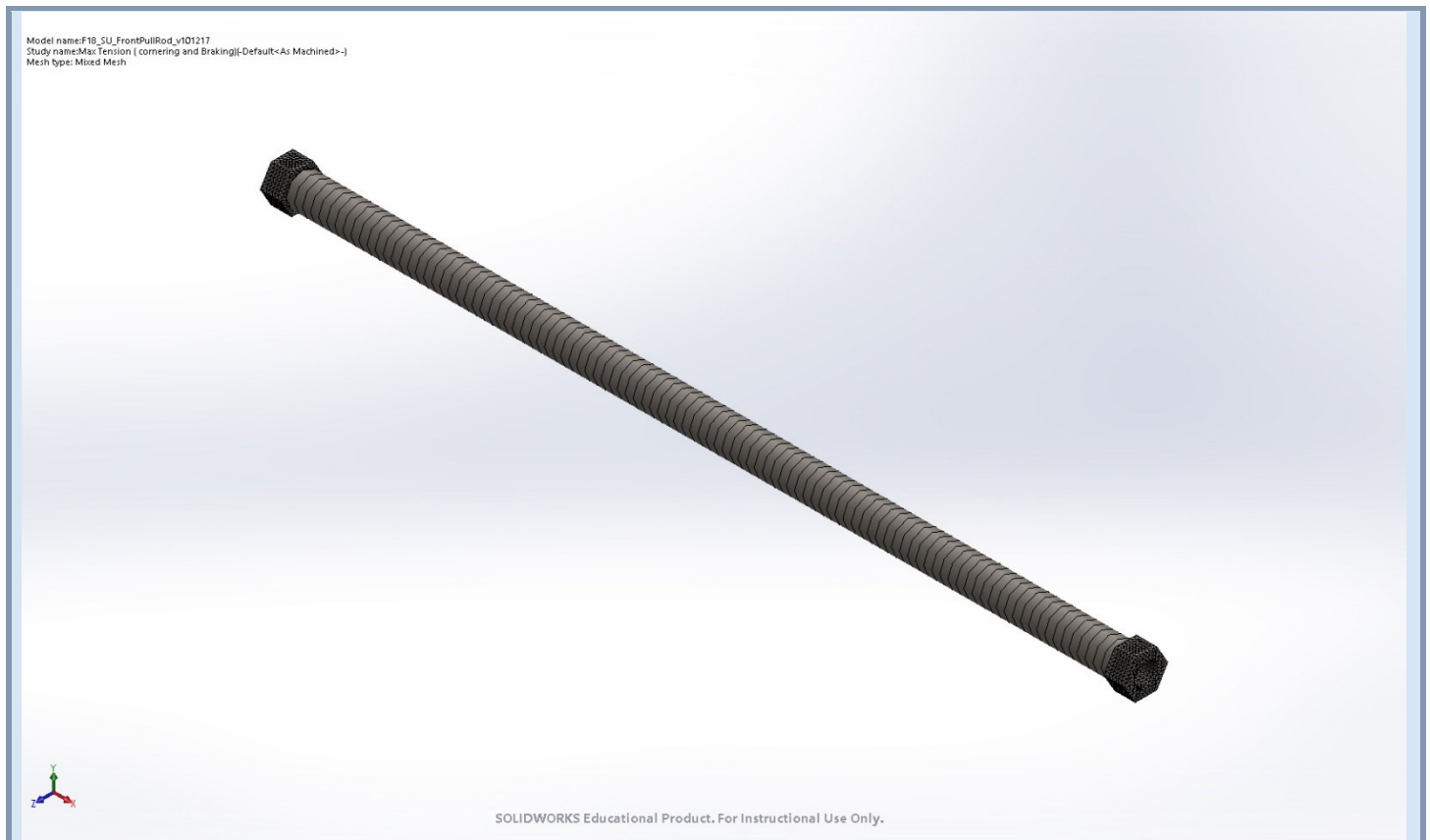
Contact	Contact Image	Contact Properties
Global Contact		Type: Bonded Components: 1 component(s) Options: Compatible mesh

Mesh information

Mesh type	Mixed Mesh
Mesher Used:	Standard mesh
Automatic Transition:	Off
Include Mesh Auto Loops:	Off
Jacobian points	4 Points
Jacobian check for shell	Off
Element Size	0.0425429 in
Tolerance	0.00212715 in
Mesh Quality Plot	High

Mesh information - Details

Total Nodes	12260
Total Elements	7414
Time to complete mesh(hh:mm:ss):	00:00:01
Computer name:	



Resultant Forces

Reaction forces

Selection set	Units	Sum X	Sum Y	Sum Z	Resultant
Entire Model	N	4546.08	-3.97861e-005	4.19617e-005	4546.08

Reaction Moments

Selection set	Units	Sum X	Sum Y	Sum Z	Resultant
Entire Model	N.m	0	0	0	1e-033

Beams

Beam Forces

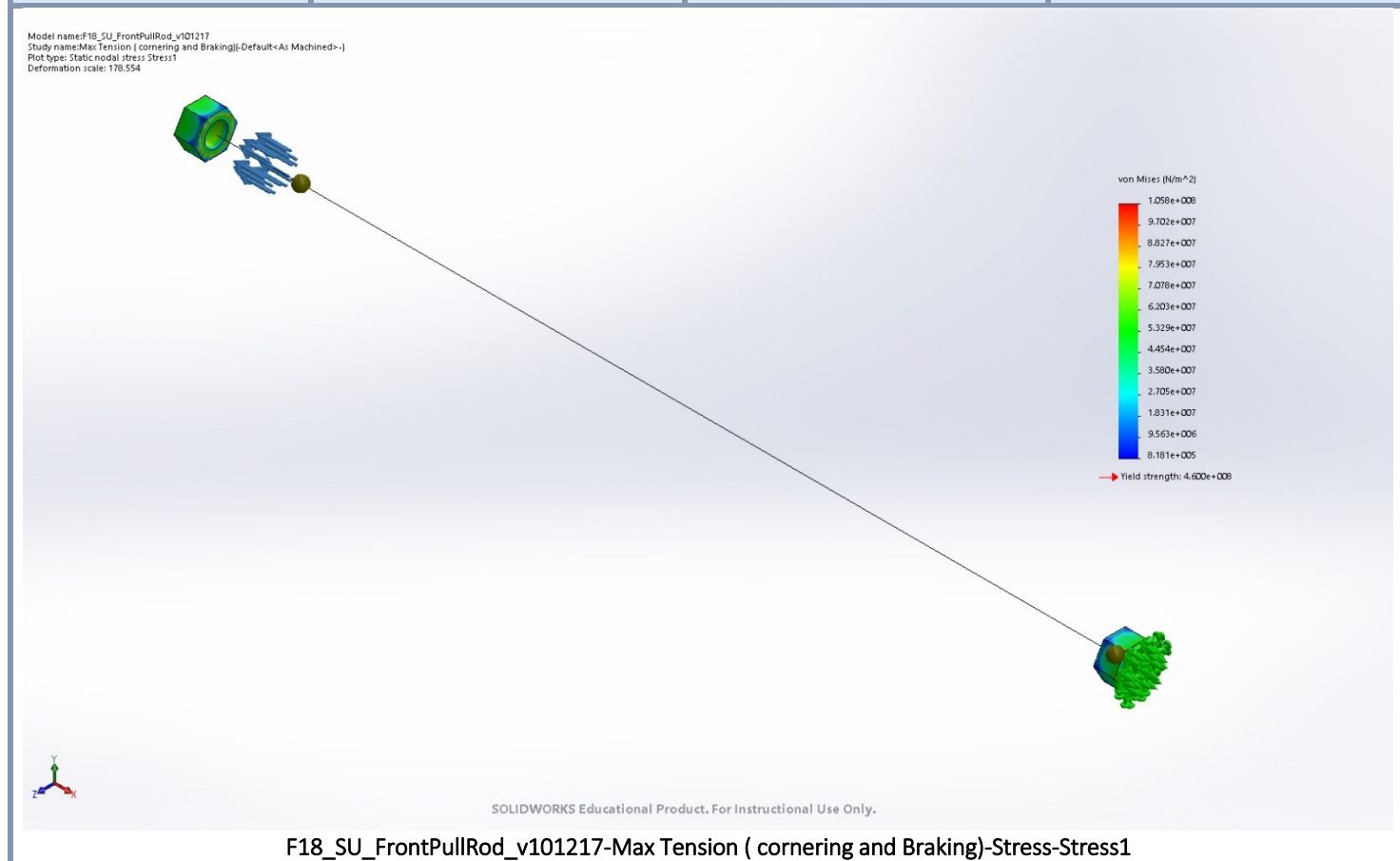
Beam Name	Joints	Axial(N)	Shear1(N)	Shear2(N)	Moment1(N.m)	Moment2(N.m)	Torque(N.m)
Beam-1(Tubing 0438ODX034ID(1))	1	-4546.08	2.72373e-009	5.30658e-009	-1.10502e-008	8.93816e-008	-1.38512e-012
	2	4546.08	-2.72368e-009	-5.30666e-009	9.5677e-009	-8.86204e-008	1.24507e-012

Beam Stresses

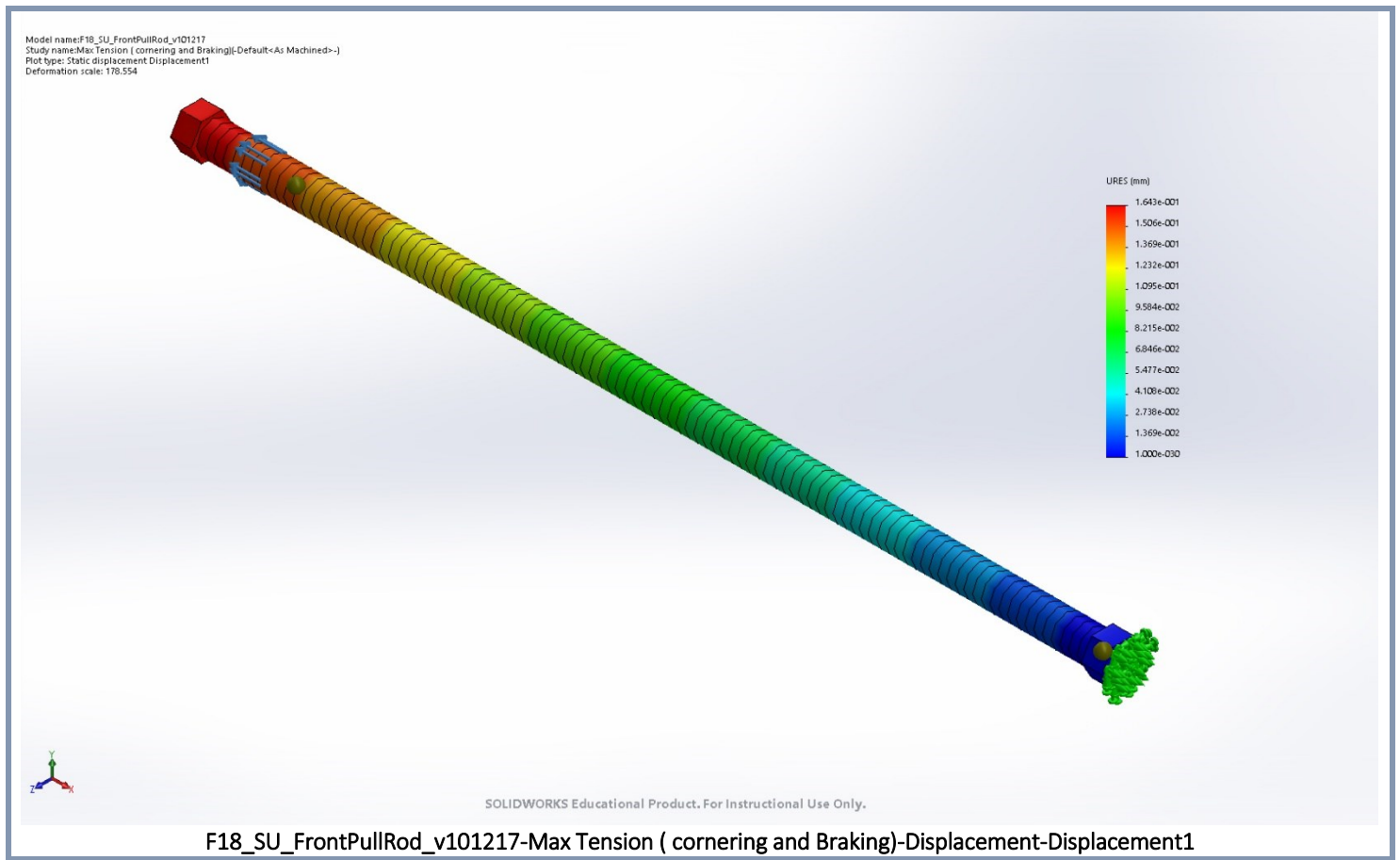
Beam Name	Joints	Axial(N/m ²)	Bending Dir1(N/m ²)	Bending Dir2(N/m ²)	Torsional (N/m ²)	Upper bound axial and bending(N/m ²)
Beam-1(Tubing 0438ODX034ID(1))	1	1.17672e+008	0.128343	1.03812	-8.04378e-006	1.17672e+008
	2	1.17672e+008	0.111124	1.02928	7.23045e-006	1.17672e+008

Study Results

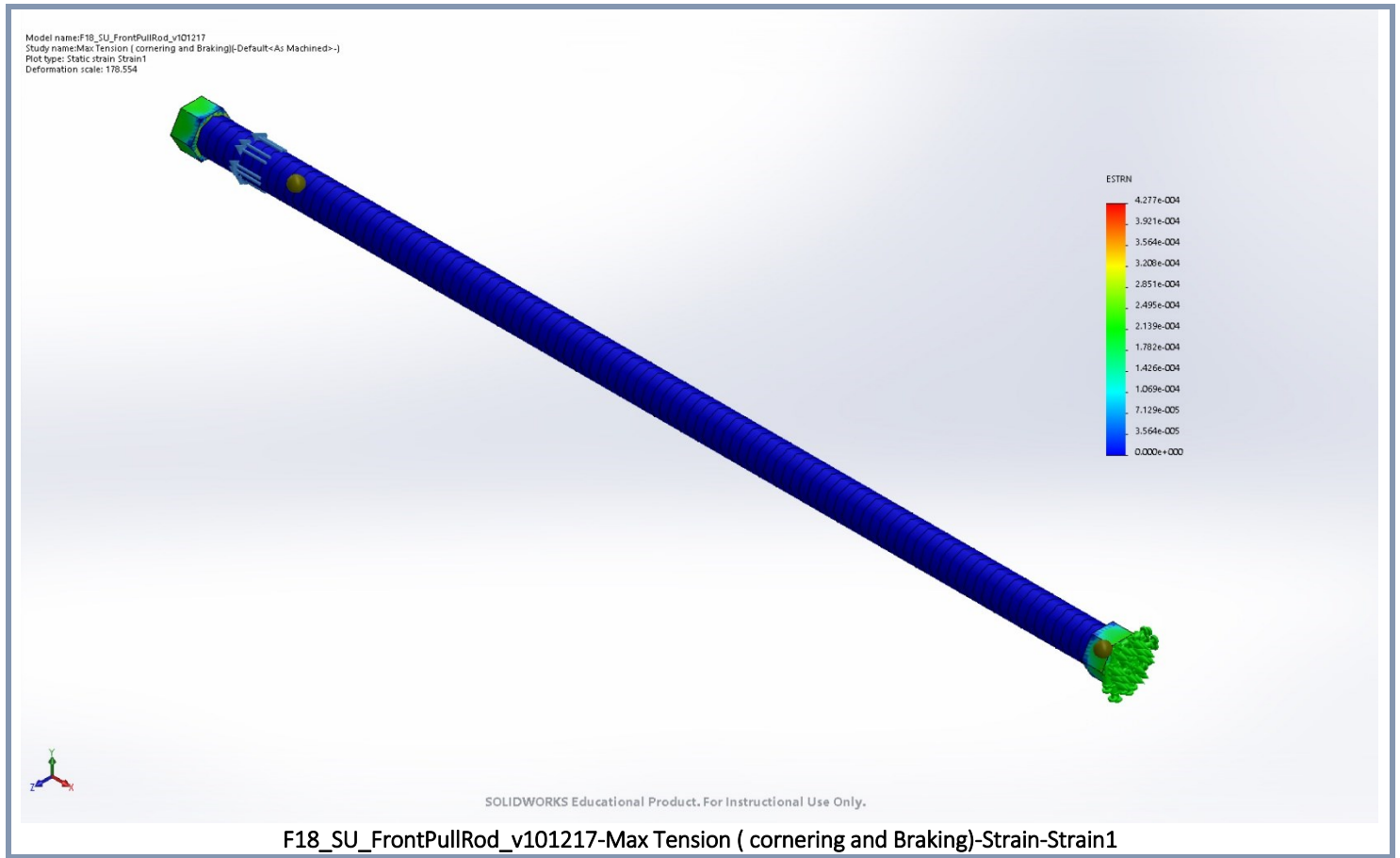
Name	Type	Min	Max
Stress1	VON: von Mises Stress	0.000e+000N/m ² Node: 12157	1.058e+008N/m ² Node: 5634



Name	Type	Min	Max
Displacement1	URES: Resultant Displacement	0.000e+000mm Node: 6151	1.643e-001mm Node: 284

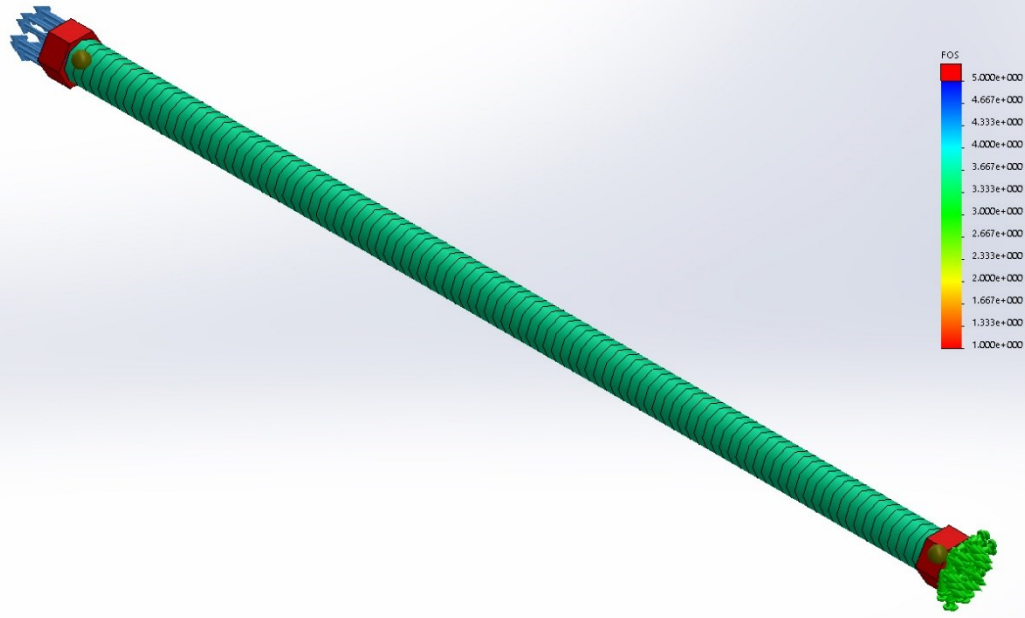


Name	Type	Min	Max
Strain1	ESTRN: Equivalent Strain	0.000e+000 Element: 7313	4.277e-004 Element: 3570



Name	Type	Min	Max
Factor of Safety1	Automatic	3.909e+000 Node: 12157	5.623e+002 Node: 10797

Model name: F18_SU_FrontPullRod_v101217
Study name: Max Tension (cornering and Braking)-Default<As Machined>-)
Plot type: Factor of Safety Factor of Safety1
Criterion: Automatic
Factor of safety distribution: Min FOS = 3.9



SOLIDWORKS Educational Product. For Instructional Use Only.

F18_SU_FrontPullRod_v101217-Max Tension (cornering and Braking)-Factor of Safety-Factor of Safety1

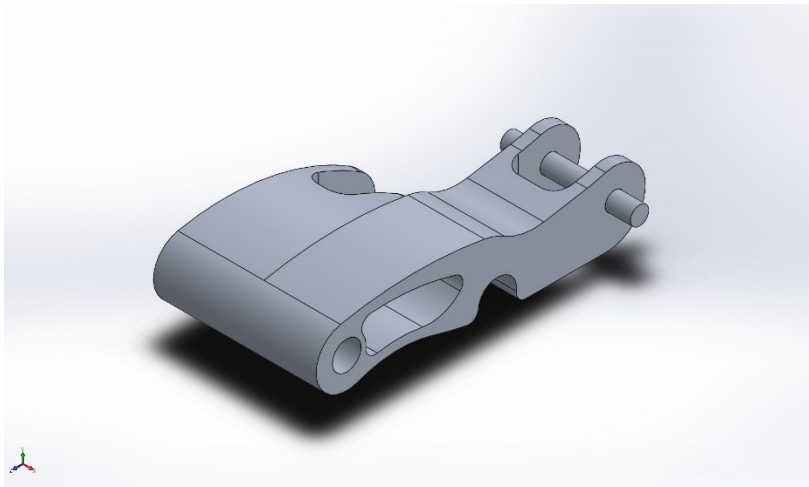
Simulation of Rocker

Date: Thursday, April 19, 2018

Designer: Solidworks

Study name: Static 1

Analysis type: Static



Description

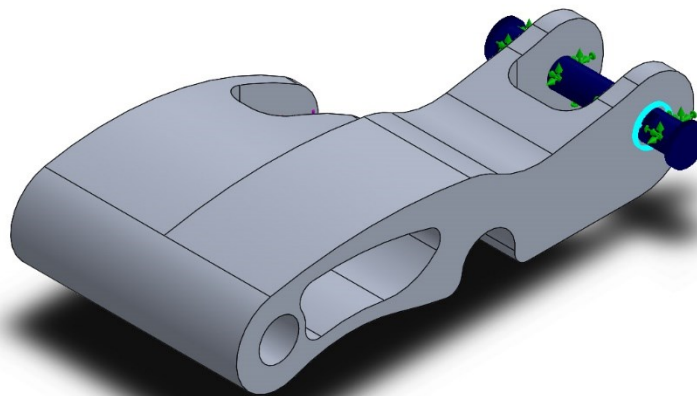
This Analysis was to determine the lightest rocker configuration that would be strong enough to withstand the forces applied to it in normal use. Multiple iterations were ran to shave material from the rocker where it wasn't needed.

Assumptions

1.5g cornering force.

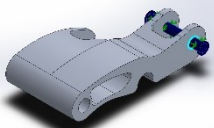
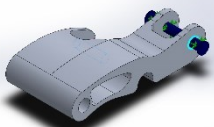
1.5g Braking force

Model Information



Model name: F18_SU_LeftRocker_v101217
Current Configuration: Default

Solid Bodies

Document Name and Reference	Treated As	Volumetric Properties	Document Path/Date Modified
3/8 (0.375) Diameter Hole2	Solid Body	Mass:0.145914 kg Volume:5.19268e-005 m ³ Density:2810 kg/m ³ Weight:1.42996 N	F:\2017-18 FSAE MQP\SolidWorks\F18_ASM_Fullcar_v031218\F18_SU_LeftRocker_v101217.SLDPRT Apr 18 14:25:49 2018
Boss-Extrude4 	Solid Body	Mass:0.00354135 kg Volume:1.26027e-006 m ³ Density:2810 kg/m ³ Weight:0.0347052 N	F:\2017-18 FSAE MQP\SolidWorks\F18_ASM_Fullcar_v031218\F18_SU_LeftRocker_v101217.SLDPRT Apr 18 14:25:49 2018
Boss-Extrude5 	Solid Body	Mass:0.00187483 kg Volume:6.672e-007 m ³ Density:2810 kg/m ³ Weight:0.0183734 N	F:\2017-18 FSAE MQP\SolidWorks\F18_ASM_Fullcar_v031218\F18_SU_LeftRocker_v101217.SLDPRT Apr 18 14:25:49 2018

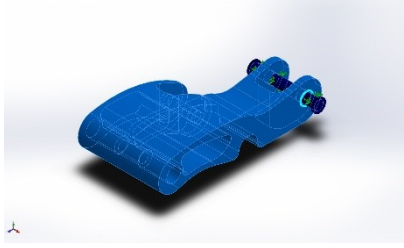
Study Properties

Study name	Static 1
Analysis type	Static
Mesh type	Solid Mesh
Thermal Effect:	On
Thermal option	Include temperature loads
Zero strain temperature	298 Kelvin
Include fluid pressure effects from SOLIDWORKS Flow Simulation	Off
Solver type	FFEPlus
Inplane Effect:	Off
Soft Spring:	Off
Inertial Relief:	Off
Incompatible bonding options	Automatic
Large displacement	On
Compute free body forces	On
Friction	Off
Use Adaptive Method:	Off
Result folder	SOLIDWORKS document (F:\2017-18 FSAE MQP\SolidWorks\F18_ASM_Fullcar_v031218)

Units

Unit system:	SI (MKS)
Length/Displacement	mm
Temperature	Kelvin
Angular velocity	Rad/sec
Pressure/Stress	N/m ²

Material Properties

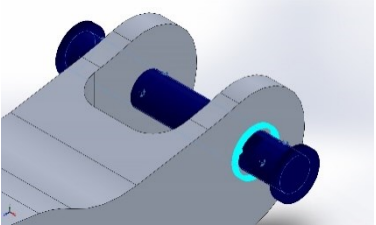
Model Reference	Properties	Components
	<p>Name: 7075-T6 (SN) Model type: Linear Elastic Isotropic Default failure criterion: Unknown Yield strength: 5.05e+008 N/m² Tensile strength: 5.7e+008 N/m² Elastic modulus: 7.2e+010 N/m² Poisson's ratio: 0.33 Mass density: 2810 kg/m³ Shear modulus: 2.69e+010 N/m² Thermal expansion coefficient: 2.4e-005 /Kelvin</p>	<p>SolidBody 1(3/8 (0.375) Diameter Hole2)(F18_SU_LeftRocker_v10 1217), SolidBody 30(Boss-Extrude4)(F18_SU_LeftRocker_v 101217), SolidBody 31(Boss-Extrude5)(F18_SU_LeftRocker_v 101217)</p>
Curve Data:N/A		

Loads and Fixtures

Fixture name	Fixture Image	Fixture Details
Fixed Hinge-1		<p>Entities: 1 face(s) Type: Fixed Hinge</p>

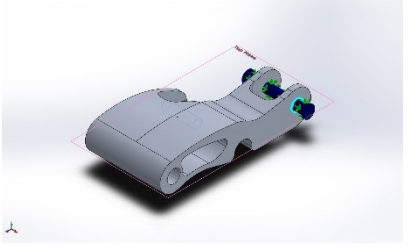
Resultant Forces

Components	X	Y	Z	Resultant
Reaction force(N)	410.872	1947.68	-1993.41	2817.08
Reaction Moment(N.m)	0	0	0	0

Fixture name	Fixture Image	Fixture Details
Fixed-1		<p>Entities: 1 face(s) Type: Fixed Geometry</p>

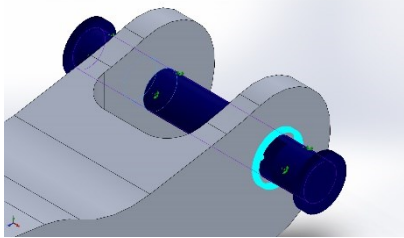
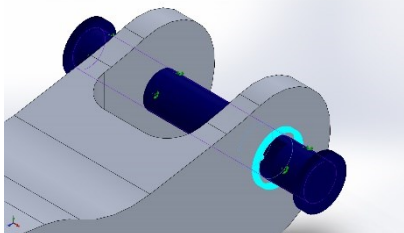
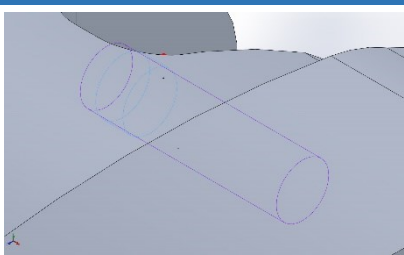
Resultant Forces

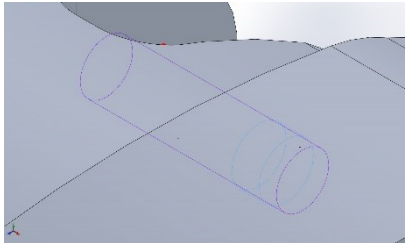
Components	X	Y	Z	Resultant
Reaction force(N)	-410.862	2500.27	1993.48	3223.99
Reaction Moment(N.m)	0	0	0	0

Load name	Load Image	Load Details
Force-1		<p>Entities: 1 face(s), 1 plane(s) Reference: Top Plane Type: Apply force Values: ---, ---, -1000 lbf</p>

Connector Definitions

Pin/Bolt/Bearing Connector

Model Reference	Connector Details	Strength Details		
 <p>Pin Connector-1</p>	<p>Entities: 2 face(s) Type: Pin Connection type: With retaining ring (No translation) Rotational stiffness value: 0 Units: SI</p>	No Data		
Connector Forces				
Type	X-Component	Y-Component	Z-Component	Resultant
Axial Force (N)	96.637	0.0021294	0.000199	-96.637
Shear Force (N)	0.049474	-2214.7	-327.06	2238.7
Torque (N.m)	3.2012e-021	7.0538e-026	6.5921e-027	-3.2012e-021
Bending moment (N.m)	-2.2124e-005	0.62355	4.0712	4.1187
 <p>Pin Connector-2</p>	<p>Entities: 2 face(s) Type: Pin Connection type: With retaining ring (No translation) Rotational stiffness value: 0 Units: SI</p>	No Data		
Connector Forces				
Type	X-Component	Y-Component	Z-Component	Resultant
Axial Force (N)	314.21	9.158e-005	-0.0057619	314.21
Shear Force (N)	-0.030475	-285.59	-1666.4	1690.7
Torque (N.m)	3.6504e-021	1.0639e-027	-6.694e-026	3.6504e-021
Bending moment (N.m)	5.1254e-005	2.0649	2.8278	3.5014
 <p>Pin Connector-5</p>	<p>Entities: 2 face(s) Type: Pin Connection type: With key (No rotation) Connection type: With retaining ring (No translation)</p>	No Data		
Connector Forces				
Type	X-Component	Y-Component	Z-Component	Resultant
Axial Force (N)	-68.511	-0.46772	0.022461	68.513
Shear Force (N)	-12.528	1849.1	292.07	1872.1
Torque (N.m)	-4.9111	-0.033527	0.0016101	4.9112
Bending moment (N.m)	0.0054353	-0.871	-1.5583	1.7852

	<p>Entities: 2 face(s) Type: Pin Connection type: With key (No rotation) Connection type: With retaining ring (No translation)</p>	<p>No Data</p>
<p>Pin Connector-6</p>		

Connector Forces

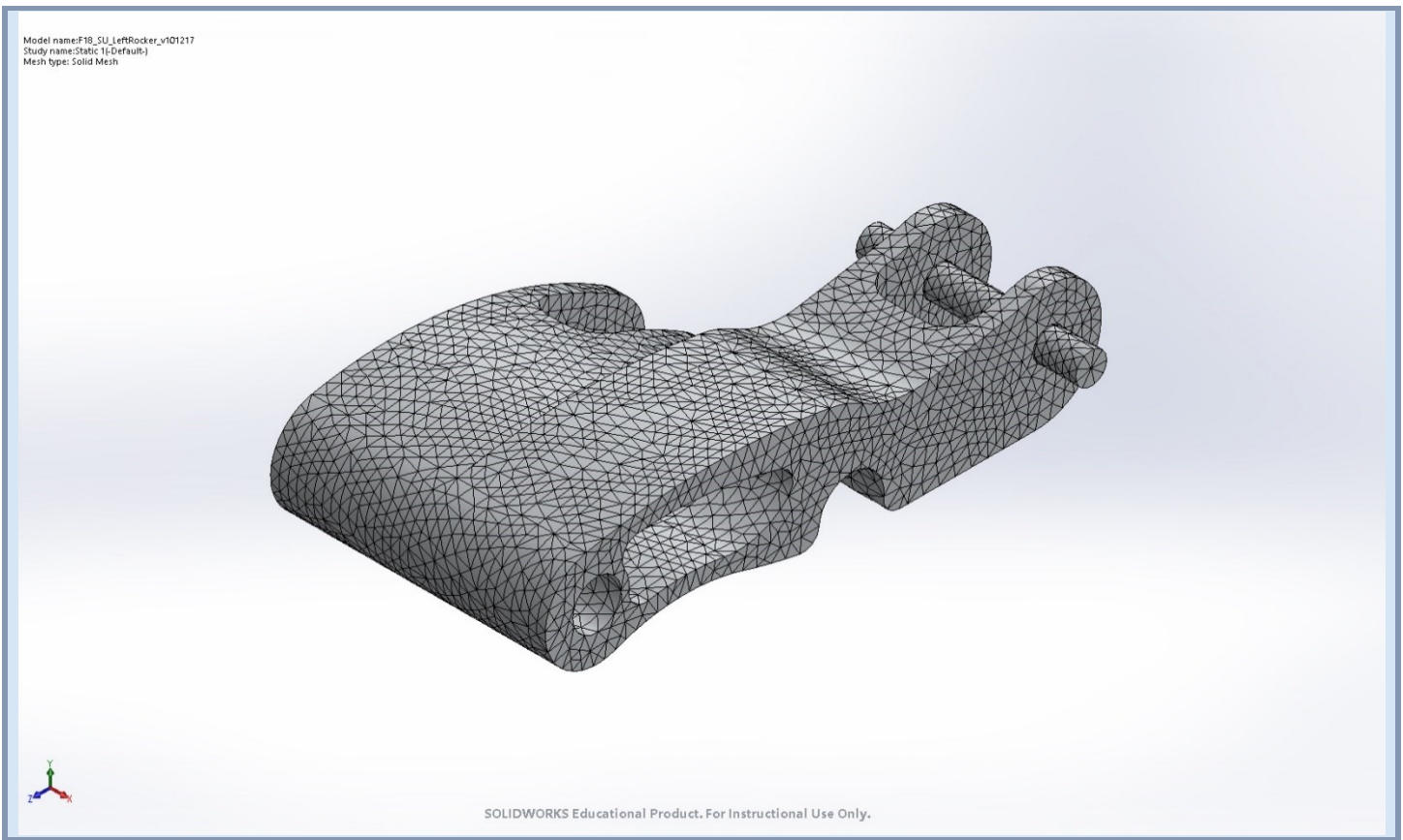
Type	X-Component	Y-Component	Z-Component	Resultant
Axial Force (N)	98.934	0.6776	-0.032228	98.936
Shear Force (N)	-17.895	2598.9	-292.06	2615.3
Torque (N.m)	4.9108	0.033634	-0.0015997	4.9109
Bending moment (N.m)	0.02426	-3.7544	-4.4629	5.8321

Mesh information

Mesh type	Solid Mesh
Mesher Used:	Curvature-based mesh
Jacobian points	4 Points
Maximum element size	0.0999924 in
Minimum element size	0.0333305 in
Mesh Quality Plot	High

Mesh information - Details

Total Nodes	61107
Total Elements	38302
Maximum Aspect Ratio	92.116
% of elements with Aspect Ratio < 3	99.4
% of elements with Aspect Ratio > 10	0.0339
% of distorted elements(Jacobian)	0
Time to complete mesh(hh:mm:ss):	00:00:02
Computer name:	



Resultant Forces

Reaction forces

Selection set	Units	Sum X	Sum Y	Sum Z	Resultant
Entire Model	N	0.00905108	4447.95	0.0714974	4447.95

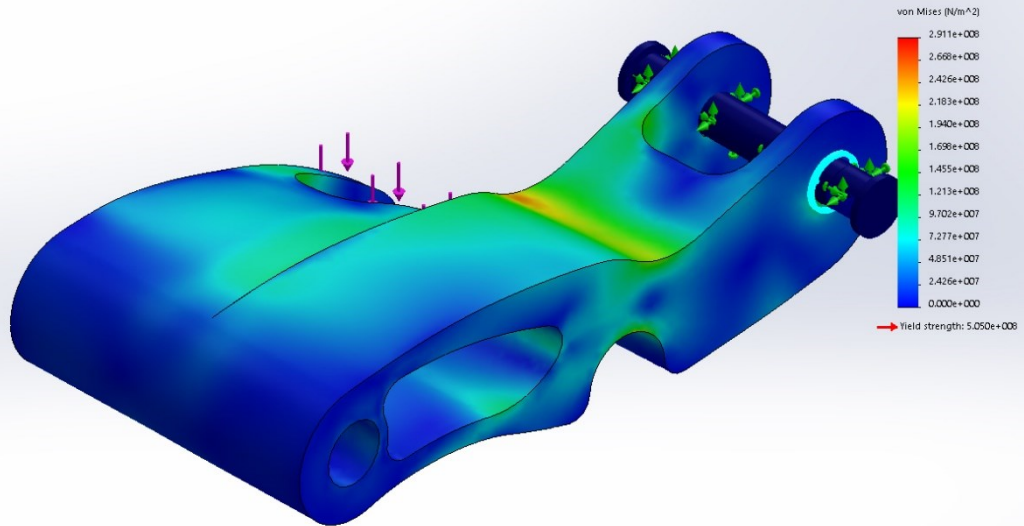
Reaction Moments

Selection set	Units	Sum X	Sum Y	Sum Z	Resultant
Entire Model	N.m	0	0	0	0

Study Results

Name	Type	Min	Max
Stress1	VON: von Mises Stress	0.000e+000N/m ² Node: 57212	2.911e+008N/m ² Node: 9357

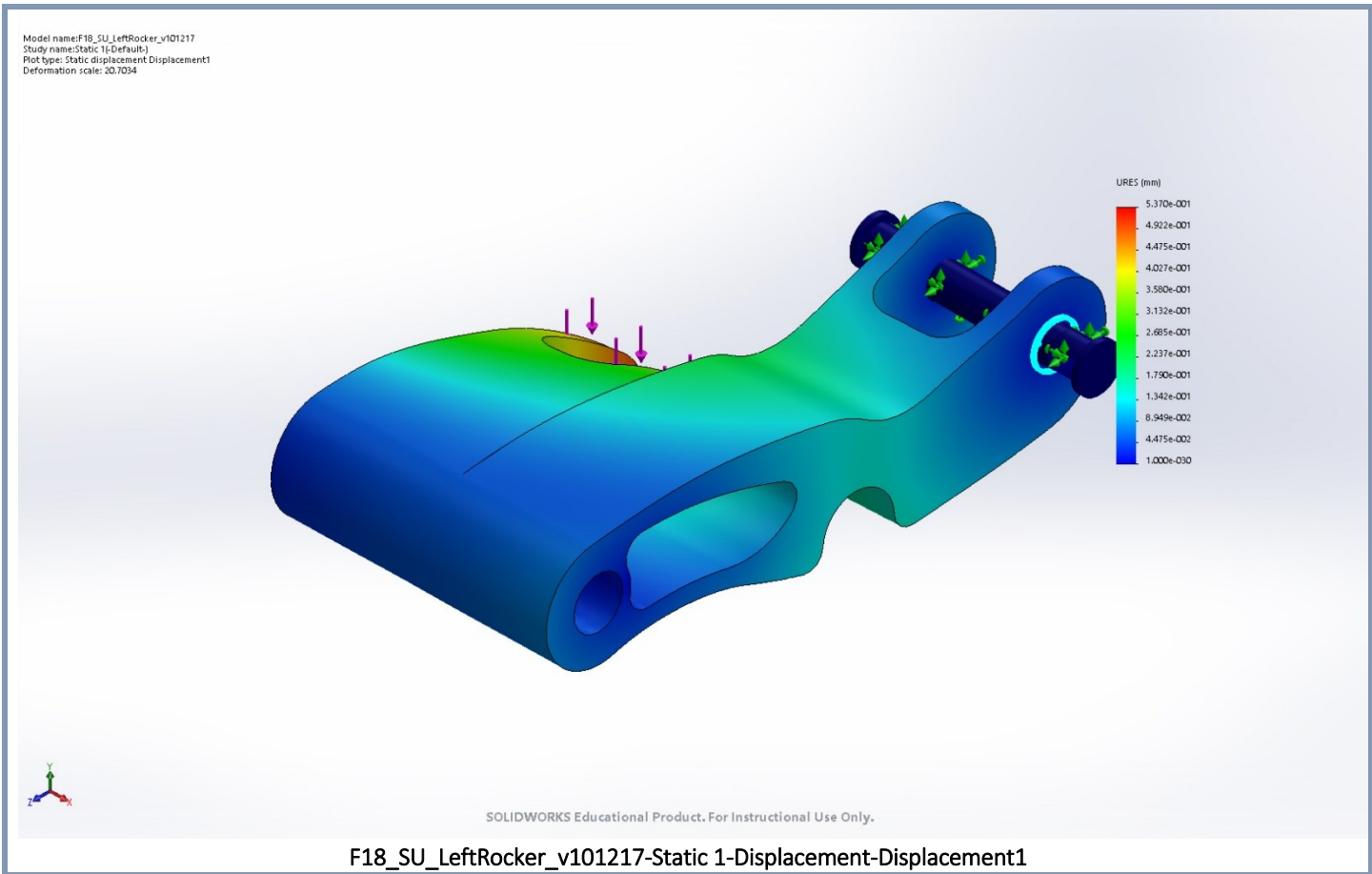
Model name:F18_SU_LeftRocker_v101217
 Study name:Static 1-Default
 Plot type: Static nodal stress Stress1
 Deformation scale: 20.7034



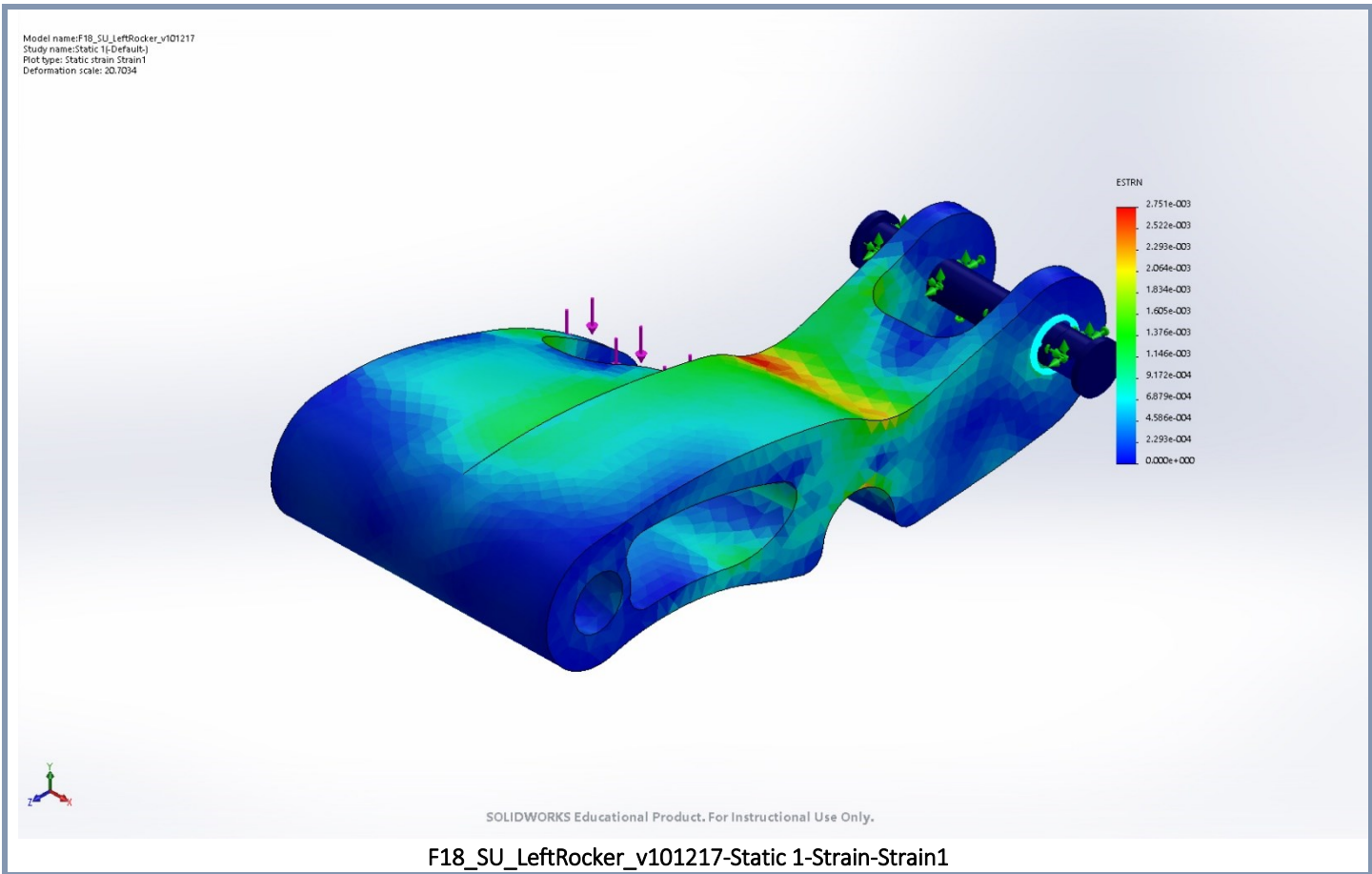
SOLIDWORKS Educational Product. For Instructional Use Only.

F18_SU_LeftRocker_v101217-Static 1-Stress-Stress1

Name	Type	Min	Max
Displacement1	URES: Resultant Displacement	0.000e+000mm Node: 57212	5.370e-001mm Node: 467

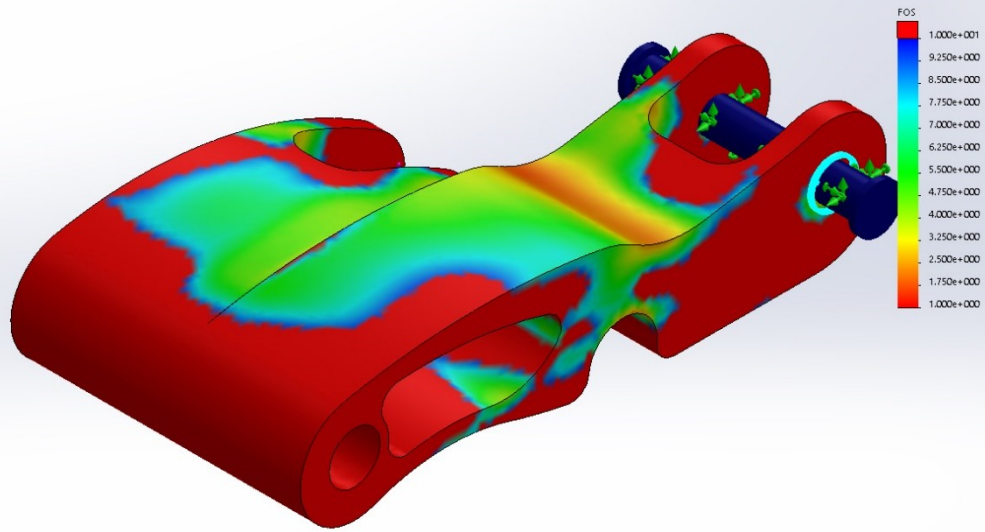


Name	Type	Min	Max
Strain1	ESTRN: Equivalent Strain	0.000e+000 Element: 36027	2.751e-003 Element: 21848



Name	Type	Min	Max
Factor of Safety1	Automatic	1.735e+000 Node: 9357	1.000e+016 Node: 57212

Model name: F18_SU_LeftRocker_v101217
Study name: Static 1 (Default)
Plot type: Factor of Safety Factor of Safety1
Criterion: Automatic
Factor of safety distribution: Min FOS = 1.7

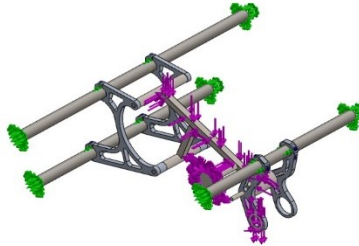


SOLIDWORKS Educational Product. For Instructional Use Only.

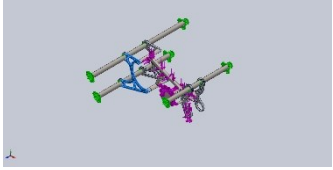
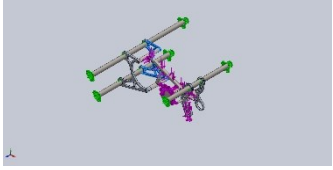
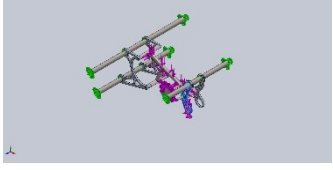
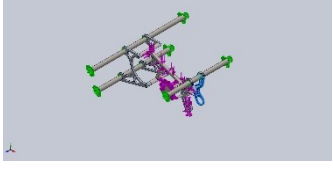
F18_SU_LeftRocker_v101217-Static 1-Factor of Safety-Factor of Safety1

Appendix G. Engine Mount FEA Simulation Report

Model Information



Model name: F18_DT_ASM_EngineMountFEA
Current Configuration: Default

Solid Bodies			
Document Name and Reference	Treated As	Volumetric Properties	Document Path/Date Modified
Cut-Extrude1 	Solid Body	Mass:0.210023 kg Volume:7.77863e-005 m ³ Density:2700 kg/m ³ Weight:2.05822 N	C:\Users\alex0\Desktop\F18_DT_EngineMountFEA_PackGo_v111317(3)\F18_DT_EngineMountFEA_PackGo_v111317\F18_DT_EngineMount_Front_v110717.SLDPRT Nov 16 21:40:45 2017
Cut-Extrude1 	Solid Body	Mass:0.210023 kg Volume:7.77863e-005 m ³ Density:2700 kg/m ³ Weight:2.05822 N	C:\Users\alex0\Desktop\F18_DT_EngineMountFEA_PackGo_v111317(3)\F18_DT_EngineMountFEA_PackGo_v111317\F18_DT_EngineMount_Front_v110717.SLDPRT Nov 16 21:40:45 2017
Cut-Extrude3 	Solid Body	Mass:0.152856 kg Volume:5.66134e-005 m ³ Density:2700 kg/m ³ Weight:1.49799 N	C:\Users\alex0\Desktop\F18_DT_EngineMountFEA_PackGo_v111317(3)\F18_DT_EngineMountFEA_PackGo_v111317\F18_DT_EngineMount_RearLeftV2.SLDPRT Dec 03 18:01:24 2017
Chamfer1 	Solid Body	Mass:0.127799 kg Volume:4.73329e-005 m ³ Density:2700 kg/m ³ Weight:1.25243 N	C:\Users\alex0\Desktop\F18_DT_EngineMountFEA_PackGo_v111317(3)\F18_DT_EngineMountFEA_PackGo_v111317\F18_DT_EngineMount_RearRightV2.SLDPRT Apr 23 11:05:51 2018

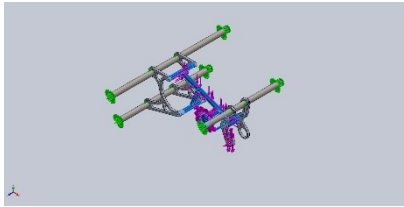
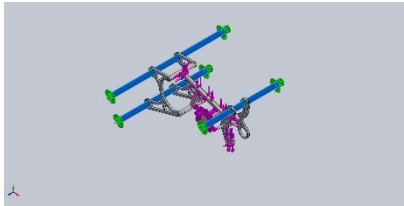
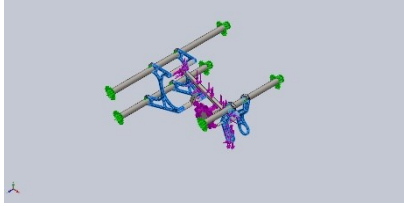
Study Properties

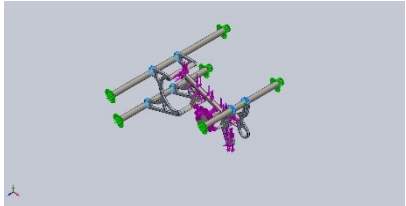
Study name	Static 1
Analysis type	Static
Mesh type	Mixed Mesh
Thermal Effect:	On
Thermal option	Include temperature loads
Zero strain temperature	298 Kelvin
Include fluid pressure effects from SOLIDWORKS Flow Simulation	Off
Solver type	Direct sparse solver
Inplane Effect:	Off
Soft Spring:	Off
Inertial Relief:	Off
Incompatible bonding options	Automatic
Large displacement	Off
Compute free body forces	Off
Friction	Off
Use Adaptive Method:	Off
Result folder	SOLIDWORKS document (C:\Users\alex0\Desktop\F18_DT_EngineMountFEA_PackGo_v111317 (3)\F18_DT_EngineMountFEA_PackGo_v111317)

Units

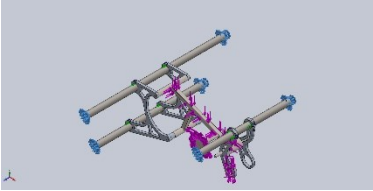
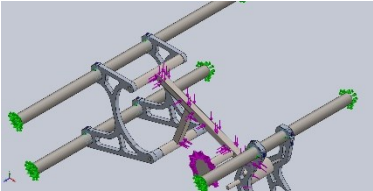
Unit system:	SI (MKS)
Length/Displacement	mm
Temperature	Kelvin
Angular velocity	Rad/sec
Pressure/Stress	N/m ²

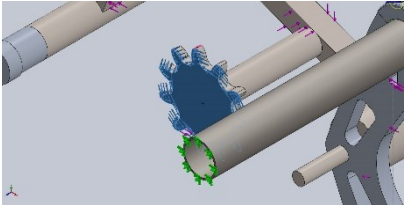
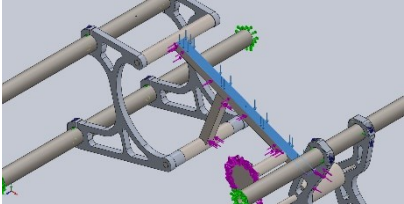
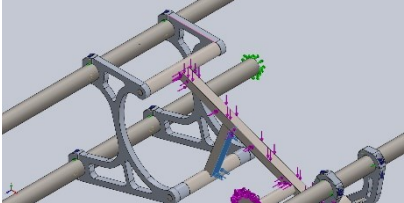
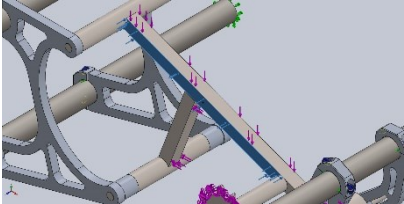
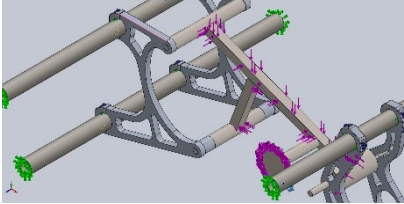
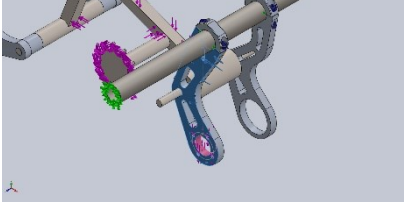
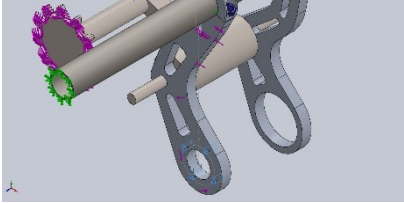
Material Properties

Model Reference	Properties	Components
	Name: Alloy Steel Model type: Linear Elastic Isotropic Default failure criterion: Max von Mises Stress Yield strength: 6.20422e+008 N/m ² Tensile strength: 7.23826e+008 N/m ² Elastic modulus: 2.1e+011 N/m ² Poisson's ratio: 0.28 Mass density: 7700 kg/m ³ Shear modulus: 7.9e+010 N/m ² Thermal expansion coefficient: 1.3e-005 /Kelvin	SolidBody 1(Cut-Extrude2)(F18_DT_2015WR450FMount_v082917-1), SolidBody 1(Boss-Extrude1)(F18_DT_EngineMount_PivotBolts-1), SolidBody 1(Boss-Extrude1)(F18_DT_EngineMount_PivotBolts-2), SolidBody 1(Boss-Extrude1)(F18_DT_EngineMount_PivotBolts-3)
Curve Data:N/A		
	Name: AISI 4130 Steel, normalized at 870C Model type: Linear Elastic Isotropic Default failure criterion: Unknown Yield strength: 4.6e+008 N/m ² Tensile strength: 7.31e+008 N/m ² Elastic modulus: 2.05e+011 N/m ² Poisson's ratio: 0.285 Mass density: 7850 kg/m ³ Shear modulus: 8e+010 N/m ²	SolidBody 1(Boss-Extrude1)(F18_DT_EngineMountFEA_BackTube-1), SolidBody 1(Boss-Extrude1)(F18_DT_EngineMountFEA_BotTube-1), SolidBody 1(Boss-Extrude1)(F18_DT_EngineMountFEA_TopTube-1)
Curve Data:N/A		
	Name: 6061-T6 (SS) Model type: Linear Elastic Isotropic Default failure criterion: Max von Mises Stress Yield strength: 2.75e+008 N/m ² Tensile strength: 3.1e+008 N/m ² Elastic modulus: 6.9e+010 N/m ² Poisson's ratio: 0.33 Mass density: 2700 kg/m ³ Shear modulus: 2.6e+010 N/m ² Thermal expansion coefficient: 2.4e-005 /Kelvin	SolidBody 1(Boss-Extrude1)(F18_DT_EngineMount_FrontSpacer-1), SolidBody 1(Boss-Extrude1)(F18_DT_EngineMount_FrontSpacer-2), SolidBody 1(Cut-Extrude1)(F18_DT_EngineMount_Front_v110717-1), SolidBody 1(Cut-Extrude1)(F18_DT_EngineMount_Front_v110717-2), SolidBody 1(Boss-Extrude1)(F18_DT_EngineMount_RearBushing-1), SolidBody 1(Cut-Extrude3)(F18_DT_EngineMount_RearLeftV2-1), SolidBody 1(Chamfer1)(F18_DT_EngineMount_RearRightV2-1)
Curve Data:N/A		

	<p>Name: 2024-T361 Model type: Linear Elastic Isotropic Default failure criterion: Max von Mises Stress Yield strength: 3.95e+008 N/m² Tensile strength: 4.95e+008 N/m² Elastic modulus: 7.24e+010 N/m² Poisson's ratio: 0.33 Mass density: 2780 kg/m³ Shear modulus: 2.8e+010 N/m² Thermal expansion coefficient: 2.32e-005 /Kelvin</p>	<p>SolidBody 1(Fillet1)(F18_DT_EngineMo unt_ShaftCollar-1), SolidBody 1(Fillet1)(F18_DT_EngineMo unt_ShaftCollar-2), SolidBody 1(Fillet1)(F18_DT_EngineMo unt_ShaftCollar-3), SolidBody 1(Fillet1)(F18_DT_EngineMo unt_ShaftCollar-4), SolidBody 1(Fillet1)(F18_DT_EngineMo unt_ShaftCollar-5), SolidBody 1(Fillet1)(F18_DT_EngineMo unt_ShaftCollar-6)</p>
<p>Curve Data:N/A</p>		

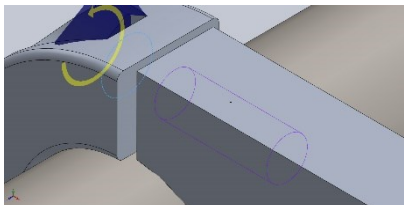
Loads and Fixtures

Fixture name	Fixture Image	Fixture Details		
Fixed-1		<p>Entities: Type:</p>	<p>6 face(s) Fixed Geometry</p>	
Resultant Forces				
Components	X	Y	Z	Resultant
Reaction force(N)	0	0	0	1e-033
Reaction Moment(N.m)	0	0	0	1e-033
Fixed Hinge-2		<p>Entities: Type:</p>	<p>6 face(s) Fixed Hinge</p>	
Resultant Forces				
Components	X	Y	Z	Resultant
Reaction force(N)	45346.5	-29624.7	387.733	54167.1
Reaction Moment(N.m)	0	0	0	1e-033

Load name	Load Image	Load Details
Torque-1		Entities: 1 face(s) Reference: Face< 1 > Type: Apply torque Value: -1400 lbf.in
Force-1		Entities: 1 face(s) Reference: Edge< 1 > Type: Apply force Values: ---, ---, 90 lbf Moments: ---, ---, --- lbf.in
Force-2		Entities: 1 face(s) Reference: Edge< 1 > Type: Apply force Values: ---, ---, 135 lbf Moments: ---, ---, --- lbf.in
Force-3		Entities: 1 face(s) Type: Apply normal force Value: 90 lbf
Force-4		Entities: 3 face(s) Reference: Edge< 1 > Type: Apply force Values: ---, ---, -1400 lbf Moments: ---, ---, --- lbf.in
Torque-2		Entities: 1 face(s) Reference: Face< 1 > Type: Apply torque Value: 240 lbf.in
Force-5		Entities: 4 face(s) Reference: Edge< 1 > Type: Apply force Values: ---, ---, 2 lbf Moments: ---, ---, --- lbf.in

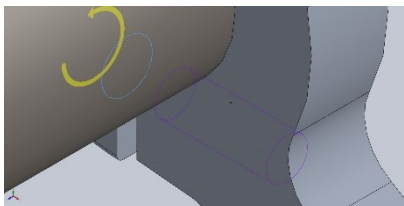
Connector Definitions

Pin/Bolt/Bearing Connector

Model Reference	Connector Details	Strength Details
 <p>Counterbore Screw-1</p>	<p>Entities: 1 edge(s), 1 face(s)</p> <p>Type: Bolt(Head/Nut diameter)(Count erbore screw)</p> <p>Head diameter: 0.375 in</p> <p>Nominal shank diameter: 0.25</p> <p>Preload (Torque): 12</p> <p>Young's modulus: 2.1e+011</p> <p>Poisson's ratio: 0.28</p> <p>Preload units: lbf.in</p>	No Data

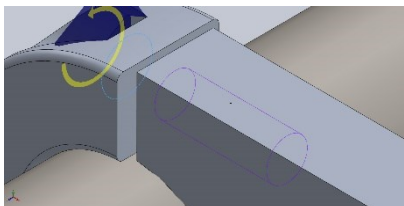
Connector Forces

Type	X-Component	Y-Component	Z-Component	Resultant
Axial Force (N)	-3852.7	8.8616	0	3852.7
Shear Force (N)	-0.043682	-18.991	-2.3932	19.142
Bending moment (N.m)	2.6271e-005	0.011421	0.34464	0.34483

 <p>Copy[1] Counterbore Screw-1</p>	<p>Entities: 1 edge(s), 1 face(s)</p> <p>Type: Bolt(Head/Nut diameter)(Count erbore screw)</p> <p>Head diameter: 0.375 in</p> <p>Nominal shank diameter: 0.25</p> <p>Preload (Torque): 12</p> <p>Young's modulus: 2.1e+011</p> <p>Poisson's ratio: 0.28</p> <p>Preload units: lbf.in</p>	No Data
---	--	---------

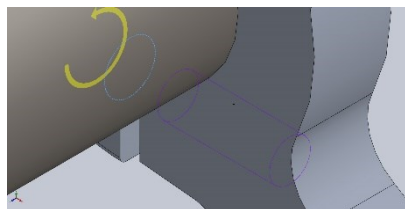
Connector Forces

Type	X-Component	Y-Component	Z-Component	Resultant
Axial Force (N)	3888.8	-8.9456	-0	-3888.8
Shear Force (N)	-0.033684	-14.643	-1.7717	14.75
Bending moment (N.m)	-0.00013886	-0.060363	0.94831	0.95023

 <p>Counterbore Screw-2</p>	<p>Entities: 1 edge(s), 1 face(s)</p> <p>Type: Bolt(Head/Nut diameter)(Count erbore screw)</p> <p>Head diameter: 0.375 in</p> <p>Nominal shank diameter: 0.25</p> <p>Preload (Torque): 12</p> <p>Young's modulus: 2.1e+011</p> <p>Poisson's ratio: 0.28</p> <p>Preload units: lbf.in</p>	No Data
---	--	---------

Connector Forces

Type	X-Component	Y-Component	Z-Component	Resultant
Axial Force (N)	-1651.9	3.7994	0	1651.9
Shear Force (N)	-0.016529	-7.1863	51.217	51.718
Bending moment (N.m)	-0.0027531	-1.197	-0.014835	1.1971



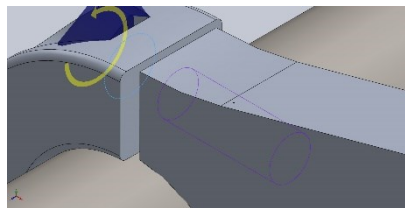
Counterbore Screw-3

Entities: 1 edge(s), 1 face(s)
Type: Bolt(Head/Nut diameter)(Count erbore screw)
Head diameter: 0.375 in
Nominal shank diameter: 0.25
Preload (Torque): 12
Young's modulus: 2.1e+011
Poisson's ratio: 0.28
Preload units: lbf.in

No Data

Connector Forces

Type	X-Component	Y-Component	Z-Component	Resultant
Axial Force (N)	-390.58	0.89851	0	390.58
Shear Force (N)	-0.054657	-23.759	71.74	75.572
Bending moment (N.m)	-0.0032338	-1.4057	0.17939	1.4171



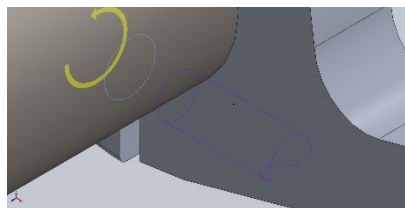
Counterbore Screw-4

Entities: 1 edge(s), 1 face(s)
Type: Bolt(Head/Nut diameter)(Count erbore screw)
Head diameter: 0.375 in
Nominal shank diameter: 0.25
Preload (Torque): 12
Young's modulus: 2.1e+011
Poisson's ratio: 0.28
Preload units: lbf.in

No Data

Connector Forces

Type	X-Component	Y-Component	Z-Component	Resultant
Axial Force (N)	-1775.7	4.0833	0	1775.7
Shear Force (N)	-0.012253	-5.3291	10.404	11.689
Bending moment (N.m)	-0.00084991	-0.36965	0.12106	0.38897



Counterbore Screw-5

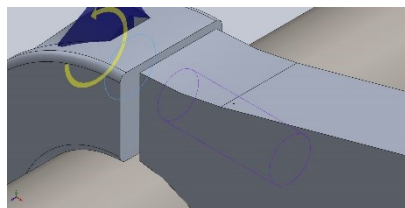
Entities: 1 edge(s), 1 face(s)
Type: Bolt(Head/Nut diameter)(Count erbore screw)
Head diameter: 0.375 in
Nominal shank diameter: 0.25
Preload (Torque): 12
Young's modulus: 2.1e+011
Poisson's ratio: 0.28
Preload units: lbf.in

No Data

Connector Forces

Type	X-Component	Y-Component	Z-Component	Resultant
Axial Force (N)	3242.8	-7.4553	-0	-3242.8
Shear Force (N)	0.084395	36.713	14.28	39.393

Bending moment (N.m)	-0.00071507	-0.31107	0.89529	0.9478
----------------------	-------------	----------	---------	--------



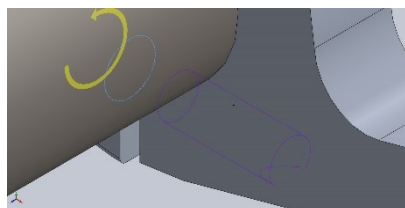
Counterbore Screw-6

Entities: 1 edge(s), 1 face(s)
Type: Bolt(Head/Nut diameter)(Count erbore screw)
Head diameter: 9.525 mm
Nominal shank diameter: 6.35
Preload (Torque): 12
Young's modulus: 2.1e+011
Poisson's ratio: 0.28
Preload units: lbf.in

No Data

Connector Forces

Type	X-Component	Y-Component	Z-Component	Resultant
Axial Force (N)	-1203.3	2.7667	0	1203.3
Shear Force (N)	-0.040537	-17.633	0.22819	17.635
Bending moment (N.m)	-0.00020014	-0.087057	-0.25433	0.26882



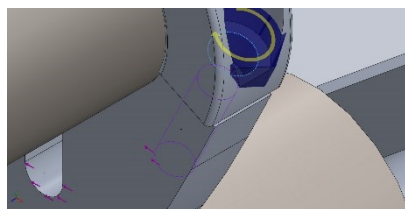
Counterbore Screw-7

Entities: 1 edge(s), 1 face(s)
Type: Bolt(Head/Nut diameter)(Count erbore screw)
Head diameter: 0.375 in
Nominal shank diameter: 0.25
Preload (Torque): 12
Young's modulus: 2.1e+011
Poisson's ratio: 0.28
Preload units: lbf.in

No Data

Connector Forces

Type	X-Component	Y-Component	Z-Component	Resultant
Axial Force (N)	-1736.5	3.993	0	1736.5
Shear Force (N)	-0.024302	-10.57	2.1878	10.794
Bending moment (N.m)	-0.00024268	-0.10556	-0.11741	0.15788



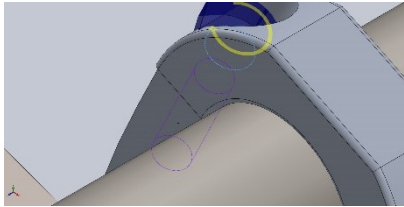
Counterbore Screw-12

Entities: 1 edge(s), 1 face(s)
Type: Bolt(Head/Nut diameter)(Count erbore screw)
Head diameter: 0.375 in
Nominal shank diameter: 0.25
Preload (Torque): 12
Young's modulus: 2.1e+011
Poisson's ratio: 0.28
Preload units: lbf.in

No Data

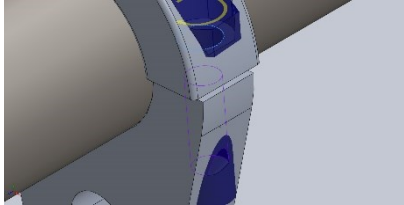
Connector Forces

Type	X-Component	Y-Component	Z-Component	Resultant
Axial Force (N)	0	0	0	0
Shear Force (N)	-327.69	159.14	-17.555	364.71
Bending moment (N.m)	0.13946	-0.067726	-6.8836	6.8853

 <p>Counterbore Screw-13</p>	Entities: 1 edge(s), 1 face(s) Type: Bolt(Head/Nut diameter)(Count erbore screw) Head diameter: 0.375 in Nominal shank diameter: 0.25 Preload (Torque): 12 Young's modulus: 2.1e+011 Poisson's ratio: 0.28 Preload units: lbf.in	No Data
--	---	---------

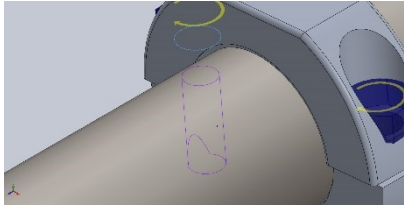
Connector Forces

Type	X-Component	Y-Component	Z-Component	Resultant
Axial Force (N)	5615.7	11563	0	12855
Shear Force (N)	71.358	-34.655	17.969	81.338
Bending moment (N.m)	-0.20135	0.097784	-1.994	2.0065

 <p>Counterbore Screw-14</p>	Entities: 1 edge(s), 1 face(s) Type: Bolt(Head/Nut diameter)(Count erbore screw) Head diameter: 0.375 in Nominal shank diameter: 0.25 Preload (Torque): 12 Young's modulus: 2.1e+011 Poisson's ratio: 0.28 Preload units: lbf.in	No Data
--	---	---------

Connector Forces

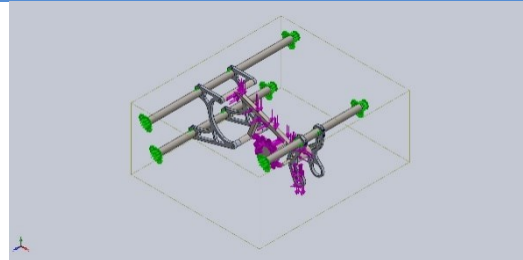
Type	X-Component	Y-Component	Z-Component	Resultant
Axial Force (N)	-0	0	0	0
Shear Force (N)	-286.85	-26.538	50.628	292.49
Bending moment (N.m)	-1.806	-0.16709	-6.8074	7.0449

 <p>Counterbore Screw-15</p>	Entities: 1 edge(s), 1 face(s) Type: Bolt(Head/Nut diameter)(Count erbore screw) Head diameter: 0.375 in Nominal shank diameter: 0.25 Preload (Torque): 12 Young's modulus: 2.1e+011 Poisson's ratio: 0.28 Preload units: lbf.in	No Data
--	---	---------

Connector Forces

Type	X-Component	Y-Component	Z-Component	Resultant
Axial Force (N)	-1070	11566	0	11615
Shear Force (N)	32.21	2.98	200.74	203.33
Bending moment (N.m)	-3.5338	-0.32693	-2.1173	4.1325

Contact Information

Contact	Contact Image	Contact Properties
Global Contact		Type: No penetration (Surface to surface) Components: 1 component(s)

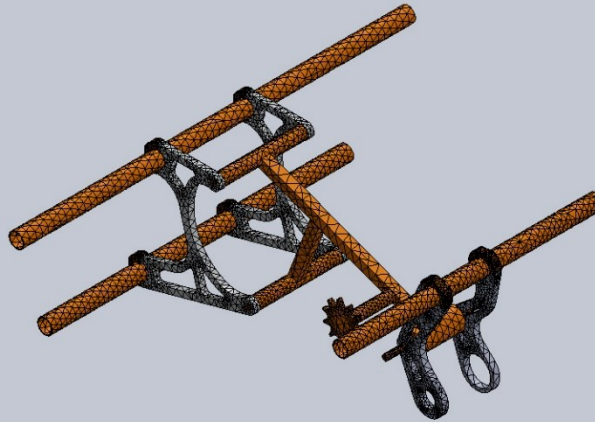
Mesh information

Mesh type	Mixed Mesh
Mesher Used:	Curvature-based mesh
Jacobian points	4 Points
Jacobian check for shell	On
Maximum element size	0.53486 in
Minimum element size	0.106972 in
Mesh Quality Plot	High
Remesh failed parts with incompatible mesh	Off

Mesh information - Details

Total Nodes	74077
Total Elements	37962
Time to complete mesh(hh:mm:ss):	00:00:05
Computer name:	

Model name:F18_DT_ASM_EngineMountFEA
Study name:Static 1(-Default-)
Mesh type: Mixed Mesh



SOLIDWORKS Educational Product. For Instructional Use Only.

Resultant Forces

Reaction forces

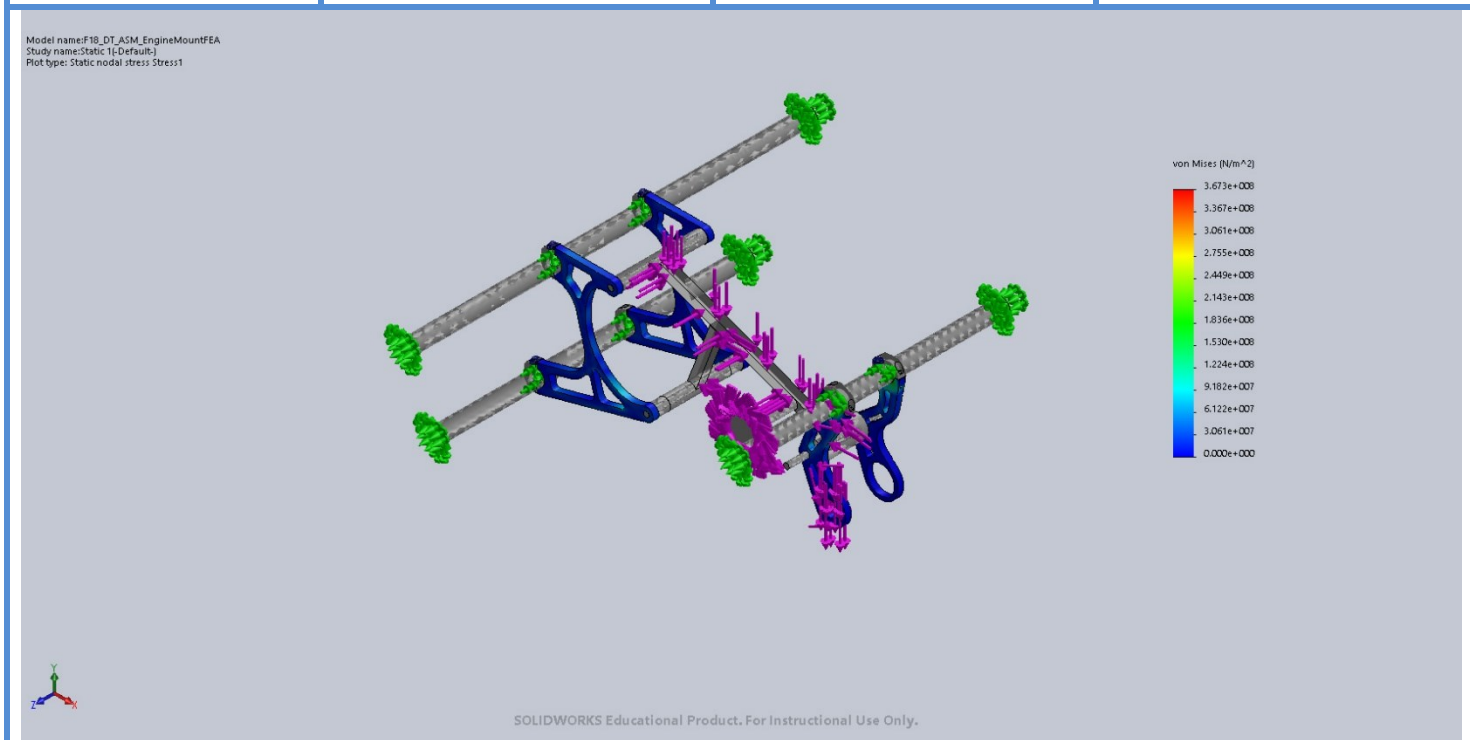
Selection set	Units	Sum X	Sum Y	Sum Z	Resultant
Entire Model	N	-5429.71	592.583	400.349	5476.6

Reaction Moments

Selection set	Units	Sum X	Sum Y	Sum Z	Resultant
Entire Model	N.m	0	0	0	1e-033

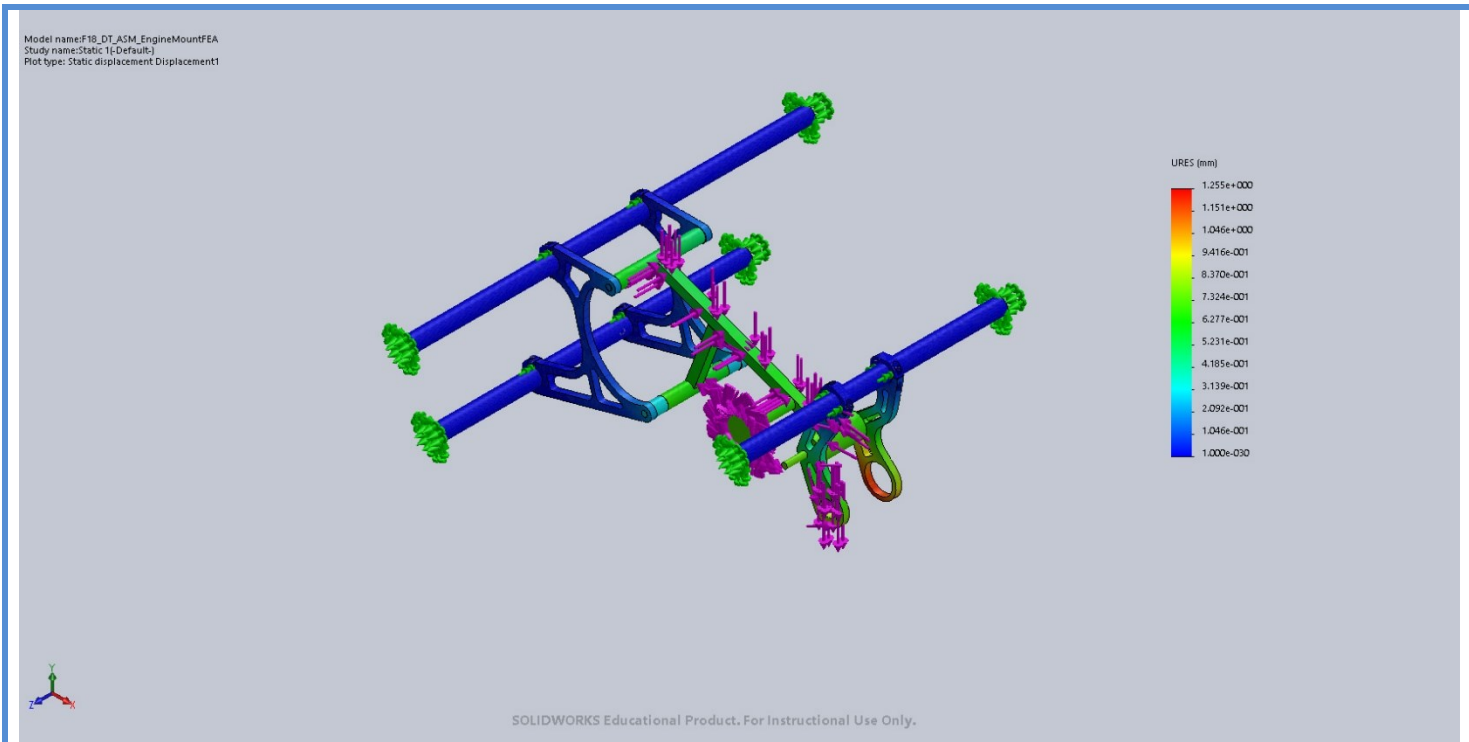
Study Results

Name	Type	Min	Max
Stress1	VON: von Mises Stress	0.000e+000N/m ² Node: 1	3.673e+008N/m ² Node: 56348



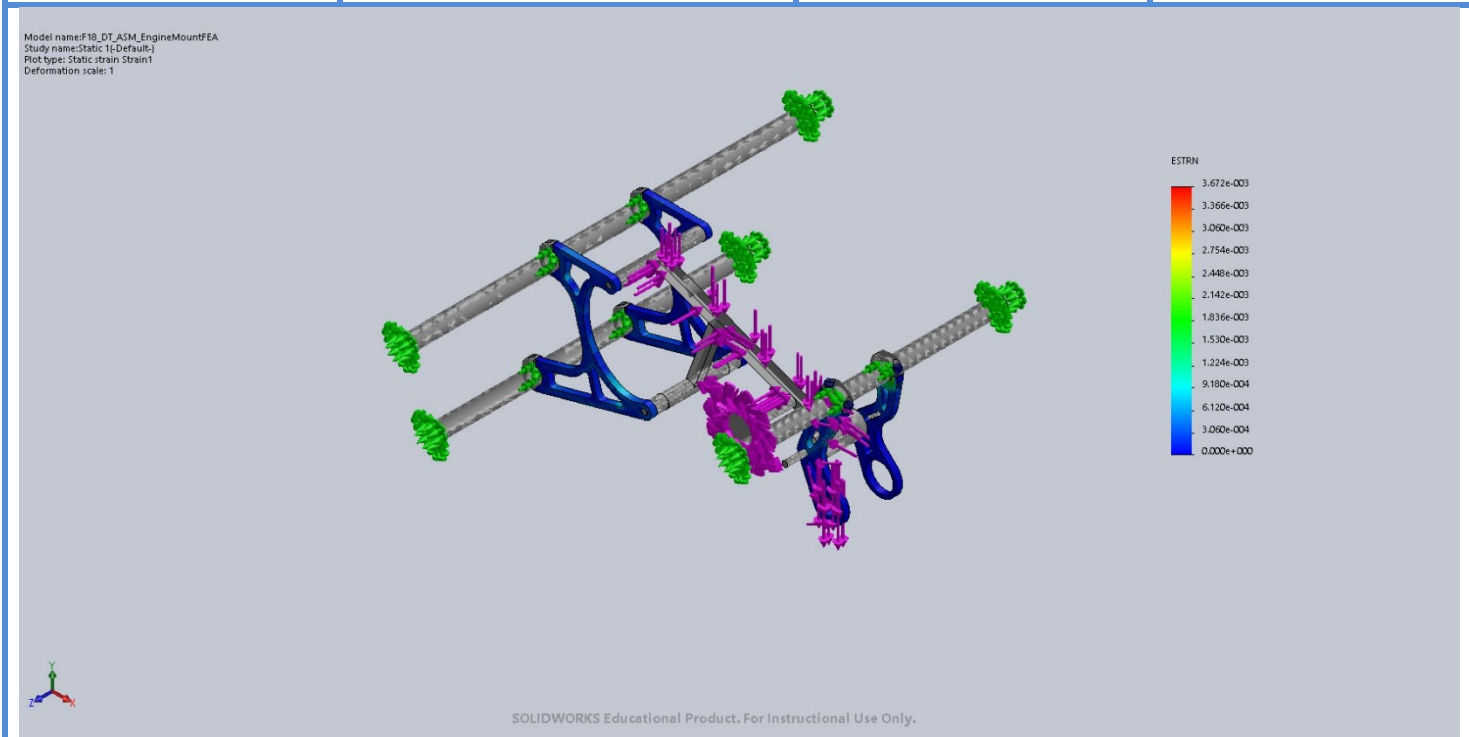
F18_DT_ASM_EngineMountFEA-Static 1-Stress-Stress1

Name	Type	Min	Max
Displacement1	URES: Resultant Displacement	0.000e+000mm Node: 7957	1.255e+000mm Node: 55541



F18_DT_ASM_EngineMountFEA-Static 1-Displacement-Displacement1

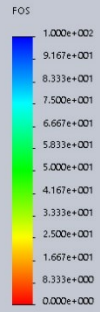
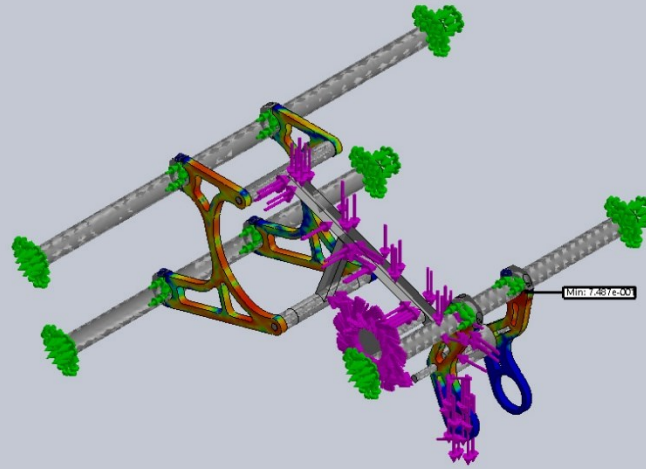
Name	Type	Min	Max
Strain1	ESTRN: Equivalent Strain	0.000e+000 Element: 1	3.672e-003 Element: 30197



F18_DT_ASM_EngineMountFEA-Static 1-Strain-Strain1

Name	Type	Min	Max
Factor of Safety1	Automatic	7.487e-001 Node: 56348	1.000e+002 Node: 1

Model name:F18_DT_ASM_EngineMountFEA
 Study name:Static 1(Default)
 Plot type: Factor of Safety Factor of Safety1
 Criterion : Automatic
 Factor of safety distribution: Min FOS = 0.75

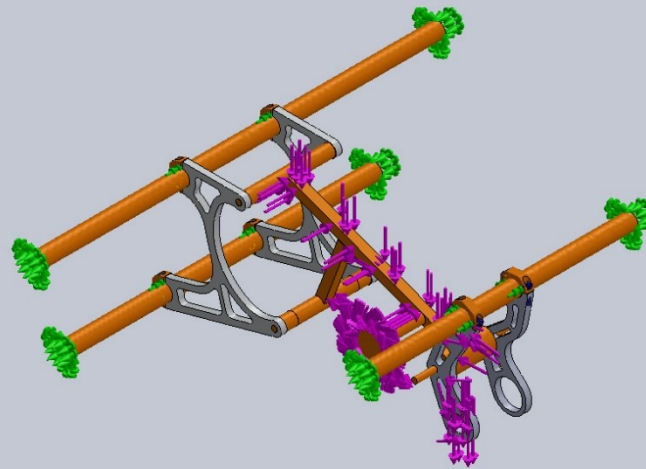


SOLIDWORKS Educational Product. For Instructional Use Only.

F18_DT_ASM_EngineMountFEA-Static 1-Factor of Safety-Factor of Safety1

Name	Type
Displacement1{1}	Deformed shape

Model name:F18_DT_ASM_EngineMountFEA
 Study name:Static 1(Default)
 Plot type: Deformed shape Displacement1{1}

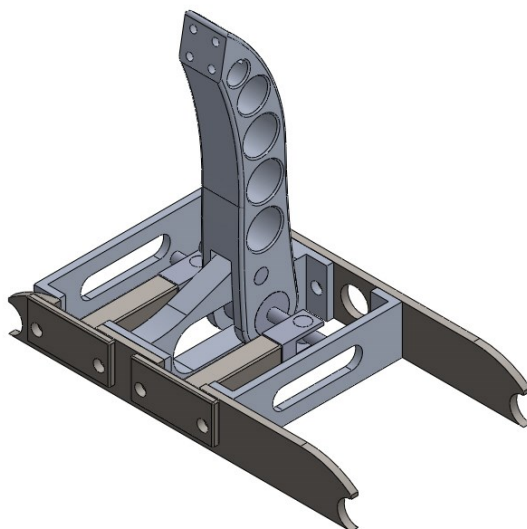


SOLIDWORKS Educational Product. For Instructional Use Only.

F18_DT_ASM_EngineMountFEA-Static 1-Displacement-Displacement1{1}

Appendix H. Pedal Assembly FEA Simulation Report

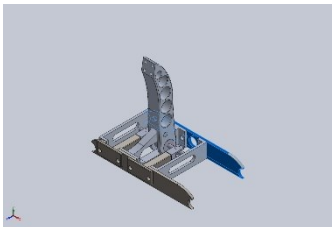
Model Information



Model name: bracket and MSs (for fea)

Current Configuration: Default

Solid Bodies

Document Name and Reference	Treated As	Volumetric Properties	Document Path/Date Modified
13/32 (0.40625) Diameter Hole1	Solid Body	Mass:0.291355 kg Volume:0.000107909 m ³ Density:2700 kg/m ³ Weight:2.85528 N	C:\Users\alex0\Desktop\MQPI\Finalized Designs\FEA\connection bracket v2.SLDPRT Oct 05 18:14:39 2017
Split Line2	Solid Body	Mass:0.56705 kg Volume:0.000210016 m ³ Density:2700.03 kg/m ³ Weight:5.55709 N	C:\Users\alex0\Desktop\MQPI\Finalized Designs\FEA\final pedal.SLDPRT Dec 06 20:22:34 2017
Mirror1 	Solid Body	Mass:0.565658 kg Volume:7.20583e-005 m ³ Density:7850 kg/m ³ Weight:5.54345 N	C:\Users\alex0\Desktop\MQPI\Finalized Designs\FEA\ms mounting bracket front V2.SLDPRT Oct 04 15:40:20 2017

<p>Mirror1</p> 	<p>Solid Body</p>	<p>Mass:0.490696 kg Volume:6.2509e-005 m³ Density:7850 kg/m³ Weight:4.80882 N</p>	<p>C:\Users\alex0\Desktop\M QP\Finalized Designs\FEA\ms mounting bracket rear V2.SLDPRT Oct 04 15:39:32 2017</p>
<p>Cut-Extrude1</p> 	<p>Solid Body</p>	<p>Mass:0.115233 kg Volume:4.2679e-005 m³ Density:2700 kg/m³ Weight:1.12929 N</p>	<p>C:\Users\alex0\Desktop\M QP\Finalized Designs\FEA\outboard connector.SLDPRT Oct 05 18:18:41 2017</p>
<p>Cut-Extrude1</p> 	<p>Solid Body</p>	<p>Mass:0.115233 kg Volume:4.2679e-005 m³ Density:2700 kg/m³ Weight:1.12929 N</p>	<p>C:\Users\alex0\Desktop\M QP\Finalized Designs\FEA\outboard connector.SLDPRT Oct 05 18:18:41 2017</p>

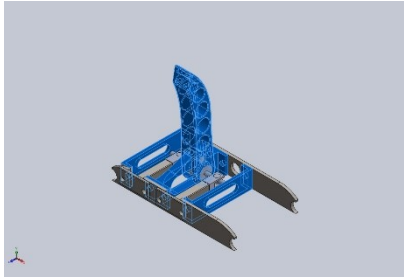
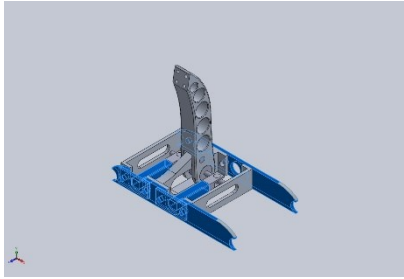
Study Properties

Study name	Static 2
Analysis type	Static
Mesh type	Mixed Mesh
Thermal Effect:	On
Thermal option	Include temperature loads
Zero strain temperature	298 Kelvin
Include fluid pressure effects from SOLIDWORKS Flow Simulation	Off
Solver type	Automatic
Inplane Effect:	Off
Soft Spring:	Off
Inertial Relief:	On
Incompatible bonding options	Automatic
Large displacement	Off
Compute free body forces	On
Friction	Off
Use Adaptive Method:	Off
Result folder	SOLIDWORKS document (C:\Users\alex0\Desktop\MQP\Finalized Designs\FEA)

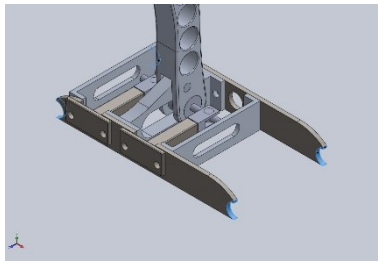
Units

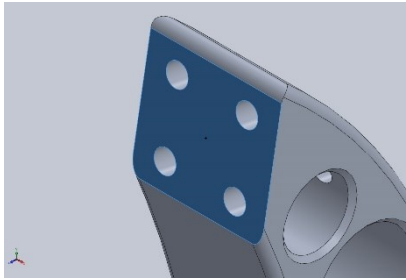
Unit system:	SI (MKS)
Length/Displacement	mm
Temperature	Kelvin
Angular velocity	Rad/sec
Pressure/Stress	N/m ²

Material Properties

Model Reference	Properties	Components
	Name: 6061-T6 (SS) Model type: Linear Elastic Isotropic Default failure criterion: Unknown Yield strength: 2.75e+008 N/m ² Tensile strength: 3.1e+008 N/m ² Elastic modulus: 6.9e+010 N/m ² Poisson's ratio: 0.33 Mass density: 2700 kg/m ³ Shear modulus: 2.6e+010 N/m ² Thermal expansion coefficient: 2.4e-005 /Kelvin	SolidBody 1(13/32 (0.40625) Diameter Hole1)(connection bracket v2-1), SolidBody 1(Split Line2)(final pedal assembly-1/final pedal-1), SolidBody 1(Cut-Extrude1)(outboard connector-1), SolidBody 1(Cut-Extrude1)(outboard connector-2)
Curve Data:N/A		
	Name: AISI 4130 Steel, normalized at 870C Model type: Linear Elastic Isotropic Default failure criterion: Unknown Yield strength: 4.6e+008 N/m ² Tensile strength: 7.31e+008 N/m ² Elastic modulus: 2.05e+011 N/m ² Poisson's ratio: 0.285 Mass density: 7850 kg/m ³ Shear modulus: 8e+010 N/m ²	SolidBody 1(Cut-Extrude1)(fea rigid supposrt-1), SolidBody 1(Cut-Extrude1)(fea rigid supposrt-2), SolidBody 1(Mirror1)(ms mounting bracket front V2-4), SolidBody 1(Mirror1)(ms mounting bracket rear V2-1)
Curve Data:N/A		

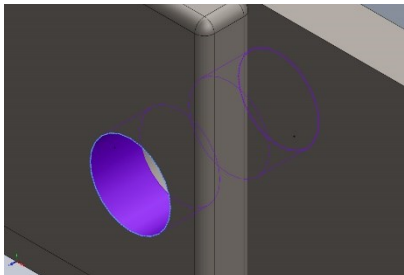
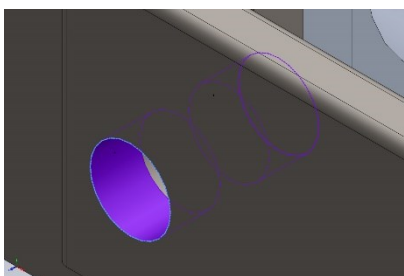
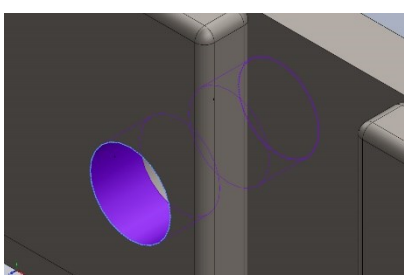
Loads and Fixtures

Fixture name	Fixture Image	Fixture Details		
Fixed-1		Entities: 8 face(s) Type: Fixed Geometry		
Resultant Forces				
Components	X	Y	Z	Resultant
Reaction force(N)	-11.892	1750.3	-1028.28	2030.04
Reaction Moment(N.m)	0	0	0	1e-033

Load name	Load Image	Load Details
Force-1		Entities: 1 face(s) Type: Apply normal force Value: 2000 N

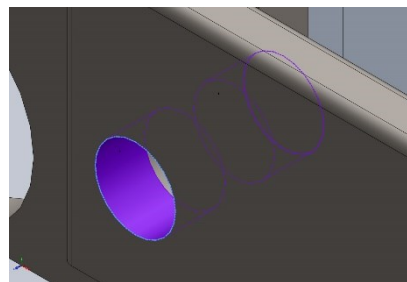
Connector Definitions

Pin/Bolt/Bearing Connector

Model Reference	Connector Details		Strength Details	
 <p>Counterbore with Nut-1</p>	Entities: Type: Head diameter: Nut diameter: Nominal shank diameter: Preload (Torque): Young's modulus: Poisson's ratio: Preload units:	2 edge(s), 2 face(s) Bolt(Head/Nut diameter)(Count erbore) 0.5625 in 0.5625 in 0.375 300 2.1e+011 0.28 lbf.in	No Data	
Connector Forces				
Type	X-Component	Y-Component	Z-Component	Resultant
Axial Force (N)	0	1.7237e-012	18929	18929
Shear Force (N)	19.05	-63.474	0	66.272
Bending moment (N.m)	-0.64807	-0.79816	7.2682e-017	1.0281
 <p>Counterbore with Nut-2</p>	Entities: Type: Head diameter: Nut diameter: Nominal shank diameter: Preload (Torque): Young's modulus: Poisson's ratio: Preload units:	2 edge(s), 2 face(s) Bolt(Head/Nut diameter)(Count erbore) 15.4781 mm 15.4781 mm 10.3188 300 2.1e+011 0.28 lbf.in	No Data	
Connector Forces				
Type	X-Component	Y-Component	Z-Component	Resultant
Axial Force (N)	0	2.4811e-012	17599	17599
Shear Force (N)	-581.52	-815.31	0	1001.4
Bending moment (N.m)	-7.5393	6.9165	-9.7508e-016	10.231
 <p>Counterbore with Nut-3</p>	Entities: Type: Head diameter: Nut diameter: Nominal shank diameter: Preload (Torque): Young's modulus: Poisson's ratio: Preload units:	2 edge(s), 2 face(s) Bolt(Head/Nut diameter)(Count erbore) 15.4781 mm 15.4781 mm 10.3188 300 2.1e+011 0.28 lbf.in	No Data	

Connector Forces

Type	X-Component	Y-Component	Z-Component	Resultant
Axial Force (N)	0	1.0595e-011	17742	17742
Shear Force (N)	585.17	-865.53	0	1044.8
Bending moment (N.m)	-7.8416	-6.9135	4.1285e-015	10.454



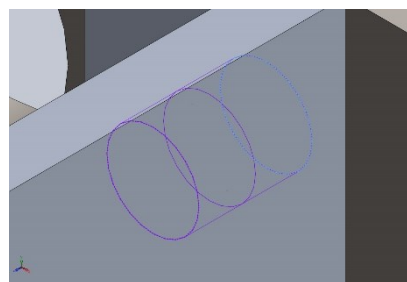
Counterbore with Nut-4

Entities: 2 edge(s), 2 face(s)
Type: Bolt(Head/Nut diameter)(Count erbore)
Head diameter: 15.4781 mm
Nut diameter: 15.4781 mm
Nominal shank diameter: 10.3188
Preload (Torque): 300
Young's modulus: 2.1e+011
Poisson's ratio: 0.28
Preload units: lbf.in

No Data

Connector Forces

Type	X-Component	Y-Component	Z-Component	Resultant
Axial Force (N)	0	1.2682e-011	17527	17527
Shear Force (N)	-10.873	7.214	0	13.048
Bending moment (N.m)	-0.61082	2.0826	-1.5069e-015	2.1703



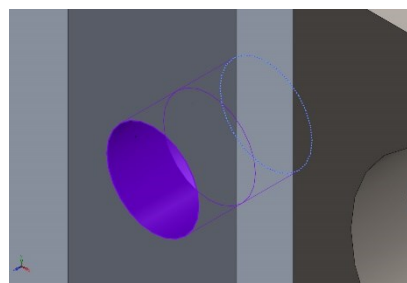
Counterbore with Nut-5

Entities: 2 edge(s), 2 face(s)
Type: Bolt(Head/Nut diameter)(Count erbore)
Head diameter: 15.4781 mm
Nut diameter: 15.4781 mm
Nominal shank diameter: 10.3188
Preload (Torque): 300
Young's modulus: 2.1e+011
Poisson's ratio: 0.28
Preload units: lbf.in

No Data

Connector Forces

Type	X-Component	Y-Component	Z-Component	Resultant
Axial Force (N)	0	0	-19608	19608
Shear Force (N)	-19.157	50.087	0	53.625
Bending moment (N.m)	-0.43341	-0.23243	0	0.4918



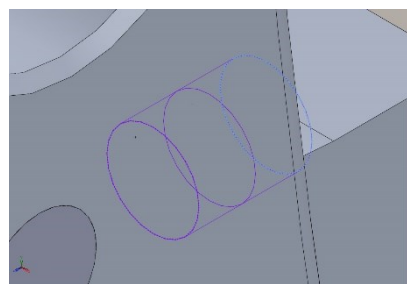
Counterbore with Nut-6

Entities: 2 edge(s), 2 face(s)
Type: Bolt(Head/Nut diameter)(Count erbore)
Head diameter: 15.4781 mm
Nut diameter: 15.4781 mm
Nominal shank diameter: 10.3188
Preload (Torque): 300
Young's modulus: 2.1e+011
Poisson's ratio: 0.28
Preload units: lbf.in

No Data

Connector Forces

Type	X-Component	Y-Component	Z-Component	Resultant
Axial Force (N)	0	-1.098e-011	-19531	19531
Shear Force (N)	-790.93	880.23	0	1183.4
Bending moment (N.m)	-4.1187	-3.9178	2.2026e-015	5.6844



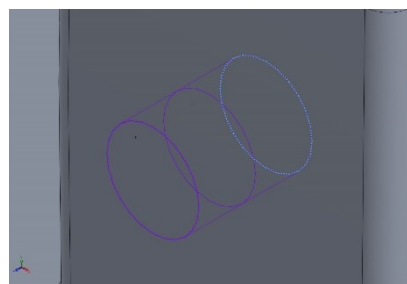
Counterbore with Nut-7

Entities: 2 edge(s), 2 face(s)
Type: Bolt(Head/Nut diameter)(Count er bore)
Head diameter: 15.4781 mm
Nut diameter: 15.4781 mm
Nominal shank diameter: 10.3188
Preload (Torque): 300
Young's modulus: 2.1e+011
Poisson's ratio: 0.28
Preload units: lbf.in

No Data

Connector Forces

Type	X-Component	Y-Component	Z-Component	Resultant
Axial Force (N)	0	-7.4963e-012	-19561	19561
Shear Force (N)	787.23	1011.3	0	1281.6
Bending moment (N.m)	-3.9159	3.7163	-1.4242e-015	5.3986



Counterbore with Nut-8

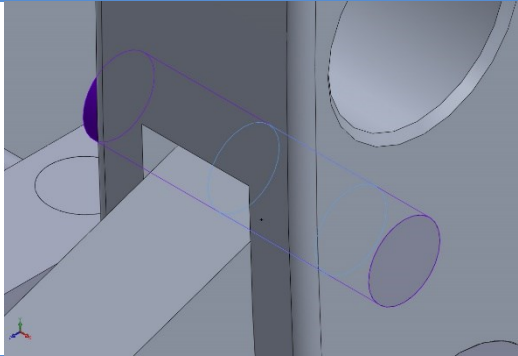
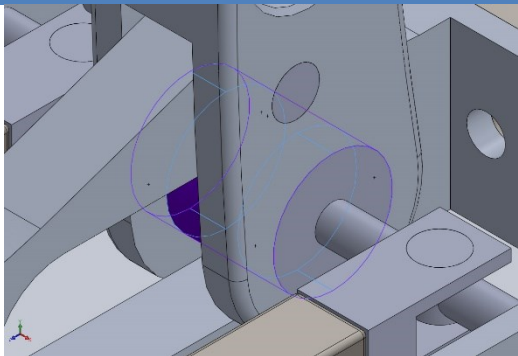
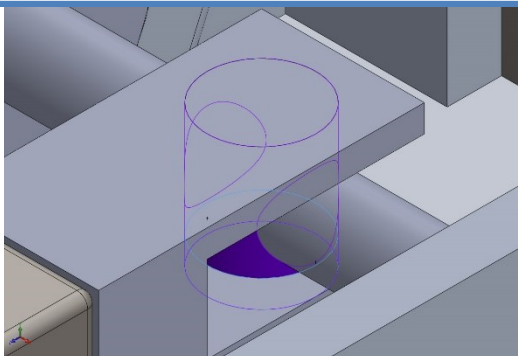
Entities: 2 edge(s), 2 face(s)
Type: Bolt(Head/Nut diameter)(Count er bore)
Head diameter: 15.4781 mm
Nut diameter: 15.4781 mm
Nominal shank diameter: 10.3188
Preload (Torque): 300
Young's modulus: 2.1e+011
Poisson's ratio: 0.28
Preload units: lbf.in

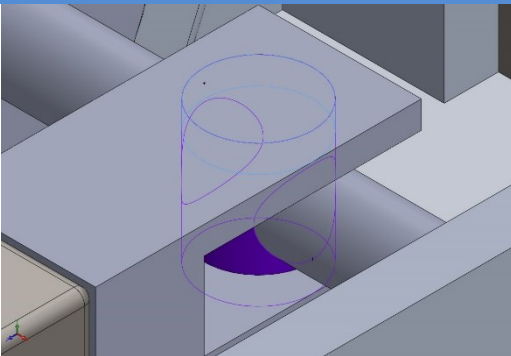
No Data

Connector Forces

Type	X-Component	Y-Component	Z-Component	Resultant
Axial Force (N)	0	0	-19600	19600
Shear Force (N)	10.965	-20.579	0	23.318
Bending moment (N.m)	0.35145	0.20973	0	0.40927

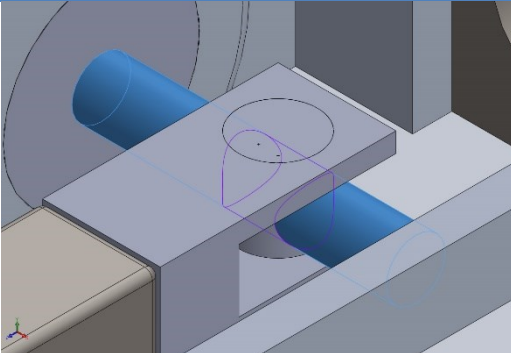
Contact Information

Contact	Contact Image	Contact Properties		
Contact Set-2		Type:	No Penetration contact pair	
		Entites:	2 face(s)	
		Advanced:	Node to surface	
Contact/Friction force				
Components	X	Y	Z	Resultant
Contact Force(N)	0.00016371	-95.684	-8472.3	8472.8
Contact Set-3		Type:	No Penetration contact pair	
		Entites:	5 face(s)	
		Advanced:	Node to surface	
Contact/Friction force				
Components	X	Y	Z	Resultant
Contact Force(N)	5.5381E-016	2.2901E-012	9.575E-013	2.4822E-012
Contact Set-6		Type:	No Penetration contact pair	
		Entites:	2 face(s)	
		Advanced:	Node to surface	
Contact/Friction force				
Components	X	Y	Z	Resultant
Contact Force(N)	1323.5	649.48	-464.42	1545.7

Contact Set-7		<p>Type: No Penetration contact pair</p> <p>Entites: 2 face(s)</p> <p>Advanced: Node to surface</p>
---------------	--	--

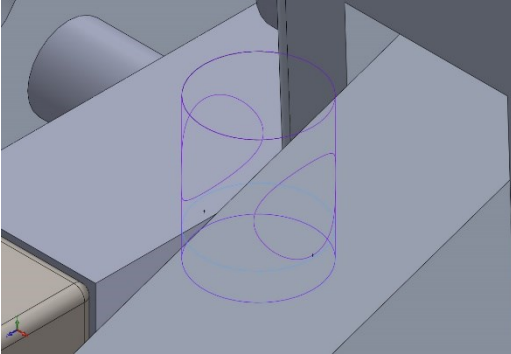
Contact/Friction force

Components	X	Y	Z	Resultant
Contact Force(N)	-965.84	670.3	-2004.7	2324

Contact Set-8		<p>Type: No Penetration contact pair</p> <p>Entites: 2 face(s)</p> <p>Advanced: Node to surface</p>
---------------	---	--

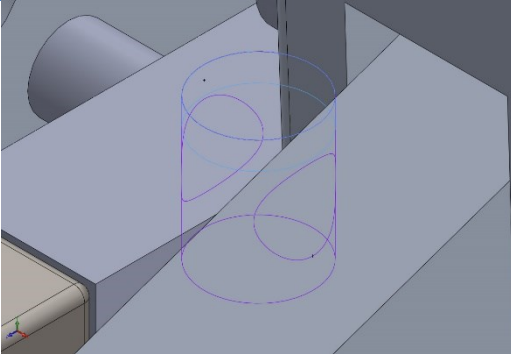
Contact/Friction force

Components	X	Y	Z	Resultant
Contact Force(N)	-1221.5	-0.61688	52.976	1222.6

Contact Set-9		<p>Type: No Penetration contact pair</p> <p>Entites: 2 face(s)</p> <p>Advanced: Node to surface</p>
---------------	---	--

Contact/Friction force

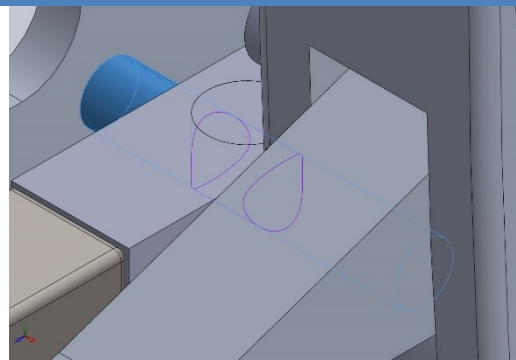
Components	X	Y	Z	Resultant
Contact Force(N)	-2212.7	1316.6	-469.37	2617.2

Contact Set-10		<p>Type: No Penetration contact pair</p> <p>Entites: 2 face(s)</p> <p>Advanced: Node to surface</p>
----------------	---	--

Contact/Friction force

Components	X	Y	Z	Resultant
Contact Force(N)	2011.5	1338.1	-4815	5387.1

Contact Set-11

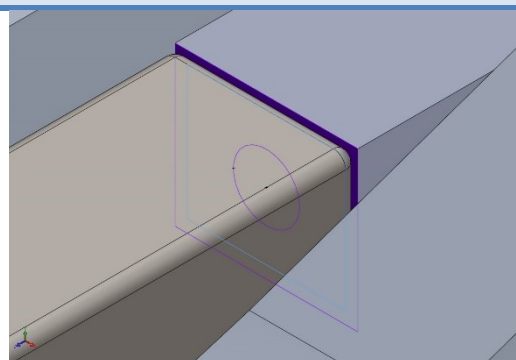


Type: No Penetration contact pair
Entites: 2 face(s)
Advanced: Node to surface

Contact/Friction force

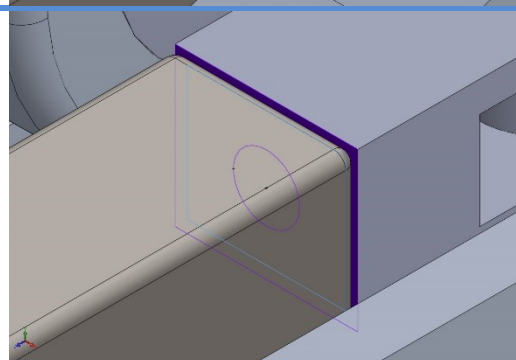
Components	X	Y	Z	Resultant
Contact Force(N)	-1403.4	-0.27055	260	1427.3

Contact Set-12



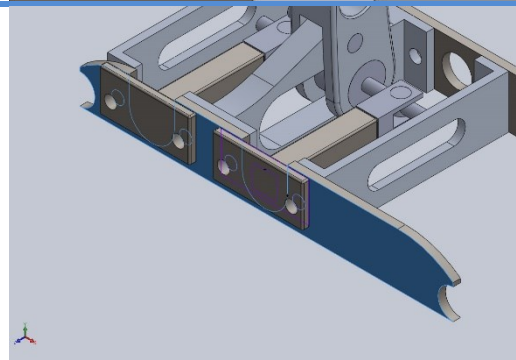
Type: Bonded contact pair
Entites: 2 face(s)

Contact Set-13



Type: Bonded contact pair
Entites: 2 face(s)

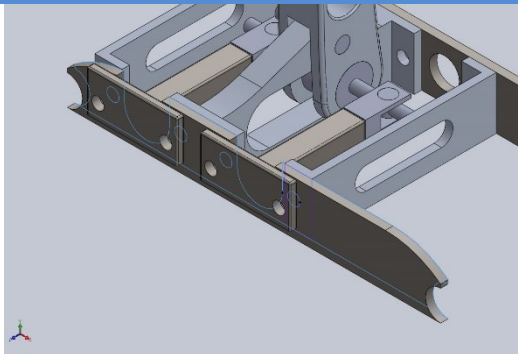
Contact Set-14



Type: No Penetration contact pair
Entites: 2 face(s)
Advanced: Node to surface

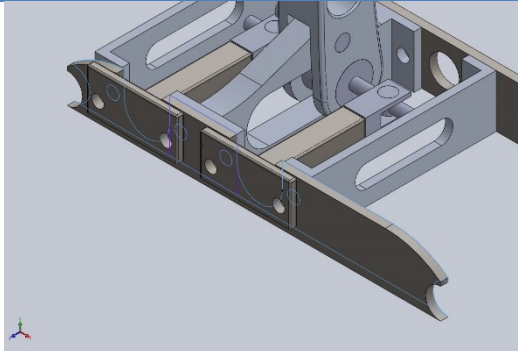
Contact/Friction force

Components	X	Y	Z	Resultant
Contact Force(N)	0	0	-31173	31173

Contact Set-15		<p>Type: No Penetration contact pair</p> <p>Entites: 2 face(s)</p> <p>Advanced: Node to surface</p>
----------------	--	--

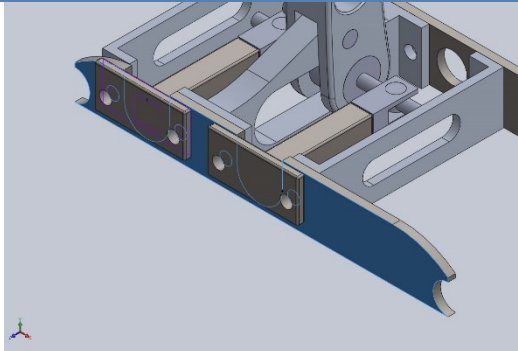
Contact/Friction force

Components	X	Y	Z	Resultant
Contact Force(N)	0	0	46305	46305

Contact Set-16		<p>Type: No Penetration contact pair</p> <p>Entites: 2 face(s)</p> <p>Advanced: Node to surface</p>
----------------	---	--

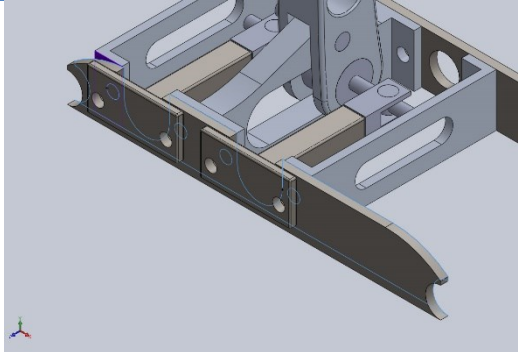
Contact/Friction force

Components	X	Y	Z	Resultant
Contact Force(N)	0	0	36698	36698

Contact Set-17		<p>Type: No Penetration contact pair</p> <p>Entites: 2 face(s)</p> <p>Advanced: Node to surface</p>
----------------	---	--

Contact/Friction force

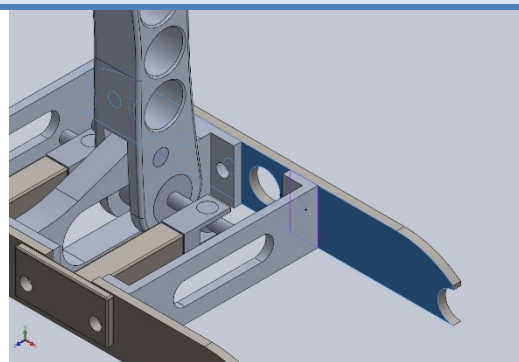
Components	X	Y	Z	Resultant
Contact Force(N)	0	0	-33070	33070

Contact Set-18		<p>Type: No Penetration contact pair</p> <p>Entites: 2 face(s)</p> <p>Advanced: Node to surface</p>
----------------	---	--

Contact/Friction force

Components	X	Y	Z	Resultant
Contact Force(N)	0	0	47163	47163

Contact Set-19

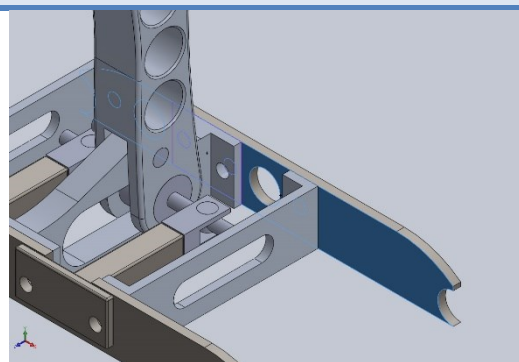


Type: No Penetration contact pair
Entites: 2 face(s)
Advanced: Node to surface

Contact/Friction force

Components	X	Y	Z	Resultant
Contact Force(N)	0	0	-59732	59732

Contact Set-20

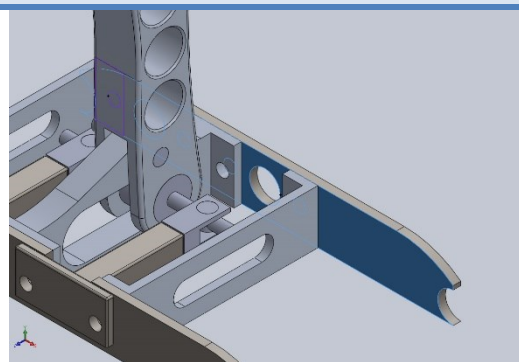


Type: No Penetration contact pair
Entites: 2 face(s)
Advanced: Node to surface

Contact/Friction force

Components	X	Y	Z	Resultant
Contact Force(N)	0	0	-39274	39274

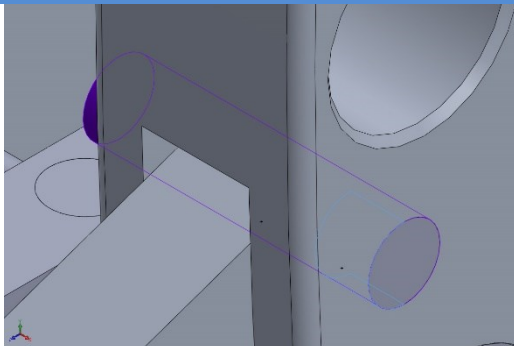
Contact Set-21



Type: No Penetration contact pair
Entites: 2 face(s)
Advanced: Node to surface

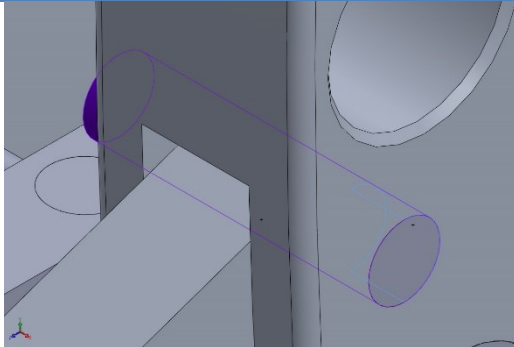
Contact/Friction force

Components	X	Y	Z	Resultant
Contact Force(N)	0	0	-59204	59204

Contact Set-24		<p>Type: No Penetration contact pair</p> <p>Entites: 2 face(s)</p> <p>Advanced: Node to surface</p>
----------------	--	--

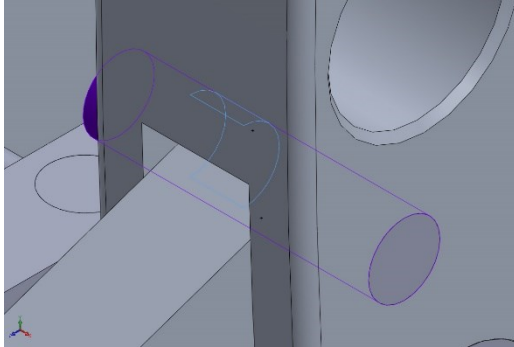
Contact/Friction force

Components	X	Y	Z	Resultant
Contact Force(N)	0.00046442	-511.62	3793	3827.4

Contact Set-25		<p>Type: No Penetration contact pair</p> <p>Entites: 2 face(s)</p> <p>Advanced: Node to surface</p>
----------------	---	--

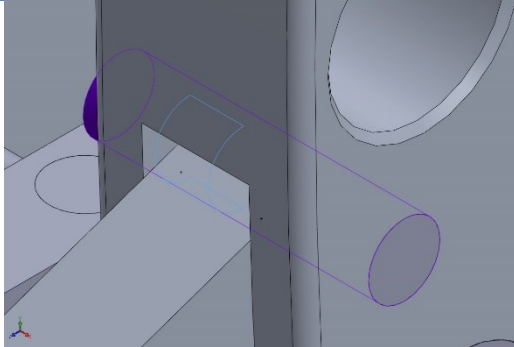
Contact/Friction force

Components	X	Y	Z	Resultant
Contact Force(N)	0.00014446	1247.1	-555.34	1365.2

Contact Set-26		<p>Type: No Penetration contact pair</p> <p>Entites: 2 face(s)</p> <p>Advanced: Node to surface</p>
----------------	---	--

Contact/Friction force

Components	X	Y	Z	Resultant
Contact Force(N)	0.00012406	1405.1	-606.68	1530.5

Contact Set-27		<p>Type: No Penetration contact pair</p> <p>Entites: 2 face(s)</p> <p>Advanced: Node to surface</p>
----------------	---	--

Contact/Friction force

Components	X	Y	Z	Resultant
Contact Force(N)	-0.0002586	-607.17	4067.3	4112.4

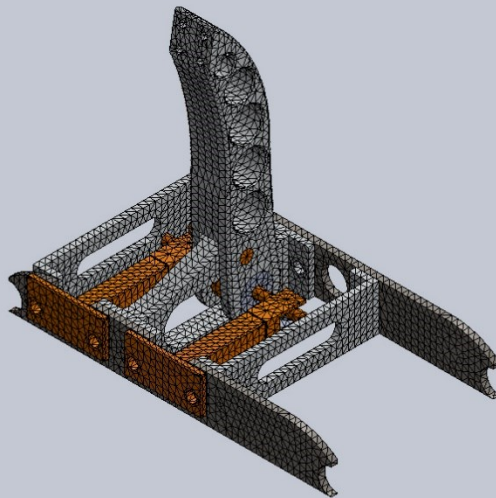
Mesh information

Mesh type	Mixed Mesh
Mesher Used:	Standard mesh
Automatic Transition:	Off
Include Mesh Auto Loops:	Off
Jacobian points	4 Points
Jacobian check for shell	On
Element Size	0.242524 in
Tolerance	0.0121262 in
Mesh Quality Plot	High
Remesh failed parts with incompatible mesh	Off

Mesh information - Details

Total Nodes	50373
Total Elements	26879
Time to complete mesh(hh:mm:ss):	00:00:09
Computer name:	

Model name:bracket and MSs (for fea)
Study name:Static 2(Default)
Mesh type: Mixed Mesh



SOLIDWORKS Educational Product. For Instructional Use Only.

Resultant Forces

Reaction forces

Selection set	Units	Sum X	Sum Y	Sum Z	Resultant
Entire Model	N	-11.892	1750.3	-1028.28	2030.04

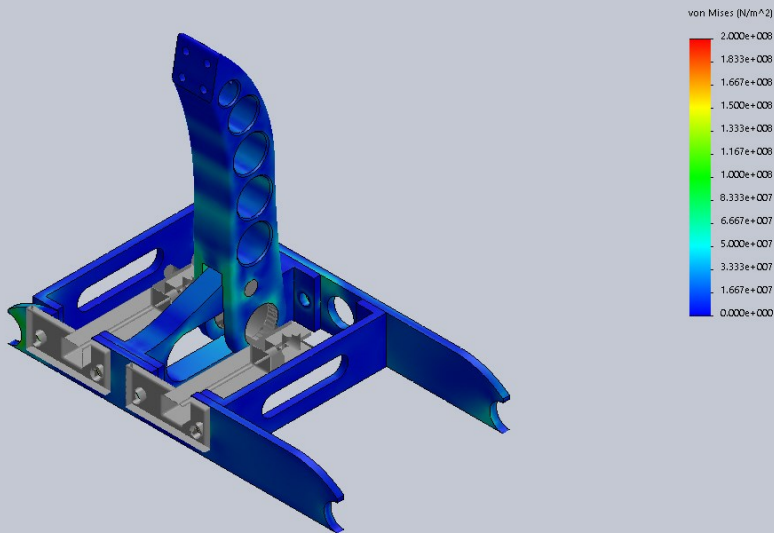
Reaction Moments

Selection set	Units	Sum X	Sum Y	Sum Z	Resultant
Entire Model	N.m	0	0	0	1e-033

Study Results

Name	Type	Min	Max
Stress1	VON: von Mises Stress	0.000e+000N/m ² Node: 42778	2.565e+008N/m ² Node: 34320

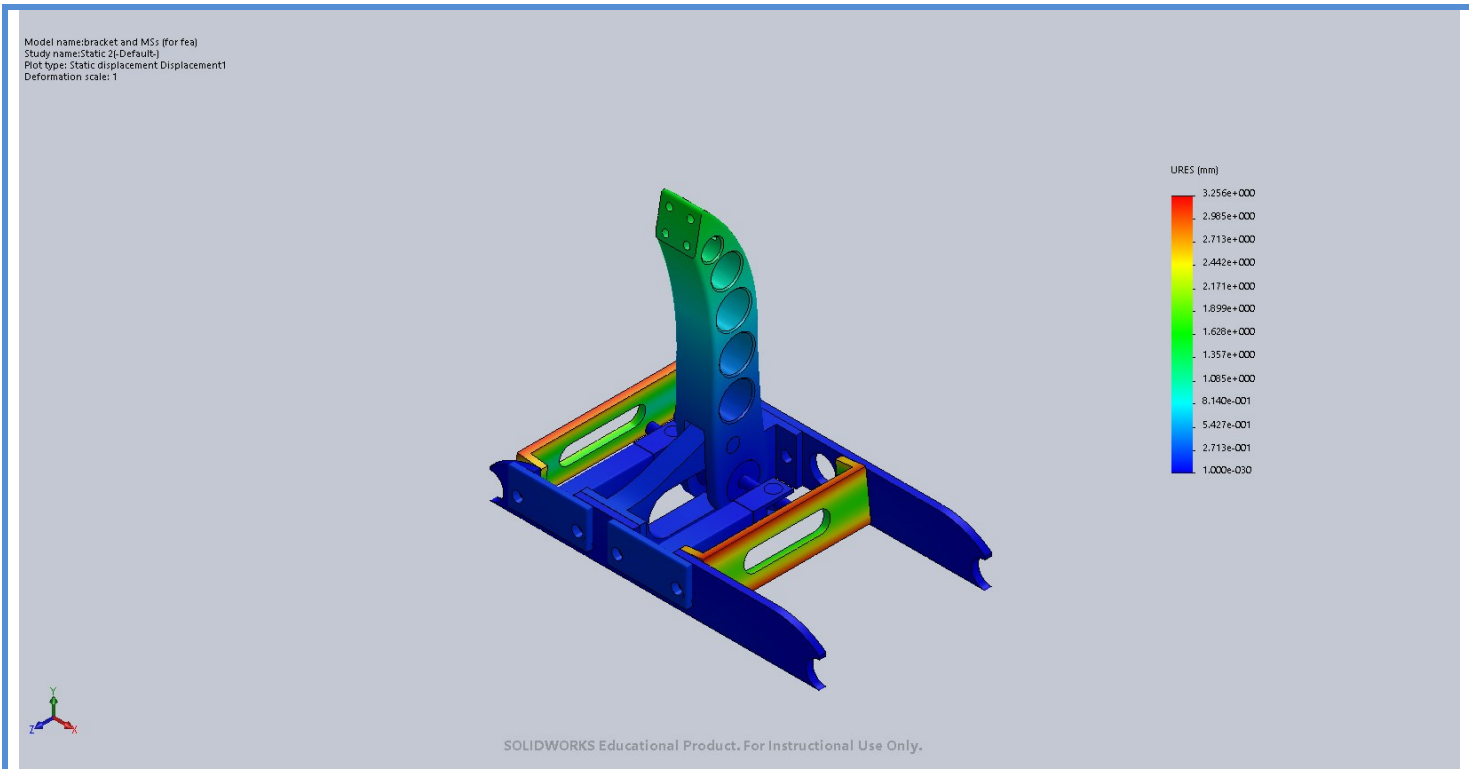
Model name:bracket and MSs (for fea)
Study name:Static 2(Default)
Plot type: Static nodal stress Stress1



SOLIDWORKS Educational Product. For Instructional Use Only.

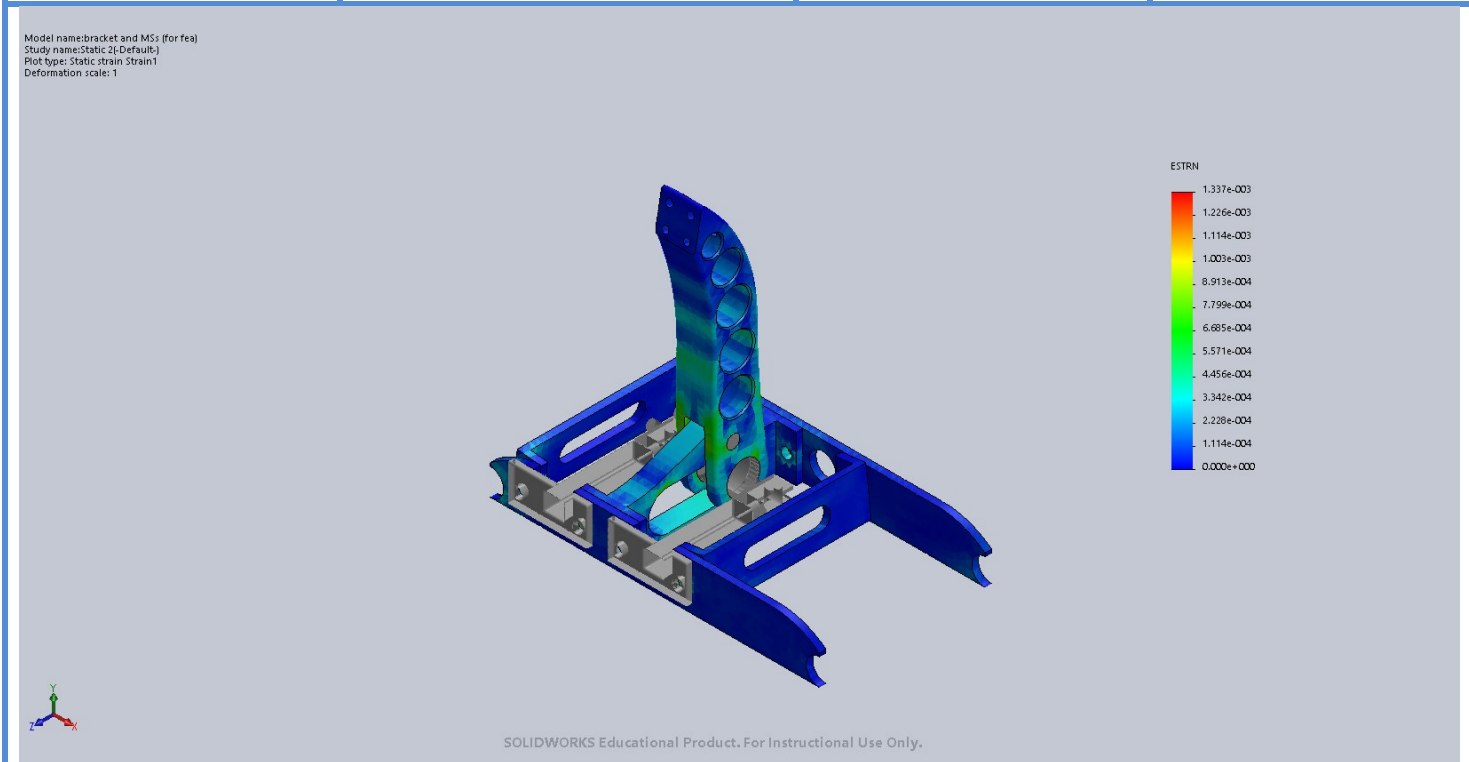
bracket and MSs (for fea)-Static 2-Stress-Stress1

Name	Type	Min	Max
Displacement1	URES: Resultant Displacement	0.000e+000mm Node: 24114	3.256e+000mm Node: 38957



bracket and MSs (for fea)-Static 2-Displacement-Displacement1

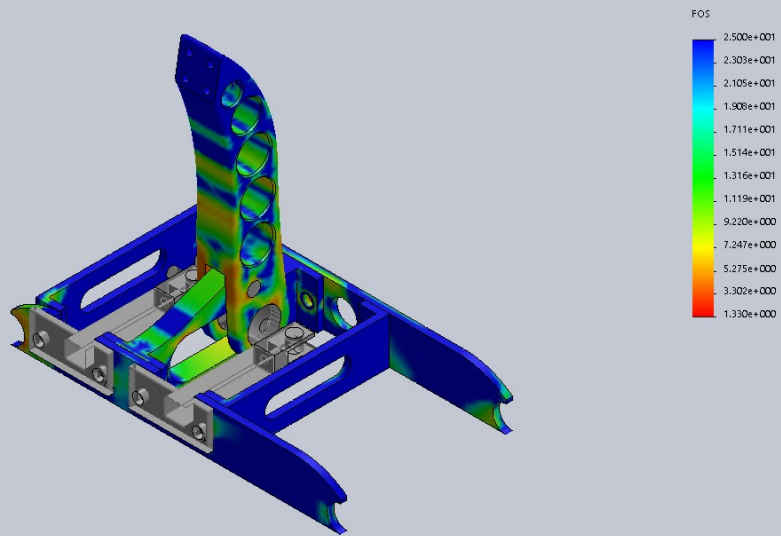
Name	Type	Min	Max
Strain1	ESTRN: Equivalent Strain	0.000e+000 Element: 23078	1.337e-003 Element: 21786



bracket and MSs (for fea)-Static 2-Strain-Strain1

Name	Type	Min	Max
Factor of Safety1	Automatic	1.330e+000 Node: 38019	3.000e+001 Node: 3

Model name: bracket and MSs (for fea)
Study name: Static 2 (Default)
Plot type: Factor of Safety-Factor of Safety1
Criterion : Automatic
Factor of safety distribution: Min FOS = 1.3



SOLIDWORKS Educational Product. For Instructional Use Only.

bracket and MSs (for fea)-Static 2-Factor of Safety-Factor of Safety1